Drivers, associations and consequences of the diel variability in high-resolution lake surface water temperature measurements

Richard Iestyn Woolway

Department of Geography

University College London

A thesis submitted for the degree of

Doctor of Philosophy

October 2014

Declaration

I, Richard Iestyn Woolway, confirm that the work presented in this thesis entitled ‘Drivers, associations and consequences of the diel variability in high-resolution lake surface water temperature measurements’, is my own. Where information has been derived from other sources, I confirm that this has been indicated in the thesis with an appropriate reference.

.....

Richard Iestyn Woolway

October, 2014

Acknowledgements

I would like to thank first and foremost, my PhD supervisors at the Centre for Ecology & Hydrology (CEH), Stephen Maberly and Ian Jones who have provided me with unending support, guidance, patience and encouragement throughout the PhD, I could not have wished for better or friendlier supervisors. I would also like to thank the Lake Ecosystems Group at CEH for hosting my PhD. A big thank you also goes to my supervisors at University College London (UCL), Gavin Simpson, Jon French and Rick Battarbee, who provided guidance during the PhD. I am very grateful for the funding provided by UCL and OTT hydrometry under the UCL Impact Studentship Scheme. I am also grateful for the travel fellowships awarded by UCL which allowed me to attend international conferences and workshops. Other travel fellowships from the Global Lake Ecological Observatory Network (GLEON) and the Networking Lake Observatories in Europe (NETLAKE) also allowed me to participate in numerous international workshops and training programs, which undoubtedly contributed greatly to my development as a scientist. Financial support for meetings and workshops inspired new research paths and gave me access to countless new friends and collaborators to exchange ideas with.

Abstract

The primary objective of this dissertation is to examine the drivers, consequences and associations of the diel variability in high-resolution lake surface water temperature. This dissertation consists of the high temporal resolution monitoring of up to 100 lakes, the creation of a predictive method to estimate the diel temperature range, and the development of an open source numerical program called Lake Heat Flux Analyzer, designed to calculate accurately the surface energy fluxes in lakes and reservoirs. A method for estimating the onset of thermal stratification from surface temperature measurements is also provided, where the association between the diel temperature range and the depth of the upper mixed layer allows accurate predictions of stratification onset with a root mean square error of 2.1 days. The relationship between the diel temperature range and lake specific characteristics is examined by a number of statistical approaches, varying from simple linear correlations to more complex additive models. The diel range in surface temperature is influenced significantly by lake surface area and water clarity. A statistically significant correlation between the diel temperature range and lake area is observed in the summer months caused by the larger lakes experiencing higher wind speeds, in turn leading to larger shear and

ultimately wind mixing, and consequently leading to greater mixing depths and thus to low diel temperature range. For 100 lakes, the diel range in surface water temperature is shown to be influenced significantly by lake surface area where the influence of lake area is most important for lakes smaller than 3.2 km^2. Compared to the seminal work in physical limnology, the work presented in this dissertation highlights the importance of much smaller, and numerically dominant, lakes which have historically been under-represented in estimates of inland waters.

Contents

List of Figures

LIST OF FIGURES

List of Tables

LIST OF TABLES

Notation

α_{sw}	Short-wave albedo
δ	Solar declination
κ	von Karman constant
ϕ_e	Similarity function for humidity
ϕ_h	Similarity function for heat
ϕ_m	Similarity function for momentum
ρ_0	Density of water surface
ρ_z	Density of air above the water surface
σ	Stefan-Boltzmann constant
τ	Momentum flux at the air-water interface
φ	Latitude
ζ	Atmospheric stability parameter
A	Amplitude

A_0	Lake surface area
$a_\oplus$	Earth's equatorial radius
AIC	Akaike Information Criteria
AICc	Second-order Akaike Information Criteria
C	Lake heat content
c	Speed of light
C_{d10N}	Neutral transfer coefficient for momentum at 10 m
C_{d10}	Transfer coefficient for momentum at 10 m
C_{dzN}	Neutral transfer coefficient for momentum
C_{dz}	Transfer coefficient for momentum
C_{e10N}	Neutral transfer coefficient for humidity at 10 m
C_{e10}	Transfer coefficient for humidity at 10 m
C_{ezN}	Neutral transfer coefficient for humidity
C_{ez}	Transfer coefficient for humidity
C_{h10N}	Neutral transfer coefficient for heat at 10 m
C_{h10}	Transfer coefficient for heat at 10 m
C_{hzN}	Neutral transfer coefficient for heat
C_{hz}	Transfer coefficient for heat

C_{pa}	Specific heat of air at constant pressure
C_{pw}	Specific heat of water at constant pressure
clf	Cloud cover fraction
E	Evaporation rate
E_s	Saturation pressure of the air
e_z	Vapour pressure of the air
g	Gravitational acceleration
GAM	Generalised Additive Model
GLM	Generalised Linear Model
H	Hour angle
h_p	Planck's constant
I_{eff}	Effective solar constant
L_λ	Spectral irradiance at a given wavelength
L_v	Latent heat of vaporization
L_w	Monin-Obukhov length scale
m	Air-mass thickness coefficient
P	Period
p	Surface air pressure

q_*	Scaling humidity term
Q_e	Latent heat flux
Q_h	Sensible heat flux
Q_{lin}	Incoming long-wave radiation
Q_{lout}	Outgoing long-wave radiation
q_o	Specific humidity at saturation pressure
Q_{sin}	Net incoming short-wave radiation
Q_s	Short-wave radiation at the water surface
Q_{tot}	Sum of surface fluxes
Q_{zmix}	Surface heating which influences the upper mixed layer
q_z	Specific humidity of the air above the lake surface
R_0	Visible component of short-wave radiation
$R_\odot$	Sun's equatorial radius
R_a	Gas constant for moist air
R_h	Relative humidity at height z_q above the water surface
R_{ref}	Angle of refraction
Ri_b	Bulk Richardson number
RSS	Residual Sum of Squares

sd	Standard deviation
T_*	Scaling potential temperature term
T_0	Surface water temperature
T_a	Transmission coefficient for absorption and scattering by aerosols
T_h	Potential temperature of the air above the water surface
T_{pg}	Transmission coefficient for absorption by permanent gases
T_R	Transmission coefficient for Rayleigh scattering
T_{v*}	Virtual potential temperature scaling parameter
T_v	Virtual air temperature
T_w	Transmission coefficient for absorption by water vapour
T_{zK}	Air temperature in Kelvin above the water surface
T_z	Air temperature at height z_t above the water surface
u_{*a}	Air-shear velocity term
u_z	Wind speed at height z_u above the water surface
V	Volume of water
W	Wedderburn Number
w_{*a}	Convective velocity scale in the atmospheric boundary layer
w_i	Akaike weight

z_{max}	Maximum lake depth
z_{mix}	Depth of the upper mixed layer
z_{oh}	Roughness length for heat
z_{oq}	Roughness length for humidity
z_o	Roughness length for momentum
Z_{SD}	Secchi depth

Chapter 1

Introduction

1.1 The importance of lakes

Lakes are bodies of water that exist across the world and provide essential provisioning, regulating, cultural and supporting ecosystem services on which humans depend. These include the transportation of commercial goods, flood regulation, food production, the support for biotic diversity, and the vital provision of water for domestic, agricultural and industrial use (e.g. Gleick, 1993; Moss, 2007). Although the global abundance of lakes is dominated by water bodies smaller than 0.1 km^2 (Downing et al., 2006; Verpoorter et al., 2014), lakes are also an important component of the global biogeochemical cycle for at least two important greenhouse gases: CO_2 (e.g. Cole et al., 2007; Kempe, 1984; Raymond et al., 2013; Tranvik et al., 2009) and CH_4 (Bastviken et al., 2004, 2011). CO_2 emissions from lakes, for example, have been shown recently to be significant relative to the terrestrial sources and sinks where global estimates for the terrestrial uptake of CO_2 is 3.0 ± 0.9 Pg C yr^{-1} (Le Quéré et al., 2009) and the global evasion

rate from lakes and reservoirs is estimated at 0.32 Pg C yr^{-1} (Raymond et al., 2013). Similarly, global CH_4 emissions expressed as CO_2 equivalents correspond to at least 25 % of the estimated terrestrial greenhouse gas sink (Bastviken et al., 2011).

Although widely distributed and important for global processes, lakes are extremely vulnerable to a wide range of stressors including climate change (e.g. Lemmin and Amouroux, 2012; Williamson et al., 2009), eutrophication (e.g. Abell et al., 2011; McDowell and Hamilton, 2013; Schindler, 1974a), invasion of alien species (e.g. Thackeray et al., 2006a; Winder et al., 2011), and acidification (e.g. Flower and Battarbee, 1983). The combination of these threats make them among the most imperilled ecosystems in the world (Dudgeon et al., 2006; Sala et al., 2000) where recent evidence suggests that freshwater systems are more threatened than marine and terrestrial ones (Millennium Ecosystem Assessment, 2005). Effective conservation and management of lakes requires a detailed understanding of how they function, which remains a formidable challenge as lakes are strongly influenced by external conditions at a hierarchy of scales (Maberly and Elliott, 2012), and the complex interactions between lake, catchment and atmosphere (Schindler, 2009). A lake and its catchment are often considered to be a single ecosystem (Likens, 1985).

1.2 The important role of physics

Physical processes play a fundamental role in lake functioning. Not least, it is through physics that the initial impacts of any changes in climate will be felt

within a lake (Livingstone et al., 2005). Lake physics also play a fundamental role in numerous chemical and biological processes in lakes as temperature, circulation patterns and turbulent mixing all set the environment in which the biology and chemistry operate. The thermal structure of lakes, for example, affects virtually all biological, chemical and physical processes, including the duration of ice cover (Magnuson et al., 2000; Weyhenmeyer et al., 2011), the solubility of dissolved oxygen and CO_2 (Kumar, 2003), species distribution (Magnuson et al., 1979), growth rates of phytoplankton (Butterwick et al., 2005; Staehr and Sand-Jensen, 2006), and the physiological and biochemical responses of fish (Breau et al., 2011; Hardewig et al., 2004).

1.3 The thermal structure of lakes

Thermal stratification is a natural phenomenon that occurs in many lakes and reservoirs as a result of the thermal expansion properties of water. The first order paradigm of thermal stratification is well established, where the vertical thermal structure of the lake is determined by the balance between turbulence, which acts to enhance mixing, and buoyancy forces, which acts to suppress turbulence and result in a vertical layering (Boehrer and Schultze, 2008). During stratification, the epilimnion, also known as the mixed layer, is defined as the part of the water column immediately below the water surface that is directly influenced by the momentum and turbulence introduced by the surface wind stress and buoyancy flux. The hypolimnion, the coolest and most dense layer, lies in contact with the bottom of the lake and is separated from the epilimnion above by a temperature-driven density gradient known as the thermocline (Fig. 1.1).

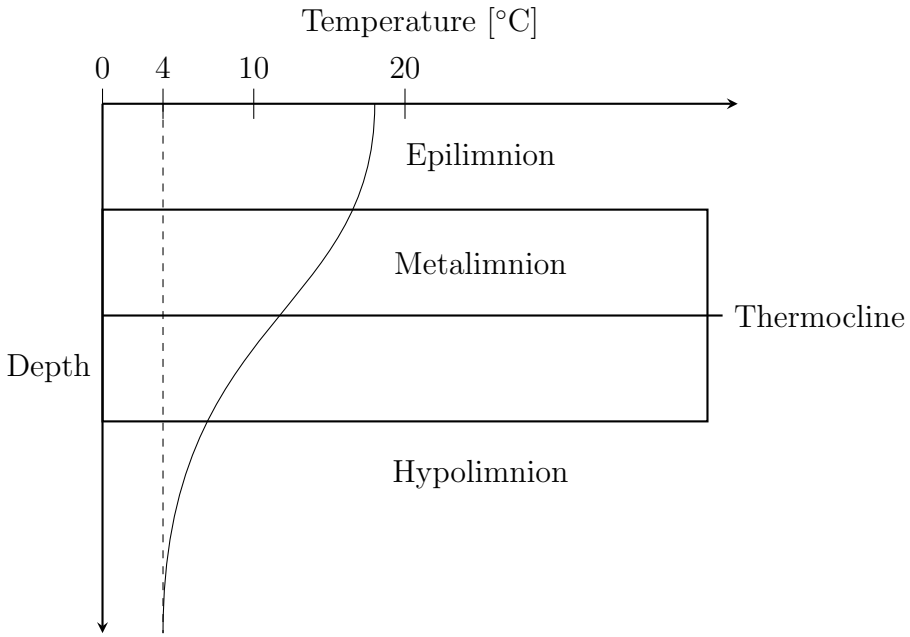

Figure 1.1: Schematic diagram of the characteristic temperature distribution in a temperate lake during summer, identifying the epilimnion, metalimnion, hypolimnion, and the region of maximum temperature gradient, the thermocline. The dashed line represents the temperature of maximum density, 3.98 °C. Redrawn from Hutter et al. (2010).

The vertical thermal structure of a lake, in particular the temperature of the upper mixed layer, is strongly influenced by climate forcing (e.g. Benson et al., 2000; Livingstone and Dokulil, 2001) or large-scale processes such as the position of the jet stream (Strong and Maberly, 2011), which ultimately, influence local weather. The influence of local weather on the thermal structure of lakes is well known. Surface water temperature has, for example, been shown to correlate strongly with air temperature over a range of spatial (e.g. Jones et al., 1997)

and temporal (e.g. Livingstone and Lotter, 1998; McCombie, 1959; Shuter et al., 1983) scales. However, the way a lake responds to local weather is also influenced by extrinsic and intrinsic lake characteristics such as lake size and water clarity, which can have a considerable effect on the thermal structure (Fischer, 1979; Hutchinson and Edmondson, 1957).

1.3.1 Climate: Large-scale atmospheric influence

Substantial year-to-year variations in lake temperature linked to regional weather patterns such as the North Atlantic Oscillation (NAO) have been discussed in great detail in recent years and have been shown to play a considerable role in aquatic ecology (e.g. Dokulil et al., 2006; George, 2007; George et al., 2004; Gerten and Adrian, 2000; Livingstone and Dokulil, 2001; Straile, 2002; Straile and Adrian, 2000; Straile and Stenseth, 2007). In north-west Europe, for example, weather, especially in winter is strongly influenced by the NAO (Hurrell, 1995), which is driven by a substantial variation in the distribution of atmospheric mass over the North Atlantic region. The NAO refers to changes in the pressure difference between the subpolar and subtropical Atlantic. Strong pressure differences between these regions result in an increase in westerly winds and mild and wet winters over Western Europe. Weak pressure differences, however, are associated with decreased westerly winds, and cold dry winters. This pressure difference can also be reversed during a negative NAO phase.

The relationship between the winter NAO and a number of lake properties in the English Lake District was investigated by George et al. (2004). A 36-year record of meteorological and limnological measurements from four lakes (Blel-

ham Tarn, Esthwaite Water, Windermere North Basin, and Windermere South Basin) were analysed and related to NAO variability. They found that winter weather conditions were strongly influenced by the NAO with, mild, wet winters being associated with strongly positive values of the North Atlantic Oscillation Index (NAOI), which is a measure of the strength of the NAO. A coefficient of determination (r^2) of up to 0.56 was calculated between the NAOI and lake surface water temperature. Other studies in the Northern Hemisphere have also found significant relationships between physical lake properties and the NAO. Livingstone (2001), for example, found a significant relationship between the NAO and ice break-up dates for five lakes, situated in Finland (Lake Kallavesi; Lake Näsijärvi), Switzerland (Lake San Murezzan), Russia (Lake Baikal), and the USA (Lake Mendota), where the winter NAO had left a detectable signal in the ice break-up dates of all five lakes at some point during the past 130 years.

Recent investigations suggest that the key physical mechanism underlying the NAO is an atmospheric phenomenon known as Rossby Wave Breaking. The physical consequence of Rossby Wave Breaking includes the latitudinal displacement of the jet stream and the corresponding changes in air temperature over continental Europe. Strong and Maberly (2011), for example, illustrated that surface water temperatures in the English Lake District were sensitive to Rossby Wave Breaking, which accounts for up to 52 % of the variance in lake surface water temperature during winter. Strong relationship were also observed during all four seasons (Strong and Maberly, 2011).

During summer, lakes in Europe are also influenced by another phenomenon known as the Gulf Stream (e.g. George and Taylor, 1995; Jennings and Allott, 2006; Nõges, 2004), which is a warm oceanic current in the North Atlantic

Ocean. The latitudinal variability of the Gulf Stream, for example, has been identified as playing a significant role on the onset of thermal stratification in the English Lake District. George and Taylor (1995) found that the thermal characteristics of Windermere (UK) were closely related to the north-south displacement of the northern wall of the Gulf Stream and during periods of northward displacement, the North Basin of Windermere became stratified earlier in the year driven by a warming of the early summer weather, consequently leading to increasing surface water temperature.

1.3.2 Weather: Local manifestation of climate

Of the numerous ways in which a climate signal can be transferred to a lake, arguably the most important is through its effect on water temperature. Lake temperature and, in turn, the thermal structure of lakes is influenced by a number of meteorological variables such as air temperature, cloud cover, relative humidity, and wind speed (Sweers, 1976), as well as one essentially astronomically determined variable, clear-sky short-wave radiation. At any given time, lake temperature tends towards an equilibrium temperature, defined as the temperature in which net heating/cooling is zero (Edinger et al., 1968). The amount of heat entering/leaving the water column is driven primarily by the exchange of radiative (net long-wave radiation, and net short-wave radiation) and non-radiative fluxes (latent and sensible heat) at the air-water interface (Fig. 1.2).

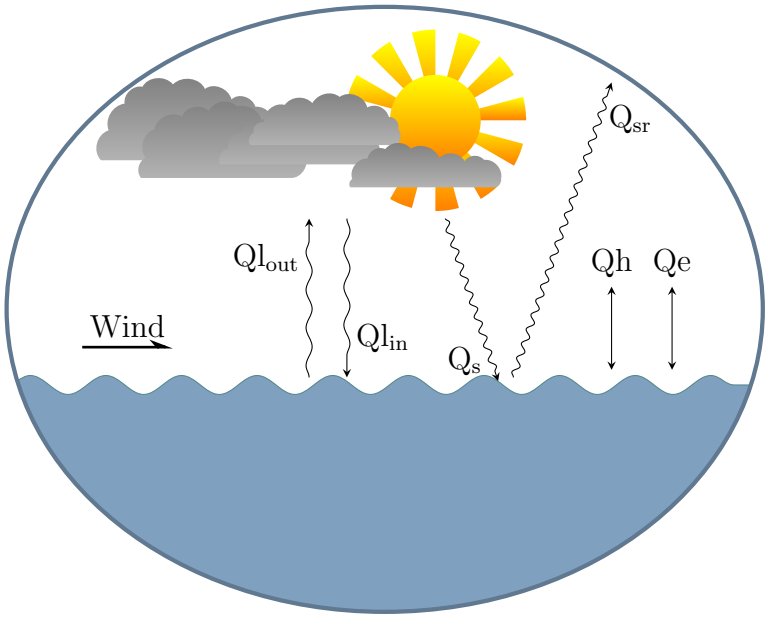

Figure 1.2: Schematic diagram illustrating the main heat exchange processes that determine the heat budget of a lake. The main heat exchange processes shown are the incoming (Q_s) and reflected (Q_{sr}) short-wave radiation, incoming (Q_{lin}) and outgoing (Q_{lout}) long-wave radiation, and the latent (Q_e) and sensible (Q_h) heat fluxes.

Many studies have calculated heat fluxes in lakes from around the world, covering temperate lakes (e.g. Hutchinson and Edmondson, 1957; Read et al., 2012), tropical (e.g. Lewis, 1973; MacIntyre et al., 2002; Verburg and Antenucci, 2010) and subtropical lakes (e.g. Imberger, 1985), as well as arctic and subarctic lakes (e.g. Eugster et al., 2003; MacIntyre et al., 2009; Vincent et al., 2008). Some of the earlier studies of surface fluxes in lakes are discussed by Myrup et al. (1979) who also include their own three-year analysis of the energy budget of Lake Tahoe, California-Nevada (USA). Other long-term studies of lake heat

budgets include a comprehensive ten-year study of the energy budget of Perch Lake, Ontario (Canada) by Robertson and Barry (1985) and a five-year analysis of Williams Lake, Minnesota (USA) by Sturrock et al. (1992). The relative importance of each of the major surface fluxes in influencing lake temperature was investigated recently by Fink et al. (2014). For Lake Constance (Germany, Switzerland, Austria), they investigated the modifications of the heat exchange processes at the lake surface from 1984 to 2011 and found that increasing absorption of short-wave radiation and long-wave radiation was responsible for lake surface warming for this period. As expected, they also illustrate that heat losses to the atmosphere by long-wave radiation and latent heat fluxes had intensified in parallel with increasing lake surface water temperature.

The majority of research on energy fluxes in lakes has been conducted at relatively long timescales, concentrating on the seasonal and intra-seasonal variation in the energy budget terms (e.g. Lenters et al., 2005; Rouse et al., 2003). Lenters et al. (2005), for example, conducted a ten-year analysis of seasonal, intra-seasonal, and inter-annual variations of evaporation rates in Sparkling Lake, northern Wisconsin (USA) and found considerable variability on a wide range of timescales. High temporal resolution studies of heat fluxes, however, are becoming increasingly common (e.g. Churchill and Kerfoot, 2007; Frempong, 1983; Heiskanen et al., 2014; Henderson-Sellers, 1986; MacIntyre et al., 2010, 2002; Pernica et al., 2014; Verburg and Antenucci, 2010) and the energy fluxes are frequently resolved at diel timescales. MacIntyre et al. (2002), for example, calculated the energy budget for Pilkington Bay, a shallow embayment of Lake Victoria (Africa), being the first surface energy budget calculated for a tropical lake over a diel timescale.

1.3.3 Local modulation by extrinsic factors

In addition to variations in regional weather, additional factors influencing lake temperature include those related to lake location. Factors such as latitude, altitude, local topographic shading and hydrology of inflows can influence the thermal structure of lakes. Latitude can influence a lake temperature through the presence of snow cover, which not only alters inflow water temperature (Livingstone et al., 2005), but can also influence light penetration at the lake surface. Schindler et al. (1990), for example, describes that even a few centimetres of snow can effectively block the penetration of light, thus radiation, into lakes, which will ultimately reduce lake temperature. The presence of snow can also act to increase the albedo of the lake, and thus lead to an increase in the amount of short-wave radiation that is reflected back to the atmosphere. On the other hand, snow can act as an insulator, so there will be less heat loss under snow compared to ice (e.g. Adams and Lasenby, 1978). Another factor, altitude, can be an important factor influencing lake temperature, where increasing altitude, thus decreasing air temperature, tends to result in a decrease in surface water temperature (e.g. Livingstone et al., 2005, 1999). Some investigations, however, have found that lake temperature is more influenced by changes in cloud cover and relative humidity than air temperature and that, at high altitude, surface water temperature can become increasingly decoupled from air temperature (e.g. Livingstone and Imboden, 1989).

At high altitude, topographic shading has been shown to modify the effects

of altitude on water temperature by depressing it below the value expected due to altitude alone (Goudsmit et al., 2000; Livingstone et al., 1999). Goudsmit et al. (2000), for example, conducted a palaeoclimatological study of Hagelseewli, a relatively deep mountain lake situated at an altitude of 2339 m above sea level in the Bernese Alps, Switzerland. They showed that surface water temperature was heavily influenced by topographic shading where the presence of a high cliff face to the south of Hagelseewli, rising to over 40° above the theoretical horizon, resulted in an extreme reduction in the amount of short-wave radiation received by the lake. A reduction in short-wave radiation ultimately resulted in the lake being completely or partially ice-covered throughout most of the year. This resulted in a reduction in the warming period, which ultimately led to cooler lake surface water temperature. Similar results were obtained by Livingstone et al. (1999) in ten Swiss Alpine lakes, where topographic shading resulted in a decrease in lake surface water temperature due to the decrease in short-wave radiation and the extension of the period of partial ice cover.

1.3.4 Local modulation by intrinsic factors

In addition to modulation by extrinsic factors, intrinsic features of the lake can also affect the thermal structure and can modify the way in which lakes respond to local meteorological forcing. Lake size is often considered as the primary factor, other than the local climate, for influencing the thermal structure of lakes. Wind speed, for example, is influenced by lake size, where larger lakes experience stronger winds (Hutchinson and Edmondson, 1957). Many investigators have even suggested that lake surface area and fetch are the most important pa-

rameters controlling momentum and energy transfer at a lake surface, and thus, the resulting upper mixed layer thickness (e.g. Davies-Colley, 1988; Gorham and Boyce, 1989; Monismith, 1985; Spigel and Imberger, 1980). Davies-Colley (1988), for example, investigated the relationship between the seasonal mixing depth of 24 lakes in New Zealand and found that the depth of the upper mixed layer was strongly correlated with lake size ($r^2 = 0.94$). Similarly, Gorham and Boyce (1989) illustrated that the depth of the thermocline in 54 Minnesota (USA) lakes, studied over a period of 4 years, varied as a function of lake size. Furthermore, they provide an empirical equation for estimating the depth of the thermocline as a function of lake size, wind stress, and the density contrast between the epilimnion and hypolimnion.

The relationship between increasing wind speed and increasing upper mixed layer depth is due to wind blowing over a lake generating a layer of high shear just below the water surface. This shear transfers wind energy from the atmosphere to the lake, leading to turbulent mixing (Fig. 1.3). Turbulent mixing, in turn, leads to an increase in the depth of the upper mixed layer (e.g. Hutchinson and Edmondson, 1957; Imberger and Hamblin, 1982; Wetzel, 1975).

Any factor which influences the wind regime over a lake can influence the thermal structure (Markfort et al., 2012; Steedman and Kushneriuk, 2000). Such local influences on the wind regime include deforestation, altering urban areas, agricultural fields, and bluff topography (e.g. France, 1997; Rask et al., 1993; Scully et al., 2000; Tanentzap et al., 2007). France (1997), for example, investigated the effect of deforestation on the depth of the thermocline in three lakes in the Experimental Lakes Area of Northwestern Ontario (Canada). He found that the removal of protective riparian trees resulted in a tripling of the measured wind

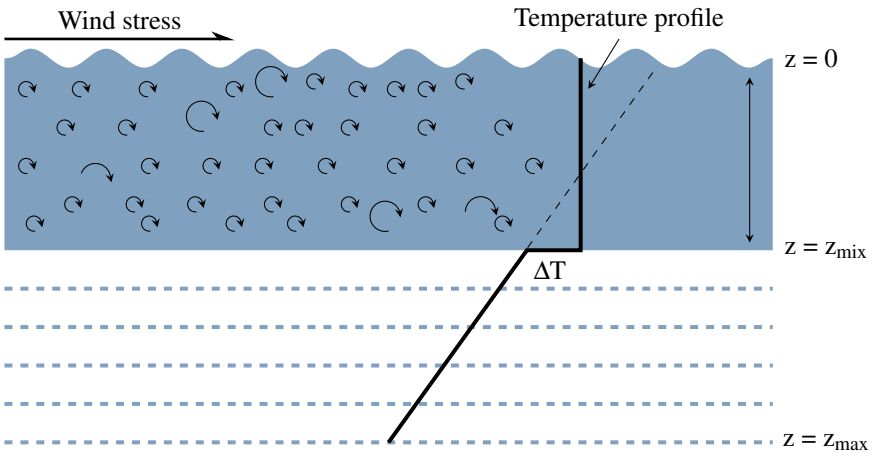

Figure 1.3: Schematic diagram illustrating the development of a mixed layer under the action of a surface wind stress. The depth (z) of the upper mixed layer (z_{mix}) and the maximum lake depth (z_{max}) are shown, as well as the temperature difference between the epilimnion and the hypolimnion, ΔT.

speeds over the lake surface, in turn, leading to a deepening of the thermocline by two metres. Similar trends were reported by Scully et al. (2000) where the effects of deforestation and re-growth on lake mixing were investigated. Using a 200-year sediment core record, they demonstrated that annual laminations of sediments indicated a fundamental change in the lake mixing regime associated with logging, which occurred between 1870 and 1890.

In addition to introducing turbulence to the surface waters by the generation of shear at the lake surface, wind stress has also been described to initiate lake currents and surface and internal waves (e.g. Csanady, 2001; Imboden and Wüest, 1995; Lemckert et al., 2004; Yeates and Imberger, 2003), all of which can influence vertical mixing (e.g. Fischer, 1979; Hutchinson and Edmondson, 1957;

Monismith and MacIntyre, 2009; Rueda-Valdivia and Schladow, 2009; Wüest and Lorke, 2003). Internal waves, for example, are a common phenomenon in lakes, and have long been recognised as having a considerable influence in determining the physical environment and ecology of the ecosystem. The history of internal wave investigations in lakes dates back to more than 100 years where the first publications on field observations were provided by Watson (1904) and Wedderburn (1907) in Loch Ness, Scotland. Subsequent studies, notably by Graf and Mortimer (1979), have investigated the details of the modal structure of internal waves by using time series of measurements with moored thermistor chains (e.g. Saggio and Imberger, 1998; Vidal et al., 2013, 2007) to measure the vertical displacement of isotherms that they cause, from which their natural modes of oscillation are then determined.

The mixing that internal waves cause has until recently been estimated only using microstructure probes, which require operators to be present and so cannot be deployed and left to obtain continuous long-term records. MacIntyre et al. (1999), for example, used a temperature-gradient microstructure probe and nutrient profiling to determine the extent of boundary mixing in Mono Lake, California (USA), and in turn investigate its effects on nutrient fluxes within the lake. An increase in the vertical flux of nutrients was observed during intense mixing events initiated by high winds. Recently, it has become possible to resolve internal wave motions and the turbulence they cause by using Acoustic Doppler Current Profilers (ADCPs) as demonstrated in a number of recent studies (Antenucci et al., 2000; Lorke and Wüest, 2005; Simpson et al., 2011). Simpson et al. (2011), for example, used ADCP measurements, in conjunction with cross-spectral analysis, to determine the modal structure of the internal wave field of

Llyn Tegid, North Wales (UK), and investigated how the internal wave motion varied with the strength of thermal stratification.

At the thermocline, Imberger (1998) described that internal waves may also enhance mixing, where the shear generated between adjacent layers in a thermally stratified lake would result in mixing and thus increase the exchange across the interface between the layers, thus leading to an increase in the depth of the upper mixed layer. Mixing, however, is thought to occur mainly through turbulence as generated by internal wave breaking at the lake periphery. For instance, cross-isopycnal mixing at the littoral zone of Lake Kinneret (Israel) was shown by Ostrovsky et al. (1996) to be a consequence of internal wave activity.

Erosion of stratification, and the subsequent change in the thermal structure of a lake, is not caused exclusively by wind stress. Processes such as convective cooling can also have a considerable effect (e.g. Eugster et al., 2003; MacIntyre et al., 2001, 2002). Throughout the seasonal cycle, for example, the lake surface is alternatively heated and cooled. Cooling at the surface creates water parcels that are slightly colder and hence denser than the water below. The cool water, therefore, sinks and is replaced by a new parcel of slightly warmer fluid, which will again be cooled and the process continues, this is known as convection. As described by Deardorff et al. (1969), however, sinking water parcels can overshoot the base of the upper mixed layer and partly penetrate into the layer below. Some energy is then available for the entrainment of heavier water from below into the upper layer, leading to a deepening of the upper mixed layer (Fig. 1.4).

Convection may be more important than wind in regulating the depth of the upper mixed layer in both tropical and small lakes (e.g. MacIntyre et al., 2002; Read et al., 2012; Snucins and Gunn, 2000). MacIntyre et al. (2002), for

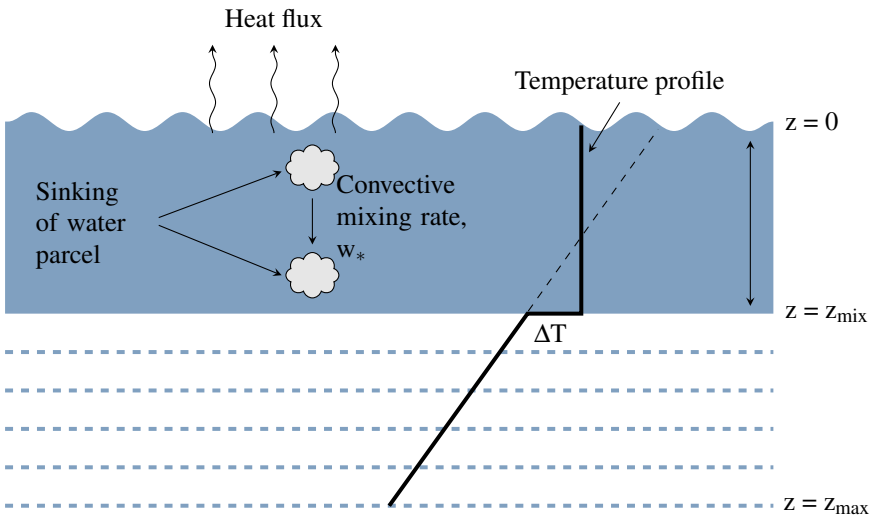

Figure 1.4: Schematic diagram illustrating the development of a mixed layer under the action of convective mixing. The initial thermal stratification is gradually eroded over the depth of the upper mixed layer, z_{mix}. The temperature inside the convecting layer is uniform, and a temperature jump of ΔT occurs between the base of the convecting layer and the water below.

example, demonstrated that surface cooling contributed 70 % of the energy for upper mixed layer deepening in Pilkington Bay (Lake Victoria, Africa). The relative contribution of wind shear and convection to turbulent mixing in the upper mixed layer was illustrated by Read et al. (2012) to vary as a function of lake size. Convection, for example, was found to be a larger mixed-layer turbulence source than wind shear for a majority of the small lakes included in their analysis, which included 40 temperate lakes of varying size (Fig. 1.5). Furthermore, seasonal patterns in wind shear and convection among the 40 lakes were shown to be dissimilar. Convection was typically lowest during spring and increased throughout the summer whereas wind shear was often highest during late spring

and commonly minimal during summer. Diel variation in wind shear and convection have also been reported. MacIntyre et al. (2001), for example, identified that during the evening, convective mixing often exceeds wind shear by up to a factor of 3, thus being a greater contributor to upper mixed layer deepening.

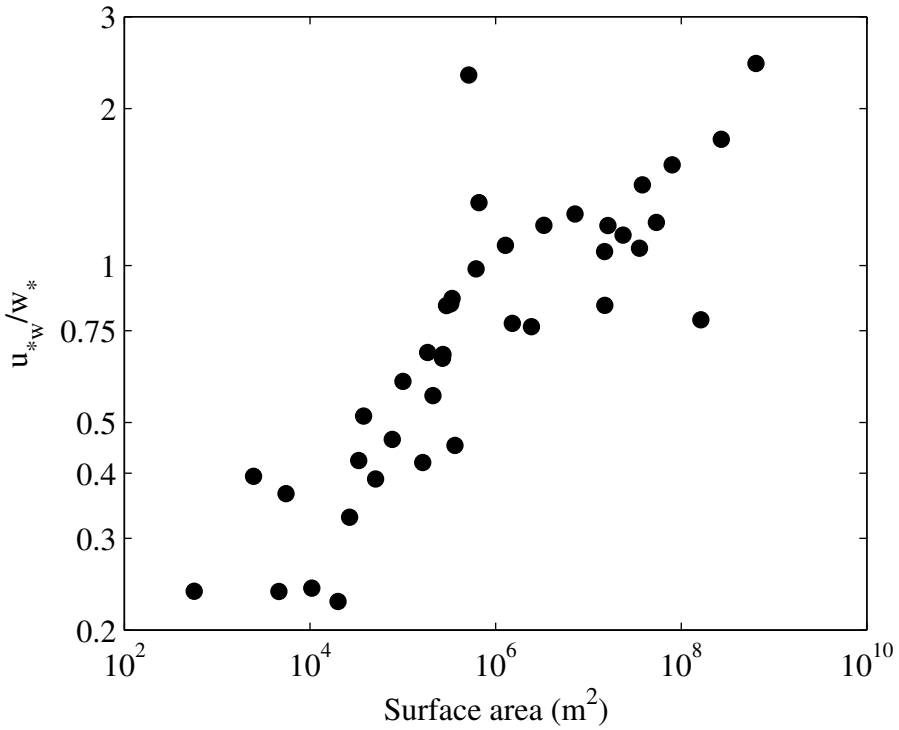

Figure 1.5: Ratio between temporally-averaged velocity scales for wind shear (u_{*w}) and convection (w_*). Re-drawn from Read et al. (2012).

As most of the heating and cooling takes place at the surface of a lake, with the exception of solar heating, part of which takes place within the water column. One key variable influencing the absorption of short-wave radiation is water clarity and a number of investigators have examined its effect on the thermal structure of lakes. Water clarity is particularly interesting from a biological viewpoint,

because it can be influenced by the number and kinds of planktonic organisms found in lakes and therefore allows a biological feedback on the thermal structure of the water column. In a comparative study of small temperate lakes in Ontario (Canada), Mazumder et al. (1990), for example, demonstrated that the depth of the upper mixed layer was directly related to water clarity, where clearer lakes had deeper mixing depths. This relationship was explained by the greater penetration of incident short-wave radiation in lakes with high water clarity. Furthermore, they showed that light penetration is primarily a function of the size distribution and biomass of algae. They demonstrated that smaller algae have greater absorption and scattering of radiation per unit mass than larger algae because their surface area per unit mass is larger. Therefore, lakes dominated by small plankton are associated with lower water clarity. Similarly, lakes with high abundance of planktivorous fish will have low water clarity, because large zooplankton, which feed on small algae, are reduced by fish predation, leading to an increase in the population of small algae, and thus a decrease in mixing depth. In another study in Ontario (Canada), Snucins and Gunn (2000) investigated the influence of water clarity on lake temperatures in 86 lakes. They demonstrated that clear lakes are more sensitive than coloured lakes to climate warming and that clear lakes exhibit large thermal changes in response to small changes in clarity.

Most studies have concluded that an increase in light penetration, associated with an increase in water clarity, is associated with an increase in mixing depth (e.g. Fee et al., 1996; Mazumder and Taylor, 1994). In general, though, water clarity is believed to have more of an influence on the thermal structure of smaller lakes where wind-induced mixing is relatively less important. Numerous

investigations from around the world have highlighted the influence of varying levels of water clarity on the depth of the upper mixed layer. In Cameroon, for example, Kling (1988) compared the mixing depths for 39 lakes and found a strong positive relationship between water clarity and the vertical thermal structure. Similar relationships have been found in Europe (e.g. Jones and Arvola, 1984) and Canada (e.g. Fee et al., 1996; Keller et al., 2006; Pérez-Fuentetaja et al., 1999; Snucins and Gunn, 2000). Keller et al. (2006), for example, used multiple linear regression analysis to investigate the relationship between a number of lake specific characteristics and the depth of the upper mixed layer for nine Boreal Shield Lakes (Canada) and found that water clarity was the best individual predictor of mixing depth ($r^2 = 0.69$). Another study in North America showed a statistical relationship between water clarity and the depth of the upper mixed layer (Mazumder and Taylor, 1994).

As well as affecting the depth of the upper mixed layer, water clarity may also influence surface water temperature where it is expected that a decrease in water clarity, resulting in an increase in the absorption of short-wave radiation, will result in an increase in surface water temperature. Previous studies, however, have found little agreement between changing water clarity and surface water temperature. Some investigators, for example, have suggested that decreasing water clarity results in lower surface temperature (Houser, 2006; Mazumder et al., 1990) others suggesting an increase in surface temperature with decreasing water clarity (De Stasio et al., 1996; Jones et al., 2005) and others higher and lower surface water temperatures at different times of the summer (Hocking and Străskraba, 1999; Jones et al., 2008). Houser (2006), for example, demonstrated that the surface water temperature of six lakes in Wisconsin (USA) was signifi-

cantly influenced by water clarity where water temperature was lower in the less transparent lakes. This was also found by Mazumder et al. (1990) who demonstrated that an increase in water clarity resulted in a decrease in surface water temperature. It was suggested that a decrease in water clarity would result in a large amount of back-radiation at night and thus a decrease in lake surface water temperature. Jones et al. (2005), however, in an experiment in two large limnetic enclosures in Blelham Tarn (UK), reported an increase of up to 1 °C with a decrease in water clarity. Furthermore, De Stasio et al. (1996) showed that a shift in water clarity, from a light attenuation coefficient of 0.1 m^{-1} to 1.2 m^{-1} would result in a surface water temperature increase of about 1 °C. Similarly, an increase from 0.2 m^{-1} to 1.0 m^{-1} change in the light attenuation coefficient was found by Sahlberg (2003) to result in a temperature increase of up to 1 °C in the Akkajaure reservoir (Sweden).

1.3.5 Seasonal cycle of thermal stratification

For many lakes of sufficient depth, the water column evolves seasonally from being isothermal in the early spring, developing stratification as the weather warms and then overturning sometime in the autumn, although the timing and duration of this process will vary among lakes. The seasonal cycle of thermal stratification is a frequently studied topic in limnology and has been shown to play an important role in the functioning of the ecosystem (e.g. Schertzer et al., 1987). It results from the seasonal variation in the surface energy fluxes and controls the water column temperature profile. During summer, for example, high input of

short-wave radiation and relatively high air temperature at the lake surface result in high surface water temperature and, if mixing processes are not too great, can lead to a steep temperature and density gradient within the water column (Fig. 1.6i) leading to a separation of the upper and lower water masses. As air temperature and short-wave radiation decreases during autumn, however, the surface water begins to cool and eventually cools to the temperature of the hypolimnion and the lake is no longer stratified (Fig. 1.6ii). If the surface water cools below 3.98 °C (the density at which freshwater has the greatest density), then the surface water becomes less dense than the bottom water and a so-called winter inverse stratification develops (Fig. 1.6iii). As the surface water heats up again during spring, the ice at the lake surface melts and the lake will once again return to a vertically isothermal state (Fig. 1.6iv). Lakes that experience this full cycle of thermal stratification are called dimictic lakes whereas lakes that only stratify once are called monomictic.

Figure 1.6: Schematic of the seasonal cycle of thermal stratification in a dimictic lake. Each sketch is accompanied by a temperature profile and the relationship between temperatures in the upper and lower regions of the lake.

Schemes to classify lakes based on temporal differences in vertical mixing compiled in Hutchinson's Treatise on Limnology (Hutchinson and Edmondson, 1957) and modified by Lewis (1983) led to an empirical classification system. Eight types of mixing (amictic, cold monomictic, dimictic, warm monomictic, and four types of polymictic lakes) were described (Table 1.1). The first mixing type described by Lewis (1983) was amictic lakes. These lakes are almost permanently ice covered and are often limited to the high latitudes and lakes situated at high altitude. Monomictic lakes are those that mix from top to bottom during one mixing period each year. These lakes can be subdivided into (i) cold monomictic lakes, which are ice covered throughout much of the year, thus inversely stratified, and mix during one brief period in summer; and (ii) warm monomictic lakes that never freeze, and are thermally stratified throughout most of the year. During winter, however, the surface waters cool and the lakes become vertically mixed. Polymictic lakes are lakes that are generally too shallow to develop long periods of thermal stratification, thus their waters can periodically mix from top to bottom throughout the ice-free period. Polymictic lakes can also be subdivided into cold and warm types, where cold polymictic lakes are those that are ice-covered in winter, and warm polymictic lakes are those that are not. These classifications are important to limnologists because they affect which species of plants and aquatic life will populate the lake. They are also useful for environmental fluid mechanics because they suggest the expected base-state of the stratification in each season.

Table 1.1: Examples of the eight lake mixing types.

Lake type	Name	Latitude, Longitude	Reference
Amictic	Vanda	77 °S, 161 °E	Goldman et al. (1967)
	Fryxell	77 °S, 163 °E	Vincent (1981)
Cold monomictic	Char	75 °N, 95 °W	Schindler et al. (1974b)
	Meretta	75 °N, 95 °W	Schindler et al. (1974c)
Continuous cold polymictic	Joseph	53 °N, 113 °W	Hickman (1979)
Discontinuous cold polymictic	Tobacco	46 °N, 82 °W	Harvey and Coombs (1971)
Dimictic	Mendota	43 °N, 89 °W	Hofman et al. (2013)
	Windermere	54 °N, 3 °W	Woolway et al. (2014)
Warm monomictic	Lanao	8 °N, 124 °E	Robertson and Ragotzkie (1990)
Discontinuous warm polymictic	Rotorua	38 °S, 176 °E	Burger et al. (2008)
Continuous warm polymictic	Sonachi	0 °N, 36 °E	MacIntyre and Melack (1982)

1.3.6 Influence on lake ecology

The thermal structure of lakes can have an important influence on lake ecology. It can, for example, influence the distribution and exposure of important abiotic conditions such as temperature, oxygen and conductivity with the potential to influence primary productivity and respiration (Reynolds, 1984; Sverdrup, 1953). A model showing the association between phytoplankton biomass and the depth of the thermocline was first derived by Sverdrup (1953), who stated that in order for the spring phytoplankton bloom to begin, it is necessary for the production of organic matter by photosynthesis to exceed the destruction by respiration. In order for this to occur, the thermocline depth must be shallower than some critical depth. Subsequent theory has incorporated nutrient levels as a second critical driver of phytoplankton dynamics in a thermally stratified water column. Klausmeier and Litchman (2001), for example, presented a model of vertical phytoplankton distribution for poorly mixed water columns, and explained that in poorly mixed waters, phytoplankton can be heterogeneously distributed, such that distinct populations are found on the sediment surface, at depth, or near the lake surface corresponding to preferred light and nutrient conditions (e.g. Clegg et al., 2007). They also showed that the phytoplankton maximum occurred at the depth for which the phytoplankton was equally limited by light and nutrients.

Aquatic predator-prey interactions may also be altered by changes in the vertical thermal structure of lakes as feeding and production rates are temperature dependent (Peters and Downing, 1984). This is particularly true for small lakes in which space, habitat heterogeneity, trophic complexity and thermal refuges are limited (e.g. Keller and Conlon, 1994; Moore et al., 1996; Post et al., 2000).

A deeper mixing depth may favour species that are less sensitive to large fluctuations in light levels, as Litchman (2000) describes for some diatom species, based on an investigation on the growth rates of four species of freshwater phytoplankton under fluctuating light conditions. During periods of mixed layer deepening, phytoplankton that have low light to nutrient needs can position themselves at the base of the thermocline and capitalise on higher nutrient levels present at the top of the hypolimnion. In contrast, buoyant cyanobacteria should be negatively influenced by a deeper thermocline due to their inability to maintain their preferred shallow position, and thus will be subjected to shading by other species positioned higher in the upper mixed layer (Huisman et al., 2004). Furthermore, fast sinking algae could benefit from greater thermocline depth as they will remain in the mixed layer for a longer duration (e.g. Winder et al., 2009).

The vertical distribution of zooplankton can be linked not only to abiotic factors such as temperature but also to the distribution of phytoplankton, invertebrates and fishes, all of which can be influenced by thermocline depth and the strength of thermal stratification (Masson et al., 2004). Leibold (1990), for example, conducted two field experiments in the early 1990s in large enclosures and found that zooplankton (*Daphnia pulicaria*) can alter their habitat in response to changes in food distribution and predators. Thackeray et al. (2006b), however, describes a more heterogeneous distribution of zooplankton being linked to stronger thermal stratification through both the active and passive movements of individuals. Consequently, phenological change in plankton seasonality can be influenced by the change in timing of thermal stratification (Thackeray et al., 2008).

The vertical partitioning of the water column, as occurs during stratification,

influences the vertical distribution of dissolved oxygen in lakes. Deeper vertical mixing of the water column, for example, could lead to greater oxygenation of the hypolimnion thus reducing anoxia at depth (Scully et al., 2000). Alternatively, restricting the supply of oxygen to the hypolimnion may lead to deoxygenation in productive lakes which can reduce the ecological niche of many species such as fish (Elliott and Bell, 2011) and lead to the release of phosphorus from the sediment to the overlying water (Morimer, 1941).

Stratification may also affect the vertical distribution of other species by providing different physical and chemical conditions at different depths and by reducing rates of water movement so that motile organisms can accumulate at preferred depths (Mellard et al., 2011). Thermal stratification may also restrict nutrient re-supply from depth to the epilimnion as was shown by George et al. (2007) where the winter effect of the NAO and the summer effect of the Gulf Stream in influencing the ecosystem is discussed. Furthermore, because nutrient concentrations are usually higher in the deeper, hypolimnetic water of stratified lakes, increased vertical mixing can make nutrients more available to epilimnetic plankton communities (Harris and Griffiths, 1987). Kristensen et al. (1992), for example, examined the frequency and importance of wind induced re-suspension in a shallow, eutrophic lake (Lake Arreso, Denmark) during storm events where the concentration of suspended solids was found to increase markedly.

The onset of thermal stratification has an important influence on lake ecology as it separates processes of production and nutrient depletion in the epilimnion from processes of decomposition and nutrient regeneration in the hypolimnion and sediment. The reduction in surface mixed layer depth that occurs as the epilimnion is formed, for example, increases light availability per unit volume

to phytoplankton (MacIntyre, 1993) which can trigger the spring bloom (Bleiker and Schanz, 1997). An earlier onset of thermal stratification can lead to an increase in the spring peak biomass of phytoplankton which can lower summer biomass of zooplankton (George and Taylor, 1995). Consequently, phenological change in plankton seasonality can be influenced by the change in timing of stratification (Thackeray et al., 2008).

The duration of thermal stratification restricts the supply of oxygen to the hypolimnion and sediment (Foley et al., 2012), leading to deoxygenation in productive lakes and potential release of phosphorus from the sediment into the water column (Morimer, 1941). Reduced oxygen concentrations at depth can also reduce the ecological niche of many species such as fish (Elliott and Bell, 2011) and stratification can affect the vertical distribution of other species by providing different physical and chemical conditions at different depths and by reducing rates of water movement so that motile organisms can accumulate at preferred depths (Mellard et al., 2011). Stratification can also influence the role of lakes in the global carbon cycle by affecting metabolism and the flux of gases between the lake and the atmosphere (Coloso et al., 2011), especially the potent greenhouse gas methane that is produced in anoxic parts of a lake (Bastviken et al., 2011).

1.4 Long-term limnological monitoring

The interaction between physics, biology and chemistry within a lake demonstrates the complexity of aquatic ecosystems. The practical consequence of the complexity in lake ecosystems is that holistic studies are needed to understand

the many different processes at work. It has become clear over the past few decades that a rich understanding of lake function requires detailed studies that range a number of temporal scales. The environmental conditions that influence lakes, and the response of lakes to those conditions, for example, are expressed differently depending on the time and distance over which they are studied. Understanding lake function is, therefore, difficult or, in most cases, impossible without long-term monitoring.

In limnology, long-term datasets are increasingly valued for the unique perspective they provide, particularly as lakes respond to both anthropogenic perturbations and long-term environmental change. Long-term data can be used to document patterns of ecosystem response to a changing climate, detect cause-effect relationships for a range of environmental conditions, define the range of natural variability, and provide a baseline from which to determine if lakes are significantly changing (e.g. Bloch and Weyhenmeyer, 2012; Carpenter and Brock, 2006; Carpenter et al., 2011; Foley et al., 2012; Maberly and Elliott, 2012; Rhodes et al., 2012; Scheffer et al., 2001; Thackeray et al., 2012; Winfield et al., 2012). Long-term surface water temperature measurements of inland water bodies, for example, are good indicators of climate change (e.g. Austin and Colman, 2008; Coats et al., 2006; Livingstone, 2003; Quayle et al., 2002; Verburg et al., 2003; Vollmer et al., 2005; Williamson et al., 2009).

Recent studies provide powerful examples of the role of long-term datasets in explaining major ecological processes in lakes. A recent long-term study in the North Basin of Windermere (UK), for example, demonstrated that climate warming in the northern hemisphere (e.g. Hari et al., 2006; Jones et al., 1999) has resulted in a significant change in zooplankton phenology and spring water

temperature (Thackeray et al., 2012). In another study within the Windermere catchment (UK), Foley et al. (2012) investigated 40 years of data collected in Blelham Tarn, and found a significant change in the vertical thermal structure of the lake. They describe that from 1968 to 2008, Blelham Tarn had experienced an earlier onset, later breakdown, and an increase of approximately 38 days in the duration of thermal stratification. These changes in stratification onset (Fig. 1.7) are comparable to those seen in other lakes. In Lake Washington (USA), for example, Winder and Schindler (2004) showed that during a 40-year period, the onset of thermal stratification had occurred 16 days earlier. Similarly, during a 17-year period in Heiligensee (Germany), Adrian et al. (1995) demonstrated that the onset of thermal stratification had occurred 3 weeks earlier. All of these observed changes have been attributed to climate change.

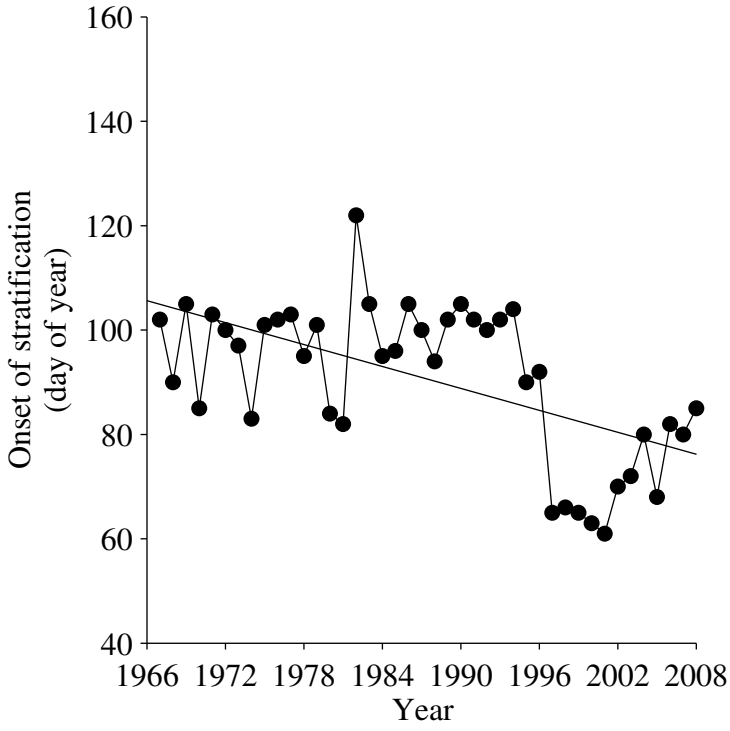

Figure 1.7: Time series in Blelham Tarn (UK) from 1968 to 2008 of annual onset of thermal stratification. Re-drawn from Foley et al. (2012).

The use of long-term data in understanding the impact of climate change has also been investigated in other lakes. In Lake Superior (USA, Canada), for example, Austin and Colman (2007) identified that climate change is having a stronger influence on lake surface water temperature than on regional air temperature. They showed that surface water temperature had increased by approximately 2.5 °C over the last four decades, which is significantly greater than the increase in regional air temperature. The difference in warming between the air and water surface is driven by a declining winter ice cover, resulting in an earlier onset of thermal stratification, and an increase in the period over which the lake warms. A reduction in the air-water temperature gradient was later shown by

Desai et al. (2009) to lead to a significant increase in surface wind speeds over the lake. Warmer summer water temperatures and longer stratified seasons have been shown to have a significant impact on lake ecology and productivity (e.g. Brooks and Zastrow, 2002; Hill and Magnuson, 1990; Lehman, 2002; Magnuson et al., 1997). In a recent study in Lake Tanganyika (East Africa), for example, O'Reilly et al. (2003) demonstrated that carbon isotope records in sediment cores suggest that primary productivity may have decreased by about 20 % due to climatic warming.

1.5 Short-term limnological monitoring

Long-term monitoring is sufficient to record decadal (e.g. Watras et al., 2014), seasonal (e.g. George, 2010) or inter-annual (e.g. Snucins and Gunn, 2000) change, but cannot resolve the processes driving many aspects of lake function. This is because physical, chemical, and biological lake properties can be completely altered by short-term, meteorologically-driven physical disturbances (e.g. Maberly, 1996; MacIntyre et al., 2009), such as strong wind events that can completely alter the vertical thermal structure. In a short-term study of Esthwaite Water (UK), for example, Frempong (1983) investigated the diel response of the thermal structure of the lake to prevailing meteorological conditions. The study was conducted over seven selected days that covered different phases of stratification. The magnitude of the diel changes in the thermal structure were shown to be controlled by the seasonal phase of stratification and the magnitude of incoming short-wave radiation. The thermal structure of the lake was also shown to

be strongly influenced by wind-induced turbulent mixing and vertical circulation induced by nocturnal cooling of the water surface through evaporative and conductive processes. In Esthwaite Water, advected energy due to lake inflow and outflow were negligible in Frempong's study. In other lakes, however, inflows can have a considerable influence on the lake, where short-term events such as flooding (e.g. De Cesare et al., 2006) in particular, can completely alter the dynamics of the system (e.g. Håkanson et al., 2000; Zohary and Ostrovsky, 2011).

In recent years, the challenge of understanding the complex dynamics in lakes has become somewhat easier as instrumented buoys capable of measuring an increasingly wide array of physical, chemical and biological parameters (Daly et al., 2011; Hart and Martinez, 2006; Porter et al., 2009) at high temporal resolution have been developed (e.g. Rouen et al., 2005). High-resolution data from instrumented buoys have been used to investigate fine-scale changes in microbial respiration in lakes (Solomon et al., 2013), the role of lake physics in ecosystem metabolism estimates (Rose et al., 2014), and the physical responses of lakes to variation in dissolved organic carbon concentrations (Read and Rose, 2013).

The value of monitoring is strengthened when it is combined with a broader, linked programme of research that includes modelling. Models are of great value in forecasting responses to future change and also help identify gaps in our understanding of how lakes function. Ecosystem functioning, however, is often predicted by numerical simulations (e.g. Arhonditsis and Brett, 2005*a*,*b*; Gal et al., 2009; Markensten et al., 2010; Trolle et al., 2011, 2008) that are calibrated to data from routine monitoring programs. Models calibrated exclusively using data from routine monitoring programs, however, may not provide adequate

insight into the causes and consequences of short-term phenomena (Harris and Griffiths, 1987) as even for the same state variable, different drivers may dominate variability at different timescales (Hanson et al., 2006). Kara et al. (2012), for example, investigated the timescale dependence in numerical simulations of physical, chemical, and biological parameters. By using a one-dimensional coupled hydrodynamic-biogeochemical model, they estimated model accuracy of predicting water surface temperature, dissolved oxygen, and phytoplankton biomass for Lake Mendota (USA) at temporal scales of hours to months. Physical and biological parameters were modelled accurately at the seasonal level, although short-term patterns, such as the diel cycle were not reproduced accurately by the model.

Recent improvements in numerical model capabilities have resulted in lake responses being simulated accurately at sub-daily timescales (e.g. Hipsey et al., 2012). Such models, however, require quality high-resolution input data, ideally measured *in situ* from high-frequency lake monitoring stations. Detailed high-frequency lake monitoring, however, is resource-demanding and currently restricted to a small proportion of the global population of lakes. In order to upscale the role of lakes in global cycles we must, therefore, explore the extent and causes of coherence among lakes.

1.6 Coherence and similarities among lakes

In limnology, temporal coherence is commonly defined as the degree to which different lakes behave similarly through time, and has been parameterised in

various ways. It has, for example, been calculated as the mean coefficient of determination calculated between all possible lake pairs (e.g. Magnuson et al., 1990), or as the mean coefficient of determination calculated between each lake and the mean time series of all other lakes (e.g. Livingstone and Dokulil, 2001). Understanding coherence is a valuable tool to extrapolate from measured to unmeasured lakes (Baines et al., 2000) and an important step in understanding the environmental factors that control the structure and functioning of the ecosystem.

The innovative work on coherence was that of Magnuson et al. (1990) who investigated the degree to which lakes within a relatively small geographic region behaved similarly through time. This investigation used data from the North Temperate Lakes Long Term Ecological Research (NTL-LTER) site in Northern Wisconsin (USA) for a 7-year period and involved the study of 37 limnological variables in 7 lakes. Two main questions were investigated during this analysis: (i) whether lakes similar in their exposure to the climate (estimated by the ratio of lake surface area/mean depth) were more temporally coherent than lakes which were dissimilar in their exposure to the climate, and (ii) whether temporal coherence in lakes progressively decreased from variables more directly influenced by the climate. The work of Magnuson et al. (1990) was carried further by Kratz et al. (1998) who extended the investigation period from 7 to 13 years and analysed 61 limnological variables. Of these variables, 9 described the physical attributes, 26 described the chemical characteristics, and the remaining 26 were biological. Similar to Magnuson et al. (1990), they demonstrated that lakes within the same geographic region respond coherently to drivers such as climate forcing and catchment processes. The most coherent variables, however,

are those with a direct, mechanistic link to climate forcing. Specifically, physical lake properties (e.g. surface water temperature) tend to vary in a more coherent way than the biological, or chemical properties.

The most comprehensive recent investigation of coherence was undertaken by Livingstone and Kernan (2009), who investigated the degree of coherence in lake surface water temperature for 25 lochs in the Grampians and Northwest Highlands of Scotland. Surface temperatures were measured from September 2000 through to December 2001 using mini thermistors with integrated data loggers. Regional coherence in surface temperature was strongest during late spring and summer when the epilimnion was thin and in autumn when surface temperature was determined by surface cooling. Regional coherence was shown to be lower in winter, presumably the result of the very low variability in surface water temperature that follows when surface temperature is near 0 °C and again in early spring when they warm up and stratify at different rates. Additional comparisons are described by Livingstone et al. (2010). They show, for example, that lake surface water temperature measurements in Finland and Estonia fluctuate extremely coherently during most of summer and early autumn. They also show that 29 lakes in Switzerland have a high degree of coherence in lake surface water temperature despite large differences in altitude, where the lakes studied range in altitude from 465 m to 2470 m above sea level.

A common theme is large-scale studies, such as those that investigate the similarities and differences among lakes, is the synthesis of several spatially disparate, often global, data sources that require collaborative efforts. Until recently, collaborative efforts at these spatial scales have been limited, mainly due to the physical separation of researchers.

1.7 Scientific monitoring networks

Environmental scientists are increasingly using networks to monitor ecosystems (Porter et al., 2005, 2009). Aquatic ecosystems, for example, have a number of networks for monitoring the environment (Table 1.2), including the National Ecological Observatory Network (NEON), the Coral Reefs Environmental Observatory Network (CREON) and the United Kingdom Lake Ecological Observatory Network (UKLEON).

Table 1.2: Examples of environmental monitoring networks.

Name	Description
National Ecological Observatory Network (NEON)	A network designed to gather and synthesise data on the impacts of climate change, land use change and invasive species on natural resources and biodiversity.
Global Ocean Observing System (GOOS)	A global system for sustained observations of the ocean.
Integrated Ocean Observing System (IOOS)	An organisation that provides quality controlled data and information on the oceans and Great Lakes.
Coral Reefs Environmental Observatory Network (CREON)	A grassroots association of scientists working to design and build sensor networks to view the marine environment.
United Kingdom Lake Ecological Observatory Network (UKLEON)	A national network of automatic lake monitoring stations that exploit state-of-the-art sensor technology and provide linked, concurrent, high temporal resolution data.
Global Observatory of Lake Responses to Environmental Change (GloboLakes)	A programme investigating the state of lakes and their response to climatic and other environmental drivers of change at a global scale through the use of a satellite-based observatory.
Networking lake observatories in Europe (NETLAKE)	A network of sites and individuals to support the development and deployment of sensor-based systems in lakes and reservoirs in Europe

Table 1.3: Summary of UKLEON lake characteristics ordered by lake area.

Name	Area (km^2)	Altitude (m)	Max. Depth (m)
Blelham Tarn	0.1	4.1	14.5
Round Loch of Glenhead	0.1	298	13.5
Llyn Conwy	0.4	455	19.0
Rostherne Mere	0.5	27	30.0
Esthwaite Water	1.0	65	15.5
Llyn Tegid	4.1	160	43.0
Bassenthwaite Lake	5.3	69	19.0
Windermere South Basin	6.7	39	42
Loch Leven	13.3	107	25.5
Loch Lomond	71.0	8	189.9
Lough Erne	110.0	46	63.0

In the United Kingdom, the primary observatory network that concentrates on lakes is the UKLEON. The primary technological objective of UKLEON is to establish the UK's first coordinated, high-resolution lake monitoring network, based on an information system that will receive, process, quality control and disseminate limnological data delivered by an integrated instrumented network of automatic lake monitoring stations. The network is composed of eleven sites that are located in England (5), Wales (2), Scotland (3), and Northern Ireland (1). The locations of the eleven UKLEON sites are shown in Fig. 1.8 and their characteristics are listed in Table 1.3.

Globally, the Global Lake Ecological Observatory Network (GLEON) is the primary organised network for limnology. GLEON is an international organisation of lake scientists with over 400 individual members from 40 countries. Its aim is to improve the understanding of lake function and management by devel-

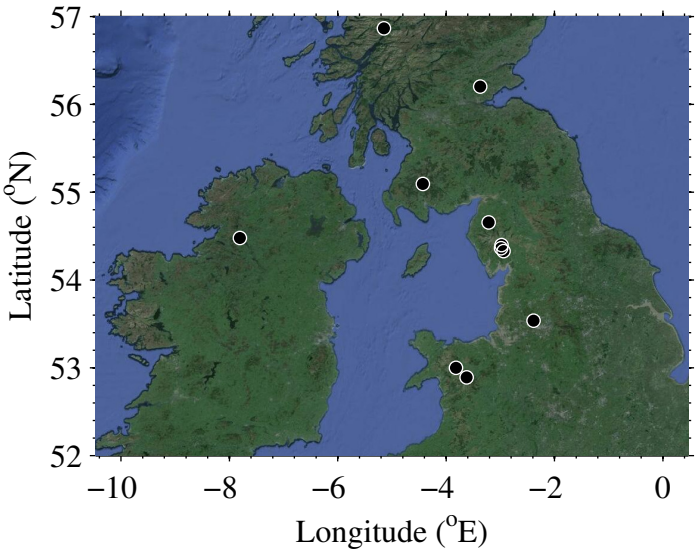

Figure 1.8: Location of lakes from the United Kingdom Lake Ecological Observatory Network (UKLEON).

oping a global, scalable, persistent network of lake ecology observatories which consist of instrumented platforms on lakes capable of sensing key limnological variables (Kratz et al., 2003).

The power of comparative research is well illustrated by the science conducted by GLEON, where the importance of lake context, such as the catchment (Klug et al., 2012), bathymetry (Read et al., 2012), and meteorology (Jennings et al., 2010) is demonstrated. However, science within GLEON focuses on many aspects of limnology, such as the response of lake structure and biology to extreme events (Jones et al., 2008), the role of wind and convection in lake physics (Read et al., 2012), the resistance and resilience of microbial communities (Shade et al., 2009), and detection of changes in ice phenology (Pierson et al., 2011). Pierson et al. (2011), for example, using GLEON data, introduced a method to estimate accurately the date of ice-on, ice-off, and the duration of ice

cover in lakes. They describe a method for detecting the presence of ice cover by recording water temperature at the lake surface and bottom. They suggest that the occurrence of ice rapidly leads to detectable levels of inverse stratification, a phenomenon which they define as occurring when the temperature at the lake surface is 0.1 °C cooler than that at the lake bottom. Similarly, the date of ice-off leads to the rapid return of isothermal conditions. Based on data from 10 lakes over a total of 43 winter seasons, they found that the timing and duration of inverse stratification monitored by recording temperatures compared well with ice cover statistics based on human observations. A Root Mean Square Error (RMSE) between the observed-based and temperature-based estimates was calculated as 7.1 days for ice-on, 6.4 days for ice-off, and 10.0 days for the duration of ice cover, leading to a relatively high degree of accuracy for detecting ice cover from *in situ* measurements, such as temperature sensors deployed at the lake.

Over the past few years, research within GLEON has focussed on developing numerical tools for analysing lake data (e.g. Read et al., 2011; Winslow et al., 2013). Read et al. (2011), for example, developed a complete open source program called 'Lake Analyzer' for calculating indices of stratification and mixing in lakes and reservoirs. These indices have been used in previous investigations around the world, to examine, for example, the effect of climate change on lake thermal structure (Hambright et al., 1994), describe potential upwelling events (e.g. MacIntyre et al., 2002; Shintani et al., 2010; Stevens and Lawrence, 1997) and processes relevant to the internal mixing of lakes (Imberger and Patterson, 1990), as well as estimating the vertical flux of oxygen (Robertson and Imberger, 1994) and ammonium (Romero et al., 1998) in lakes (Table 1.4). Addi-

tional analytical tools introduced by GLEON include the 'rLakeAnalyzer' package (Winslow et al., 2013), which is an R (R Core Team, 2013) translation of the MATLAB based lake physics toolset (Read et al., 2011), and the 'Lake Metabolizer' package (http://cran.r-project.org/web/packages/LakeMetabolizer/), which is a collection of lake metabolism functions that can be used to calculate the metabolic activity of individual organisms and whole ecosystems. These tools are useful to the limnological community as they not only process data from multiple lakes rapidly, but also provide a mean of calculating processes using the same method, thereby facilitating global comparisons.

Table 1.4: Indices calculated by Lake Analyzer including example references of where the metrics have been used.

Metric	Units	Description	Example publications
Lake Number	-	A dimensionless index describing the balance between the stabilising force of thermal stratification and the destabilising force supplied by wind.	Imberger and Patterson (1989); Robertson and Imberger (1994); Wain and Rehman (2010).
Epilimnion depth	m	The vertical portion of the water column which is directly influenced by the surface drivers of wind and convective cooling.	von Einem and Granéli (2010).
Metalimnion depth	m	The region within the water column that the thermocline occupies.	Garneau et al. (2013).
Hypolimnion depth	m	The region within the water column directly below the metalimnion.	Foley et al. (2012).
Thermocline depth	m	The depth of the maximum change in water density with respect to change in depth.	Hambright et al. (1994).
Buoyancy frequency	s^{-2}	The angular frequency at which a vertically displaced parcel will oscillate within a statically stable environment.	MacIntyre et al. (2002).
Schmidt stability	J m^{-2}	The resistance to mechanical mixing due to the potential energy inherent in the stratification of the water column.	Hutchinson and Edmondson (1957); Idso (1973); Kling (1988).
Wedderburn Number	-	Describes the likelihood of upwelling events under stratified conditions.	Shintani et al. (2010).

1.8 Research aims and objectives

The use of high-frequency data to examine coherence in lake surface water temperature has just begun (Livingstone et al., 2010; Livingstone and Kernan, 2009). As yet, though, coherence on diel timescales has not been investigated. A precursor to studying diel coherence is to understand the influence of lake morphometry on the diel range in surface water temperature. This is the overarching aim of this dissertation. However, this dissertation goes beyond the drivers of the diel range in lake surface water temperature to investigate the consequences and associations of the diel temperature range. The above aims are delivered through four specific objectives:

1. To establish an automated methodology for processing the driving atmospheric data that influence lake water temperature (i.e. the surface energy fluxes), and to develop a predictive method for estimating the diel range in surface water temperature.

2. To investigate the diel range in lake surface water temperature for a case study lake, and determine how it varies throughout the year. It is also hypothesised that the magnitude of the diel range in lake surface water temperature can be influenced by thermal stratification to the extent that important information about the vertical thermal structure of lakes may be gleaned from surface water temperature measurements alone; this is investigated in the context of this work.

3. To examine the diel range in lake surface water temperature among lakes, within the same geographic area, driven by essentially the same climate,

but characterised by different morphometric features.

4. To determine the extrinsic and intrinsic drivers of the diel range of lake surface water temperature for a global sample of lakes.

Chapter 2

Research design & methodology

2.1 Introduction

In this chapter, the methods followed to address the specific research aims and objectives described in Chapter 1 are discussed. The chapter begins by describing the study sites selected for this dissertation as well as the data collected from each site. A detailed description of the methods used to investigate the diel range in lake surface water temperature is then provided, including a detailed introduction into wavelet analysis and the methods followed to calculate the expected diel temperature range. This chapter also introduces a program called 'Lake Heat Flux Analyzer', which was developed during this PhD project to calculate the surface energy fluxes with lake buoy data. The statistical techniques used for investigating the relationship between lake specific characteristics and the diel temperature range are then described.

2.2 Study sites

The data used in this dissertation were collected from 100 lakes from around the world with a wide range of morphological and bathymetric features (Table 2.1). The lakes vary between 2468 m^2 and 1.63 $\times$ 10^8 m^2 in surface area, between 0.08 m^{-1} and 5.7 m^{-1} in the vertical attenuation coefficient for photosynthetically available radiation (K_d), between 0 m and 2464 m in altitude, and lie in latitudes between 38.768 °S and 59.846 °N (Fig. 2.1). Most sites are restricted to surface water temperature measurements, although some (24) also have meteorological and depth-resolved temperature measurements.

The data used to address the specific aims and objectives highlighted in Chapter 1 varied depending on the data requirements of the individual objective. Data from each lake were collected by several instruments, monitored and maintained by different organisations from different countries (Fig. 2.2) where lake specific information such as lake location, altitude and bathymetry were provided by the individual data providers. The lakes situated in the United Kingdom are maintained by the Centre for Ecology & Hydrology (CEH), the Environment Agency (EA), Natural Resources Wales (NRW), the United Kingdom Upland Waters Monitoring Network (UKUWMN), and the Scottish Environment Protection Agency (SEPA). Nine of the 42 UK lakes are part of the UKLEON. Data from the UKLEON lakes can be viewed at http://data.ecn.ac.uk/ukleon/.

Data from the Swiss lakes (as well as a number of Scottish lochs) were collected as part of the Swiss Sectretariat for Education and Science and the European Commission within the framework of the European Union Environment and Climate projects EMERGE (European mountain lake ecosystems: region-

alisation, diagnostic & socio-economic evaluation), CLIME (Climate and lake impacts in Europe), and Euro-limpacs. Data from lake Iseo is freely available (e.g. Pilotti et al., 2013) and can be found at http://www.ing.unibs.it/hydraulics/.

Lakes from the United States of America and New Zealand (as well as some from Europe) were provided from individual members of the GLEON. A list of GLEON lakes can be found at http://www.gleon.org/members/lakes. Data for Lake Washington, Lake Sammamish and Lake Union are available to download from the King County website (https://green.kingcounty.gov/lake-buoy/default.aspx).

Table 2.1: Study sites used in this dissertation including the water quality and meteorological parameters available for each lake and the duration of data available. Lakes without names are identified by the identification number employed by Livingstone and Kernan (2009)

Lake Name	Country	Data source	Latitude (°N)	Mean K_d (m^{-1})	Area (km^2)	Altitude (m)	Water temperature profile (°C)	Surface temperature (°C)	Wind speed ($m\ s^{-1}$)	Short-wave radiation ($W\ m^{-2}$)	Relative humidity (%)	Air temperature (°C)	Start date (mmm-YY)	End date (mmm-YY)
Acton	USA	GLEON	39.5702	1.62	2.53	263		✓					May-10	Sep-10
Bachalpsee	Switzerland	EMERGE	46.67	-	0.0803	2265		✓					Jun-00	Sep-00
Bänzlauiseeli, Unteres	Switzerland	EMERGE	46.6897	-	0.0207	2177		✓					Jun-00	Sep-00
Bassenthwaite	England	UKLEON	54.6537	0.55	5.3	69	✓	✓	✓	✓	✓	✓	Jan-09	Dec-12
Blelham Tarn	England	UKLEON	54.3961	0.64	0.1	41	✓	✓	✓	✓	✓	✓	Jan-08	Dec-11
Bolger	USA	GLEON	46.2305	5.1	0.010633	483		✓					Jun-13	Sep-13
Brotherswater	England	EA	54.5063	0.31	0.19	161		✓					Jan-11	Aug-11
Burgäschisee	Switzerland	EMERGE	47.1695	-	0.21	465		✓					Jun-00	Sep-00
Burgseeli	Switzerland	EMERGE	46.6975	-	0.0525	613		✓					Jun-00	Sep-00
Burnmoore Tarn	England	UKUWMN	54.4285	0.50	0.239	252		✓					Jan-13	Aug-13
Buttermere	England	EA	54.5312	0.16	0.93	100		✓					Feb-99	Dec-99
Castle	Denmark	GLEON	55.934	2.1	0.223046	28	✓	✓	✓	✓	✓	✓	Apr-06	Nov-06
Celyn	Wales	NRW	52.9493	-	3.236	299		✓					Jun-12	Sep-12
Clatto	Scotland	CEH	56.4991	0.65	0.094	153							Mar-09	Nov-09

Coniston	England	EA	54.3381	0.24	4.70	44		✓					Feb-11	Dec-11
Conwy	Wales	UKLEON	52.9993	0.54	0.4	454		✓					Jan-07	Oct-07
Crampton	USA	GLEON	46.2105	0.818	0.258925	512	✓	✓	✓	✓	✓	✓	Jun-05	Sep-05
Crystal Bog	USA	GLEON	46.0076	3.45	0.005524	503		✓					May-08	Oct-08
Crystal Lake	USA	GLEON	46.002	0.38	0.34	501	✓	✓	✓	✓	✓	✓	May-11	Sep-11
Cwm Mynach	Wales	UKUWMN	52.7947	0.28	0.057	285		✓					Jan-13	Aug-13
Dittligsee	Switzerland	EMERGE	46.7564	-	0.0602	652		✓					Jun-00	Sep-00
Egelmösli	Switzerland	EMERGE	46.945	-	0.0152	550		✓					Jun-00	Sep-00
Elterwater	England	EA	54.4272	0.69	0.17	53		✓					Mar-11	Aug-11
Ennerdale	England	EA	54.5222	0.29	3	113		✓					Feb-11	Aug-11
Erken	Sweden	GLEON	59.846	0.4	23.6742	11	✓	✓	✓	✓	✓	✓	Apr-08	Oct-08
Esthwaite Water	England	UKLEON	54.3583	0.56	1	65	✓	✓	✓	✓	✓	✓	Jan-05	Dec-09
Feeagh	Ireland	GLEON	53.943	0.96	3.327559	14		✓					Jan-10	Dec-10
Flemington	Scotland	CEH	57.5424	4.8	0.14	40		✓					Jan-10	Aug-10
Flueseeli	Switzerland	EMERGE	46.4096	-	0.0347	2045		✓					Jul-00	Sep-00
Gadenlauisee	Switzerland	EMERGE	46.7209	-	0.0082	2155		✓					Jul-00	Oct-00
Gantrischseeli	Switzerland	EMERGE	46.7118	-	0.0141	1578		✓					Jun-00	Sep-00
Gorm Lochan	Scotland	EMERGE	57.1719	-	0.0164	870		✓					Jan-01	Oct-01
Grane Langsø	Denmark	GLEON	56.0181	0.18	0.11	82		✓					May-12	Nov-12
Grasmere	England	EA	54.4484	0.39	0.64	62		✓					Jan-07	Dec-07
Hagelseeli	Switzerland	EMERGE	46.6893	-	0.0064	2410		✓					Jun-00	Sep-00
Hagelseewli	Switzerland	EMERGE	46.673	-	0.0249	2339		✓					Jun-00	Sep-00
Harp	Canada	GLEON	45.3796	0.64	1.513724	327		✓					Jan-13	Oct-13
Häxeseeli	Switzerland	EMERGE	46.6803	-	0.0243	2464		✓					Jun-00	Sep-00
Hinterburgseeli	Switzerland	EMERGE	46.718	-	0.045	1514		✓					Jun-00	Sep-00

Hummingbird	USA	GLEON	46.2437	5.7	0.007862	516		✓					Jun-13	Sep-13
Iseo	Italy	WRR	45.724	0.49	60.9	185	✓	✓	✓	✓	✓	✓	Jan-12	Jul-12
Jekl Bog	USA	GLEON	45.9945	1.9	0.002468	499		✓					May-11	Jun-11
Kinneret	Israel	GLEON	32.817	0.5	163.268	0	✓	✓	✓	✓	✓	✓	Jan-05	Dec-05
Lawrence	USA	GLEON	42.4409	0.53	0.051	274	✓	✓	✓	✓	✓	✓	Apr-09	Oct-09
Llyn Llagi	Wales	UKUWMN	53.0145	0.34	0.051	380		✓					Jan-13	Jul-13
Llyn Padarn	Wales	NRW	53.128	0.48	0.97	316		✓					Jun-12	Nov-12
Loch a' Mhadaidh	Scotland	EMERGE	57.7126	0.25	0.311	570		✓					Jan-01	Oct-01
Loch an Fhuar-thuill Mhoir	Scotland	EMERGE	57.4524	0.36	0.0536	770		✓					Jan-01	Oct-01
Loch Bhuic Moir	Scotland	EMERGE	57.2785	0.6	0.0355	540		✓					Jan-01	Sep-01
Loch Chon	Scotland	UKUWMN	56.213	0.55	1.057	96		✓					Jan-13	Sep-13
Loch Coire Fionnaraich	Scotland	UKUWMN	57.4921	0.55	0.093	236		✓					Jan-13	Aug-13
Loch Coire Mhic Fherchair	Scotland	EMERGE	57.5912	0.13	0.1005	600		✓					Jan-01	Sep-01
Loch Gorm	Scotland	EMERGE	57.6813	0.25	0.2161	540		✓					Jan-01	Oct-01
Loch Grannoch	Scotland	UKUWMN	55.0021	0.8	1.114	214		✓					Jan-13	Sep-13
Loch Lomond	Scotland	UKLEON	56.105	0.53	71	7.6		✓					Apr-08	Dec-08
Loch Nagar	Scotland	UKUWMN	56.959	0.19	0.099	788		✓					Jan-13	Sep-13
Loch nan Eun	Scotland	EMERGE	56.885	0.85	0.1446	790		✓					Jan-01	Oct-01
Loch Tinker	Scotland	UKUWMN	56.2273	0.44	1.1×10^{-1}	418		✓					Jan-13	Sep-13
Loch Toll Lochan	Scotland	EMERGE	57.4955	0.72	0.0755	520		✓					Jan-01	Oct-01
Lochan a' Chnapaich	Scotland	EMERGE	57.8098	0.39	0.056	690		✓					Jan-01	Oct-01
Loweswater	England	CEH	54.5825	0.5	0.6	125	✓	✓	✓	✓	✓	✓	Jan-09	Dec-09
Meienfallseeli	Switzerland	EMERGE	46.5869	-	0.0152	1900		✓					Jun-00	Oct-00
Mendota	USA	GLEON	43.105	0.82	38.2824	259	✓	✓	✓	✓	✓	✓	Apr-09	Nov-09
Moossee	Switzerland	EMERGE	47.0221	-	0.3035	521		✓					Jun-00	Oct-00

Morris	USA	GLEON	46.2575	2.63	0.058819	506		✓					May-13	Aug-13
Mouser Bog	USA	GLEON	45.998	2.44	0.037833	494	✓	✓	✓	✓	✓	✓	May-11	Aug-11
Ngaroto	New Zealand	GLEON	-37.954	3.6	1.08	33		✓					Jan-12	Dec-12
North Sparkling Bog	USA	GLEON	46.005	2.54	4.6×10^{-3}	497							May-09	Dec-09
Oberstockensee	Switzerland	EMERGE	46.6872	-	0.1181	1665		✓					Jun-00	Sep-00
Priest Pot	England	CEH	54.3721	1.44	0.01	66		✓					Jun-02	Sep-02
Rostherne Mere	England	UKLEON	53.354	0.85	0.5	27		✓					Jan-11	Dec-11
Rotoiti	New Zealand	GLEON	-38.037	0.54	34.6	279	✓	✓	✓	✓	✓	✓	Feb-08	Sep-08
Rotorua	New Zealand	GLEON	-38.082	0.63	79.8555	280	✓	✓	✓	✓	✓	✓	Jan-08	Dec-09
Round Loch of Glenhead	Scotland	UKLEON	55.0933	0.39	0.127	298		✓					Jan-13	Jul-13
Sägistalsee	Switzerland	EMERGE	46.6796	-	0.0725	1935		✓					Jun-00	Sep-00
Sammamish	USA	KG	47.6	0.34	19.8	9		✓					May-06	Dec-06
SC0084	Scotland	EMERGE	57.5168	0.16	0.0964	670		✓					Jan-01	Oct-01
Schwarzsee	Switzerland	EMERGE	46.6657	-	0.4554	1046		✓					Jun-00	Sep-00
Scoat Tarn	England	UKUWMN	54.4812	0.17	0.043	602		✓					Jan-13	Jul-13
Seebergsee	Switzerland	EMERGE	46.5774	-	0.0576	1831		✓					Jun-00	Sep-00
Seebodensee	Switzerland	EMERGE	46.7235	-	0.0073	2042		✓					Jun-00	Sep-00
South Trout	USA	GLEON	46.029	0.39	14.9184	495	✓	✓	✓	✓	✓	✓	Jun-05	Nov-05
Sparkling Lake	USA	GLEON	46.008	0.39	0.618453	497	✓	✓	✓	✓	✓	✓	May-11	Oct-11
St. Gribsø	Denmark	GLEON	55.985	2.3	0.100285	50	✓	✓	✓	✓	✓	✓	Apr-06	Nov-06
Strathclyde	Scotland	SEPA	55.793	-	0.82	18		✓					Jun-13	Sep-13
Sulsseewli	Switzerland	EMERGE	46.6175	-	0.0201	1920		✓					Jun-00	Sep-00
Sulsseewli, Oberes	Switzerland	EMERGE	46.6121	-	0.0072	2191		✓					Jun-00	Sep-00
Sunapee	USA	GLEON	43.391	0.39	16.2489	333	✓	✓	✓	✓	✓	✓	May-08	Oct-08
Tarawera	New Zealand	GLEON	-38.198	0.08	41	298		✓					Jan-12	Dec-12

Tegid	Wales	UKLEON	52.8885	0.58	4.1	164	✓	✓	✓	✓	✓	✓	Jan-09	Dec-11
Triebtenseewli	Switzerland	EMERGE	46.5527	-	0.0966	2365		✓					Jun-00	Oct-00
Trout Bog	USA	GLEON	46.041	2.89	0.010478	495	✓	✓	✓	✓	✓	✓	May-04	Nov-04
Ullswater	England	EA	54.5761	0.32	8.9	145		✓					Jan-11	Dec-11
Union	USA	KG	47.639	0.33	2.35	5		✓					Apr-06	Dec-06
Waikaremoana	New Zealand	GLEON	-38.768	0.13	54	600	✓	✓	✓	✓	✓	✓	May-09	Oct-09
Washington	USA	KG	47.618	0.2	88	0		✓					Feb-06	Dec-06
West Long	USA	GLEON	46.2356	1.578	0.048658	513		✓					Jun-13	Sep-13
Windermere	England	UKLEON	54.35	0.45	6.70	39	✓	✓	✓	✓	✓	✓	Jan-07	Dec-12
Wingra	USA	GLEON	43.0537	3.2	1.30	257		✓					Jul-04	Sep-04
Wintergreen	USA	GLEON	42.398	1.3	0.164	275	✓	✓	✓	✓	✓	✓	Jul-09	Oct-09

CEH Centre for Ecology & Hydrology; EA Environment Agency; EMERGE European Mountain lake Ecosystems: Regionalisation, diagnostic & socio-economic Evaluation; GLEON Global Lake Ecological Observatory Network; KG King Cross major lakes monitoring; NRW Natural Resources Wales; SEPA Scottish Environment Protection Agency; UKLEON United Kingdom Lake Ecological Observatory Network; UKUWMN United Kingdom Upland Waters Monitoring Network; WRR (Pilotti et al., 2013).

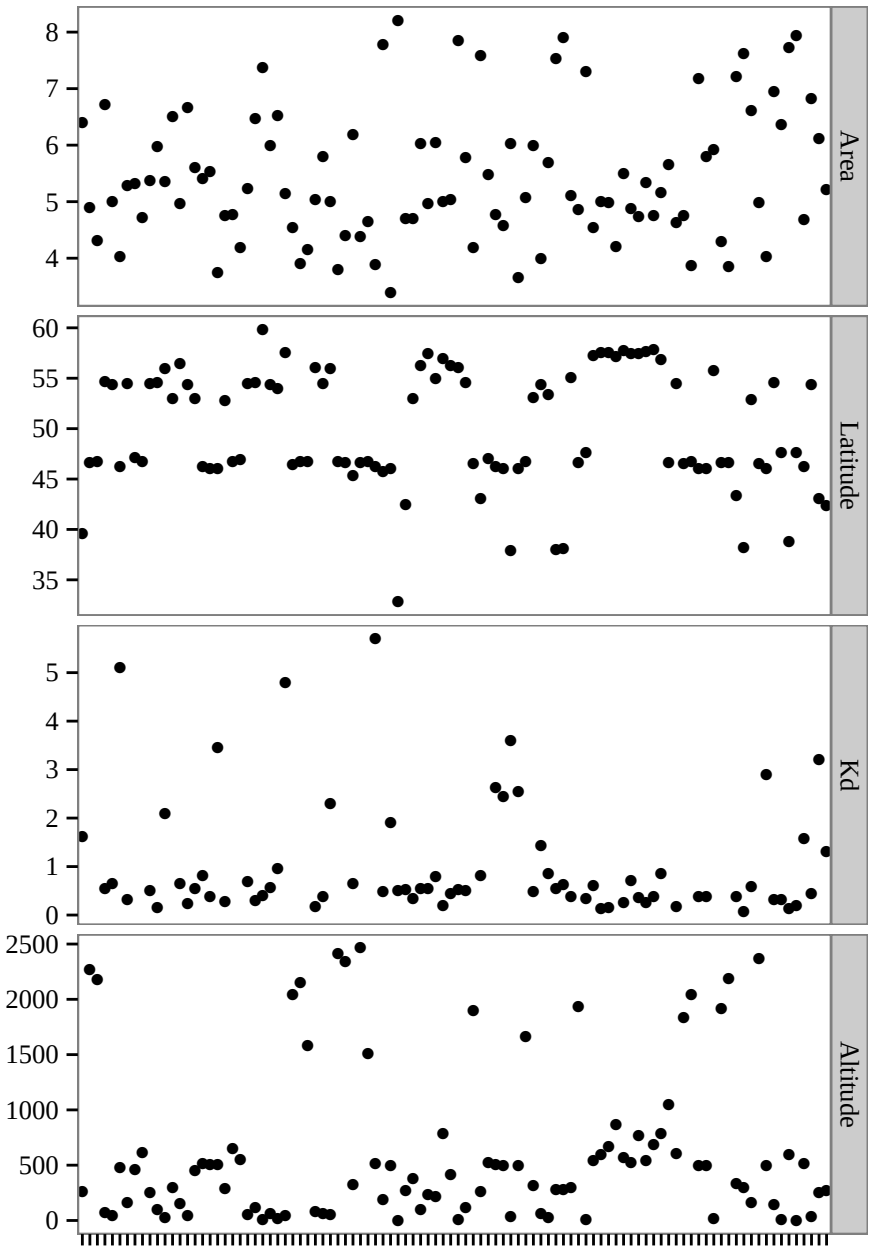

Figure 2.1: The general characteristics of the lakes included in this dissertation. Area is shown in base 10 logarithm (m^2); Latitude is shown as absolute latitude (°); K_d has units of m^{-1}; and altitude has units of metres.

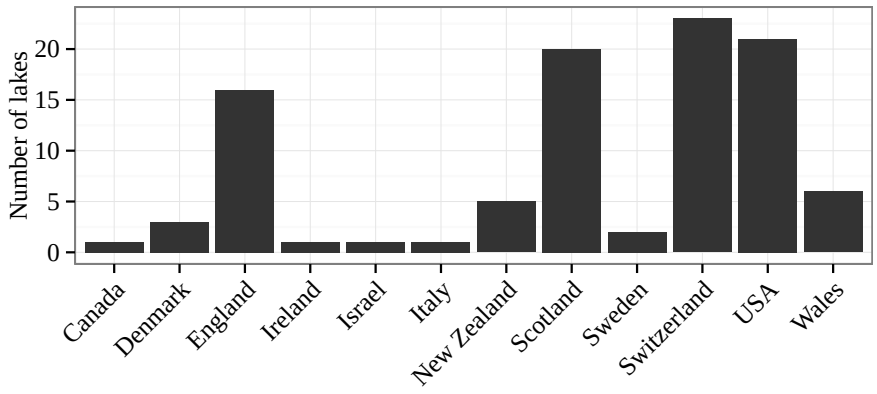

Figure 2.2: Individual countries from which the data used in this dissertation originated.

2.3 Surface water temperature measurements

Surface water temperatures were measured on each site by different instruments. All of the surface water temperature measurements were recorded by instruments with a typical temperature range of -5 °C to +40 °C and relative accuracies to within 1 °C. Although the uncertainty in water temperature measurements can vary from those suggested by the manufacturers, for example due to biofouling in the lake, in this dissertation it is assumed that these errors will be minimal. Specifically, as the comparisons made in this dissertation are on relatively long time-scales (e.g. annually), it is assumed that the uncertainties associated with these measurements will be small. Surface water temperatures were recorded at high temporal resolution (usually between 1 and 15-minute intervals). For all of the lakes included in this dissertation, surface water temperature measurements (actually, near-surface) were recorded at a depth of 1 m below the water surface.

2.4 Meteorological and depth-resolved temperature measurements

Depth-resolved water temperature and meteorological measurements were recorded by monitoring buoys located on each lake (24 lakes in total). The exact variables measured vary among the lakes, but a fully functional monitoring station includes measurements of wind speed and direction, short-wave radiation, relative humidity and temperature profiles with depth (Fig. 2.3). The example provided here is a monitoring station deployed on the UKLEON sites, known as an Automatic Water Quality Monitoring Station (AWQMS). For the UKLEON lakes, temperature sensors were assembled specifically for each lake with the number of sensors and depth intervals chosen according to the depth of the water column and the mixing characteristics of the lake. For specific information on the monitoring stations deployed on each lake, please refer to the appropriate data source.

2.5 Diel surface water temperature range

The magnitude of the diel surface water temperature range in each lake was evaluated by two methods: (1) by calculating the absolute difference between the maximum and minimum daily lake surface water temperature, and (2) by calculating the magnitude of the diel cycle in lake surface water temperature using wavelet analysis. Wavelet analysis was used as it can resolve the entire diel cycle, unlike the observed range which only uses two points within any 24 hour period. The wavelet analysis method was only used on a small subset (7) of

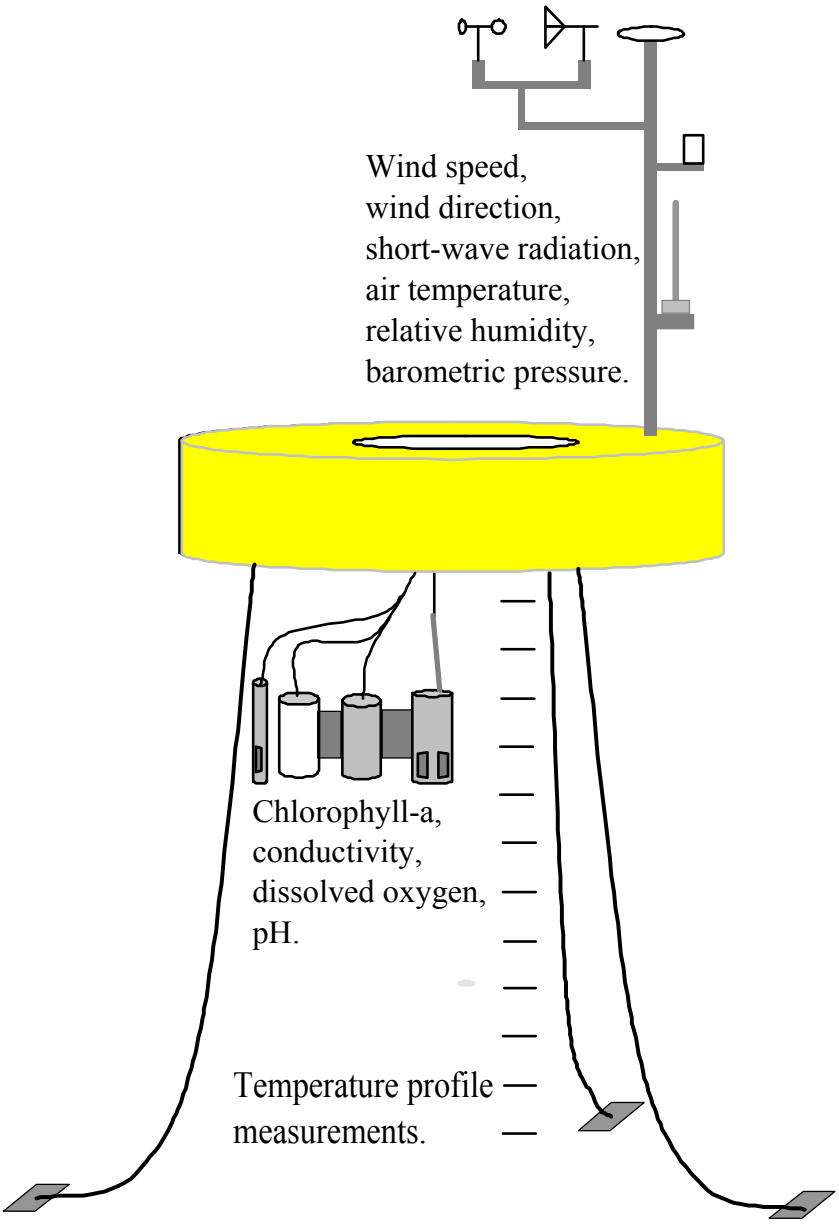

Figure 2.3: Example of a water quality monitoring station.

the lakes, however. These two methods are discussed in the following sections.

2.5.1 Observed diel surface water temperature range

The observed diel surface water temperature range was calculated as the absolute difference between the maximum and minimum lake surface water temperature for a given day (Fig. 2.4). In order to ensure consistency between each day, however, the observed diel range was only considered if at least 80% of the data were available for each 24 hour period. For hourly data, for example, 20 measurements were needed before the diel surface water temperature range was used. In addition, for a specific month to be considered in annual comparisons, 50 % of that month needed to have sufficient data (i.e. at least two weeks of 24 hour data for a given month).

2.5.2 Magnitude of the diel range in lake surface water temperature from wavelet analysis

The magnitude of the diel range in lake surface water temperature was evaluated by wavelet analysis. The main focus of this section is to describe the wavelet transform and the concept of analysing data in the frequency domain. This section begins by describing Fourier transforms, which is an alternative representation of a time series in terms of its frequency components. The Fourier transform has various forms, such as the Fourier series used for the representation of periodic signals, the discrete Fourier transform used for the representation of time signals, and the short-time Fourier transform, which is essentially a time-frequency representation, detailing how the frequency components of a signal

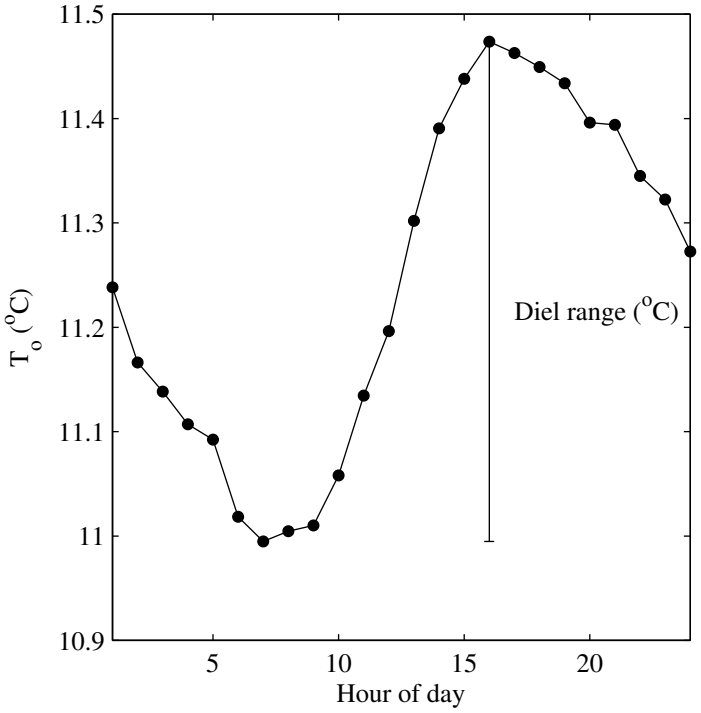

Figure 2.4: Example calculation of the diel surface water temperature range for Esthwaite Water (UK) in 2009.

changes with time. There are also different wavelet transforms, the wavelet series, the discrete wavelet transform, and the continuous wavelet transform. As the continuous wavelet transform was the only wavelet transform used in this dissertation, the description of wavelet analysis is limited to this method. Only a brief description of wavelet transform analysis is provided here, and for a more detailed view of wavelet analysis the reader is referred to Percival and Walden (2006) or Torrence and Compo (1998) where a practical guide to wavelet analysis is provided.

2.5.3 Fourier Transforms

The Fourier transform is one of the most widely applied signal processing tools in the environmental sciences. It reveals the frequency composition of a time series by transforming it from the time domain into the frequency domain. The Fourier transform makes use of the Fourier series, which represents a function as an infinite sum of sinusoids and it decomposes a signal into different frequencies. The main disadvantage of using Fourier transforms for analysing non-stationary data, however, is that the computation is performed over all times, thus making no distinction between stationary and transient parts of a signal. To illustrate these limitations, a synthetic time series composed of a sine wave of a known frequency and amplitude is generated and analysed using the Fourier transform. The time series with periodic components were composed as:

$$\begin{aligned} x(t) &= \sin(2\pi 5t) && \text{when } 0 \leq t \leq 2, \\ x(t) &= \sin(2\pi 10t) && \text{when } 2 \leq t \leq 4. \end{aligned} \tag{2.1}$$

The synthetic time series represents a signal where its periodicity varies in time (t). The first half of the signal has a frequency of five cycles per second and the second half has a frequency of ten cycles per second. The Fourier transform captures the information about the different frequencies that make up the signal, as identified by the peaks in the spectrum but fails to capture any information regarding the time of frequency change (Fig. 2.5).

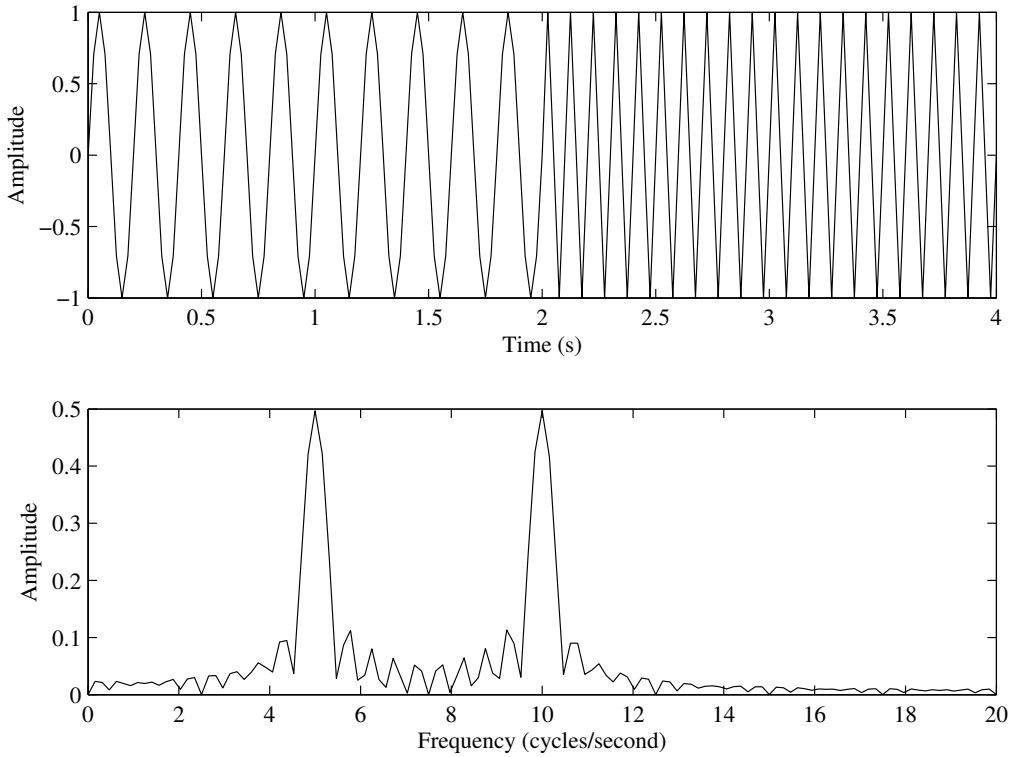

Figure 2.5: Synthetic time series (upper panel) and the corresponding Fourier transform (lower panel).

2.5.4 Short-time Fourier transforms

A straightforward solution to overcome the limitations of the Fourier transform is to introduce an analysis window of certain length that moves along the signal through time to perform a 'time-localised' Fourier transform, this method is known as the short-time Fourier transform (Gabor, 1946). The short-time Fourier transform corrects the deficiency of Fourier transforms for non-stationary data by analysing a small section of a signal at a given time. This adaptation can then be used to map a signal into a two-dimensional function of time and frequency. To compute the short-time Fourier transform the original signal is multiplied by

a window function, and then the Fourier transform is computed in each window. By repeating this procedure for the duration of the signal, the Fourier transform of the entire series can be calculated, resulting in a two-dimensional representation of the signal (Fig. 2.6). The size of the window chosen is related to the time and frequency resolution of the short-time Fourier transform, where the shorter the window, the higher the time resolution. This is usually accompanied by a poor frequency resolution. For a long window, however, the frequency resolution is high, but the time resolution is low. A feature of this transform is that the window is of constant length throughout the analysis, meaning that the transform has a fixed-resolution in both time and frequency. The inherent drawback of this method arises when high and low-frequency components of the series do not lie within the frequency range of the window (Kaiser, 2011). A window of certain size, for example, will sample more oscillations at short wavelengths compared to long wavelengths. Thus, the robustness of the method is dependent on the frequency of the series. Similar to the Fourier transform, the use and limitation of the short-time Fourier transform is demonstrated by applying equation 2.1 to the analysis. The short-time Fourier transform can clearly capture the periodicity of the synthetic time series, but the issue of time resolution is evident (Fig. 2.6).

2.5.5 Continuous wavelet transform

Wavelet transform represents the next logical step in analysing the frequency components of a signal. That is a windowing technique with variable-sized regions. Wavelet analysis allows the use of long time intervals where precise low-

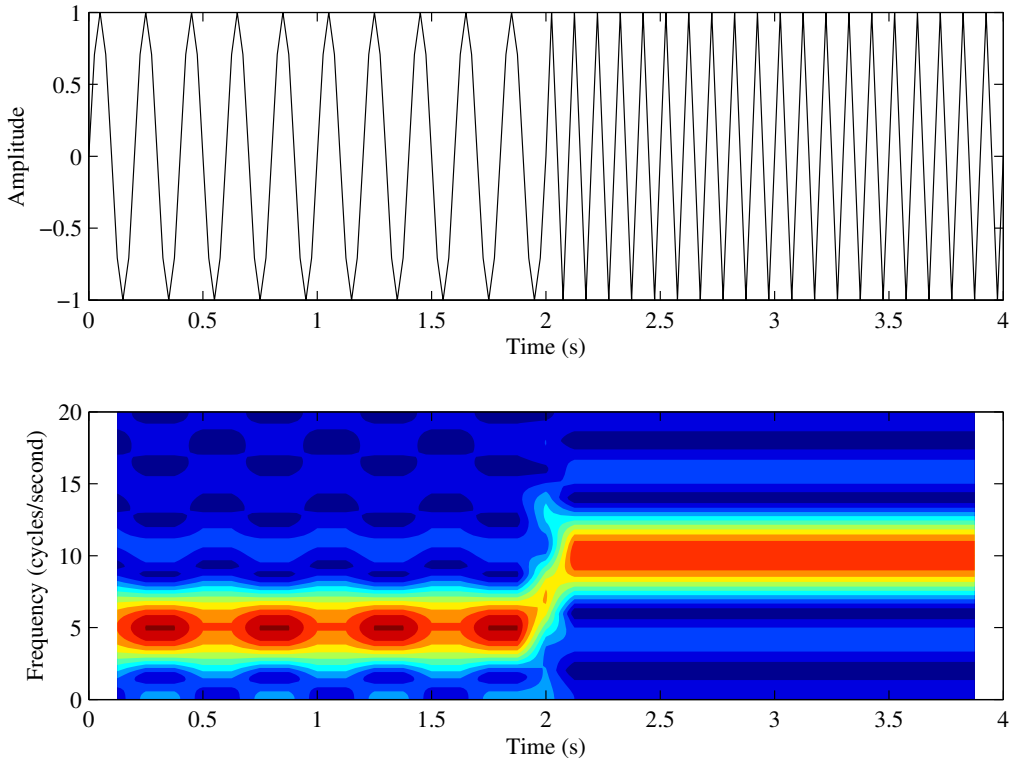

Figure 2.6: Synthetic time series (upper panel) and the corresponding short-time Fourier transform (lower panel).

frequency information is required, and shorter regions where high-frequency information is required. This makes wavelet analysis suitable for signals that have both low-frequency/high-duration components and high-frequency/short-duration components, which is the case for some environmental time series. Another important distinction from the short-time Fourier transform is that wavelet analysis is not limited to using sinusoidal analysing functions. Rather, a large selection of localised waveforms, known as wavelet functions, can be used. For that reason, among others, wavelet analysis has become increasingly popular in a range of disciplines in science, particularly in atmospheric and oceanic sciences

(e.g. Thiebaut and Vennel, 2010), and more recently in ecological time series (e.g. Winder and Cloern, 2010).

A number of different wavelet functions are available for use when applying the continuous wavelet transform. When choosing an appropriate wavelet function it is important to consider the strengths and weaknesses of the different types, where the choice of function depends on the desired analysis, the nature of the time series, and the features present in the data (Torrence and Compo, 1998). The analysis described in this dissertation involved capturing the oscillatory behaviour of a time series of unknown frequencies. As it is expected that the wavelet spectra at adjacent times will be highly correlated we choose one of the common non-orthogonal wavelet functions, the Morlet wavelet (e.g. Grinsted et al., 2004). An issue with wavelet analysis is the loss in statistical power at the start and end of the time series. Regions where edge effects become important, as shown by the cone of influence, were excluded from the analyses in this dissertation. Further information on the cone of influence and its calculation can be found in Torrence and Compo (1998).

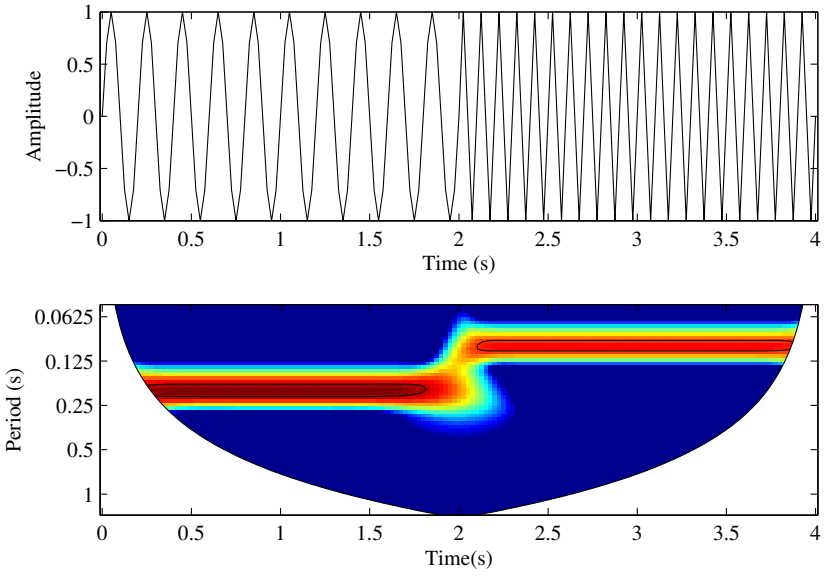

Figure 2.7: Synthetic time series (upper panel) and the continuous wavelet transform (lower panel). Solid black lines in the wavelet spectra represent the features that are statistically significant ($p < 0.05$). The continuous wavelet spectra is shown in base 2 logarithm, and illustrate how the strength of the periodicities changes with time. The wavelet coefficients that were within the cone of influence (i.e. white spaces near the start and end of the time series) are removed.

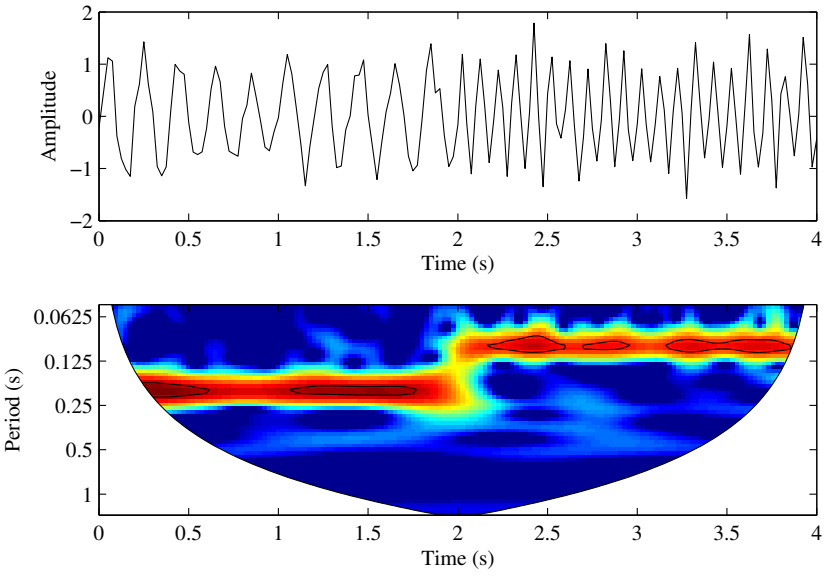

Figure 2.8: Same as Fig. 2.7 but with a Gaussian noise added to the synthetic time series.

The continuous wavelet transform clearly captures the periodicity of the synthetic time series (Fig. 2.7). The continuous wavelet transform also provides information on the significance of the features in the spectra. This is achieved by comparing the wavelet coefficients with a background spectra, where the nature of the background spectra depends on the nature of the data. For environmental time series, for example, a red-noise background is often used. A red-noise background noise has increasing variance with increasing scale, or decreasing frequency, and is characteristic of an environmental data series (e.g. Grinsted et al., 2004). Once the appropriate background spectra is chosen, the spectrum is then compared to the expected spectrum at a pre-determined confidence interval (e.g. $p < 0.05$). If the wavelet power of the time series exceeds the power of the background spectra, the time series variance can be considered as a significant feature of the spectra. If the wavelet power of the time series does not exceed the power of the background spectra the time series variance will not be considered as a significant feature of the spectra. As an example, a Gaussian noise is added to equation 2.1 and the wavelet spectra is once again computed. The computed spectra demonstrates that some features are no longer significant (Fig. 2.8).

Since the wavelet spectrum presents a large amount of information, it is often desirable to condense this information by averaging the results over a range of times or periods. One useful technique is to average the variance over time and then compare the spectral power at different periods. This is referred to as the global wavelet transform (GWT) and results in a graph of variance versus period, where similar to the Fourier transform, time information is lost (Percival and Walden, 2006). The GWT is very useful in determining the relative differences in the dominant frequencies of the spectra. During this dissertation

the GWT was used to compare the diel cycle in lake surface water temperature among different lakes.

2.5.6 Detecting the onset of thermal stratification from the diel surface water temperature range

A lake is generally considered to be stratified when the temperature difference between the surface and the bottom is greater than 1 °C (e.g. Stefan et al., 1996). The onset of thermal stratification can thus be defined as the time when the temperature difference between the surface and bottom of the lake first exceeds 1 °C. During this dissertation, two methods are proposed for detecting the onset of thermal stratification from high temporal resolution (15-minute) surface water temperature measurements. The accuracy of using the diel range as an estimate of the onset of thermal stratification is investigated by applying two methods based on the calculation of (1) the absolute difference in the diel surface temperature range, and (2) the magnitude of the diel range from wavelet analysis.

From the observed diel surface water temperature range, the onset of thermal stratification was estimated as the time where the diel range first exceeds 1 °C. The onset of stratification from wavelet analysis was estimated to be the time when the power of the wavelet signal became significant, that is, when it first exceeded 1. This denotes the time that the wavelet coefficients become a significant feature of the power spectra when compared to background noise. In order to avoid the detection of transient stratification events, in all cases the onset of stratification is defined as the time when the criterion mentioned was maintained for a period of at least 48 hours, which was mainly chosen to remove the influ-

ence of diurnal stratification events. To illustrate the use of wavelet analysis for this purpose, a synthetic time series with known period (P = 12) and amplitude (A = 5) was generated (Fig. 2.9a). A Gaussian noise was then added to the signal (Fig. 2.9b) and the wavelet coefficients were computed (Fig. 2.9c). The signal is only shown as being a significant feature of the spectra when it is significantly different from the background noise. It is, therefore, proposed that the timing of the onset of thermal stratification can be detected by measuring changing surface water temperature over time.

2.6 Theoretical diel surface water temperature range

One of the main objectives of this dissertation is to determine the drivers of the diel range in lake surface water temperature and to understand the role of lake specific features in influencing the diel cycle. To have a better understanding of the drivers of the diel temperature range, a theoretical approximation is provided. The diel surface water temperature range is driven by the amount of heating/cooling taking place over a diel cycle and may be estimated by calculating the change in heat content over a diel period. The heat content (C), for a fully mixed layer, may be calculated as:

$$C = \rho_0 \times C_{pw} \times V \times T_0, \tag{2.2}$$

where $\rho_0 = 10^3 \times \left(1 - 1.9549 \times 10^{-5} \left|T_0 - 3.84\right|^{1.68}\right)$ is the density (kg m^{-3}) of the water surface (Henderson-Sellers, 1986), C_{pw} is the specific heat of water at

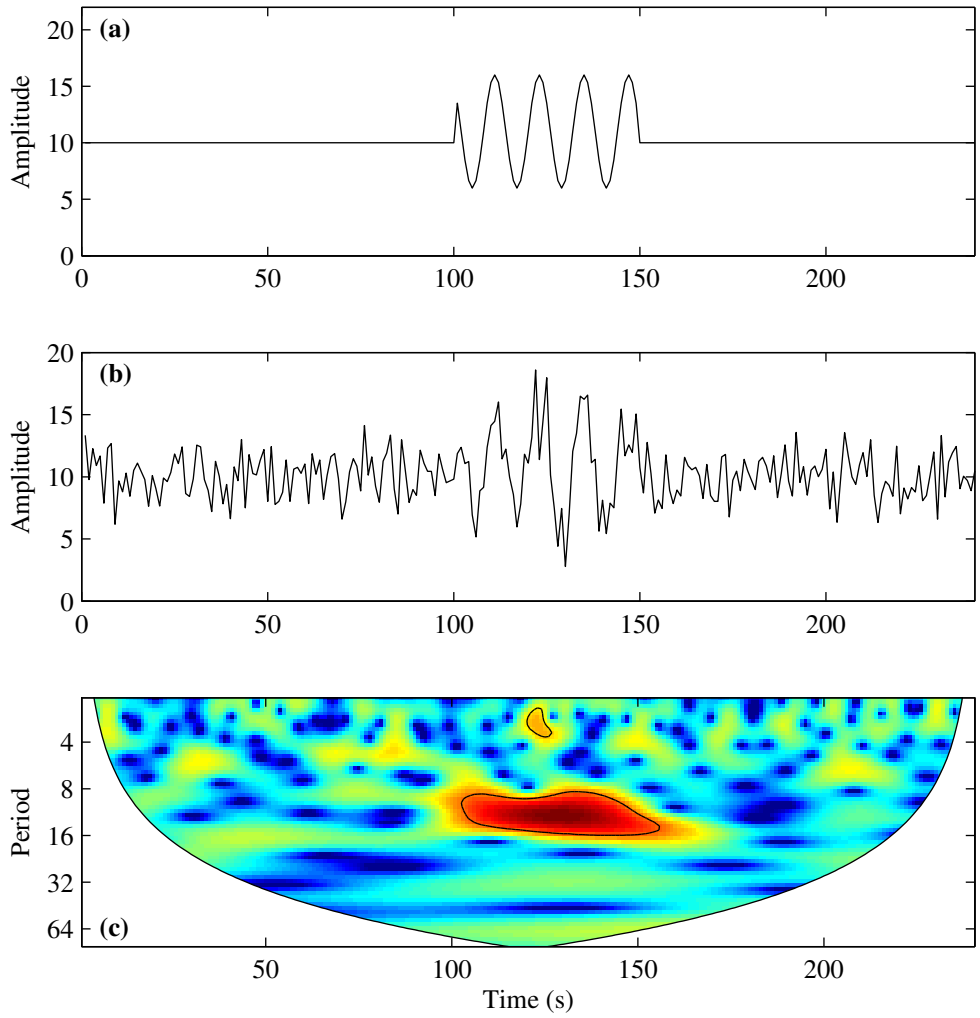

Figure 2.9: (a) Synthetic time series with amplitude of 5 and a period of 12, (b) the time series with a Gaussian noise, and (c) wavelet spectra of the synthetic time series with a Gaussian noise.

constant pressure (4186 J kg^{-1} °C^{-1}), V is the volume of water (m^3) within the upper mixed layer (z_{mix}) and T_0 is the lake surface water temperature (°C). Equation 2.2 can be used to determine the expected change in surface temperature over a given time period as:

$$\rho_0 C_{pw} V T_{02} = \rho_0 C_{pw} V T_{01} + \Delta t Q_{zmix} A_0, \tag{2.3}$$

$$\rho_0 C_{pw} V T_{02} - \rho_0 C_{pw} V T_{01} = \Delta t Q_{zmix} A_0,$$

$$\rho_0 C_{pw} V \left(T_{02} - T_{01}\right) = \Delta t Q_{zmix} A_0,$$

$$T_{02} - T_{01} = \frac{\Delta t Q_{zmix} A_0}{\rho_0 C_{pw} V},$$

$$\therefore \Delta T_0 = \frac{\Delta t Q_{zmix} A_0}{\rho_0 C_{pw} V},$$

where Δt is the heating period for a given day (taken to be 12 h, or 43200 s), A_0 is lake surface area (m^2), and Q_{zmix} is the amount of surface heating which influences the upper mixed layer (J m^{-2} s^{-1} or W m^{-2}), which can be estimated as:

$$Q_{zmix} = Q_{tot} - \left[R_0 \exp^{(-K_d z_{mix})}\right], \tag{2.4}$$

where Q_{tot} is the sum of surface fluxes (W m^{-2}), $R_0 \exp^{(-K_d z_{mix})}$ expresses the amount of energy that reaches the base of the upper mixed layer according to Beer's law, where R_0 is the visible component of short-wave radiation (W m^{-2}), K_d is the vertical attenuation coefficient for photosynthetically available radiation (m^{-1}), and z_{mix} was defined as the first depth where the temperature difference was > 0.2 °C relative to the surface temperature located at 1 m (e.g. Thompson, 1976).

2.7 Calculating the volume of water within the upper mixed layer

To calculate the volume of water within the upper mixed layer, previous information on lake bathymetry is required. Bathymetric maps or depth-sounder data, for example, can be used to provide information on the area at each depth between the lake surface and the maximum lake depth, and thus, can be used to estimate the volume of water within the upper mixed layer. Bathymetric data for Blelham Tarn, Bassenthwaite Lake, Loweswater, and Windermere were taken from bathymetric maps presented by Ramsbottom (1976) and for Esthwaite Water from depth-sounder data presented by Mackay et al. (2012). For locations where neither of these datasets exist, lake volume can be estimated by assuming that a lake has a conical shape constrained by surface area and maximum depth. By assuming a conically shaped lake (Fig. 2.10), the amount of water within the entire lake may be estimated as:

$$V = \frac{1}{3}\pi R^2 \left(z_2 + z_1\right), \tag{2.5}$$

where R is the radius of the lake surface, z_1 is the depth of the upper mixed layer, and z_2 is the difference between the maximum lake depth and the depth of the upper mixed layer. The volume of water beneath the upper mixed layer may be estimated as:

$$V = \frac{1}{3}\pi r^2 z_2, \tag{2.6}$$

where r is the radius of the lake at the base of the upper mixed layer. The volume of water within the upper mixed layer can, therefore, be estimated as the differ-

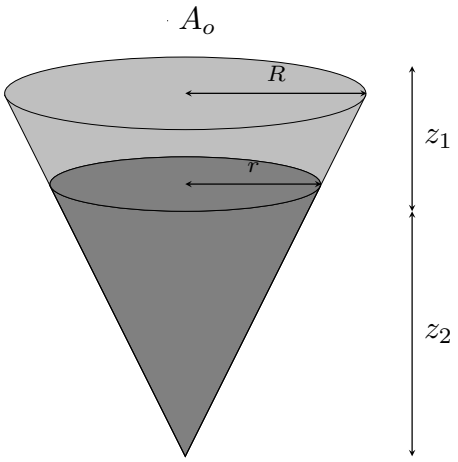

Figure 2.10: Schematic of a conically shaped lake with the surface mixed layer shown by the light grey region.

ence between the volume of the entire lake by the volume in the lower portion of the lake (Fig. 2.10). This is known as the volume of the frustum of a cone and can be simplified as:

$$V = \frac{\pi}{3}\left(R^2 + Rr + r^2\right) z_1, \tag{2.7}$$

where r can be estimated from similar triangles as:

$$\frac{R}{r} = \frac{z_2 + z_1}{z_2}, \tag{2.8}$$

$$r = \frac{Rz_2}{z_2 + z_1}. \tag{2.9}$$

2.8 Calculating the sum of surface fluxes

The sum of surface fluxes, Q_{tot}, was calculated as:

$$Q_{tot} = Q_{sin} + Q_{lin} - Q_{lout} - Q_e - Q_h, \tag{2.10}$$

where Q_{sin} is the net incoming short-wave radiation (W m^{-2}), Q_{lin} is the incoming long-wave radiation (W m^{-2}), Q_{lout} is the outgoing long-wave radiation (W m^{-2}), Q_e is the latent heat flux (W m^{-2}), and Q_h is the sensible heat flux (W m^{-2}). To calculate these fluxes, a variety of input variables are required: surface water temperature, air temperature (T_z) at height z_t (m) above the water surface (°C), relative humidity (R_h) at height z_q (m) above the water surface (%), wind speed (u_z) at height z_u (m) above the water surface (m s^{-1}), and short-wave radiation (Q_s) measured at the lake surface (W m^{-2}). In addition, the measurement height of the sensors above the water surface is needed.

2.8.1 Incident and reflected short-wave radiation

The amount of short-wave radiation reaching the lake surface can be measured directly, using relatively inexpensive radiometers. The short-wave albedo, α_{sw}, however, influences the amount of radiation that is reflected back to the atmosphere, and thus influences the amount of radiation that penetrates beneath the water surface. Incoming short-wave radiation, Q_{sin} (W m^{-2}), by taking the short-wave albedo into account, can be expressed as:

$$Q_{sin} = Q_s\,(1 - \alpha_{sw})\,. \tag{2.11}$$

Here, α_{sw} is estimated from Fresnel's equation as:

$$\alpha_{sw} = \frac{1}{2}\left[\frac{\tan^2\left(Z - R_{ref}\right)}{\tan^2\left(Z + R_{ref}\right)} + \frac{\sin^2\left(Z - R_{ref}\right)}{\sin^2\left(Z + R_{ref}\right)}\right], \tag{2.12}$$

where R_{ref} is the angle of refraction calculated from Snell's law as:

$$R_{ref} = \sin^{-1}\left(\frac{\sin\left(Z\right)}{\eta}\right), \tag{2.13}$$

where η = 1.33 is the index of refraction (Kirk, 1994) and Z is the solar zenith angle calculated as a function of latitude (φ), solar declination (δ) and the hour angle (H) as:

$$Z = \cos^{-1}\left(\sin\left(\frac{2\varphi\pi}{360}\right)\sin\left(\frac{2\delta\pi}{360}\right) + \cos\left(\frac{2\varphi\pi}{360}\right)\cos\left(\frac{2\delta\pi}{360}\right)\cos H\right), \tag{2.14}$$

$$\begin{aligned}\delta = \frac{180}{\pi}(&0.006918 - 0.399912\cos\left(\gamma\right) + 0.070257\sin\gamma \\ &- 0.006758\cos 2\gamma + 0.000907\sin 2\gamma - 0.002697\cos 3\gamma \\ &+ 0.00148\sin 3\gamma),\end{aligned} \tag{2.15}$$

$$\gamma = 2\pi\left(DOY - 1\right)/365, \tag{2.16}$$

$$H = \left(\pi/12\right)\left(t_{noon} - t_{solar}\right), \tag{2.17}$$

where DOY is the decimal day of year (e.g. Jan 10$^{\text{th}}$ = 10), t_{noon} is the local solar noon and t_{solar} is local solar time.

2.8.2 Long-wave radiation

The net long-wave heat flux (W m^{-2}) across the air-water interface comprises two main components: (i) incoming long-wave radiation and (ii) outgoing long-wave radiation. The bulk formulae may be expressed as:

$$Q_{lnet} = Q_{lin} - Q_{lout}, \tag{2.18}$$

where in the absence of direct measurements, these are estimated from frequently measured variables.

During this dissertation, outgoing long-wave radiation was estimated as:

$$Q_{lout} = \varepsilon_w \sigma T_{0K}^4, \tag{2.19}$$

where ε_w = 0.972 (Davies et al., 1971) is the emissivity of water, $\sigma = 5.67 \times 10^8$ is the Stefan-Boltzmann constant (W m^{-2} K^{-4}), and T_{0K} is the surface water temperature in Kelvin. Incoming long-wave radiation was estimated following the methods of Crawford and Duchon (1999) as used in other limnological studies (e.g. Jakkila et al., 2009; Read et al., 2012). Following this method, the incoming long-wave radiation was estimated as:

$$Q_{lin} = \left\{ clf + (1 - clf) \left(1.22 + 0.06 \sin \left[(\text{month} + 2) \frac{\pi}{6} \right] \right) \left(\frac{e_z}{T_{zK}} \right)^{1/7} \right\} \sigma T_{zK}^4, \tag{2.20}$$

where month is the numerical month (e.g. January = 1), T_{zK} is air temperature in Kelvin, and e_z is the vapour pressure of the air (hPa) calculated as $e_z = R_h E_s$ where E_s is the saturation vapour pressure estimated based on the saturation

vapour pressure of the air calculated following Lowe (1977) as:

$$E_s = a_0 + T_z\left(a_1 + T_z\left(a_2 + T_z\left(a_3 + T_z\left(a_4 + T_z\left(a_5 + a_6 T_z\right)\right)\right)\right)\right), \tag{2.21}$$

where a_0 to a_6 (°C) are given by:

$$\begin{aligned}
a_0 &= 6.107799961, \\
a_1 &= 4.436518521 \times 10^{-1}, \\
a_2 &= 1.428945805 \times 10^{-2}, \\
a_3 &= 2.650648471 \times 10^{-4}, \\
a_4 &= 3.031240396 \times 10^{-6}, \\
a_5 &= 2.034080948 \times 10^{-8}, \\
a_6 &= 6.136820929 \times 10^{-11}.
\end{aligned}$$

The cloud cover fraction, clf, is estimated as:

$$clf = 1 - s, \tag{2.22}$$

where s is the ratio of the measured short-wave radiation (i.e. Q_s) to the clear-sky short-wave radiation, I_c. The clear-sky short-wave radiation is estimated as:

$$I_c = I_{eff}\left(\cos Z\right) T_R T_{pg} T_w T_a, \tag{2.23}$$

where I_{eff} is the effective solar constant, calculated following (Meyers and Dale, 1983) as:

$$I_{eff} = 1353\left\{1 + 0.034 \times \cos\left[2\pi\left(DOY - 1\right)/365\right]\right\}, \tag{2.24}$$

and T_i represent the transmission coefficients for Rayleigh scattering R, absorption by permanent gases pg and water vapour, w, and absorption and scattering by aerosols, a.

An empirical relationship to account for the effects of Rayleigh scattering and absorption by permanent gases was given by Kondratyev (1969). Atwater and Brown (1974) later modified this expression to account for the isotropic nature of Rayleigh scattering with one-half of the scattered radiation being in the forward direction. This formula may be expressed as:

$$T_R T_{pg} = 1.021 - 0.084\left[m\left(0.000949p + 0.051\right)\right]^{0.5}, \tag{2.25}$$

where p is the surface pressure (mb) calculated as a function of altitude as:

$$p = \left[101325\left(1 - \text{altitude} \times 2.25577 \times 10^{-5}\right)^{5.25588}\right]/100, \tag{2.26}$$

and m is the air mass thickness coefficient, calculated as:

$$m = 35\cos Z\left(1244\cos^2 Z + 1\right)^{-0.5}, \tag{2.27}$$

where $\cos Z$ is the cosine of the solar zenith angle (equation 2.14). A formula by McDonald (1960) is used to account for water vapour absorption in the atmo-

sphere, T_w, which may be calculated as:

$$T_w = 1 - 0.077\,(pw \times m)^{0.3}, \tag{2.28}$$

where pw is the precipitable water which is estimated as:

$$pw = \exp\left[(0.1133 - \ln(G+1)) + 0.0393T_d\right], \tag{2.29}$$

T_d (°F) is the dew point temperature estimated as:

$$T_d = \frac{[243.5 \times \ln(e_z/6.112)]}{[17.67 - \ln(e_z/6.112)]} + 33.8, \tag{2.30}$$

and G is an empirically-derived constant for different seasons and latitudes (Table 2.2).

As standard meteorological observations cannot be used to estimate the aerosol attenuation, T_a is calculated as a residual from clear sky conditions. The relation follows an expression given by Houghton (1954) which is:

$$T_a = 0.95^m. \tag{2.31}$$

Once I_c was calculated from equation 2.23, direct observations of solar irradiance were then used to calculate s and clf in equation 2.22. As clf increases from 0 to 1, calculated values of clf less than zero are adjusted back to zero to be physically realistic (Crawford and Duchon, 1999).

As the calculation of incoming long-wave radiation is based on the ratio of clear-sky and measured short-wave radiation, incoming long-wave radiation can-

Table 2.2: Seasonal and latitudinal mean values of G (Smith, 1966).

Latitudinal zone (°)	Winter	Spring	Summer	Autumn	Annual average
0-10	3.37	2.85	2.80	2.64	2.91
10-20	2.99	3.02	2.70	2.93	2.91
20-30	3.60	3.00	2.98	2.93	3.12
30-40	3.04	3.11	2.92	2.94	3.00
40-50	2.70	2.95	2.77	2.71	2.78
50-60	2.52	3.07	2.67	2.93	2.79
60-70	1.76	2.69	2.61	2.61	2.41
70-80	1.60	1.67	2.24	2.63	2.03
80-90	1.11	1.44	1.94	2.02	1.62

not be calculated at night. In this dissertation, night-time incoming long-wave radiation values are estimated as the mean of the daytime values. This adds an additional source of uncertainty in these estimates, but in comparison to more widely-used incoming long-wave formulae (e.g. Gill, 1982), which are daily averages, this method has been shown to provide a more accurate representation of incoming long-wave radiation (Crawford and Duchon, 1999).

2.8.3 Bulk algorithms for momentum, sensible and latent heat fluxes

The air-water fluxes of momentum (τ, N m^{-2}), heat (Q_h, W m^{-2}), and moisture (Q_e, W m^{-2}) are parametrized by bulk algorithms that relate surface layer data to surface fluxes using formulae based on similarity theory and empirical rela-

tionships. The standard procedure involves the calculation of roughness lengths for momentum, heat, and moisture (z_o, z_{oh}, z_{oq}) and the corresponding transfer coefficients (C_d, C_h, C_e) from observed wind speed (u), temperature (T), and humidity (q) profiles, via an iteration routine involving a friction velocity term u_{*a}, a scaling potential temperature T_*, and a scaling humidity q_*. Using the above terms, surface fluxes for momentum, sensible heat, and latent heat can be calculated as:

$$\tau = C_{dz}\rho_z u_z^2 = \rho_z u_{*a}^2, \tag{2.32}$$

$$Q_h = \rho_z C_{pa} C_{hz} u_z (T_0 - T_z) = -\rho_z C_{pa} u_{*a} T_*, \tag{2.33}$$

$$Q_e = \rho_z L_v C_{ez} u_z (q_0 - q_z) = -\rho_z L_v u_{*a} q_*, \tag{2.34}$$

where $\rho_z = 100p/[R_a(T_z + 273.16)]$ is the density (kg m^{-3}) of the overlying air (Verburg and Antenucci, 2010), and $R_a = 287(1 + 0.608q_z)$ is the gas constant for moist air (J kg^{-1} °C^{-1}); C_{pa} = 1006 is the specific heat of air at constant pressure (J kg^{-1} °C^{-1}); $L_v = 2.501 \times 10^6 - 2370 \times T_0$ is the latent heat of vaporisation (J kg^{-1}); $q_0 = 0.622 \times e_{sat}/[p + (0.622 - 1)e_{sat}]$ is the specific humidity at saturation pressure (kg kg^{-1}), e_{sat} is the saturated vapour pressure (hPa) calculated following Bolton (1980) as $e_{sat} = 6.11 \exp[17.27T_0/(237.3 + T_0)]$; $q_z = 0.622 \times e_z/[p + (0.622 - 1)e_z]$ is the specific humidity of the air (kg kg^{-1}) at height z_q (m) above the water surface, $e_z = R_h e_s/100$, and $e_s = 6.11 \exp[17.27T_z/237.3 + T_z]$ is the saturated vapour pressure (hPa) at z_t. Here, C_{dz}, C_{hz} and C_{ez} are transfer coefficients for heights z_u, z_t and z_q, respectively.

A variety of bulk flux algorithms are presently used in the literature (e.g. Fairall et al., 2003, 1996; Verburg and Antenucci, 2010; Zeng et al., 1998).

While these algorithms all use equations (2.32) to (2.34) to calculate the surface fluxes, they differ in the parameterization of the transfer coefficients, the treatment of free convective conditions and surface layer gustiness. In this dissertation, the turbulent fluxes were calculated following Zeng et al. (1998), which applies Monin-Obukhov similarity theory to the atmospheric boundary layer. This theory states that wind, temperature and humidity profile gradients depend on unique functions of the stability parameter, ζ, where $\zeta = zL_w^{-1}$:

$$\frac{\kappa z_u}{u_{*a}}\frac{du}{dz} = \phi_m(\zeta), \qquad \frac{\kappa z_t}{T_*}\frac{dT}{dz} = \phi_h(\zeta), \qquad \frac{\kappa z_q}{q_*}\frac{dq}{dz} = \phi_e(\zeta), \tag{2.35}$$

where L_w is the Monin-Obukhov length scale (m), κ is the von Karman constant (= 0.41), and ϕ_m, ϕ_h and ϕ_e are the similarity functions that relate the fluxes of momentum, heat, and moisture to the mean profile gradients of wind, temperature and humidity, respectively. According to Brutsaert (1982), the Monin-Obukhov length scale is a measure of the ratio of the reduction of potential energy due to wind mixing and the growth of atmospheric stratification due to surface fluxes and may be calculated following Monin and Obukhov (1954) as:

$$L_w = \frac{-\rho_z u_{*a}^3 T_v}{\kappa g\left(\frac{Q_h}{C_{pa}} + 0.61 \times \frac{(T_z+273.16)Q_e}{L_v}\right)}, \tag{2.36}$$

where $T_v = (T_z + 273.16) \times (1 + 0.61 q_z)$ is the virtual air temperature (K) and $g = 9.78033\left(1 + \left(0.0053\sin^2|\varphi| - 5.8\times10^{-6}\sin^2|\varphi|\right)\right)$ is the gravitational acceleration (m s^{-2}), where the standard value of 9.81 m s^{-2} is given at latitude $\sim$45.5°.

Following Zeng et al. (1998), the differential equations for ϕ_m, ϕ_h and ϕ_e can

be integrated between the roughness length and the measurement height to obtain wind, temperature and moisture gradients in the atmospheric boundary layer and the corresponding scaling parameters used in calculating the turbulent surface fluxes. The roughness length of momentum (z_o) was calculated following Smith (1998) as:

$$z_o = \left(\frac{\alpha_1 u_{*a}^2}{g}\right) + \left(\frac{\alpha_2 v_a}{u_{*a}}\right), \tag{2.37}$$

where α_1 is the Charnock constant (= 0.013), α_2 = 0.11, and v_a is the kinematic viscosity of air (= 1.5×10^{-5} m^2 s^{-1}). The functional form of Brutsaert (1982) is then used to estimate the roughness length of heat (z_{ot}) and humidity (z_{oq}) as:

$$z_{oq} = z_{ot} = z_o \exp\left(-b_1 Re^{0.25} - b_2\right), \tag{2.38}$$

where $b_1 = 2.67$, $b_2 = -2.57$, and Re = $u_{*a} z_o / v_a$ is the roughness Reynolds number.

Using the Monin-Obukhov similarity theory, the flux-gradient relations for momentum, $\phi_m(\zeta)$, are:

$$\phi_m(\zeta) = 5 + \zeta \qquad \text{for} \quad \zeta > 1 \,(\text{very stable}) \tag{2.39}$$

$$\phi_m(\zeta) = 1 + 5\zeta \qquad \text{for} \quad 0 \leq \zeta \leq 1 \,(\text{stable}) \tag{2.40}$$

$$\phi_m(\zeta) = (1 - 16\zeta)^{-1/4} \qquad \text{for} \quad -1.574 \leq \zeta < 0 \,(\text{unstable}) \tag{2.41}$$

$$\phi_m(\zeta) = \left(0.7\kappa^{2/3}\right)(-\zeta)^{1/3} \qquad \text{for} \quad \zeta < -1.574 \,(\text{very unstable}) \tag{2.42}$$

and for sensible and latent heat, where $\phi_e(\zeta) = \phi_h(\zeta)$, are:

$$\phi_e(\zeta) = 5 + \zeta \qquad \text{for} \quad \zeta > 1 \,(\text{very stable}) \tag{2.43}$$

$$\phi_e(\zeta) = 1 + 5\zeta \qquad \text{for} \quad 0 \leq \zeta \leq 1 \,(\text{stable}) \tag{2.44}$$

$$\phi_e(\zeta) = (1 - 16\zeta)^{-1/2} \qquad \text{for} \quad -0.465 \leq \zeta < 0 \,(\text{unstable}) \tag{2.45}$$

$$\phi_e(\zeta) = 0.9\kappa^{4/3}(-\zeta)^{-1/3} \qquad \text{for} \quad \zeta < -0.465 \,(\text{very unstable}) \tag{2.46}$$

where to ensure continuous functions of $\phi_m(\zeta)$, $\phi_h(\zeta)$ and $\phi_e(\zeta)$ we can match the relations for very unstable conditions at ζ_m = -1.574 for $\phi_m(\zeta)$ and $\zeta_h = \zeta_e$ = -0.465 for $\phi_h(\zeta) = \phi_e(\zeta)$. The flux gradient relations can then be integrated to yield wind profiles, and the corresponding friction velocity, u_{*a}, as:

$$\phi_m = \frac{\kappa z_u}{u_{*a}} \frac{du}{dz} = 5 + \zeta, \tag{2.47}$$

$$\phi_m = \frac{\kappa z_u}{u_{*a}} \frac{du}{dz} = 5 + \left(\frac{z_u}{L_w}\right),$$

and then by re-arranging for du and integrating between z_o and z_u we obtain

$$du = \frac{u_{*a}}{\kappa}\left\{\left(\ln\left(\frac{L_w}{z_o}\right) + 5\right) + \left[5\ln\left(\frac{z_u}{L_w}\right) + \left(\frac{z_u}{L_w}\right) - 1\right]\right\},$$

$$u_z - u_0 = \frac{u_{*a}}{\kappa}\left\{\left(\ln\left(\frac{L_w}{z_o}\right) + 5\right) + \left[5\ln\left(\frac{z_u}{L_w}\right) + \left(\frac{z_u}{L_w}\right) - 1\right]\right\},$$

$$u_z = \frac{u_{*a}}{\kappa}\left\{\left(\ln\left(\frac{L_w}{z_o}\right) + 5\right) + \left[5\ln\left(\frac{z_u}{L_w}\right) + \left(\frac{z_u}{L_w}\right) - 1\right]\right\}, \tag{2.48}$$

$$u_{*a} = u_z\kappa\left\{\left(\ln\left(\frac{L_w}{z_o}\right) + 5\right) + \left[5\ln\left(\frac{z_u}{L_w}\right) + \left(\frac{z_u}{L_w}\right) - 1\right]\right\}^{-1}, \tag{2.49}$$

$$u_{10} = \frac{u_{*a}}{\kappa}\left\{\left(\ln\left(\frac{L_w}{z_o}\right) + 5\right) + \left[5\ln\left(\frac{10}{L_w}\right) + \left(\frac{10}{L_w}\right) - 1\right]\right\}, \tag{2.50}$$

for very stable conditions ($\zeta > 1$),

$$\phi_m = \frac{\kappa z_u}{u_{*a}} \frac{du}{dz} = 1 + 5\zeta, \tag{2.51}$$

$$\phi_m = \frac{\kappa z_u}{u_{*a}} \frac{du}{dz} = 1 + 5\left(\frac{z_u}{L_w}\right),$$

and then by re-arranging for du and integrating between z_o and z_u we obtain

$$du = \frac{u_{*a}}{\kappa}\left[\ln\left(\frac{z_u}{z_o}\right) + 5\left(\frac{z_u}{L_w}\right)\right],$$

$$u_z - u_0 = \frac{u_{*a}}{\kappa}\left[\ln\left(\frac{z_u}{z_o}\right) + 5\left(\frac{z_u}{L_w}\right)\right],$$

$$u_z = \frac{u_{*a}}{\kappa}\left[\ln\left(\frac{z_u}{z_o}\right) + 5\left(\frac{z_u}{L_w}\right)\right], \tag{2.52}$$

$$u_{*a} = u_z \kappa \left[\ln\left(\frac{z_u}{z_o}\right) + 5\left(\frac{z_u}{L_w}\right)\right]^{-1}, \tag{2.53}$$

$$u_{10} = \frac{u_{*a}}{\kappa}\left[\ln\left(\frac{10}{z_o}\right) + 5\left(\frac{10}{L_w}\right)\right], \tag{2.54}$$

for stable conditions ($0 < \zeta < 1$),

$$\phi_m = \frac{\kappa z_u}{u_{*a}} \frac{du}{dz} = \left[1 - 16\zeta\right]^{-1/4}, \tag{2.55}$$

$$\phi_m = \frac{\kappa z_u}{u_{*a}} \frac{du}{dz} = \left[1 - 16\left(\frac{z_u}{L_w}\right)\right]^{-1/4},$$

and then by re-arranging for du and integrating between z_o and z_u we obtain

$$du = \frac{u_{*a}}{\kappa}\left[\ln\left(\frac{z_u}{z_o}\right) - \psi_m\left(\frac{z_u}{L_w}\right)\right],$$

$$u_z - u_0 = \frac{u_{*a}}{\kappa}\left[\ln\left(\frac{z_u}{z_o}\right) - \psi_m\left(\frac{z_u}{L_w}\right)\right],$$

$$u_z = \frac{u_{*a}}{\kappa}\left[\ln\left(\frac{z_u}{z_o}\right) - \psi_m\left(\frac{z_u}{L_w}\right)\right], \tag{2.56}$$

$$u_{*a} = u_z\kappa\left[\ln\left(\frac{z_u}{z_o}\right) - \psi_m\left(\frac{z_u}{L_w}\right)\right]^{-1}, \tag{2.57}$$

$$u_{10} = \frac{u_{*a}}{\kappa}\left[\ln\left(\frac{10}{z_o}\right) - \psi_m\left(\frac{10}{L_w}\right)\right], \tag{2.58}$$

for unstable conditions ($\zeta_m < \zeta < 0$), and

$$\phi_m = \frac{\kappa z_u}{u_{*a}}\frac{du}{dz} = \left(0.7\kappa^{2/3}\right)\left(-\zeta\right)^{1/3}, \tag{2.59}$$

$$\phi_m = \frac{\kappa z_u}{u_{*a}}\frac{du}{dz} = \left(0.7\kappa^{2/3}\right)\left(-\frac{z_u}{L_w}\right)^{1/3},$$

and then by re-arranging for du and integrating between z_o and z_u we obtain

$$du = \frac{u_{*a}}{\kappa}\left\{\left[\ln\left(\frac{\zeta_m L_w}{z_o}\right) - \psi_m(\zeta_m)\right] + 1.14\left[\left(-\frac{z_u}{L_w}\right)^{1/3} - (-\zeta_m)^{1/3}\right]\right\},$$

$$u_z - u_0 = \frac{u_{*a}}{\kappa}\left\{\left[\ln\left(\frac{\zeta_m L_w}{z_o}\right) - \psi_m(\zeta_m)\right] + 1.14\left[(-\zeta_m)^{1/3} - (-\zeta_m)^{1/3}\right]\right\},$$

$$u_z = \frac{u_{*a}}{\kappa}\left\{\left[\ln\left(\frac{\zeta_m L_w}{z_o}\right) - \psi_m(\zeta_m)\right] + 1.14\left[(-\zeta_m)^{1/3} - (-\zeta_m)^{1/3}\right]\right\}, \tag{2.60}$$

$$u_{*a} = u_z\kappa\left\{\left[\ln\left(\frac{\zeta_m L_w}{z_o}\right) - \psi_m(\zeta_m)\right] + 1.14\left[\left(-\frac{z_u}{L_w}\right) - (-\zeta_m)^{1/3}\right]\right\}^{-1}, \tag{2.61}$$

$$u_{10} = \frac{u_{*a}}{\kappa}\left\{\left[\ln\left(\frac{\zeta_m L_w}{z_o}\right) - \psi_m(\zeta_m)\right] + 1.14\left[\left(-\frac{10}{L_w}\right)^{1/3} - (-\zeta_m)^{1/3}\right]\right\}, \tag{2.62}$$

for very unstable conditions ($\zeta < \zeta_m = -1.574$) where

$$\psi_m(\zeta) = 2\ln\left(\frac{1+\chi}{2}\right) + \ln\left(\frac{1+\chi^2}{2}\right) - 2\tan^{-1}\chi + \frac{\pi}{2}, \tag{2.63}$$

is the stability function for momentum under stable conditions and

$$\chi = (1-16\zeta)^{1/4}. \tag{2.64}$$

Under stable conditions ($\zeta > 0$), the wind speed u_z is defined as:

$$u_z = \max[u_z, 0.1], \tag{2.65}$$

and for unstable cases ($\zeta < 0$), u_z is given by:

$$u_z = \left[u_z^2 + (\beta_* w_{*a})^2\right]^{1/2}, \tag{2.66}$$

where w_{*a} is the convective velocity scale in the atmospheric boundary layer, defined as:

$$w_{*a} = \left(-\frac{g}{T_v} T_{v*} u_{*a} z_i \right)^{1/3}, \tag{2.67}$$

where z_i is the convective boundary layer height (= 1000 m), β_* = 1, and T_{v*} is the virtual potential temperature scaling parameter, calculated as:

$$T_{v*} = T_* \left(1 + 0.61 q_z/100\right) + 0.61 \times T_h, \tag{2.68}$$

where $T_h = (T_z + 273.16) \times (100/p)^{(287.1/1004.67)}$ is the potential temperature, which is the temperature that a parcel of air would acquire if it was adiabatically brought to a standard reference pressure. The flux gradient relations for heat follow a similar manner to that of wind, but by integrating the flux gradients for heat we obtain

$$\phi_h = \frac{\kappa z_t}{T_*} \frac{dT}{dz} = 5 + \zeta, \tag{2.69}$$

$$\phi_h = \frac{\kappa z_t}{T_*} \frac{dT}{dz} = 5 + \left(\frac{z_t}{L_w} \right),$$

and then by re-arranging for dT and integrating between z_{ot} and z_t we obtain

$$dT = \frac{T_*}{\kappa} \left\{ \left[\ln \left(\frac{L_w}{z_{ot}} \right) + 5 \right] + \left[5 + \ln \left(\frac{z_t}{L_w} \right) + \left(\frac{z_t}{L_w} \right) - 1 \right] \right\},$$

$$T_z - T_0 = \frac{T_*}{\kappa} \left\{ \left[\ln \left(\frac{L_w}{z_{ot}} \right) + 5 \right] + \left[5 + \ln \left(\frac{z_t}{L_w} \right) + \left(\frac{z_t}{L_w} \right) - 1 \right] \right\},$$

$$T_z = \frac{T_*}{\kappa}\left\{\left[\ln\left(\frac{L_w}{z_{ot}}\right)+5\right]+\left[5+\ln\left(\frac{z_t}{L_w}\right)+\left(\frac{z_t}{L_w}\right)-1\right]\right\}+T_0, \tag{2.70}$$

$$T_* = T_z\kappa\left\{\left\{\left[\ln\left(\frac{L_w}{z_{ot}}\right)+5\right]+\left[5+\ln\left(\frac{z_t}{L_w}\right)+\left(\frac{z_t}{L_w}\right)-1\right]\right\}+T_0\right\}^{-1}, \tag{2.71}$$

$$T_{10} = \frac{T_*}{\kappa}\left\{\left[\ln\left(\frac{L_w}{z_{ot}}\right)+5\right]+\left[5+\ln\left(\frac{10}{L_w}\right)+\left(\frac{10}{L_w}\right)-1\right]\right\}+T_0, \tag{2.72}$$

for very stable conditions ($\zeta > 1$),

$$\phi_h = \frac{\kappa z_t}{T_*}\frac{dT}{dz} = 1+5\zeta, \tag{2.73}$$

$$\phi_h = \frac{\kappa z_t}{T_*}\frac{dT}{dz} = 1+5\left(\frac{z_t}{L_w}\right),$$

and then by re-arranging for dT and integrating between z_{ot} and z_t we obtain

$$dT = \frac{T_*}{\kappa}\left[\ln\left(\frac{z_t}{z_{ot}}\right)+5\left(\frac{z_t}{L_w}\right)\right],$$

$$T_z - T_0 = \frac{T_*}{\kappa}\left[\ln\left(\frac{z_t}{z_{ot}}\right)+5\left(\frac{z_t}{L_w}\right)\right],$$

$$T_z = \frac{T_*}{\kappa}\left[\ln\left(\frac{z_t}{z_{ot}}\right)+5\left(\frac{z_t}{L_w}\right)\right]+T_0, \tag{2.74}$$

$$T_* = T_z\kappa\left\{\left[\ln\left(\frac{z_t}{z_{ot}}\right)+5\left(\frac{z_t}{L_w}\right)\right]+T_0\right\}^{-1}, \tag{2.75}$$

$$T_{10} = \frac{T_*}{\kappa}\left[\ln\left(\frac{10}{z_{ot}}\right) + 5\left(\frac{10}{L_w}\right)\right] + T_0, \tag{2.76}$$

for stable conditions $(0 < \zeta < 1)$,

$$\phi_h = \frac{\kappa z_t}{T_*}\frac{dT}{dz} = (1 - 16\zeta)^{-1/2}, \tag{2.77}$$

$$\phi_h = \frac{\kappa z_t}{T_*}\frac{dT}{dz} = \left(1 - 16\left(\frac{z_t}{L_w}\right)\right)^{-1/2},$$

and then by re-arranging for dT and integrating between z_{ot} and z_t we obtain

$$dT = \frac{T_*}{\kappa}\left[\ln\left(\frac{z_t}{z_{ot}}\right) - \psi_h\left(\frac{z_t}{L_w}\right)\right],$$

$$T_z - T_0 = \frac{T_*}{\kappa}\left[\ln\left(\frac{z_t}{z_{ot}}\right) - \psi_h\left(\frac{z_t}{L_w}\right)\right],$$

$$T_z = \frac{T_*}{\kappa}\left[\ln\left(\frac{z_t}{z_{ot}}\right) - \psi_h\left(\frac{z_t}{L_w}\right)\right] + T_0, \tag{2.78}$$

$$T_* = T_z\kappa\left\{\left[\ln\left(\frac{z_t}{z_{ot}}\right) - \psi_h\left(\frac{z_t}{L_w}\right)\right] + T_0\right\}^{-1}, \tag{2.79}$$

$$T_{10} = \frac{T_*}{\kappa}\left[\ln\left(\frac{10}{z_{ot}}\right) - \psi_h\left(\frac{10}{L_w}\right)\right] + T_0, \tag{2.80}$$

for unstable conditions $(\zeta_h < \zeta < 0)$, and

$$\phi_h = \frac{\kappa z_t}{T_*}\frac{dT}{dz} = 0.9\kappa^{4/3}(-\zeta)^{-1/3}, \tag{2.81}$$

$$\phi_h = \frac{\kappa z_t}{T_*}\frac{dT}{dz} = 0.9\kappa^{4/3}\left(-\frac{z_t}{L_w}\right)^{-1/3}, \tag{2.82}$$

and then by re-arranging for dT and integrating between z_{ot} and z_t we obtain

$$dT = \frac{T_*}{\kappa}\left\{\left[\ln\left(\frac{\zeta_h L_w}{z_{ot}}\right) - \psi_h(\zeta_h)\right] + 0.8\left[(-\zeta_h)^{-1/3} - \left(-\frac{z_t}{L_w}\right)^{-1/3}\right]\right\},$$

$$T_z - T_0 = \frac{T_*}{\kappa}\left\{\left[\ln\left(\frac{\zeta_h L_w}{z_{ot}}\right) - \psi_h(\zeta_h)\right] + 0.8\left[(-\zeta_h)^{-1/3} - \left(-\frac{z_t}{L_w}\right)^{-1/3}\right]\right\},$$

$$T_z = \frac{T_*}{\kappa}\left\{\left[\ln\left(\frac{\zeta_h L_w}{z_{ot}}\right) - \psi_h(\zeta_h)\right] + 0.8\left[(-\zeta_h)^{-1/3} - \left(-\frac{z_t}{L_w}\right)^{-1/3}\right]\right\} + T_0, \tag{2.83}$$

$$T_* = T_z \kappa\left\{\left\{\left[\ln\left(\frac{\zeta_h L_w}{z_{ot}}\right) - \psi_h(\zeta_h)\right] + 0.8\left[(-\zeta_h)^{-1/3} - \left(-\frac{z_t}{L_w}\right)^{-1/3}\right]\right\} + T_0\right\}^{-1}, \tag{2.84}$$

$$T_{10} = \frac{T_*}{\kappa}\left\{\left[\ln\left(\frac{\zeta_h L_w}{z_{ot}}\right) - \psi_h(\zeta_h)\right] + 0.8\left[(-\zeta_h)^{-1/3} - \left(-\frac{10}{L_w}\right)^{-1/3}\right]\right\} + T_0, \tag{2.85}$$

for very unstable conditions ($\zeta < \zeta_h = -0.465$), where the stability function for temperature and humidity ($\psi_h = \psi_e$) is given by

$$\psi_h = \psi_e = 2\ln\left(\frac{1+\chi^2}{2}\right). \tag{2.86}$$

The calculation for q_* is the same as those for T_* except that $[T_z - T_0]$ and z_{ot} are replaced by $[q_z - q_0]$ and z_{oq} respectively:

$$\phi_e = \frac{\kappa z_q}{q_*}\frac{dq}{dz} = 5 + \zeta, \tag{2.87}$$

$$\phi_e = \frac{\kappa z_q}{q_*}\frac{dq}{dz} = 5 + \left(\frac{z_q}{L_w}\right),$$

and then by re-arranging for dq and integrating between z_{oq} and z_q we obtain

$$dq = \frac{q_*}{\kappa}\left\{\left[\ln\left(\frac{L_w}{z_{oq}}\right)+5\right]+\left[5+\ln\left(\frac{z_q}{L_w}\right)+\left(\frac{z_q}{L_w}\right)-1\right]\right\},$$

$$q_z - q_0 = \frac{q_*}{\kappa}\left\{\left[\ln\left(\frac{L_w}{z_{oq}}\right)+5\right]+\left[5+\ln\left(\frac{z_q}{L_w}\right)+\left(\frac{z_q}{L_w}\right)-1\right]\right\},$$

$$q_z = \frac{q_*}{\kappa}\left\{\left[\ln\left(\frac{L_w}{z_{oq}}\right)+5\right]+\left[5+\ln\left(\frac{z_q}{L_w}\right)+\left(\frac{z_q}{L_w}\right)-1\right]\right\}+q_0, \tag{2.88}$$

$$q_* = q_z\kappa\left\{\left\{\left[\ln\left(\frac{L_w}{z_{oq}}\right)+5\right]+\left[5+\ln\left(\frac{z_q}{L_w}\right)+\left(\frac{z_q}{L_w}\right)-1\right]\right\}+q_0\right\}^{-1}, \tag{2.89}$$

$$q_{10} = \frac{q_*}{\kappa}\left\{\left[\ln\left(\frac{L_w}{z_{oq}}\right)+5\right]+\left[5+\ln\left(\frac{10}{L_w}\right)+\left(\frac{10}{L_w}\right)-1\right]\right\}+q_0, \tag{2.90}$$

for very stable conditions ($\zeta > 1$),

$$\phi_e = \frac{\kappa z_q}{q_*}\frac{dq}{dz} = 1 + 5\zeta, \tag{2.91}$$

$$\phi_e = \frac{\kappa z_q}{q_*}\frac{dq}{dz} = 1 + 5\left(\frac{z_q}{L_w}\right),$$

and then by re-arranging for dq and integrating between z_{oq} and z_q we obtain

$$dq = \frac{q_*}{\kappa}\left[\ln\left(\frac{z_q}{z_{oq}}\right) + 5\left(\frac{z_q}{L_w}\right)\right],$$

$$q_z - q_0 = \frac{q_*}{\kappa}\left[\ln\left(\frac{z_q}{z_{oq}}\right) + 5\left(\frac{z_q}{L_w}\right)\right],$$

$$q_z = \frac{q_*}{\kappa}\left[\ln\left(\frac{z_q}{z_{oq}}\right) + 5\left(\frac{z_q}{L_w}\right)\right] + q_0, \tag{2.92}$$

$$q_* = q_z\kappa\left\{\left[\ln\left(\frac{z_q}{z_{oq}}\right) + 5\left(\frac{z_q}{L_w}\right)\right] + q_0\right\}^{-1}, \tag{2.93}$$

$$q_{10} = \frac{q_*}{\kappa}\left[\ln\left(\frac{10}{z_{oq}}\right) + 5\left(\frac{10}{L_w}\right)\right] + q_0, \tag{2.94}$$

for stable conditions $(0 < \zeta < 1)$,

$$\phi_e = \frac{\kappa z_q}{q_*}\frac{dq}{dz} = (1 - 16\zeta)^{-1/2}, \tag{2.95}$$

$$\phi_e = \frac{\kappa z_q}{q_*}\frac{dq}{dz} = \left(1 - 16\left(\frac{z_q}{L_w}\right)\right)^{-1/2},$$

and then by re-arranging for dq and integrating between z_{oq} and z_q we obtain

$$dq = \frac{q_*}{\kappa}\left[\ln\left(\frac{z_q}{z_{oq}}\right) - \psi_e\left(\frac{z_q}{L_w}\right)\right],$$

$$q_z - q_0 = \frac{q_*}{\kappa}\left[\ln\left(\frac{z_q}{z_{oq}}\right) - \psi_e\left(\frac{z_q}{L_w}\right)\right],$$

$$q_z = \frac{q_*}{\kappa}\left[\ln\left(\frac{z_q}{z_{oq}}\right) - \psi_e\left(\frac{z_q}{L_w}\right)\right] + q_0, \tag{2.96}$$

$$q_* = q_z\kappa\left\{\left[\ln\left(\frac{z_q}{z_{oq}}\right) - \psi_e\left(\frac{z_q}{L_w}\right)\right] + q_0\right\}^{-1}, \tag{2.97}$$

$$q_{10} = \frac{q_*}{\kappa}\left[\ln\left(\frac{10}{z_{oq}}\right) - \psi_e\left(\frac{10}{L_w}\right)\right] + q_0, \tag{2.98}$$

for unstable conditions ($\zeta_e < \zeta < 0$), and

$$\phi_e = \frac{\kappa z_q}{q_*}\frac{dq}{dz} = 0.9\kappa^{4/3}\left(-\zeta\right)^{-1/3}, \tag{2.99}$$

$$\phi_e = \frac{\kappa z_q}{q_*}\frac{dq}{dz} = 0.9\kappa^{4/3}\left(-\frac{z_q}{L_w}\right)^{-1/3}, \tag{2.100}$$

and then by re-arranging for dq and integrating between z_{oq} and z_q we obtain

$$\begin{aligned} dq = \frac{q_*}{\kappa}\Bigg\{&\left[\ln\left(\frac{\zeta_e L_w}{z_{oq}}\right) - \psi_e\left(\zeta_e\right)\right] \\ &+0.8\left[\left(-\zeta_e\right)^{-1/3} - \left(-\frac{z_q}{L_w}\right)^{-1/3}\right]\Bigg\}, \end{aligned}$$

$$\begin{aligned} q_z - q_0 = \frac{q_*}{\kappa}\Bigg\{&\left[\ln\left(\frac{\zeta_e L_w}{z_{oq}}\right) - \psi_e\left(\zeta_e\right)\right] \\ &+0.8\left[\left(-\zeta_e\right)^{-1/3} - \left(-\frac{z_q}{L_w}\right)^{-1/3}\right]\Bigg\}, \end{aligned}$$

$$\begin{aligned} q_z = \frac{q_*}{\kappa}\Bigg\{&\left[\ln\left(\frac{\zeta_e L_w}{z_{oq}}\right) - \psi_e\left(\zeta_e\right)\right] \\ &+0.8\left[\left(-\zeta_e\right)^{-1/3} - \left(-\frac{z_q}{L_w}\right)^{-1/3}\right]\Bigg\} + q_0, \end{aligned} \tag{2.101}$$

$$q_* = q_z \kappa \left\{ \left\{ \left[\ln\left(\frac{\zeta_e L_w}{z_{oq}}\right) - \psi_e(\zeta_e) \right] + 0.8 \left[(-\zeta_e)^{-1/3} - \left(-\frac{z_q}{L_w}\right)^{-1/3} \right] \right\} + q_0 \right\}^{-1}, \tag{2.102}$$

$$q_{10} = \frac{q_*}{\kappa} \left\{ \left[\ln\left(\frac{\zeta_e L_w}{z_{oq}}\right) - \psi_e(\zeta_e) \right] + 0.8 \left[(-\zeta_e)^{-1/3} - \left(-\frac{10}{L_w}\right)^{-1/3} \right] \right\} + q_0, \tag{2.103}$$

for very unstable conditions ($\zeta < \zeta_e = -0.465$).

The transfer coefficients for momentum(C_{dz}), sensible heat (C_{hz}) and latent heat (C_{ez}) can be calculated by re-arranging equations 2.32 to 2.34 as:

$$\tau = C_{dz} \rho_z u_z^2 = \rho_z u_{*a}^2, \tag{2.104}$$

$$C_{dz} = \rho_z u_{*a}^2 \Big/ \rho_z u_z^2, \tag{2.105}$$

$$C_{dz} = u_{*a}^2 \Big/ u_z^2, \tag{2.106}$$

$$Q_h = \rho_z C_{pa} C_{hz} u_z (T_0 - T_z) = \rho_z C_{pa} u_{*a} T_*, \tag{2.107}$$

$$C_{hz} = \rho_z C_{pa} u_{*a} T_* \Big/ \rho_z C_{pa} u_z (T_0 - T_z), \tag{2.108}$$

$$C_{hz} = -u_{*a} T_* \Big/ u_z (T_0 - T_z). \tag{2.109}$$

$$Q_e = \rho_z L_v C_{ez} u_z (q_0 - q_z) = -\rho_z L_v u_{*a} q_*, \tag{2.110}$$

$$C_{ez} = \rho_z L_v u_z (q_0 - q_z) \Big/ -\rho_z L_v u_{*a} q_*, \tag{2.111}$$

$$C_{ez} = -u_{*a} q_* \Big/ u_z (q_0 - q_z). \tag{2.112}$$

2.8.4 Development of Lake Heat Flux Analyzer

As part of the PhD project, a program called 'Lake Heat Flux Analyzer' was developed for calculating the surface energy fluxes in lakes according to the methods described in this chapter. The program was written in MATLAB and is free to download (https://github.com/GLEON/HeatFluxAnalyzer) under the GNU Public Licence. Users without access to MATLAB can use the online web interface for Lake Heat Flux Analyzer (http://heatfluxanalyzer.gleon.org/) which runs the program on a remote server based on unique input files and allows users to download results after completion.

Full performance of Lake Heat Flux Analyzer requires various input files, including data on water temperature, wind speed, short-wave radiation, relative humidity, and air temperature as well as a configuration file (Table 2.3). The program can also accept net long-wave radiation data, incoming long-wave radiation data and photosynthetically available radiation data. Data requirements vary depending on the user-defined output selections (Table 2.4), which allows the program to be flexible with respect to data sources, instead of requiring all potential data files or functions for each program to be run. This structure not only increases program speed but also allows users with data limitations to use the program as some calculations require fewer inputs. Additional information regarding input file format as well as a step-by-step guide to using the program is provided in the user manual, which can be found on the web interface (http://heatfluxanalyzer.gleon.org/).

Table 2.3: Table of input parameters for the Lake Heat Flux Analyzer program. Specific data format requirements are provided in the user manual.

Input	Units	Description
.wtr	°C	Tab delimited text file of surface water temperature measurements
.wnd	m s^{-1}	Tab delimited text file of wind speed measurements
.airT	°C	Tab delimited text file of air temperature measurements
.rh	%	Tab delimited text file of relative humidity measurements
.sw	W m^{-2}	Tab delimited text file of short-wave radiation measurements
.lwnet	W m^{-2}	Tab delimited text file of net long-wave radiation measurements.
.lw	W m^{-2}	Tab delimited text file of incoming long-wave radiation measurements.
.par	mmol m^{-2} s^{-1}	Tab delimited text file of photosynthetically available radiation measurements. This file is only used when a .sw file is missing.
z_u	m	Height of wind measurement
z_q	m	Height of humidity measurement
z_t	m	Height of air temperature measurement
Output resolution	s	Output resolution of results
alt	m	Altitude of lake
φ	°N	Latitude of lake
Max wind speed	m s^{-1}	Maximum wind speed allowed
Min wind speed	m s^{-1}	Minimum wind speed allowed

Additional parameters are also calculated by Lake Heat Flux Analyzer. These include evaporation rates (mm day^{-1}), calculated as:

$$E = \frac{Q_e}{\rho_0 \times L_v}, \tag{2.113}$$

and the transfer coefficients at a height of 10 m above the lake surface, calculated

Table 2.4: Table of output variables from the Lake Heat Flux Analyzer program including a list of input files required for the corresponding outputs.

Output	Description	.wtr	.wnd	.airT	.rh	.sw
u_{*a}	Air friction velocity	✓	✓	✓	✓	
u_{*aN}	Air friction velocity (neutral)		✓			
T_{10}	Air temperature at 10 m	✓	✓	✓	✓	
E	Evaporation	✓	✓	✓	✓	
Q_{lin}	Incoming long-wave radiation	✓		✓	✓	✓
Q_e	Latent heat flux	✓	✓	✓	✓	
τ	Momentum flux	✓	✓	✓	✓	
L_w	Monin-Obukhov length scale	✓	✓	✓	✓	
Q_{lnet}	Net long-wave radiation	✓		✓	✓	✓
Q_{lout}	Outgoing long-wave radiation	✓				
Q_{sr}	Reflected short-wave radiation					✓
rh_{10}	Relative humidity at 10 m	✓	✓	✓	✓	
Q_h	Sensible heat flux	✓	✓	✓	✓	
C_{hz}	Transfer coefficient for heat	✓	✓	✓	✓	
C_{hzN}	Transfer coefficient for heat (neutral)		✓			
C_{h10}	Transfer coefficient for heat at 10 m	✓	✓	✓	✓	
C_{h10N}	Transfer coefficient for heat at 10 m (neutral)		✓			
C_{ez}	Transfer coefficient for humidity	✓	✓	✓	✓	
C_{ezN}	Transfer coefficient for humidity (neutral)		✓			
C_{e10}	Transfer coefficient for humidity at 10 m	✓	✓	✓	✓	
C_{e10N}	Transfer coefficient for humidity at 10 m (neutral)		✓			
C_{dz}	Transfer coefficient for momentum	✓	✓	✓	✓	
C_{dzN}	Transfer coefficient for momentum (neutral)		✓			
C_{d10}	Transfer coefficient for momentum at 10 m	✓	✓	✓	✓	
C_{d10N}	Transfer coefficient for momentum at 10 m (neutral)		✓			
u_{10}	Wind speed at 10 m	✓	✓	✓	✓	
u_{10N}	Wind speed at 10 m (neutral)		✓			

as:

$$C_{h10} = Q_h \Big/ \rho_z C_{pa} u_{10} (T_0 - T_{10}), \tag{2.114}$$

$$C_{e10} = Q_e \Big/ \rho_z L_v u_{10} (q_0 - q_{10}), \tag{2.115}$$

$$C_{d10} = u_{*a}^2 \Big/ u_{10}^2. \tag{2.116}$$

The neutral transfer coefficients at a height of 10 m are also calculated as:

$$C_{d10N} = \left[\kappa \Big/ \ln \left(\frac{10}{z_o} \right) \right]^2, \tag{2.117}$$

$$C_{e10N} = C_{e10N} = \kappa^2 \Big/ \left[\ln \left(\frac{10}{z_o} \right) \ln \left(\frac{10}{z_{oq}} \right) \right], \tag{2.118}$$

where z_o and z_{oq} are calculated under neutral atmospheric conditions, that is $\zeta = 0$.

2.9 The penetration of short-wave radiation into the upper mixed layer

Short-wave radiation that penetrates beneath the depth of the upper mixed layer is primarily confined within the visible (0.4 to 0.7 μm) part of the short-wave spectrum. To determine the amount of short-wave radiation that penetrates beneath the depth of the upper mixed layer, however, the percentage of short-wave radiation that lies within the visible range must, therefore, be calculated. This can be achieved by firstly calculating the amount of short-wave radiation that

reaches the earth's surface and then calculating the percentage of the radiation that is confined within the visible range. For example, the amount of radiation that reaches earth may be estimated according to Planck's law as:

$$L_\lambda = \frac{2h_p c^2}{\lambda^5 \exp\left(\frac{hc}{\lambda k T_K}\right) - 1}, \tag{2.119}$$

where L denotes the spectral radiance (W m^{-2}), $k = 1.38066 \times 10^{-23}$ is the Boltzmann constant (J K^{-1}), T_K is temperature in Kelvin, $c = 3 \times 10^8$ is the speed of light (m s^{-1}), $h_p = 6.626 \times 10^{-34}$ is Planck's constant (m^2 kg s^{-1}), and λ is wavelength (m). To determine the amount of radiation that reaches earth, equation 2.119 may be solved for a black body with a temperature of 5800 K (i.e. the surface temperature of the sun). This represents the energy flow from the Sun, per unit of solid angle, across a unit area which is right next to the Sun's surface. To calculate the solar spectrum as measured outside the earth's atmosphere (Fig 2.11), however, L_λ must be multiplied by the square of the ratio of the sun's equatorial radius ($R_\odot$) to earth's orbital radius ($a_\oplus$) as:

$$\left(\frac{R_\odot}{a_\oplus}\right)^2 = \left(\frac{696342 \text{ km}}{152098232 \text{ km}}\right)^2 \approx 2177 \times 10^{-5}. \tag{2.120}$$

In addition, the fact that the Sun emits in all directions needs to be accounted for, which means applying Lambert's cosine law, which essentially states that after integrating over a solid angle an extra factor of π needs to be included.

To determine the amount of energy that reaches earth's surface, the influence of scattering and absorption within the earth's atmosphere must also be included. These processes not only significantly reduce the intensity of solar irradiance but

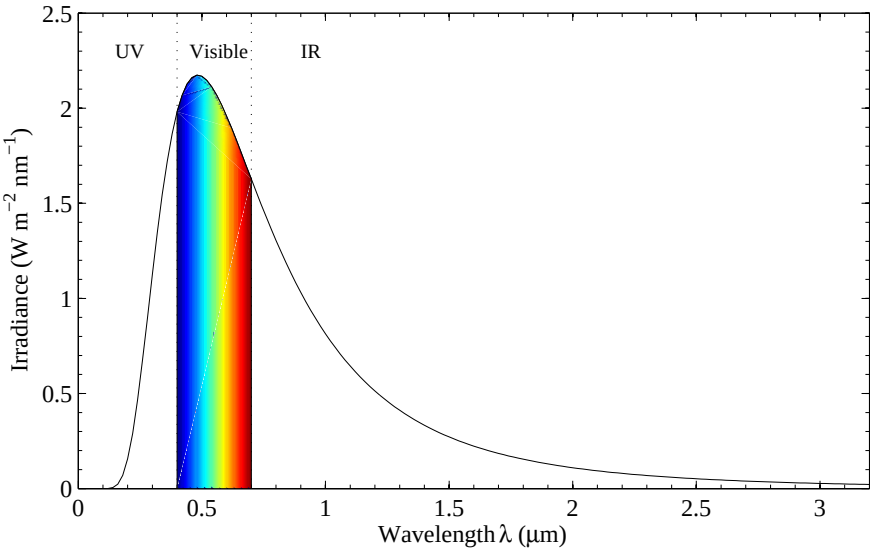

Figure 2.11: Blackbody spectrum for T = 5800 K outside of earth's atmosphere.

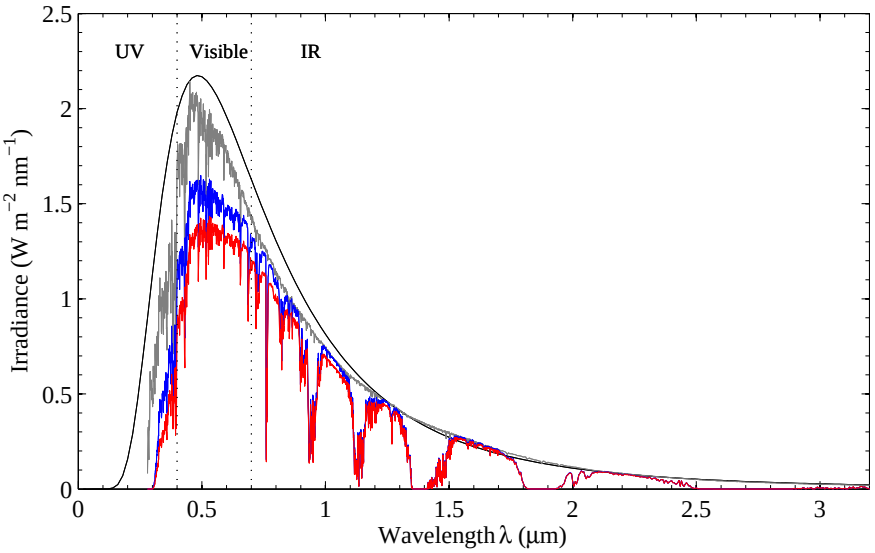

Figure 2.12: Energy curve for a black body at 5800K (black line), outside (grey) and inside (blue) the earth's atmosphere, and at the earth's surface (red line).

also change the spectral distribution of the energy (i.e. will alter the shape of the energy curve in Fig 2.11). To account for these effects, the model presented by Gueymard et al. (2002) was used (Fig 2.12). By integrating between the ultraviolet, visible and infrared portions of the short-wave spectrum we are able to calculate the proportion of energy in each region. The percentage of energy confined within each section is then calculated as the ratio of the energy within that region and the energy within the entire spectra (Table 2.5).

By calculating the percentage of ultraviolet ($0.1\ \mu\text{m} \leq \lambda < 0.4\ \mu\text{m}$), visible

Table 2.5: Proportion of different wavelengths to the total energy distribution at the earth's surface calculated following Gueymard et al. (2002).

	Wavelength	% of total	% of total
Ultraviolet	$0.1\ \mu\text{m} \leq \lambda < 0.28\ \mu\text{m}$	0	-
	$0.28\ \mu\text{m} \leq \lambda < 0.315\ \mu\text{m}$	0.1	6.7
	$0.315\ \mu\text{m} \leq \lambda < 0.4\ \mu\text{m}$	6.6	
Visible light	$0.4\ \mu\text{m} \leq \lambda < 0.7\ \mu\text{m}$	42.0	42.0
Infrared	$0.7\ \mu\text{m} \leq \lambda < 0.8\ \mu\text{m}$	11.4	
	$0.8\ \mu\text{m} \leq \lambda < 0.825\ \mu\text{m}$	2.3	
	$0.825\ \mu\text{m} \leq \lambda < 0.9\ \mu\text{m}$	7.2	
	$0.9\ \mu\text{m} \leq \lambda < 0.925\ \mu\text{m}$	1.7	
	$0.925\ \mu\text{m} \leq \lambda < 1\ \mu\text{m}$	4.0	49.8
	$1\ \mu\text{m} \leq \lambda < 1.2\ \mu\text{m}$	10.1	
	$1.2\ \mu\text{m} \leq \lambda < 1.8\ \mu\text{m}$	12.2	
	$1.8\ \mu\text{m} \leq \lambda < 2\ \mu\text{m}$	0.1	
	$2\ \mu\text{m} \leq \lambda < 2.4\ \mu\text{m}$	0.6	
	$> 2.4\ \mu\text{m}$	0.1	

($0.4\ \mu\text{m} \leq \lambda < 0.7\ \mu\text{m}$), and infrared ($0.7\ \mu\text{m} \leq \lambda$) radiation within the energy spectrum, the relative importance of each of these bands becomes evident. At the

earth's surface, for example, the ultraviolet range accounts for 6.7 % of the total short-wave radiation, visible light accounts for 42 % of the short-wave spectrum, and infrared accounts for 49.8 % of the short-wave spectrum. The attenuation coefficient, however, can influence the amount of radiation that penetrates to a given depth in the water column, and thus, the amount of radiation that penetrates to a certain depth in the water column is lower.

The attenuation coefficient can differ greatly with wavelength. For the visible range, the attenuation coefficient can be calculated following a number of different methods, listed here in order of preferential data sources, 1) exponential fits of *in situ* measurements of downwelling irradiance in the 0.4 to 0.7 μm range, 2) a model which includes the attenuating properties of water, dissolved organic carbon concentration, and chlorophyll *a* (Morris et al., 1995), or 3) a function of Secchi depth (Kirk, 1994). For the majority of the lakes studied in this dissertation, K_d estimates were provided by the individual data provider for a given lake. For the lakes in the English Lake District, however, K_d was estimated as a function of Secchi depth (z_{SD}) as:

$$K_d = c_1 / z_{SD}, \tag{2.121}$$

where c_1 is a constant which is dependent on the optical properties of the lake water in which K_d is estimated.

For lakes in the English Lake District, K_d, was calculated from depth-profiles using a cosine-corrected sensor (Li-Cor Li-A92SA), which measures in the spectral range 0.4 to 0.7 μm, and compared to contemporaneous readings of Secchi depth. A total of 67 measurements were made over a year, approximately

fortnightly, at three Cumbrian lakes (Esthwaite Water, Bassenthwaite Lake and Derwent Water) which had contrasting optical properties. Secchi depth ranged between 1.5 and 7.0 m which covered the range of Secchi depths measured here. The best fit to the data was produced using K_d = 1.75/Secchi depth (adjusted r^2 = 0.85; $p < 0.001$) and this produced an average difference between measured and estimated K_d of between 0.03 and 0.06 m^{-1} for the three lakes. Therefore, K_d was estimated as $K_d = 1.75/z_{SD}$ for all of the lakes in the English Lake District.

For the infrared range of the spectrum, the attenuation coefficient depends less on in-water properties and more on general water properties, and thus the values reported by Jellison and Melack (1993) are used in this dissertation. For the ultraviolet range, however, the values reported by Olesen and Maberly (2001) for the attenuation coefficient were used (Fig. 2.13).

To calculate the percentage of short-wave radiation that reaches a particular depth (e.g. I_{1m} is the percentage of short-wave radiation reaching a depth of 1 m) in the water column, the Beer Lambert law was used as:

$$I_{1m} = I_0 \exp^{(-K_d z_{mix})}, \tag{2.122}$$

where I_0 is the radiation measured at the lake surface. Using the attenuation coefficients calculated for lakes in the English Lake District, a limited proportion of ultraviolet and infrared radiation is calculated to penetrate beneath a depth of 1.5 m (Table 2.6), which is the minimum upper mixed layer depth calculated for these lakes, only the visible component of short-wave radiation was considered as having a substantial influence on the upper mixed layer. The percentage of short-wave radiation that penetrates beneath the upper mixed layer can, therefore,

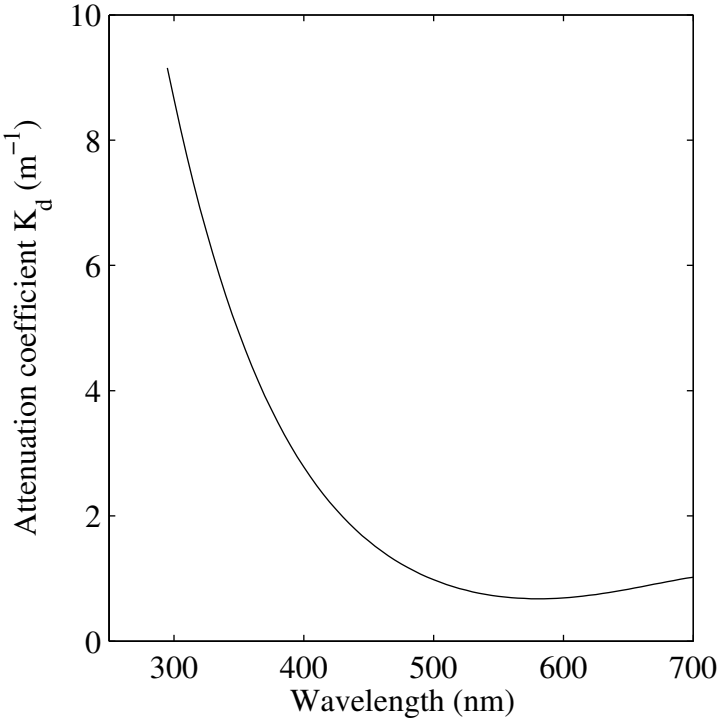

Figure 2.13: Attenuation coefficient in Esthwaite Water. Re-drawn from Olesen and Maberly (2001).

be approximated solely as a function of the radiation within the visible range. From these calculations, it is safe to assume that the visible component of short-wave radiation is the only part of the short-wave spectrum that penetrates beneath the depth of the upper mixed layer. Furthermore, the visible component of short-wave radiation, R_0 in equation 2.4, can be estimated from short-wave radiation measurements at the lake surface as:

$$R_0 = Q_{sin} \times 0.42, \tag{2.123}$$

which expresses R_0 in energy units (i.e. W m^{-2}).

Table 2.6: Same as Table 2.5 but also including the percentage of radiation that reaches a depth of 1.5 m.

	Wavelength	% of total	% of total	K_d (m^{-1})	% of total at 1.5 m
Ultraviolet	$0.1\ \mu m \leq \lambda < 0.28\ \mu m$	0		-	0
	$0.28\ \mu m \leq \lambda < 0.315\ \mu m$	0.1	6.7	8.2	4.6×10^{-7}
	$0.315\ \mu m \leq \lambda < 0.4\ \mu m$	6.6		4.5	4.8×10^{-3}
Visible light	$0.4\ \mu m \leq \lambda < 0.7\ \mu m$	42.0	42.0	c_1/z_{SD}	-
Infrared	$0.7\ \mu m \leq \lambda < 0.8\ \mu m$	11.4		1.1	2.2
	$0.8\ \mu m \leq \lambda < 0.825\ \mu m$	2.3		2.25	0.08
	$0.825\ \mu m \leq \lambda < 0.9\ \mu m$	7.2		3.4	0.04
	$0.9\ \mu m \leq \lambda < 0.925\ \mu m$	1.7		14.7	4.5×10^{-10}
	$0.925\ \mu m \leq \lambda < 1\ \mu m$	4.0	49.8	26	4.6×10^{-17}
	$1\ \mu m \leq \lambda < 1.2\ \mu m$	10.1		448	1.4×10^{-291}
	$1.2\ \mu m \leq \lambda < 1.8\ \mu m$	12.2		870	0
	$1.8\ \mu m \leq \lambda < 2\ \mu m$	0.1		4335	0
	$2\ \mu m \leq \lambda < 2.4\ \mu m$	0.6		7800	0
	$> 2.4\ \mu m$	0.1		-	-

2.10 Statistical methods

During this dissertation, a number of statistical approaches were used to investigate the relationship between lake specific features and the diel temperature range. The basic statistical approaches used include means, medians, standard deviations, Pearson's correlations and Spearman's rank correlation (Manly, 2008). In this section, the statistical modelling techniques used in this dissertation are described, including linear regression models, generalised linear models and generalised additive models.

2.10.1 A simple linear model

This section introduces the statistical methods for a linear model. A simple linear regression is a statistical model that assumes a linear relationship between a continuous response variable y and one or more, usually continuous, predictor variables, $X = x_1, ..., x_n$. Consider the case of a single predictor variable x and its relationship to y. A simple form for such a model is:

$$y_i = \beta_0 + x_i\beta_1 + \varepsilon_i, \tag{2.124}$$

where β_0 is the intercept i.e. the mean of the probability distribution of y when $x = 0$, β_1 is the slope, which measures the rate of change in y for a per-unit change in x, and ε_i is the residual error i.e. the information not explained by the model. The main idea behind the linear model is to estimate the values of β_0 and β_1. These parameters can be estimated using least-squares, solving this model

by minimizing the Residual Sum of Squares (RSS) as:

$$RSS = \sum_{i=1}^{n} \varepsilon_i^2 = \sum_{i=1}^{n} (y_i - \hat{y}_i)^2 = \sum_{i=1}^{n} (y_i - \beta_0 - \beta_1 x_i)^2, \tag{2.125}$$

where $\hat{y}_i$ is is the predicted value. A simple linear regression model is a very useful tool to model the relationship between one predictor and one explanatory variable.

Several predictor variables are often needed to explain an observed phenomena. A regression model that can include a number of predictors is, therefore, commonly used. This model is called a multiple linear regression, commonly expressed as:

$$y_i = \beta_0 + x_{1i}\beta_1 + x_{2i}\beta_2 + ... + x_{mi}\beta_m + \varepsilon_i, \tag{2.126}$$

where we have $m+1$ parameters to estimate, one for the intercept and one for each of the m predictors x_m. A number of assumptions are made when using a multiple linear regression model. These assumptions include normality and homogeneity of residuals, and the independence of observations i.e. the y values for one observation should not be influenced by the y values of another observation.

2.10.2 Generalised linear model

Generalised linear models (GLMs) are a synthesis and extension of linear regression models. A GLM, for example, extends the types of data and error distributions that can be modelled beyond the Gaussian (normally distributed) data of linear regression. A GLM consists of three components (i) a random component, specifying the conditional distribution of the response y_i given the values

of the explanatory data; (ii) a linear predictor function (η_i):

$$\eta_i = \beta_0 + x_{1i}\beta_1 + x_{2i}\beta_2 + ... + x_{ki}\beta_k, \tag{2.127}$$

where X_{ij} are prescribed functions of the explanatory variables; and (iii) a smooth and invertible link function $g(\cdot)$, which transforms the expectation of the response $\mu_i \equiv E(Y_i)$ to the linear predictor:

$$g(\mu_i) = \eta_i = \beta_0 + x_{1i}\beta_1 + x_{2i}\beta_2 + ... + x_{ki}\beta_k. \tag{2.128}$$

This allows for the residuals to be non-normally distributed and is what separates GLMs from a linear model. While there is a great deal to explore further with regards to generalised linear models, the main point here is to note that they are essentially a generalisation of the typical linear model.

2.10.3 Generalised additive model

A Generalised Additive Model (GAM) is a semi-parametric extension of the GLM in which the linear predictors depend on smooth functions of some predictor variables. For a single covariate, for example, a GAM has the form:

$$g(\mu_i) = \eta_i = \beta_0 + f_1(x_{1i}), \tag{2.129}$$

where f_1 is a smoothing function (Hastie and Tibshirani, 1990). A GAM consisting of smooth terms for several variables has the form:

$$g(\mu_i) = \eta_i = \beta_0 + f_1(x_{1i}) + f_2(x_{2i}) + ... + f_k(x_{ki}) = \sum_{k=1}^{m} f_k(x_{ki}). \quad (2.130)$$

The smooth functions can be one of many types. One example is a spline, which is a smooth polynomial function that is piecewise-defined, and possesses a high degree of smoothness at the places where the polynomial pieces connect. This is the smoother used in this dissertation. In all other respects, GAM's are similar to GLM's (link functions, error distributions, etc.), the main difference being that the amount of smoothing can be controlled.

2.10.4 Statistical model selection

When conducting statistical analyses, it is important to estimate the effect of a predictor variable on a response variable and it's precision. In certain instances, however, it is also essential to assess whether the effect of a given predictor is sufficiently important to include in a statistical model. This is an issue of model selection and is often the case in observational studies, where a number of variables are believed to explain a given process or pattern. In this dissertation, a GAM is used to explain the observed variation in the diel temperature range with a number of lake specific characteristics (e.g. lake surface area, altitude, latitude, water clarity). To test which predictor variable or which combination of predictor variables best explained the observed pattern, a set of candidate models are specified, which are made up of every possible combination of predictor variables. In order to select the 'best' model, the candidate models are ranked according to the

relative support for each candidate model according to the Akaike Information Criterion (AIC), which is defined as (Burnham and Anderson, 1998):

$$AIC = -2\log(\log L) + 2k, \tag{2.131}$$

where k is the number of estimated parameters included in the model (i.e. number of predictor variables and the intercept) and logL is the maximized log-likelihood function for the estimated model. The AIC penalises for the addition of parameters, and thus selects a model that fits well but has a minimum number of parameters. For small datasets (i.e. n/k $<\sim$40), the second-order Akaike Information criterion (AICc) is commonly used. The AICc can be calculated as:

$$AICc = -2(\log L) + 2k + \frac{[2k(k+1)]}{(n-k-1)}. \tag{2.132}$$

As sample size increases, the last terms of the AICc approaches zero, and the AICc tends to yield the same conclusions as the AIC (Burnham and Anderson, 1998).

The absolute values of the AIC have no meaning. It becomes useful, however, when comparing the AIC of a series of candidate models. The model with the lowest AIC, for example, is the best model among all models specified for the data. It is important to note, however, that if only poor models are considered, the AIC will select the best of the poor models. Two measures associated with the AIC can be used to compare models: ΔAIC and Akaike weights (w_i). The ΔAIC_i is a measure of the AIC of each model relative to the best model, and is

calculated as:

$$\Delta AIC = AIC_i - \min(AIC), \tag{2.133}$$

where AIC_i is the AIC value for model i and $\min(\mathrm{AIC})$ is the AIC value of the best model. As a rule of thumb, a ΔAIC of less than 4 suggests substantial evidence for the model, a ΔAIC between 4 and 7 indicate that the model has considerably less support, and a ΔAIC of less than 10 indicates that the model is very unlikely (Burnham and Anderson, 1998). Akaike weights provide another measure of the strength of evidence for each model, and represent the ratio of $\Delta\mathrm{AIC}_i$ values for each model relative to the entire set of candidate models. The Akaike weight, w_i, can be calculated as:

$$w_i = \frac{\exp\left(-\frac{1}{2}\Delta\mathrm{AIC}_i\right)}{\sum_{r=1}^{R} \exp\left(-\frac{1}{2}\Delta_r\right)}, \tag{2.134}$$

where Δ_r is the $\Delta\mathrm{AIC}_i$ of model r i.e. one of the candidate models. The Akaike weight indicates the probability that the model is the best among the whole set of candidate models. An Akaike weight of 0.60, for example, indicates that given the data, the model has a 60 % chance of being the best one among those considered in the set of candidate models. Furthermore, the Akaike weights of the best model can be compared with the competing models to determine to what extent is one model better than another. These are termed evidence ratios and can be calculated as:

$$\text{Evidence ratio} = \frac{w_j}{w_i}, \tag{2.135}$$

where model j is compared against model i. This method can be used to assess the degree of uncertainty regarding the best model, and for small evidence ratios,

it can suggest that the rank of the models may change if a different dataset of the same size was used (Burnham and Anderson, 1998). Akaike weights are also useful to give a measure of the relative importance of a predictor variable, which can be achieved by simply multiplying the Akaike weights with the parameter estimate among all of the candidate models that include that predictor variable:

$$\text{Model average estimate} = \hat{\theta} = \sum_{i=1}^{R} w_i \hat{\theta}_i, \tag{2.136}$$

where $\hat{\theta}_i$ is the parameter estimate for model i.

Chapter 3

Accurate calculation of surface energy fluxes with high-frequency lake buoy data

3.1 Introduction

As part of the PhD project, a program called 'Lake Heat Flux Analyzer' was developed to calculate accurately the surface energy fluxes in lakes with high-frequency lake buoy data (Chapter 2). Lake Heat Flux Analyzer is openly available and can be used to process data from multiple lakes rapidly. It provides a means of calculating the surface fluxes using a consistent method, thereby facilitating global comparisons of high-frequency data from lake buoys. In this chapter, some of the outputs of the program are shown for Esthwaite Water (United Kingdom) in 2009. To demonstrate its use for lakes globally, the surface energy fluxes for two additional lake datasets (Lake Mendota, USA, and Rotorua, New

Zealand) are shown.

3.2 Meteorological conditions at Esthwaite Water

In 2009, air temperature for Esthwaite Water had a clear and expected seasonal cycle (Fig. 3.1), varying from, on average, less than 5 °C in winter to more than 15 °C in summer, but with much day-to-day and within day variation. The average wind speed at the reference height (2.14 m) was about 2.4 m s^{-1} with little systematic seasonal pattern (Fig. 3.2), although summer (Jun, July, August) average wind speeds were marginally lower than the winter (Jan, Feb) ones, calculated as 2.3 and 2.4 m s^{-1}, respectively. The relative humidity was continuously high, averaging 86 % with summer humidities typically being lower than the winter ones (Fig. 3.3). Daily-averaged humidity virtually never dropped below 60 % but frequently exceeded 90 %. Incoming short-wave radiation was highly variable at both the diel and seasonal time scale with an annual average of 108 W m^{-2} (Fig. 3.4). Maximum hourly-averaged incoming short-wave radiation, however, was much greater, reaching 950 W m^{-2} in mid-June, corresponding to the summer solstice. Surface water temperature, similar to air temperature, followed a typical annual pattern, being high in summer and low in winter (Fig. 3.5). Unlike air temperature, however, the surface water temperature varied much less at diel timescales, often fluctuating by less than 2 °C of the daily-averaged temperature.

By examining the hourly data, the diel cycle in the meteorological variables may be diagnosed (Fig. 3.6). It is clear that air and water temperature, wind speed, incoming short-wave radiation and relative humidity change sys-

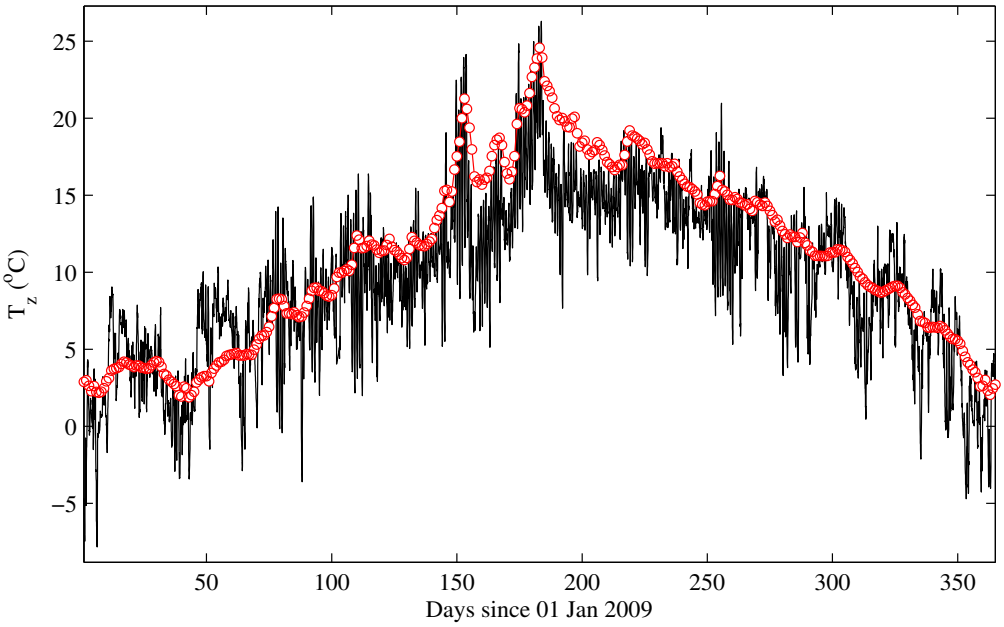

Figure 3.1: Hourly (black) and daily-averaged (red) air temperature measurements for Esthwaite Water at a height of 2.14 m above the lake surface.

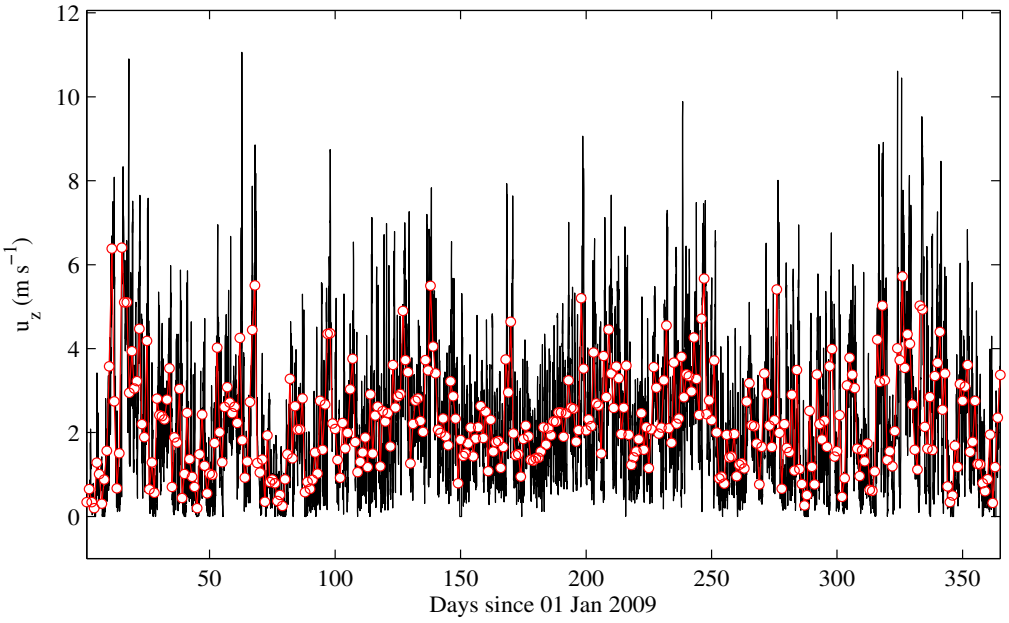

Figure 3.2: Hourly (black) and daily-averaged (red) wind speed measurements for Esthwaite Water at a height of 2.85 m above the lake surface.

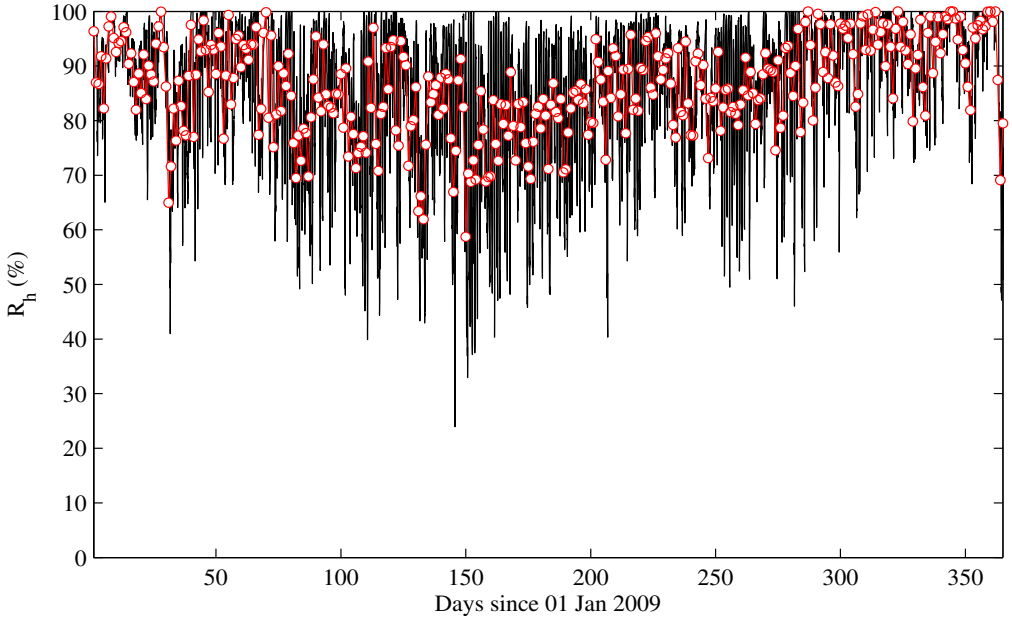

Figure 3.3: Hourly (black) and daily-averaged (red) relative humidity measurements for Esthwaite Water at a height of 2.14 m above the lake surface.

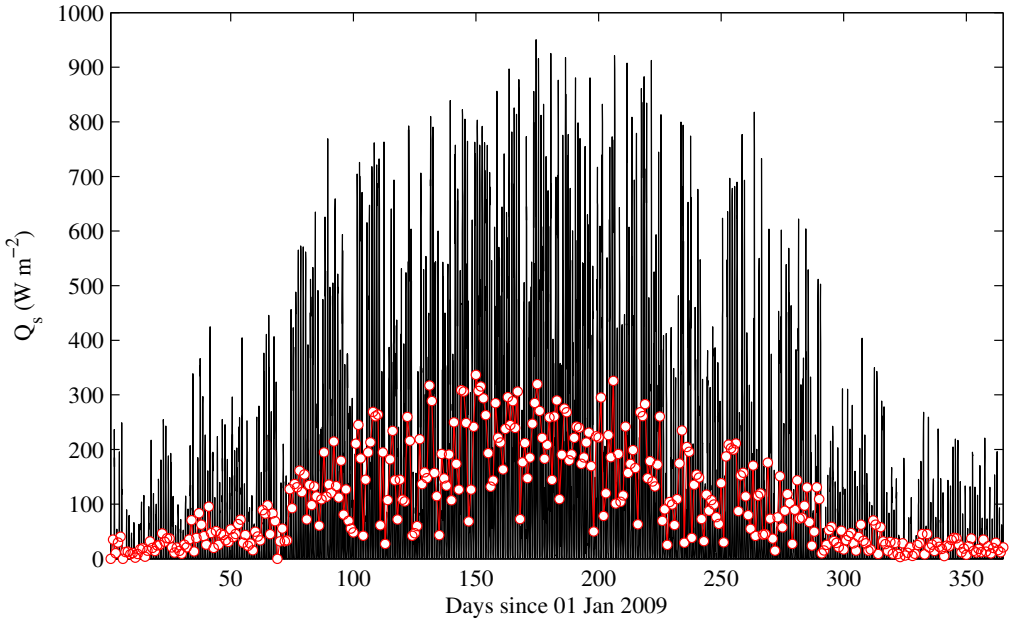

Figure 3.4: Hourly (black) and daily-averaged (red) short-wave radiation measurements for Esthwaite Water.

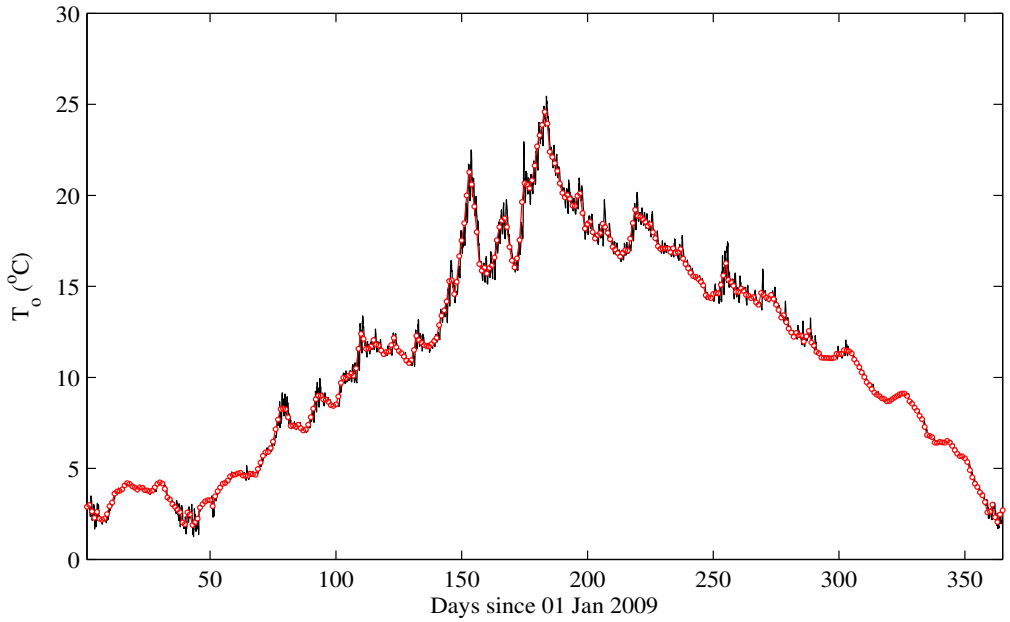

Figure 3.5: Hourly (black) and daily-averaged (red) surface water temperature measurements for Esthwaite Water.

tematically through the day. Air temperatures on average rose by approximately 3 °C from the early morning to mid-afternoon. The amplitude of change in surface water temperature during a diel cycle was generally lower than that of air temperature, rising by approximately 0.5 °C from the early morning to mid-afternoon (Fig. 3.6a). Relative humidities correspondingly dropped by about 15 % between these times (Fig. 3.6b). Incoming short-wave radiation varied by just over 300 W m^{-2} over a diel cycle, reaching a maximum at approximately 1500 (Fig. 3.6c). The most interesting change, however, was arguably in wind speed, which was characterised by late afternoon wind speeds being more than 50 % greater than the night-time ones (Fig. 3.6d).

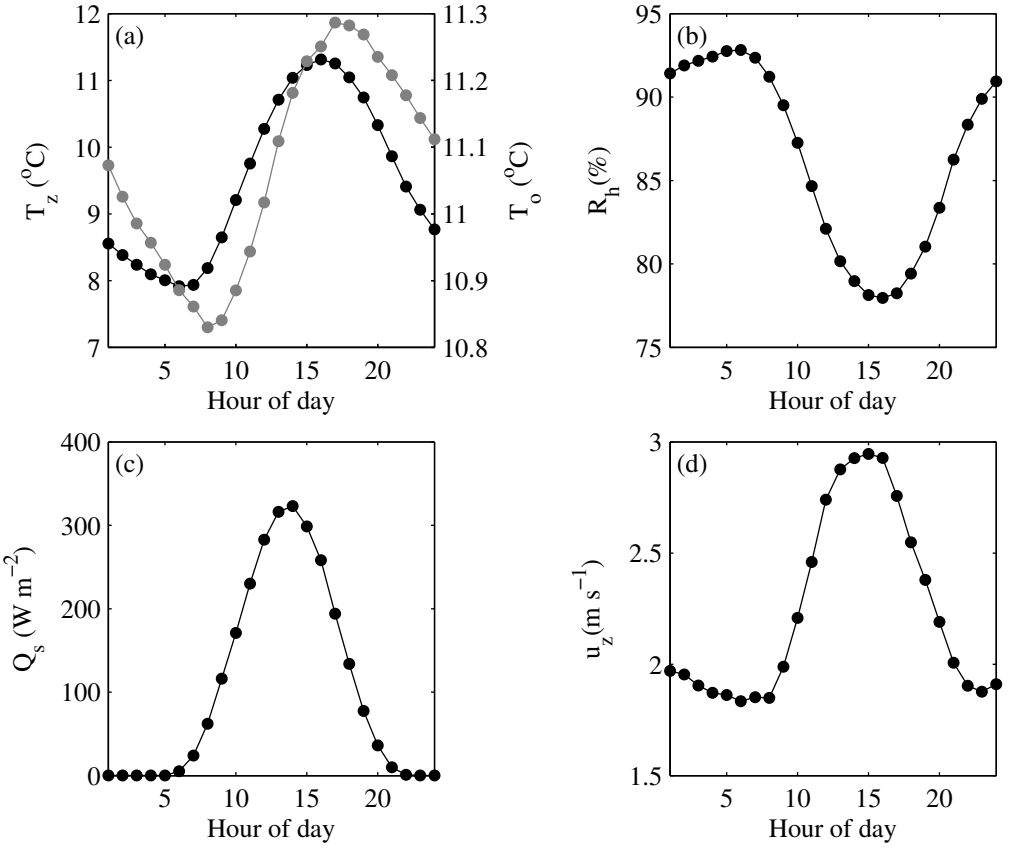

Figure 3.6: Annually-averaged diel cycle in (a) air (T_z, black) and surface water (T_0, grey) temperature, (b) relative humidity, (c) incoming short-wave radiation, and (d) wind speed.

3.3 Temporal variability in surface energy fluxes at Esthwaite Water

There was a recognisable seasonal cycle among the majority of the heat flux components as well as the total surface heat flux in Esthwaite Water. There was also a large daily and intra-annual variation in the heat fluxes. In 2009, the reflected short-wave radiation was highly variable with minimal seasonal

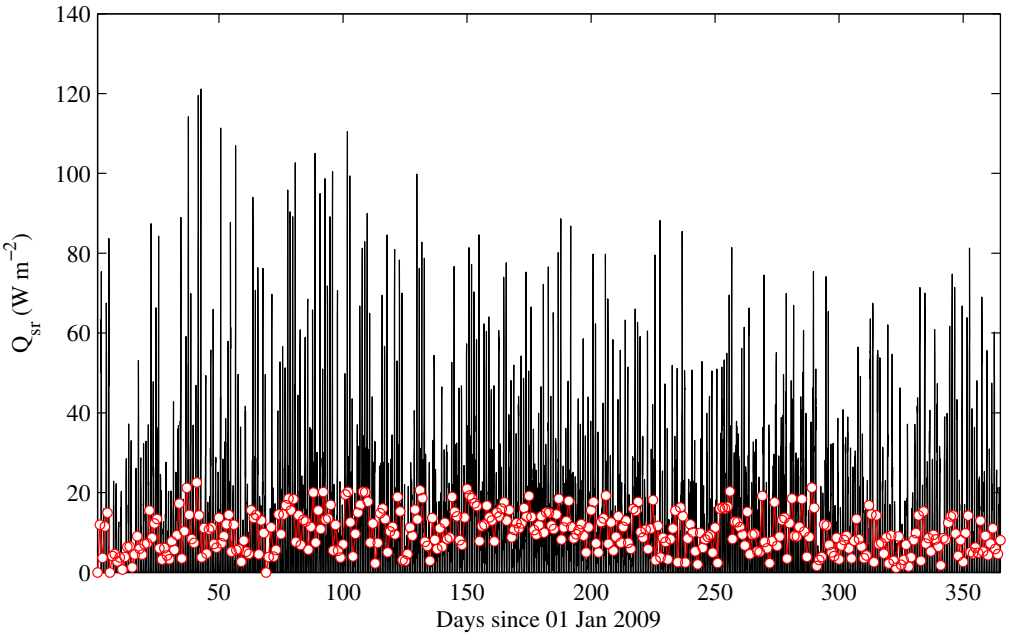

Figure 3.7: Hourly (black) and daily-averaged (red) reflected short-wave radiation, Q_{sr}, estimates for Esthwaite Water.

pattern (Fig. 3.7). Maximum reflected short-wave radiation (120 W m^{-2}) was calculated in February, which was over an order of magnitude greater than the annual mean reflected short-wave radiation (10 W m^{-2}). Incoming long-wave radiation (Fig. 3.8a), which acts to warm the lake surface, was substantially lower than the outgoing long-wave radiation (Fig. 3.8b) through the year, being 54 W m^{-2} lower on average (i.e. annual average for the hourly data). Incoming long-wave radiation was more variable than the outgoing long-wave radiation at diel timescales, being driven by the diel range in the main driving variables, air and water temperature, respectively.

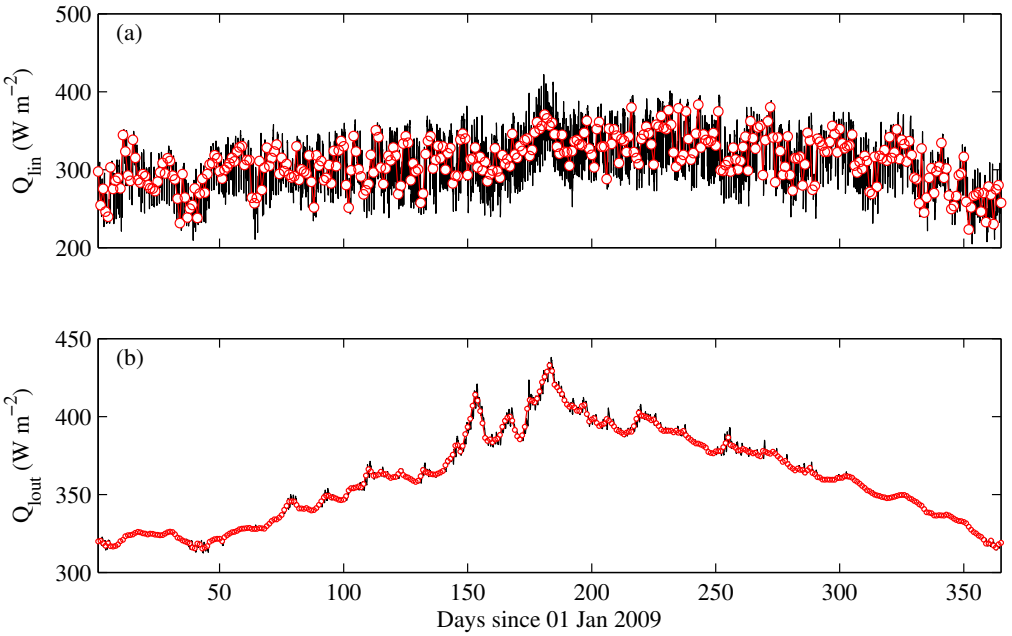

Figure 3.8: Hourly (black) and daily-averaged (red) (a) incoming, Q_{lin}, and (b) outgoing, Q_{lout}, long-wave radiation estimates for Esthwaite Water.

Although usually smaller than the radiative fluxes, the two turbulent fluxes of latent and sensible heat (Fig. 3.9) are important as they can both be either warming or cooling fluxes. They therefore act as a feedback mechanism, cooling the lake if it becomes warmer than the overlying air and warming the lake if it becomes cooler than the air. Both latent and sensible heat fluxes follow a seasonal cycle, being large in summer and low in winter (Fig. 3.9). Of the two turbulent fluxes, the larger in Esthwaite Water is the latent heat flux (Fig. 3.9a), being 19 W m^{-2} larger on average (i.e. annual average for the hourly data). The latent heat flux can also be negative (i.e. heat entering the lake), e.g. during dew formation, as is seen on day of year 320. The sensible heat flux (Fig. 3.9), however, may be larger than the latent heat flux during certain periods of the year, as

occurred in Esthwaite Water during winter. On day of year 325, for example, the sensible heat flux was 18 W m^{-2} higher than the latent heat flux.

The total surface heat flux demonstrates a clear seasonal cycle being predominantly positive (i.e. heating) in summer and negative (i.e. cooling) in winter (Fig. 3.10). From the hourly-averaged data, heat can be seen to be leaving the lake at the start of the year, but starts entering the lake around March, reaching its maximum in May-June and then starts leaving the lake again in September. As the total surface heat flux is the sum of its constituent parts the seasonal cycle was not necessarily the same as any of the individual heat fluxes. Incoming short-wave radiation, for example, was a large contributor to the total daily surface heat flux in Esthwaite Water during the stratified period (Fig. 3.11a), often being up to three times larger than the net long-wave radiation, which is generally a cooling term, and an order of magnitude larger than the reflected short-wave radiation. During the non-stratified period, however, incoming long-wave radiation is the dominant heating term. As outgoing long-wave radiation is often greater than the incoming long-wave radiation, net long-wave radiation is, therefore, predominantly a cooling term through most of the year. Of the surface turbulent fluxes (Fig. 3.11b), the latent heat flux is the largest contributor to the total surface heat flux in Esthwaite Water, being twice that of the sensible heat flux for the selected period.

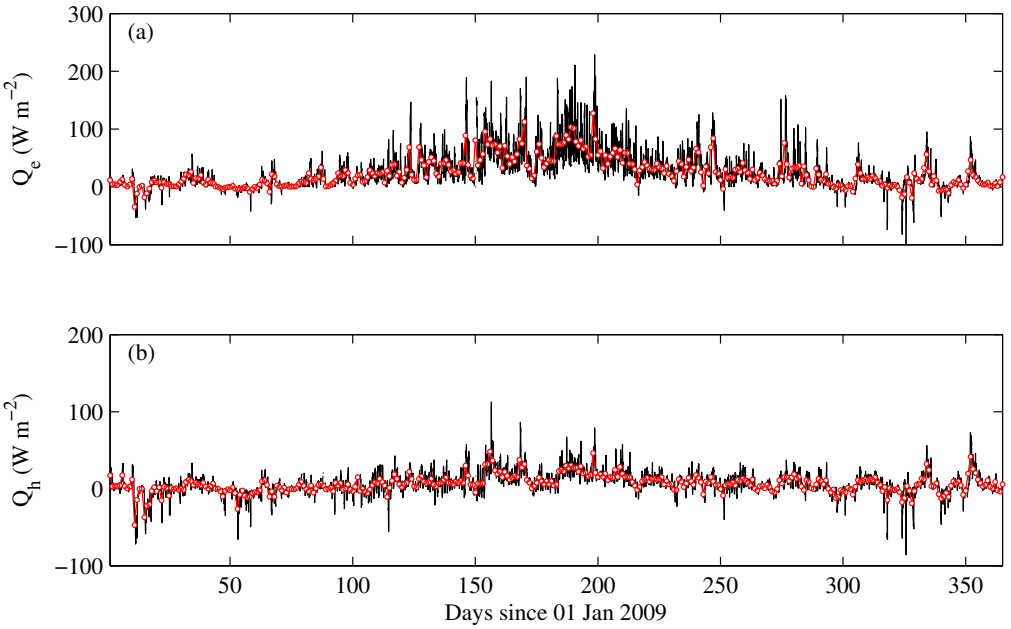

Figure 3.9: Hourly (black) and daily-averaged (red) (a) latent, Q_e, and (b) sensible, Q_h, heat flux estimates for Esthwaite Water.

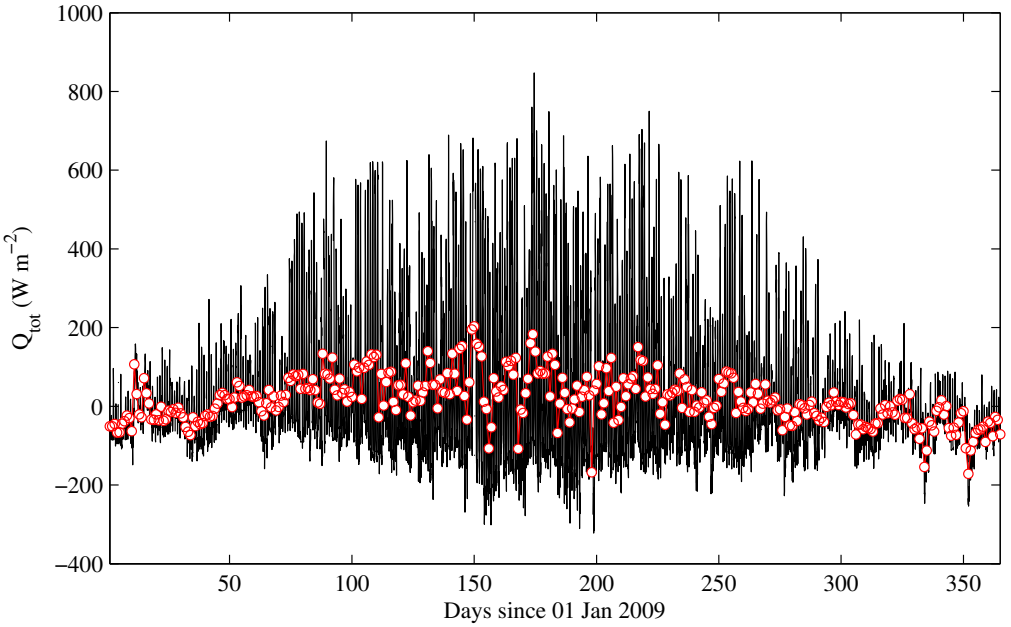

Figure 3.10: Hourly (black) and daily-averaged (red) total surface heat flux, Q_{tot}, estimates for Esthwaite Water.

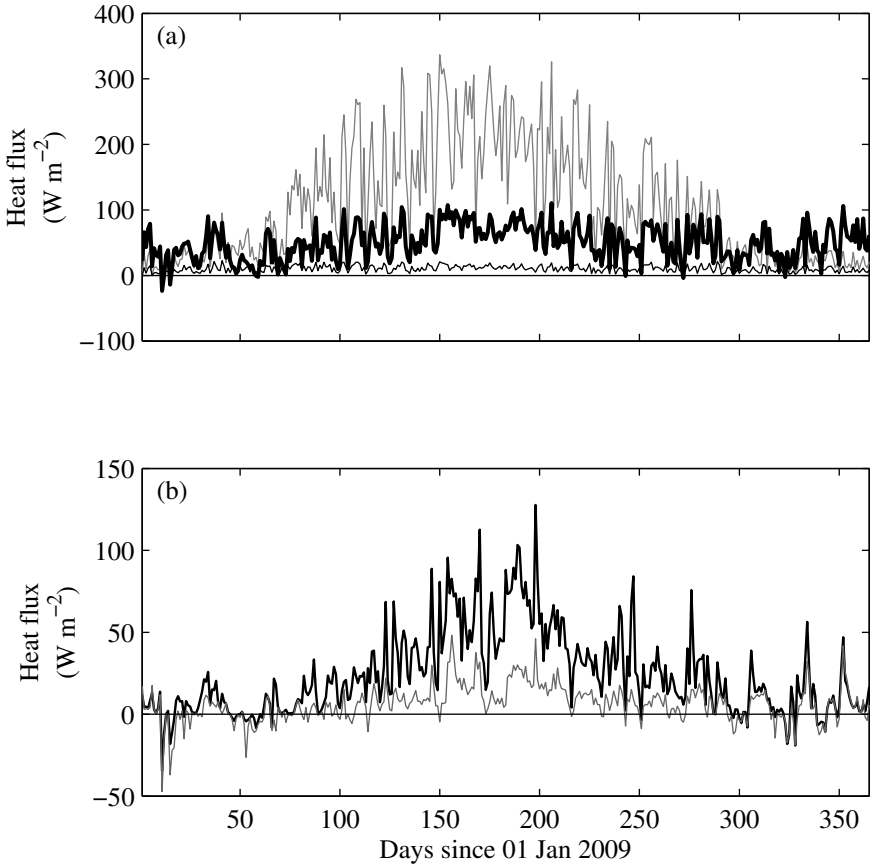

Figure 3.11: Time series of daily-averaged (a) incoming (grey) and reflected (thin black) short-wave radiation, and net long-wave radiation (thick line); (b) latent (black) and sensible (grey) heat flux in Esthwaite Water.

Hourly output of Lake Heat Flux Analyzer demonstrated a distinct diel cycle in both of the turbulent surface fluxes as well as the total surface heat flux (Fig. 3.12). It is clear that both latent and sensible heat fluxes change systematically throughout the day (Fig. 3.12a). The latent surface heat flux, for example, rose by approximately 10 W m^{-2} from early morning to the mid-afternoon. The sensible heat flux, however, was highest in early morning and lowest in mid-afternoon, where an annually-averaged diel range of 9 W m^{-2} was calculated.

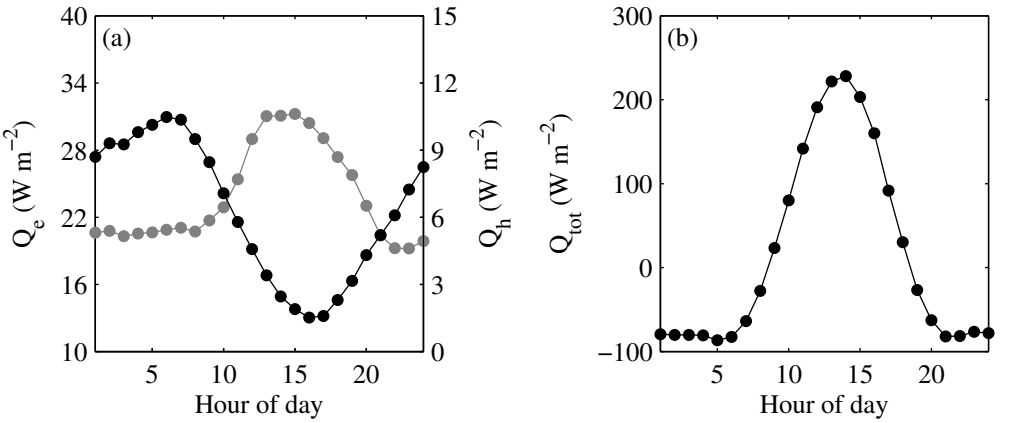

Figure 3.12: Annually-averaged diel cycle in (a) latent (Q_e, grey) and sensible (Q_h, black) heat flux, and (b) total surface heat flux (Q_{tot}).

The annually-averaged total surface heat flux varied by just over 310 W m^{-2} over a diel cycle, reaching a maximum of 228 W m^{-2} at approximately 1400 to 1500 (Fig. 3.12b).

Meteorological forcing, and thus, the surface energy fluxes are highly variable. It is therefore essential to be able to investigate these at a range of temporal scales. This is illustrated by examining a seven-day period during summer, in which, the hourly-averaged wind speed varied from $<$ 1 to 8 m s^{-1}. Differences between wind speed at the measurement height (2.85 m) and those estimated at a height of 10 m by Lake Heat Flux Analyzer were variable throughout the study period (Fig. 3.13a). On day of year 301, for example, the estimated wind speed at 10 m was approximately 40 % greater than at the measurement height, whereas on day of year 297 they were about equal. During low-wind conditions the stability parameter ($z_u L_w^{-1}$) was negative (Fig. 3.13b), often reaching the lower threshold of -15 that is commonly used as a cut-off during the computation of the stability parameter (e.g. Imberger and Patterson, 1990; MacIntyre et

al. 2002), and the drag coefficient was high (Fig. 3.13c). Furthermore, as the stability parameter approached zero, the drag coefficients at 10 m closely matched those calculated at the measurement height. When the stability parameter approached zero during high winds, the transfer coefficient was generally low. The need to calculate transfer coefficients accurately at high-resolution is illustrated by the large changes evident in the drag coefficient, varying by over an order of magnitude within a 24 hour period (e.g. day 296-297). When the atmosphere was stable ($z_u L_w^{-1} > 0$), C_{d10} was lower than C_{dz} and when the atmosphere was unstable ($z_u L_w^{-1} < 0$), estimates of C_{d10} were higher than C_{dz}. The momentum flux, τ, also varied by an order of magnitude, closely following the change in wind speed, where a sharp increase or decrease in wind speed was reflected in an increase or decrease in the momentum flux (Fig. 3.13d).

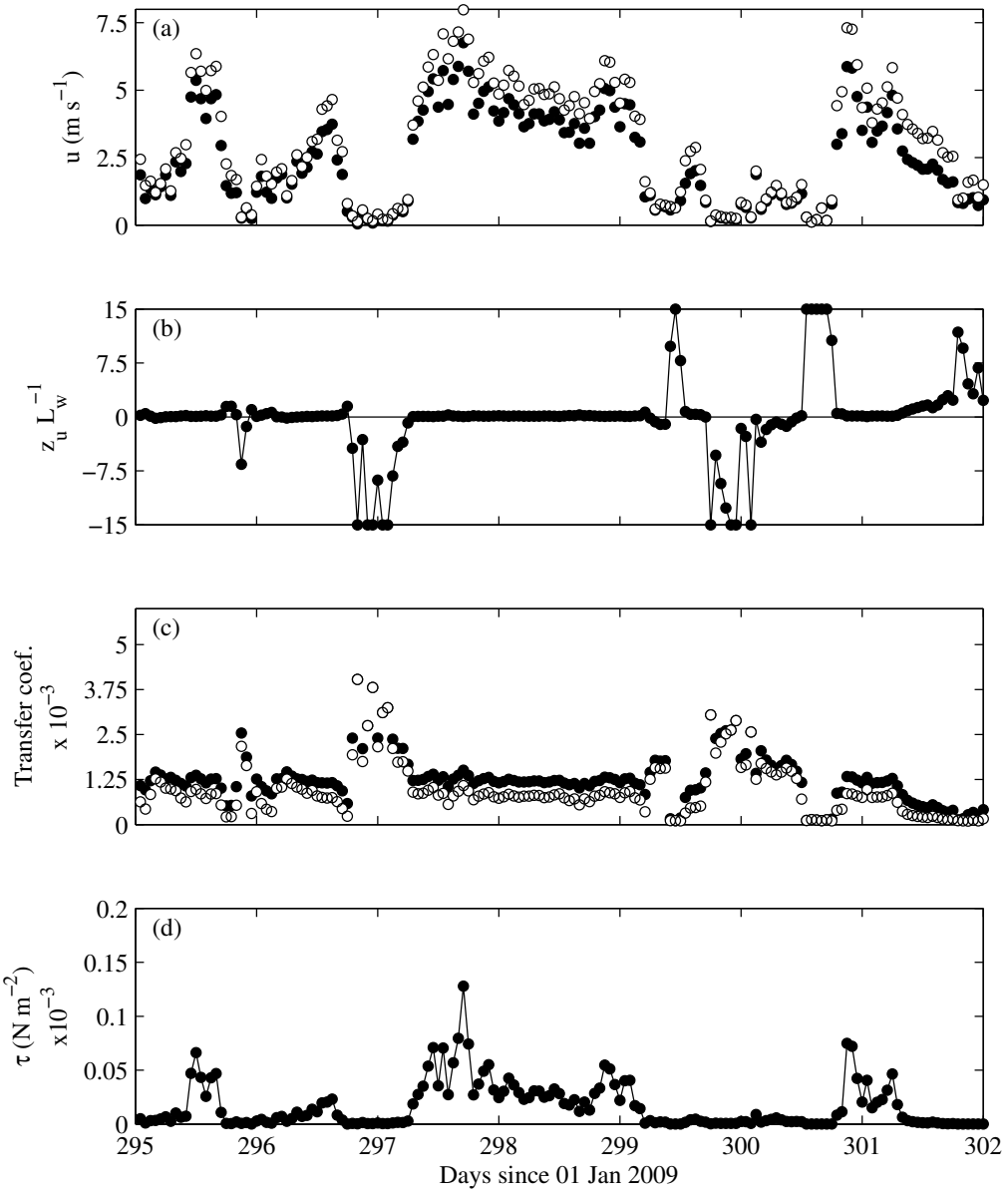

Figure 3.13: High-frequency (hourly) measurements for seven days during the stratified period in Esthwaite Water of (a) wind speed at the measurement height (closed circles) and those estimated at 10 m (open circles); (b) atmospheric stability parameter, $z_u L_w^{-1}$, bounded by ± 15; (c) transfer coefficient for momentum (i.e. drag coefficient) at the measurement height (closed circles) and 10 m (open circles); (d) shear stress (i.e. momentum flux) at the water surface.

An example 24 hour period during spring (Fig. 3.14) highlights the variability in air temperature at high temporal resolution as well as the variability with height above the water surface (Fig. 3.14a). When the atmospheric boundary layer was stable, air temperature at 10 m was marginally higher than at the measurement height. As expected, the transfer coefficient for sensible heat at the measurement height was consistently higher than that at 10 m (Fig. 3.14b). Similar to the transfer coefficient for momentum, the transfer coefficient for heat varied substantially over a 24 hour period. There was also a large hourly variation in the sensible heat flux (Fig. 3.14c), despite the minimal change in lake surface water temperature.

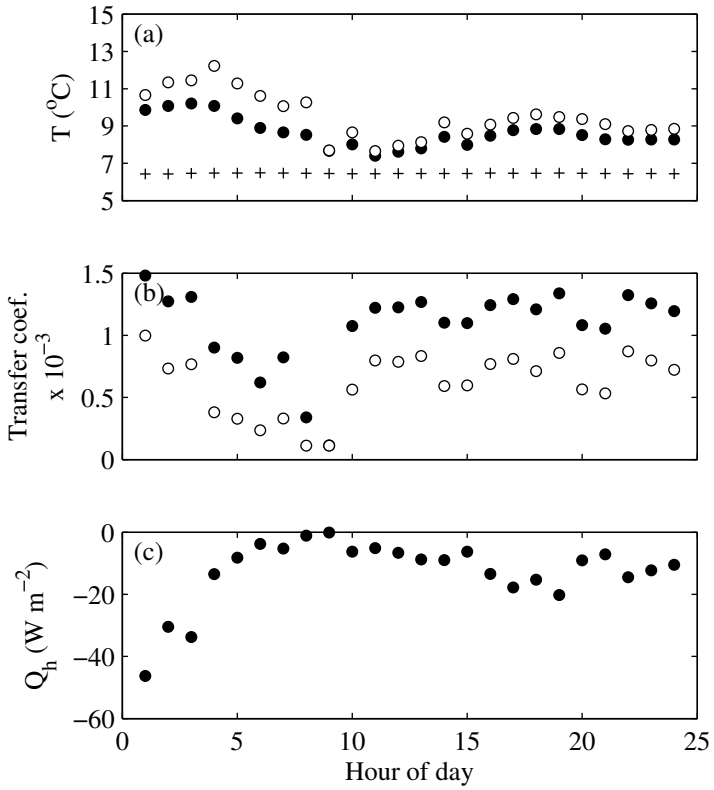

Figure 3.14: High-frequency (hourly) measurements for a 24 hour period in Esthwaite Water, showing (a) air temperature at the measurement height (closed circles), air temperature estimated at 10 m (open circles) and water temperature (plus sign); (b) transfer coefficient for sensible heat at the measurement height (closed circles) and 10 m (open circles); (c) sensible heat flux. Note that negative values represent heat entering the lake.

The transfer coefficients can be calculated following a number of different methodologies, including simple approaches using constants or equations that relate the transfer coefficient to measured wind speeds (e.g. Jones et al., 2005; Mackay et al., 2011; Vachon and Prairie, 2013). As surface flux estimates are sensitive to the choice of transfer coefficient algorithms used (Blanc, 1985; Zeng

et al., 1998), the latent and sensible heat fluxes estimates may vary substantially. In Esthwaite Water, for example, by using (i) constant transfer coefficients of $C_e = C_h$ = 0.00135 (Hicks, 1972; Pond et al., 1974), (ii) transfer coefficient calculated by assuming neutral atmospheric conditions but correcting for measurement height (e.g. MacIntyre et al., 2002), and (iii) transfer coefficients calculated following the methods outlined in Chapter 2, a large variation in the turbulent heat fluxes are calculated. For the latent heat flux, using different transfer coefficient schemes resulted in a maximum bias of up to 30 W m^{-2} in the hourly-averaged estimates for the selected period (Fig. 3.15) and an annually-averaged bias of 55 W m^{-2}. The two-week period shown illustrates large temporal variability in the surface flux estimates at a diel timescale. Similarly, the sensible heat flux estimates vary substantially depending on the transfer coefficient scheme used. For the hourly-averaged data, a maximum bias of 8 W m^{-2} is calculated for the sensible heat flux during the selected period (Fig. 3.16) and an annually-averaged bias of 33 W m^{-2}.

Even small uncertainties in the turbulent surface fluxes can lead to large uncertainties in the total surface heat flux. By calculating the sensible and latent heat fluxes using the three different schemes described above, and then using these values when calculating the total surface heat flux, large differences in the total surface heat flux estimates are calculated (Fig. 3.17). Different transfer coefficient schemes resulted in a maximum monthly-averaged bias of up to 25 W m^{-2} in the total surface heat flux estimates. This error can be put into context by considering its net effect on a lake over an entire year. As an example, Esthwaite Water has a volume (V_{tot}) of about 6 $\times$ 10^6 m^3 and a surface area (A_0) of about 1 $\times$ 10^6 m^2. A bias (ε_{Qtot}) of only 1 W m^{-2} in the surface fluxes estimates would

cause an error in the average change in temperature (ΔT_0) over a year of:

$$\Delta T_0 = \frac{A_0 \times \varepsilon_{Qtot} \times \Delta t}{V_{\text{tot}} \times C_{pw} \times \rho_0}, \tag{3.1}$$

$$\Delta T_0 = \frac{\left(1 \times 10^6\right) \times 1 \times 365 \times 86400}{\left(6 \times 10^6\right) \times 4186 \times 1000}, \tag{3.2}$$

$$\Delta T_0 = 1.26^{\circ}\text{C}, \tag{3.3}$$

where C_{pw} = 4186 J kg^{-1} $^{\circ}$C^{-1} is the specific heat capacity of water at constant pressure, ρ_0 = 1000 kg m^{-3} is an estimate for the density of water, and Δt is time in seconds over a year. An error of 1 W m^{-2} in calculating the surface fluxes, would therefore, translate to being more than a degree in temperature over a year for the whole lake. Thus, a bias in the total surface heat flux can then translate to large errors in predicted water temperatures from numerical models, which often use constants for the transfer coefficient (e.g. Hipsey et al., 2012).

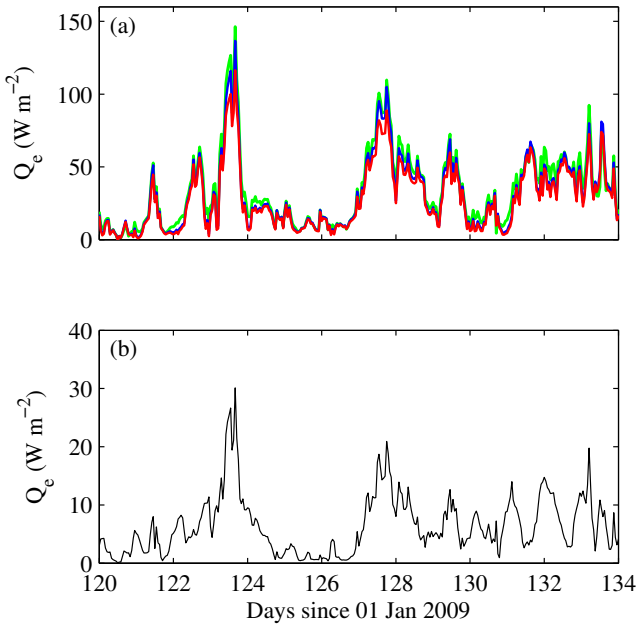

Figure 3.15: Hourly-averaged (a) latent heat flux, Q_e, estimates for Esthwaite Water using a constant transfer coefficient of 0.00135 (red), transfer coefficient calculated by assuming neutral atmospheric conditions but correcting for measurement height (blue), and transfer coefficients calculated following the methods outlined in Chapter 2 (green), and (b) the range in estimated Q_e.

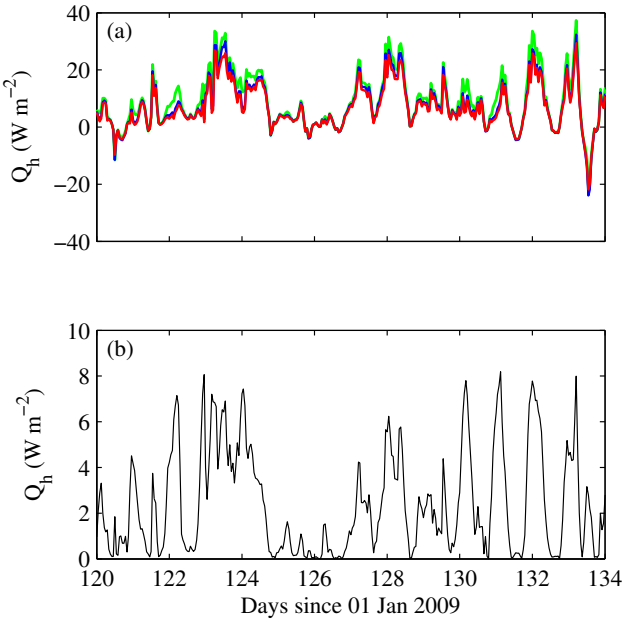

Figure 3.16: Same as Fig. 3.15 but for the sensible heat flux, Q_e

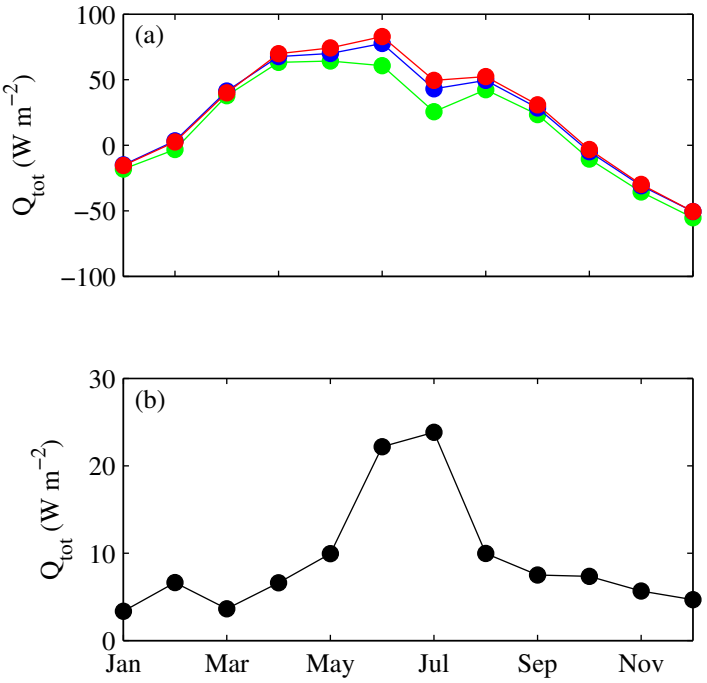

Figure 3.17: Monthly-averaged (a) total surface heat flux, Q_{tot}, estimates for Esthwaite Water using a constant transfer coefficient of 0.00135 (red), transfer coefficient calculated by assuming neutral atmospheric conditions but correcting for measurement height (blue), and transfer coefficients calculated following the methods outlined in Chapter 2 (green), and (b) the range in estimated Q_{tot}.

3.4 Estimating the diel temperature range in Esthwaite Water

By using the calculated surface energy fluxes, the expected diel temperature range for Esthwaite Water can be estimated following the methods presented in Chapter 2. The observed diel temperature range was highly correlated with the estimated diel temperature range for Esthwaite Water with a Spearman's

rank correlation of 0.83. For Esthwaite Water, the greatest diel surface temperature range is expected when the amount of surface heating influencing the upper mixed layer, Q_{zmix}, is large and when the depth of the upper mixed layer is shallow (Fig. 3.18). Average heating of 300 W m^{-2} acting upon a 2 m upper mixed layer, for example, would increase the surface temperature by as much as 2.5 °C for a given day. With either decreased heating or increased upper mixed layer depth, the expected diel temperature change will decrease. For example, a diel temperature range of more than 1 °C is only likely to take place for upper mixed layer depths of less than 4 m, while for surface heating less than 100 W m^{-2} only the shallower surface layers will exhibit a diel temperature range of greater than 0. 5 °C.

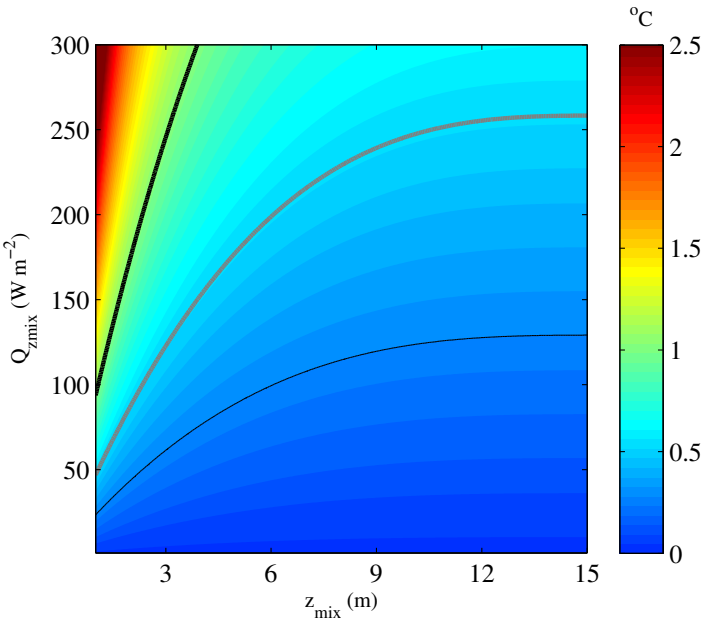

Figure 3.18: Contour plot of the expected diel temperature range for Esthwaite Water as a function of net energy input into the upper mixed layer and upper mixed layer depth. The thick black line refers to an estimated diel range of 1 °C, the thick grey line refers to an estimated diel range of 0.5 °C, and the thin black line refers to an expected diel range of 0.25 °C.

3.5 Global comparisons using Lake Heat Flux Analyzer

Despite recent efforts to develop transfer coefficient algorithms no single method is consistently used to calculate the energy fluxes in lakes. An additional source of uncertainty in comparing surface fluxes is that data are often measured at different heights above the water surface on different lakes. Lake Heat Flux Analyzer, however, can calculate the surface fluxes for many lakes in a consistent

way, by correcting for measurement heights, thus allowing a robust comparison among sites.

For the three example lakes shown here, the daily-averaged wind speed estimated at a height of 10 m varied considerably (Fig. 3.19) among the lakes. As expected, u_{10} was highest for the largest lake Rotorua and lowest for the smallest lake Esthwaite Water. Rotorua, for example, experienced an annually-averaged wind speed of approximately 6 m s^{-1} whereas Esthwaite Water experienced an annually-averaged wind speed of approximately 2.3 m s^{-1}, thus being 3 times larger on average. Lake Mendota experienced an annually-averaged wind speed of 5.2 m s^{-1}, being slightly lower than that estimated for Rotorua, but substantially larger than that estimated for Esthwaite Water.

There was also a considerable difference in the total surface heat flux, Q_{tot} (Fig. 3.20). As expected, Q_{tot} was predominantly positive during summer and negative in winter. The total surface heat flux for Rotorua was generally low during the selected period, as the months shown represent winter in New Zealand. All three lakes demonstrated a seasonal pattern in Q_{tot} , although Lake Mendota experienced the greatest magnitude throughout the period shown. The maximum estimated total surface heat flux for Lake Mendota, for example, was approximately 800 W m^{-2}, which was more than double the maximum total surface heat flux measured for Esthwaite Water.

Daily-averaged data are often not ideal for comparison because of the large amount of intra-annual variability. Longer averages can also be obtained from the Lake Heat Flux Analyzer program to illustrate better the difference among sites. Lake Heat Flux Analyzer can also be used to calculate evaporation. For the three lakes shown here, monthly-averaged evaporation rates were lowest for

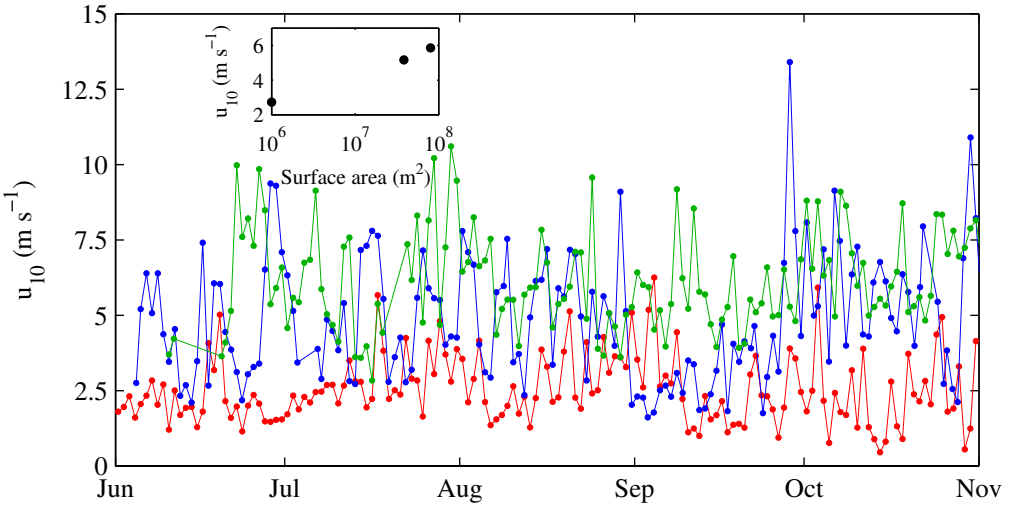

Figure 3.19: Time series of daily-averaged wind speed estimated at a height of 10 m above the lake surface, u_{10}, for Esthwaite Water (red), Lake Mendota (blue) and Rotorua (green) and the relationship between the annually-averaged wind speed and lake surface area for the three lakes (inset).

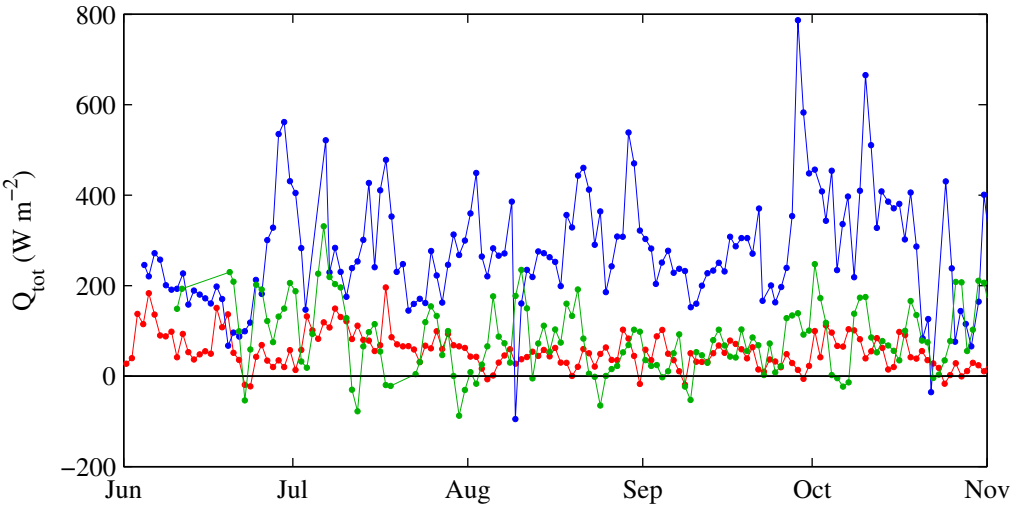

Figure 3.20: Time series of daily-averaged total surface energy fluxes, Q_{tot}, for Esthwaite Water (red), Lake Mendota (blue) and Rotorua (green).

Esthwaite Water and highest for Lake Mendota during the specified months (Fig. 3.21). Seasonal patterns in the evaporation rates occur and were largest in summer and smallest in winter for these lakes. For the Northern Hemisphere lakes, evaporation rates for Lake Mendota were considerably higher than for Esthwaite Water, on occasion being five times as large. For Rotorua, evaporation rates were lowest in July, which corresponds to winter, and highest in November, corresponding to late spring.

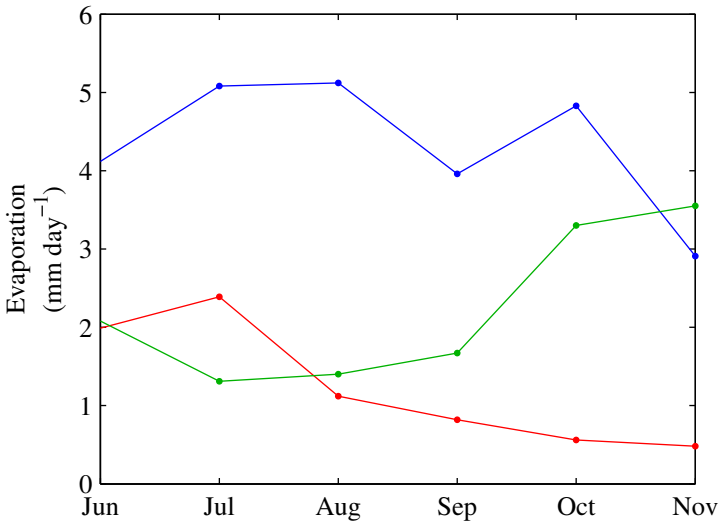

Figure 3.21: Monthly-averaged evaporation rates for Esthwaite Water (red), Lake Mendota (blue) and Rotorua (green).

Chapter 4

A novel method for estimating the onset of thermal stratification in lakes from surface water measurements

4.1 Introduction

In this chapter, the seasonal evolution of the diel cycle in lake surface water temperature is investigated for seven temperate lakes that range in surface area from 0.1 to 79.8 km^2 and cover maximum depths of 15 to 42 m (Table 4.1). The primary aim is to relate the magnitude of the diel temperature cycle to the onset of thermal stratification and to determine if stratification onset can be detected from surface temperature measurements. The results shown here are published as an article in Water Resources Research (doi: 10.1002/2013WR014975).

Table 4.1: The general characteristics of the lakes studied in this investigation and the years studied; lakes are shown in descending order according to their surface area. Note that the day of year for Rotorua has been altered to be comparable with Northern Hemisphere times (i.e. day of year + 182).

Lake	Latitude (°N), Longitude (°E)	Area (km^2)	Max. Depth (m)	Mean depth (m)	Average onset of stratification (day of year)	Year investigated (total number of years)
Rotorua	-38.08°, 176.27°	79.8	22	10	79	2008-2009 (1)
Lake Mendota	43.11°,-89.42°	39.4	25	12	127	2009 (1)
Windermere South Basin	54.35°, -2.94°	6.7	42	17	91	2007-2009, 2011, and 2012 (5)
Bassenthwaite Lake	54.65°, -3.22°	5.3	19	5	92	2010 and 2012 (2)
Llyn Tegid	52.88°, -3.63°	4.1	42	24	80	2009 and 2011 (2)
Esthwaite Water	54.36°, -2.96°	1.0	16	6	81	2005, 2007, and 2009 (3)
Blelham Tarn	54.36°, -2.98°	0.1	15	7	83	2008, 2009, and 2011 (3)

4.2 Vertical water column temperature profiles: temporal variability in mixing and stratification

Each of the 17 time series of water column temperature included in this analysis demonstrated a period of thermal stratification in the summer, and periods of isothermal conditions in winter. To demonstrate the temporal variability in water column temperature as well as the variability in the mixing of these lakes, a one year temperature profile for each lake is shown (Fig. 4.1 to 4.7). During the analysis period, Blelham Tarn, Esthwaite Water, Lake Mendota, Llyn Tegid, and Windermere (Figures 4.1, 4.2, 4.3, 4.4 and 4.5) mixed twice per year, and thus, are classified as dimictic. These five lakes were virtually isothermal (temperature difference between top and bottom less than 1 °C) between October and April and by early May had stratified into a warm upper epilimnion and a cool lower hypolimnion, which persisted until mid-September. The largest temperature difference between top and bottom for these lakes was recorded for Lake Mendota (18.2 °C) in mid-July. Among the UK lakes, the largest temperature difference between top and bottom was recorded for Esthwaite Water (16.3 °C).

High-frequency variations in water column temperature were evident among all of the dimictic lakes. In Lake Mendota, for example, the presence of internal waves is clearly visible in the temperature profile data, which can be seen as the rapid oscillations of the isotherms. High-frequency temperature variations are also visible in the other dimictic lakes. Alternating periods of heating and cooling, for example, are observed in each of the remaining dimictic lakes, which can ultimately lead to transient stratification events. As expected, transient stratification periods are also evident in the polymictic lakes, Bassenthwaite Lake

and Rotorua (Figures 4.6 and 4.7), where short periods of defined stratification seldom lasted longer than a week before the occurrence of convective and wind-driven destratification events vertically mixed the water column. Bassenthwaite Lake, for example, is intermittently stratified between May and September, and in overturn for the remainder of the year. During the stratified period, however, the vertical temperature difference in Bassenthwaite Lake is relatively small in comparison to the other UK lakes. As a result, the vertical structure of the water column is readily broken down. Rotorua experienced similar short-term mixing patterns as Bassenthwaite Lake. Compared to Bassenthwaite Lake, however, Rotorua is much larger (Table 4.1), and due to the relationship between wind mixing and lake size as well as the differences in climate and latitude (MacIntyre and Melack, 2009), the temperature difference between top and bottom is much lower in Rotorua.

All of the lakes studied here demonstrated a clear seasonal stratification cycle typical of temperate lakes. The onset of thermal stratification, estimated here as when the difference between the top and bottom temperature first exceeded 1 °C, however, varied among the lakes. For the UK lakes, for example, the earliest onset of thermal stratification occurred in Llyn Tegid (average day of year = 80) and the latest onset of thermal stratification occurred in Bassenthwaite Lake (average day of year = 92). The largest of the dimictic lakes, Lake Mendota, became thermally stratified last, where the difference between the top and bottom temperature did not exceed 1 °C until day of year 127.

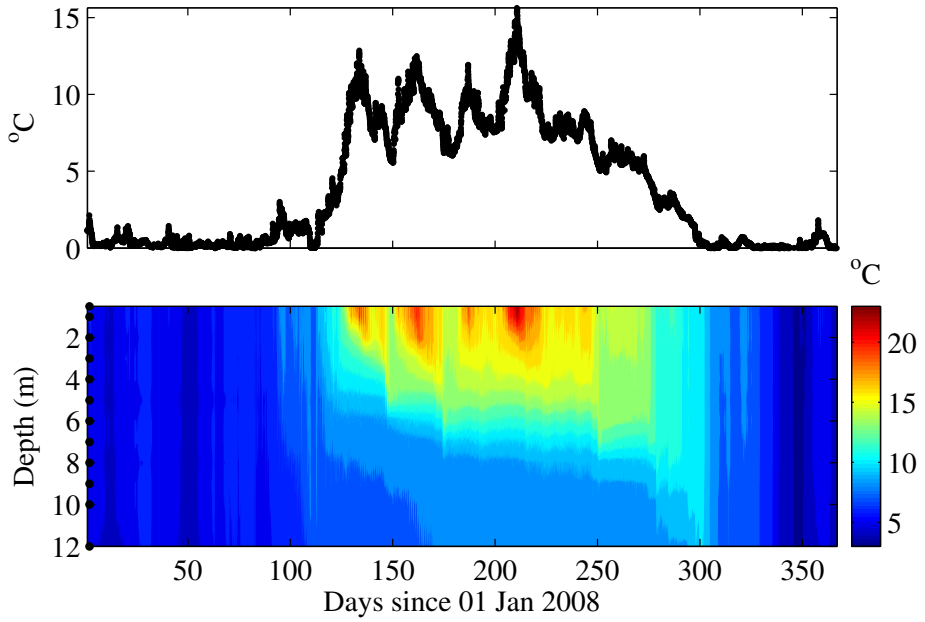

Figure 4.1: Temperature difference between top and bottom temperature (upper panel) and the water column temperature profiles (lower panel) for Blelham Tarn, 2008. Thermistor depths are shown by the black filled circles on the left side of the lower panel.

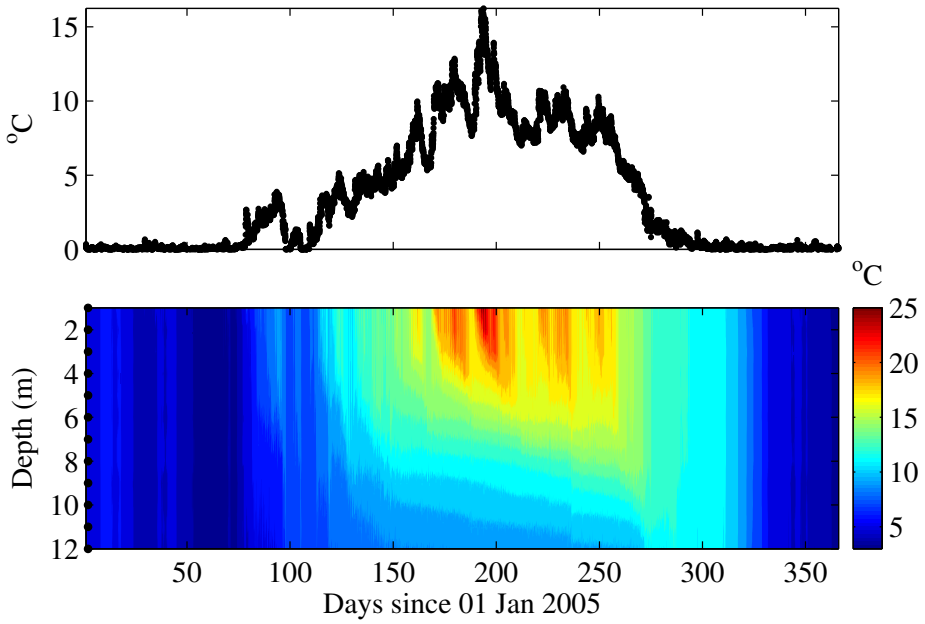

Figure 4.2: Same as Fig. 4.1 but for Esthwaite Water, 2005.

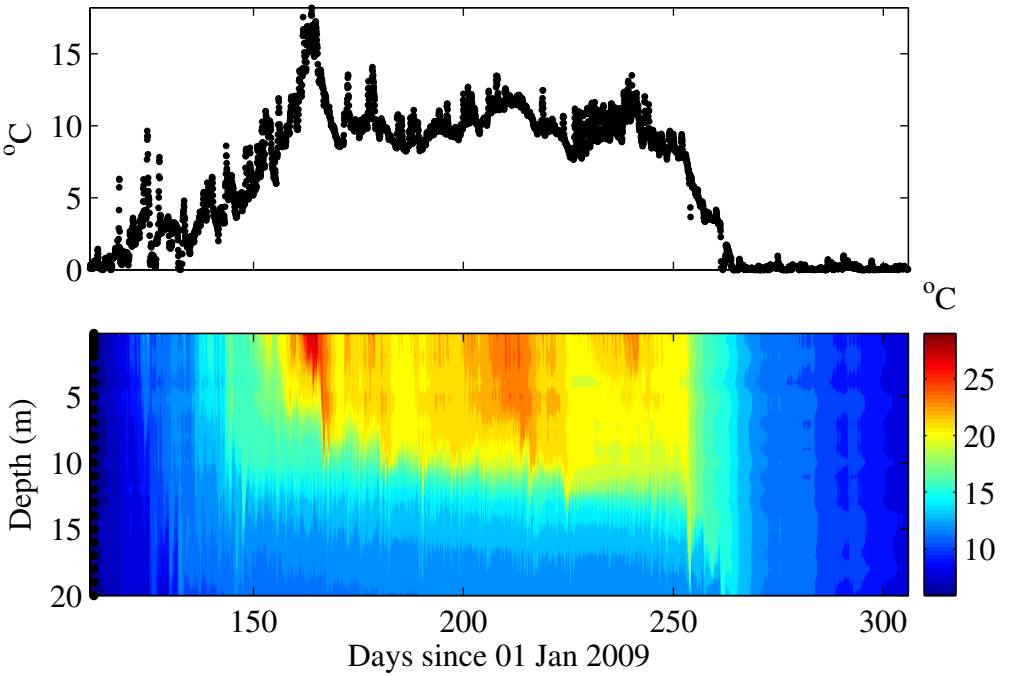

Figure 4.3: Same as Fig. 4.1 but for Lake Mendota, 2009.

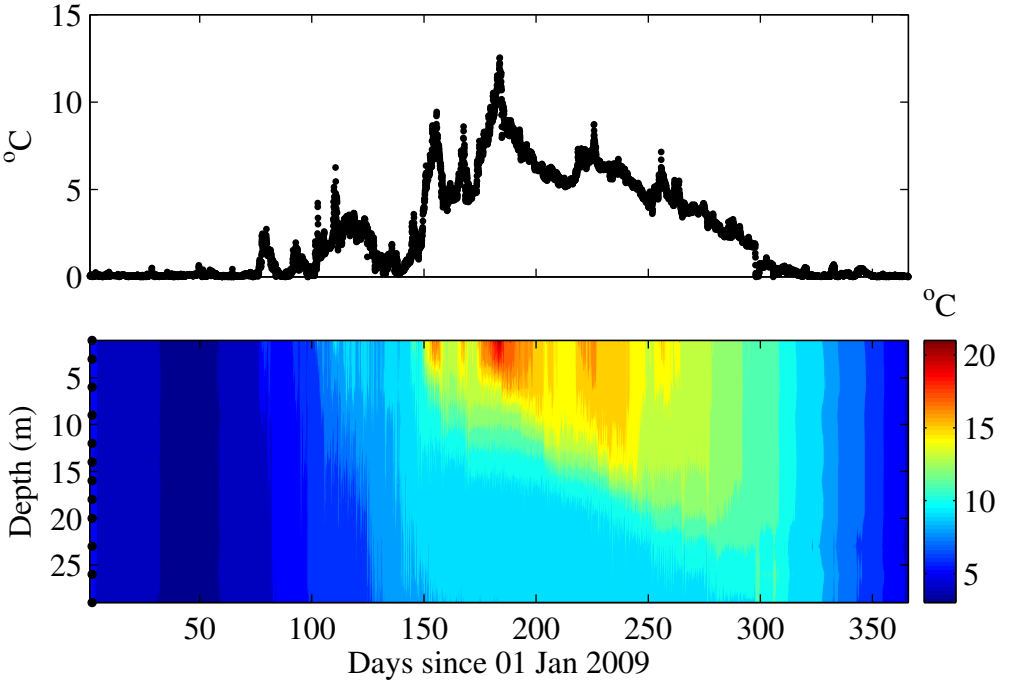

Figure 4.4: Same as Fig. 4.1 but for Llyn Tegid, 2009.

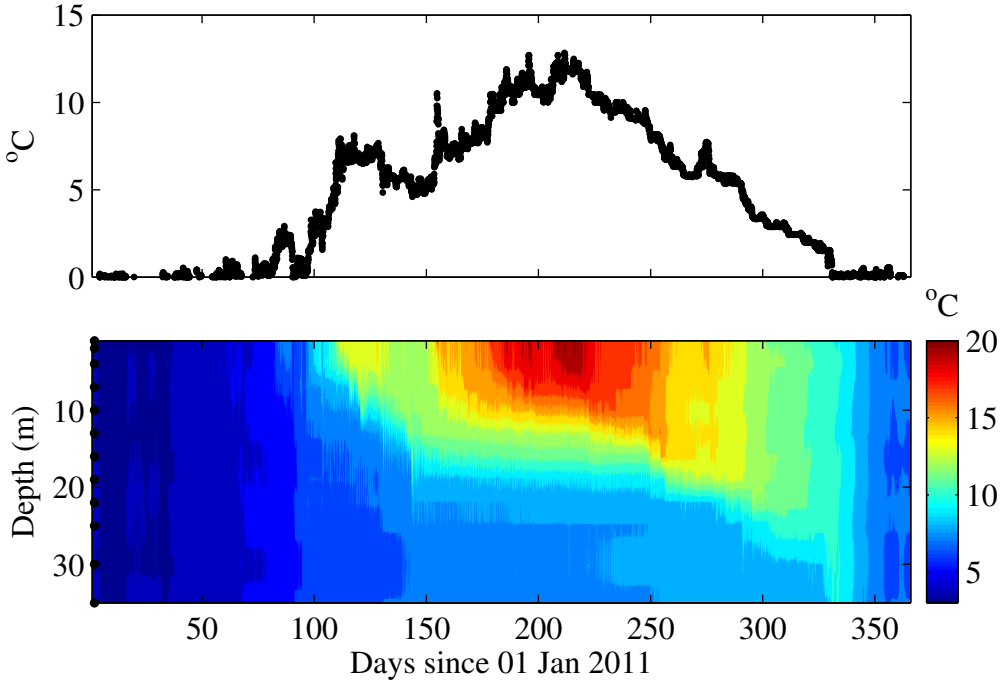

Figure 4.5: Same as Fig. 4.1 but for Windermere, 2011.

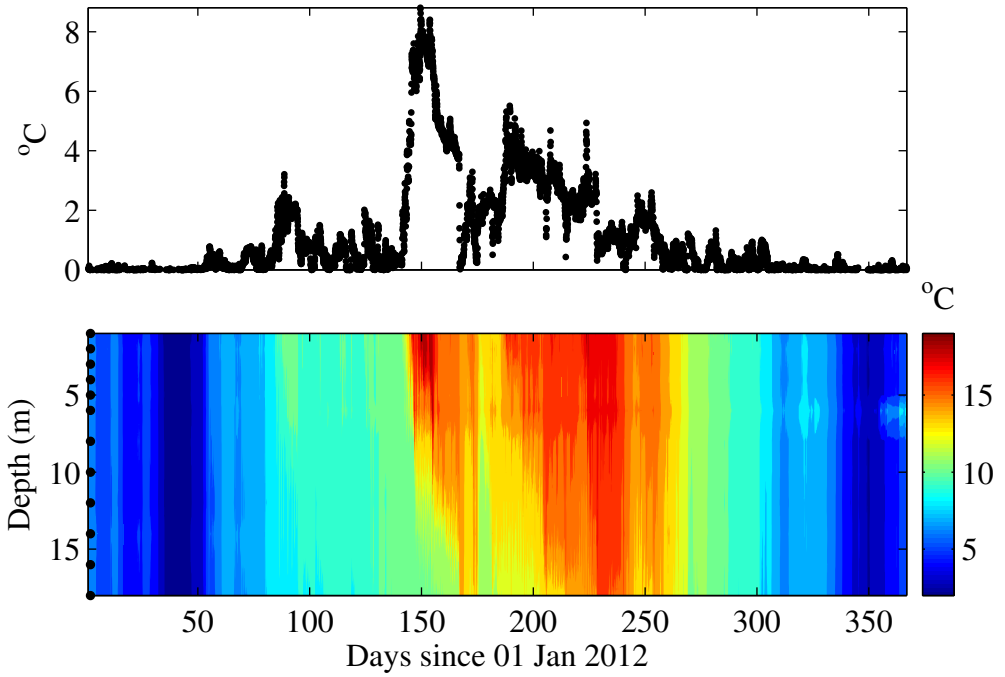

Figure 4.6: Same as Fig. 4.1 but for Bassenthwaite Lake, 2012.

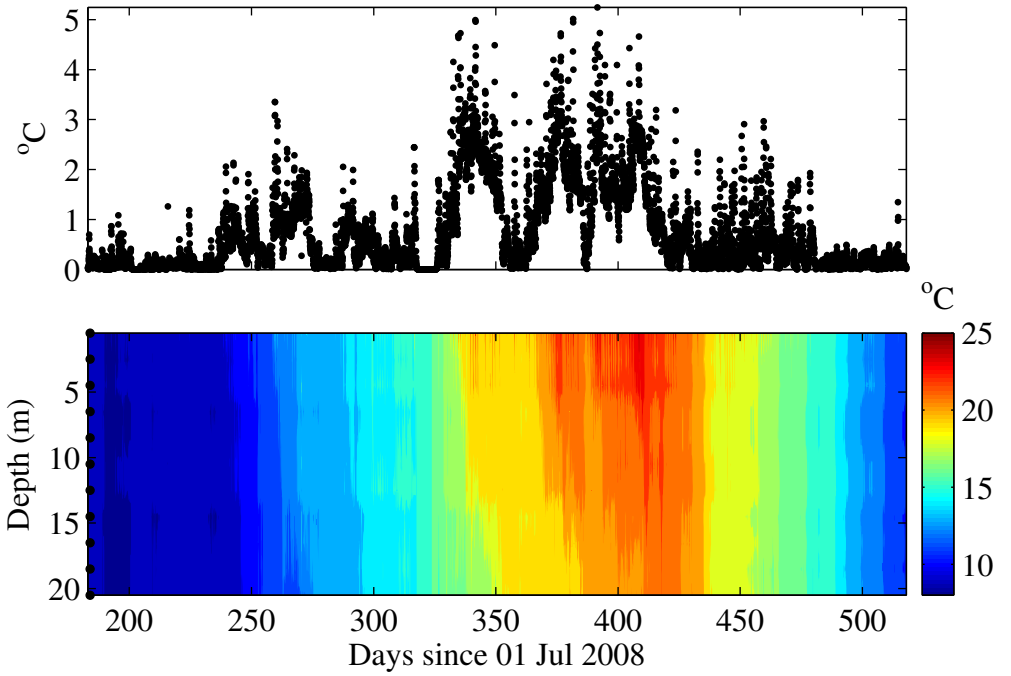

Figure 4.7: Same as Fig. 4.1 but for Rotorua, 2008-09.

4.3 Wavelet transform of surface temperature measurements

The diel range in lake surface water temperature for each lake included in this investigation was evaluated by computing the wavelet coefficients of the time series. Similar to the examples shown for the water temperature profiles (Fig. 4.1 to 4.7), the wavelet coefficients for one year for each lake is shown (Fig. 4.8 to 4.14). Surface water temperature for each lake followed a clear seasonal cycle, being low in winter and high in summer. By computing the wavelet coefficients of surface water temperature, short-term temperature fluctuations become evident among all of the lakes. The diel signal for each lake followed a clear seasonal cycle that was significant during summer when surface water temperature

was high and non-significant during winter. The periods that are significant are those that are enclosed by the black contour lines overlaying the wavelet spectra. Diel fluctuations were observed in the dimictic (Fig. 4.8 to 4.12) and polymictic lakes (Figures 4.13 and 4.14) thus illustrating that the 24 hour cycle was a dominant feature among all of the lakes. There was also high power at low-frequency (four to eight days) in four of the seven lakes shown here (Bassenthwaite Lake, Blelham Tarn, Esthwaite Water, and Llyn Tegid), indicating strong signals at the scale of weather systems (e.g. Lafrenière and Sharp, 2003). However, the power was non-significant at the annual scale, as illustrated by the global wavelet transform. The dominance of the diel cycle was clearly illustrated by the global wavelet transform where a peak in the power spectra was calculated at a period of 24 hours. The power around the 24 hour cycle is the dominant feature among all of the lakes, indicating strong diel signatures in the time series. Furthermore, the time-averaged power spectrum (i.e. GWT) at a period of 24 hours varied among the lakes, thus, illustrating the different magnitudes of the diel temperature cycle. For the years shown, the diel signal was strongest for Esthwaite Water (1.38) and Blelham Tarn (1.14), and weakest for Llyn Tegid (0.40) and Windermere (0.56). This implies that Esthwaite Water is more responsive to diel temperature changes in 2005 than Windermere was in 2011. As the data shown are from different years, a straightforward comparison between the diel cycles of the different lakes has little meaning. This does demonstrate, however, that the method presented in this chapter is used on a number of lake types with varying strengths of their diel temperature signal.

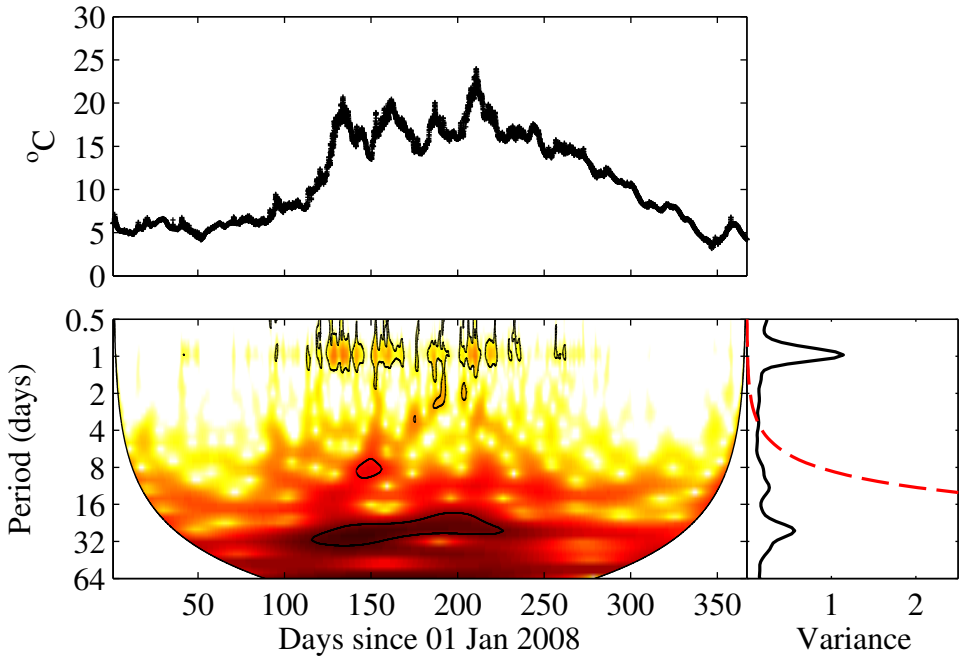

Figure 4.8: Surface water temperature (upper panel) and the wavelet power spectrum of surface water temperature (lower panel) for Blelham Tarn, 2008. The left side of the bottom panel shows the continuous wavelet spectrum and the solid black lines represent the features of the spectra that are significant ($p < 0.05$). The continuous wavelet spectra are shown in base 2 logarithm, and illustrate how the strength of the periodicities change with time. The right side of the bottom panel illustrates the global wavelet spectra where the black line encloses the time-averaged spectra and the dashed red line shows the 95 % significance level. The power values are coded from white for low power to dark red for high power.

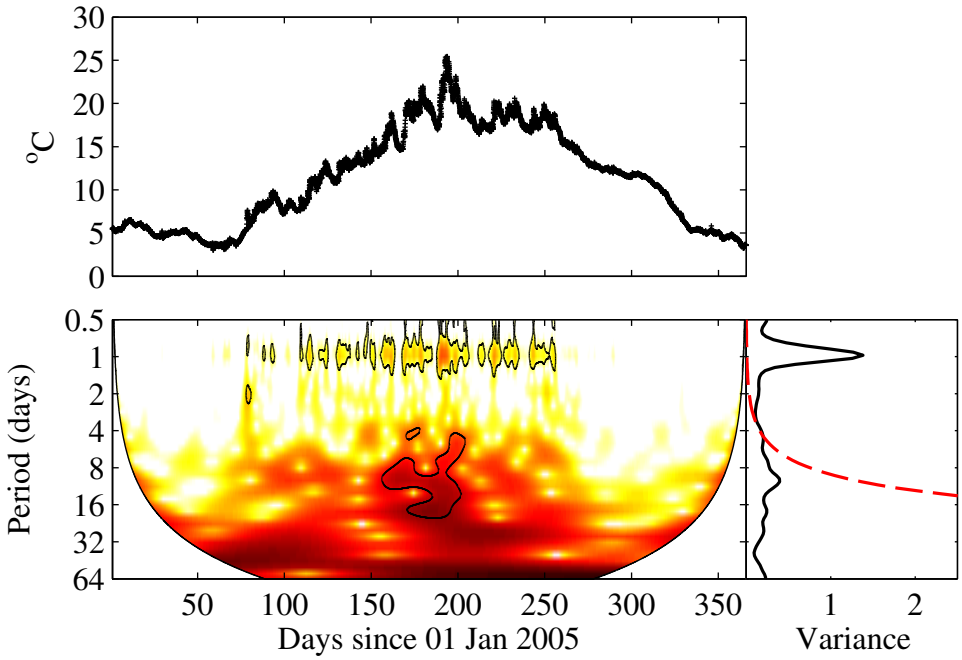

Figure 4.9: Same as Fig. 4.8 but for Esthwaite Water, 2005.

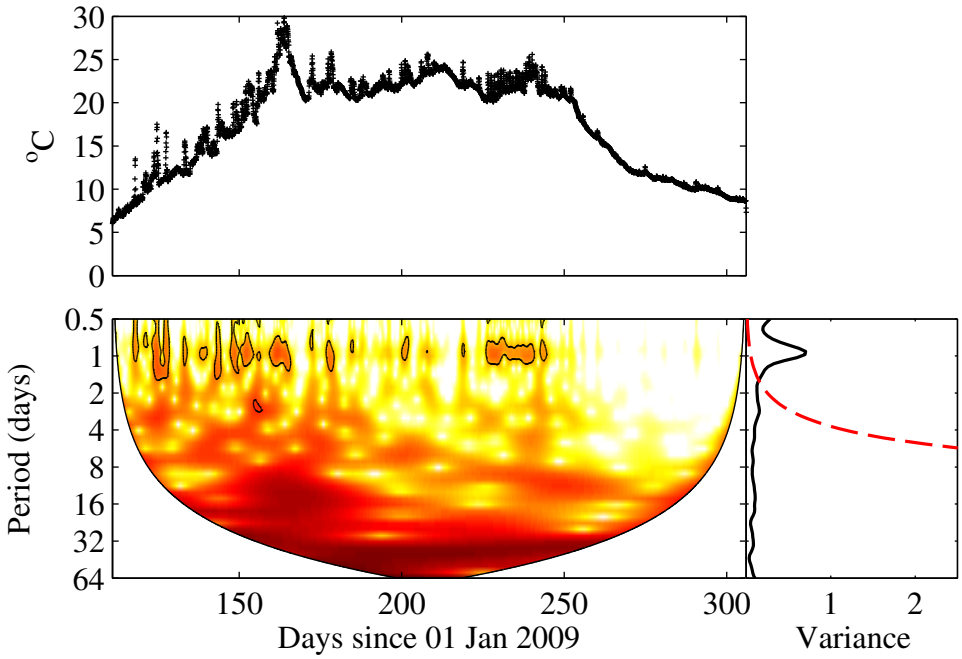

Figure 4.10: Same as Fig. 4.8 but for Lake Mendota, 2009.

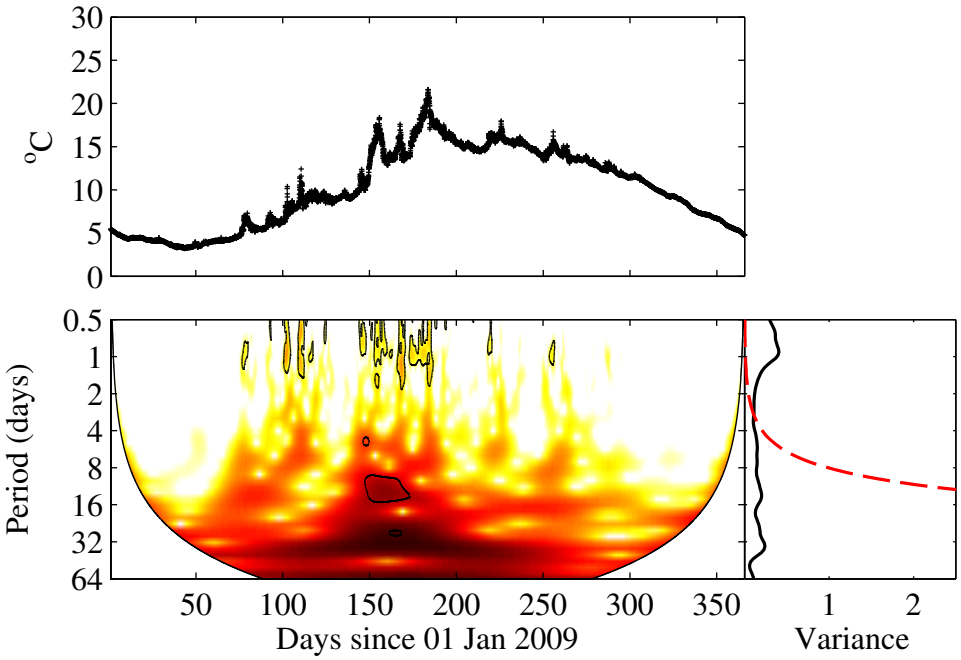

Figure 4.11: Same as Fig. 4.8 but for Llyn Tegid, 2009.

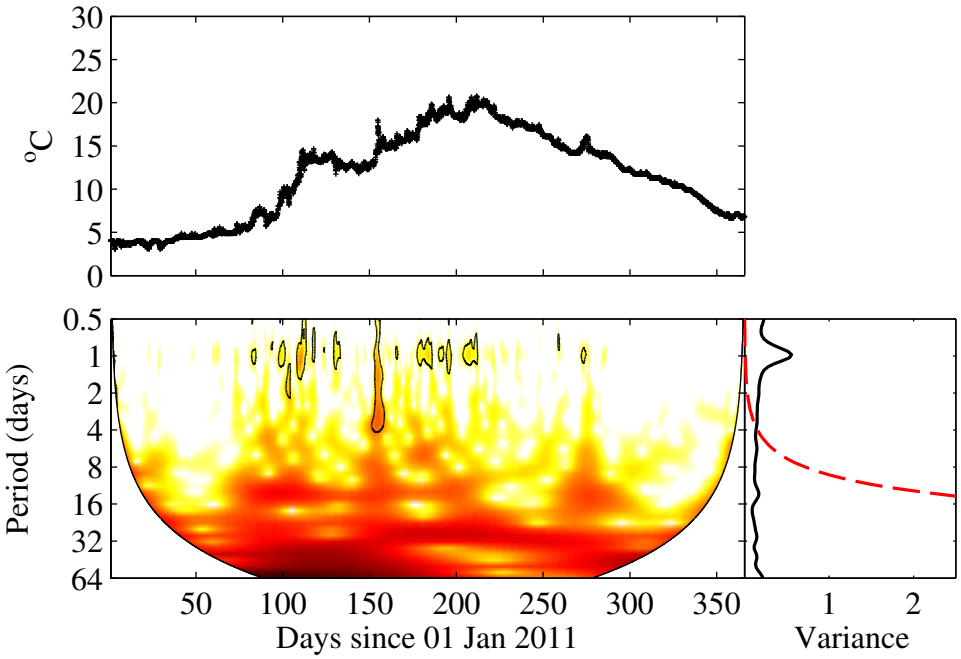

Figure 4.12: Same as Fig. 4.8 but for Windermere, 2011.

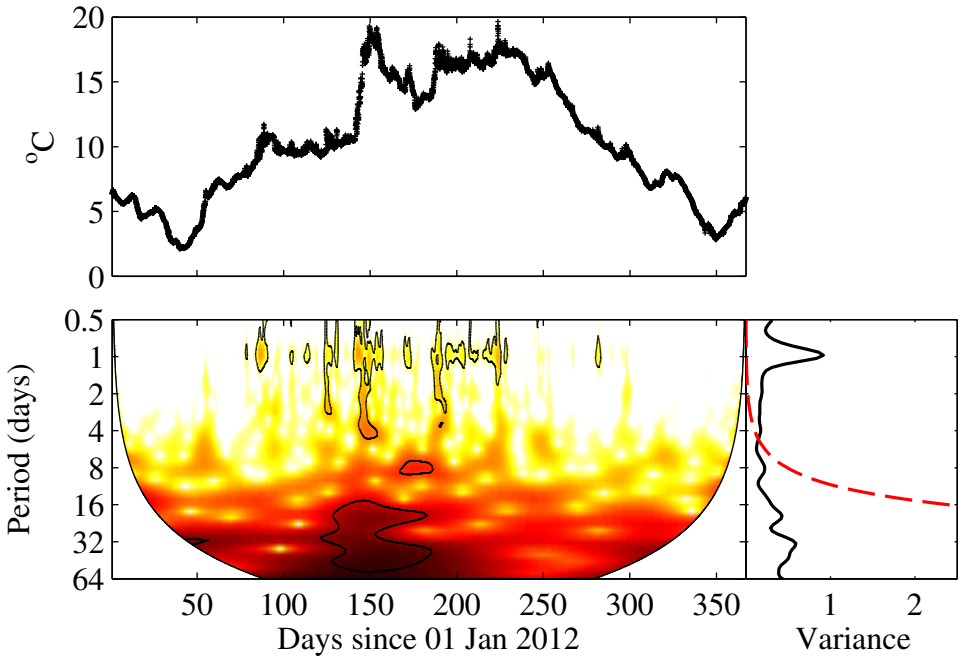

Figure 4.13: Same as Fig. 4.8 but for Bassenthwaite, 2012.

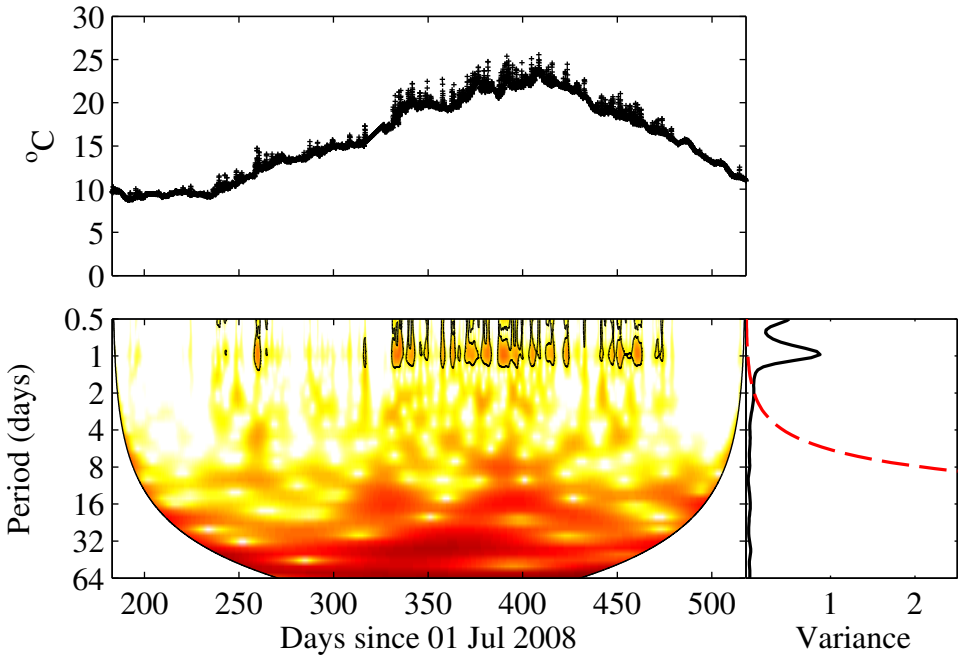

Figure 4.14: Same as Fig. 4.8 but for Rotorua, 2008-09.

4.4 Correlation between observed diel temperature range and wavelet power at a period of 24 hours

The observed diel surface temperature range, calculated as the difference between the maximum and minimum lake surface water temperature for each day was highly correlated with the wavelet power at a period of 24 hours (Fig. 4.15). The statistical dependence (evaluated by Spearman's rank correlation, r_s) between the observed diel surface temperature range and the wavelet power at 24 hours was high ($p < 0.001$) for all of the lakes. The relationship between these variables, however, was drastically different at times when the observed diel temperature range was less than 1 °C where wavelet power shows a strong dependence on the observed temperature range, unlike those periods where the diel temperature range was greater than 1 °C. A heteroskedastic relationship is evident among all of the lakes (Fig. 4.15), where the variability between the wavelet power at a period of 24 hours and the observed diel surface temperature range increased at higher values. During the stratified period, the observed diel temperature range closely followed the wavelet power, where a sharp increase or decrease in the observed diel temperature range was reflected in an increase or decrease in the wavelet power (Fig. 4.16).

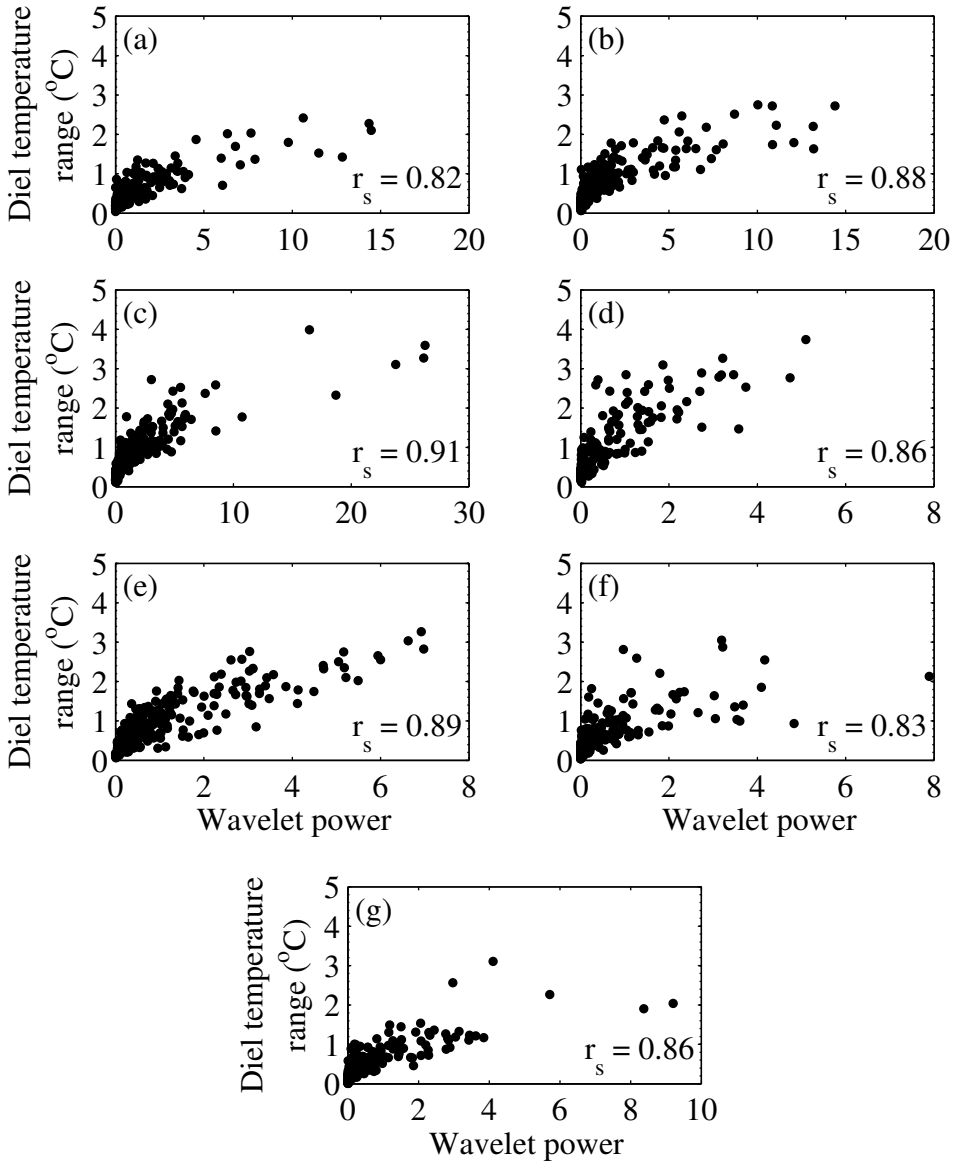

Figure 4.15: Example correlations between the observed diel temperature range and the wavelet power at a period of 24 hours for (a) Bassenthwaite Lake, 2012; (b) Blelham Tarn, 2008; (c) Esthwaite Water, 2005; (d) Lake Mendota, 2009; (e) Rotorua, 2008-09; (f) Llyn Tegid, 2009; and (g) Windermere, 2011. A non-parametric test (Spearman's rank correlation) was used to evaluate the statistical dependence between paired variables. Correlations are significant at the $p < 0.001$ level. Note the different scales for each x-axis.

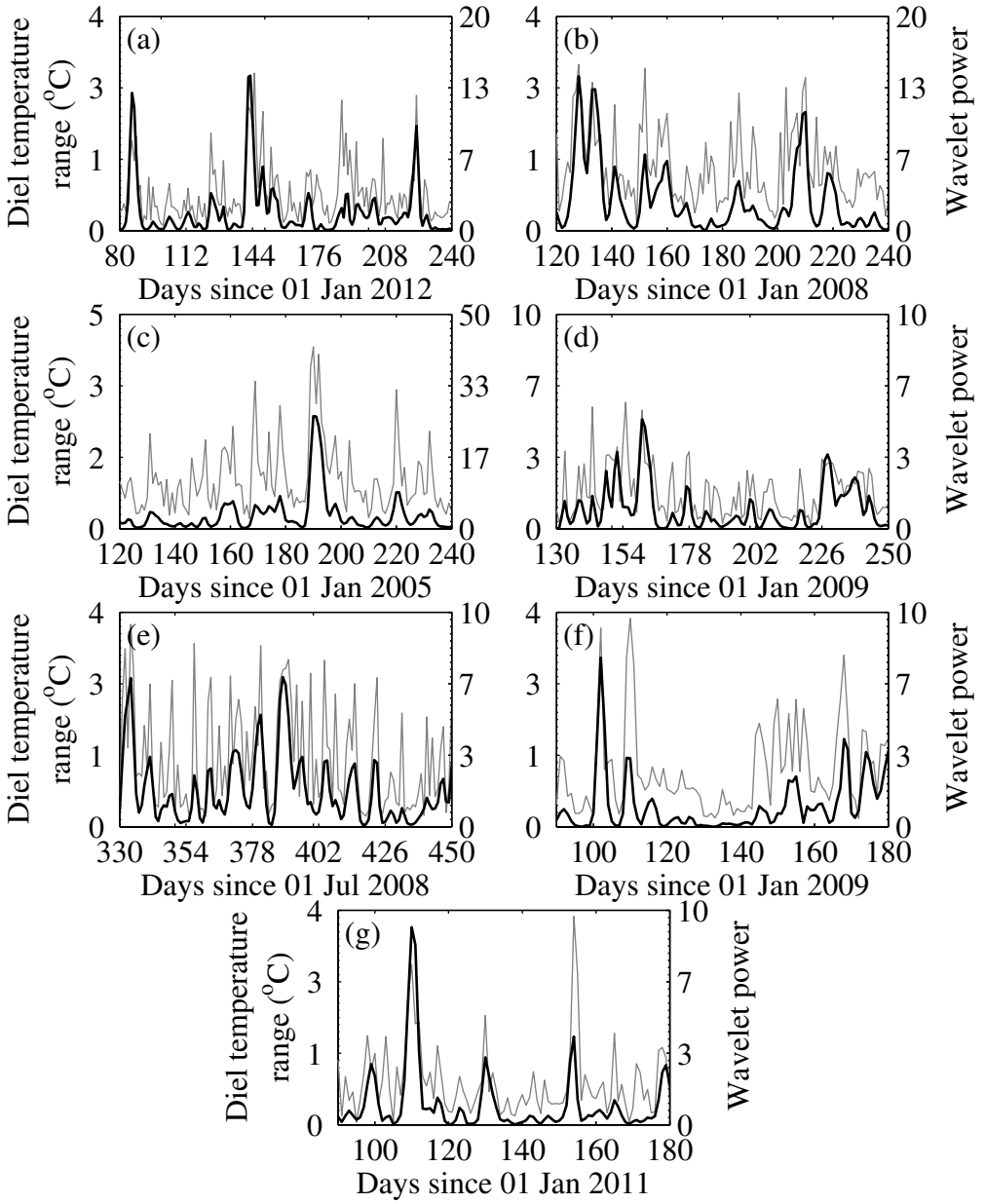

Figure 4.16: Example comparison of the observed diel surface temperature range (grey) and the wavelet power at a period of 24 hours (black) for (a) Bassenthwaite Lake, 2012; (b) Blelham Tarn, 2008; (c) Esthwaite Water, 2005; (d) Lake Mendota, 2009; (e) Rotorua, 2008-09; (f) Llyn Tegid, 2009; and (g) Windermere, 2011. Note the different scales for each of the lakes.

4.5 Estimating the onset of thermal stratification from the diel temperature range

As explained in Chapter 2, the onset of thermal stratification was estimated from the diel temperature range as (i) the time that the diel temperature range first exceeded 1 °C, and (ii) the first time that the wavelet power at a period of 24 hours was greater than unity (i.e. when the diel cycle was statistically significant). Therefore, to assess the accuracy of using the diel temperature range to estimate the onset of thermal stratification, stratification onset was first calculated from the temperature profiles as the first time that the difference between top and bottom temperature exceeded 1 °C. The estimated onset of stratification from methods (i) and (ii) were then calculated and compared against the actual onset dates. By using the 24 hour signal from the wavelet coefficients, the onset of thermal stratification could be estimated accurately. It could also be estimated relatively well using the observed diel surface temperature range (Fig. 4.17). Using the wavelet method allowed the onset of stratification to be estimated with a root mean square error (RMSE) of 2.1 days. The observed temperature range method was not as accurate but still allowed stratification onset to be estimated with a RMSE of 11.8 days on average.

4.6 Frequency of temperature measurements needed to estimate the onset of stratification

In order to determine the effect of sampling frequency on the accuracy of estimating the onset of thermal stratification, the high-resolution surface temperature measurements were down-sampled to produce data series with frequencies ranging from two to eight hours. That is, the high-resolution data were used to extract two to eight hour interval data, and then for each temperature series, the onset of thermal stratification was estimated using both of the proposed methods. This revealed that the accuracy of estimating the onset of thermal stratification declined with lower frequency data (Fig. 4.18). Using the wavelet method, for example, resulted in the accuracy to drop from having a RMSE of 2.1 days for the 15 minute temporal resolution data to a RMSE of approximately 15 days for the 8 hour temporal resolution data.

By down-sampling the measured data and re-estimating the onset of thermal stratification using the two methods, the data revealed that the greatest loss in accuracy for the wavelet method was between a sampling resolution of 1 and 2 hours where, on average, the accuracy of the method dropped from 2.5 to 7 days. This means that the accuracy of estimating the onset of thermal stratification will be reduced greatly when using two instead of one hour resolution data, but will be influenced less by using four instead of six hour resolution data. Similarly, the observed diel surface temperature range approach was also sensitive to sampling frequency. Down-sampling to a temporal resolution of 8 hours, for example, increased the RMSE to about 24 days (Fig. 4.18).

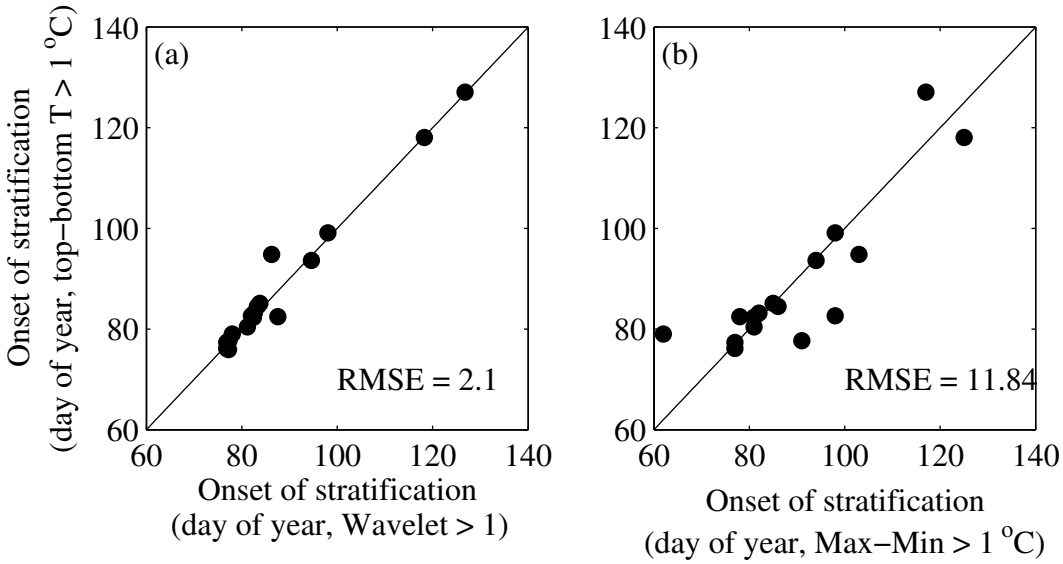

Figure 4.17: Comparison of the day of year when the observed temperature difference between the lake surface and bottom first exceeded 1 °C with (a) the day of year when the wavelet power at the 24 hour scale became significant; and (b) the day of year when the diel surface temperature range exceeded 1 °C. The root mean square error (RMSE) is shown in the bottom right corner.

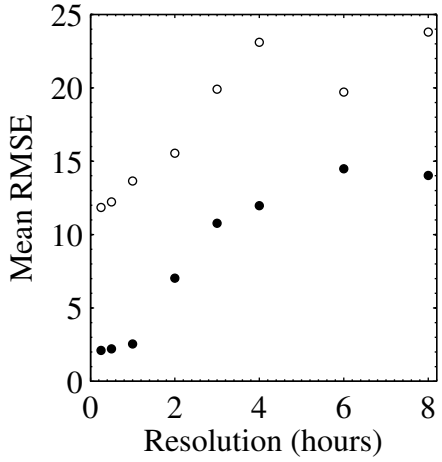

Figure 4.18: Comparison of the root mean square error (RMSE) associated with estimating the onset of thermal stratification from the observed diel temperature range (open circles) and wavelet power (closed circles) for different frequencies of data collection.

Chapter 5

A comparison of the diel range in lake surface water temperature from five lakes in the English Lake District

5.1 Introduction

In the following chapter, the diel range in lake surface water temperature for five neighbouring lakes is investigated. The aim here is to assess if the diel range in lake surface water temperature differs among lakes driven by essentially the same climate, but characterised by different morphometric features. In Chapter 3 and 4 it was shown that the diel range in lake surface water temperature can be influenced by the depth of the upper mixing layer. It was also demonstrated that a rapid transition from a mixed to a thermally stratified water column would

result in high diel surface temperature variations to the extent that the onset of thermal stratification could be detected accurately. The depth of the upper mixed layer, however, is known to be influenced by factors such as lake area and water clarity (e.g. Fee et al., 1996; Mazumder and Taylor, 1994). The aim of this chapter is to assess if the diel temperature range can also be related to these lake specific factors. Five lakes from the English Lake District were chosen for this investigation. The lakes range in surface area from 0.1 to 6.7 km^2 and cover maximum depths of 14.5 to 42 m (Table 5.1).

Table 5.1: General characteristics of the five study lakes, shown in descending order according to their surface area. Meteorological measurement heights are provided for wind speed (z_u), air temperature (z_t), and relative humidity (z_q).

Lake	Area (km^2)	Max. Depth (m)	Mean depth (m)	Annual mean K_d (m^{-1})	Annual mean u_{10} ($m\ s^{-1}$)	Altitude (m)	z_u (m)	z_u (m)	z_u (m)
Windermere South Basin	6.7	42.0	16.8	0.46	3.2	39	2.65	2.45	2.45
Bassenthwaite Lake	5.3	19.0	5.3	0.70	3.7	69	2.65	2.45	2.45
Esthwaite Water	1.0	15.5	6.4	0.82	2.3	65	2.85	2.14	2.14
Loweswater	0.6	16.0	8.4	0.66	2.9	125	2.65	2.45	2.45
Blelham Tarn	0.1	14.5	6.8	0.87	1.6	41	2.65	2.45	2.45

5.2 Depth-resolved temperature profiles

There was a period of thermal stratification during summer, and isothermal conditions in winter, in each of the five study lakes (Fig. 5.1). All of the lakes became thermally stratified on approximately day of year 80 but experienced a number of transient destratification periods throughout the summer, especially in Bassenthwaite Lake (Fig. 5.1a). The total duration of stratified days among the lakes varied from approximately four months to about seven months. As expected, surface water temperatures for each of the five lakes followed a pronounced seasonal cycle, being low in winter and high in summer. Lowest monthly-averaged surface water temperatures were measured during February, varying between 2.8 °C for Bassenthwaite Lake and 4.2 °C for Blelham Tarn. Highest monthly-averaged surface water temperatures were in July, again varying between the temperature of Bassenthwaite Lake and Blelham Tarn. Among the five lakes, the highest monthly-averaged surface water temperature was 19.8 °C, measured in the smallest lake, Blelham Tarn. The maximum difference in surface water temperature among the neighbouring lakes occurred in December, where surface water temperature in Bassenthwaite Lake were 2.8 °C cooler than the warmest lake for that month, Windermere South Basin. Similarly, a 2.7 °C temperature difference occurred in April where the maximum and minimum monthly-averaged surface water temperatures were measured in Blelham Tarn and Windermere South Basin, respectively.

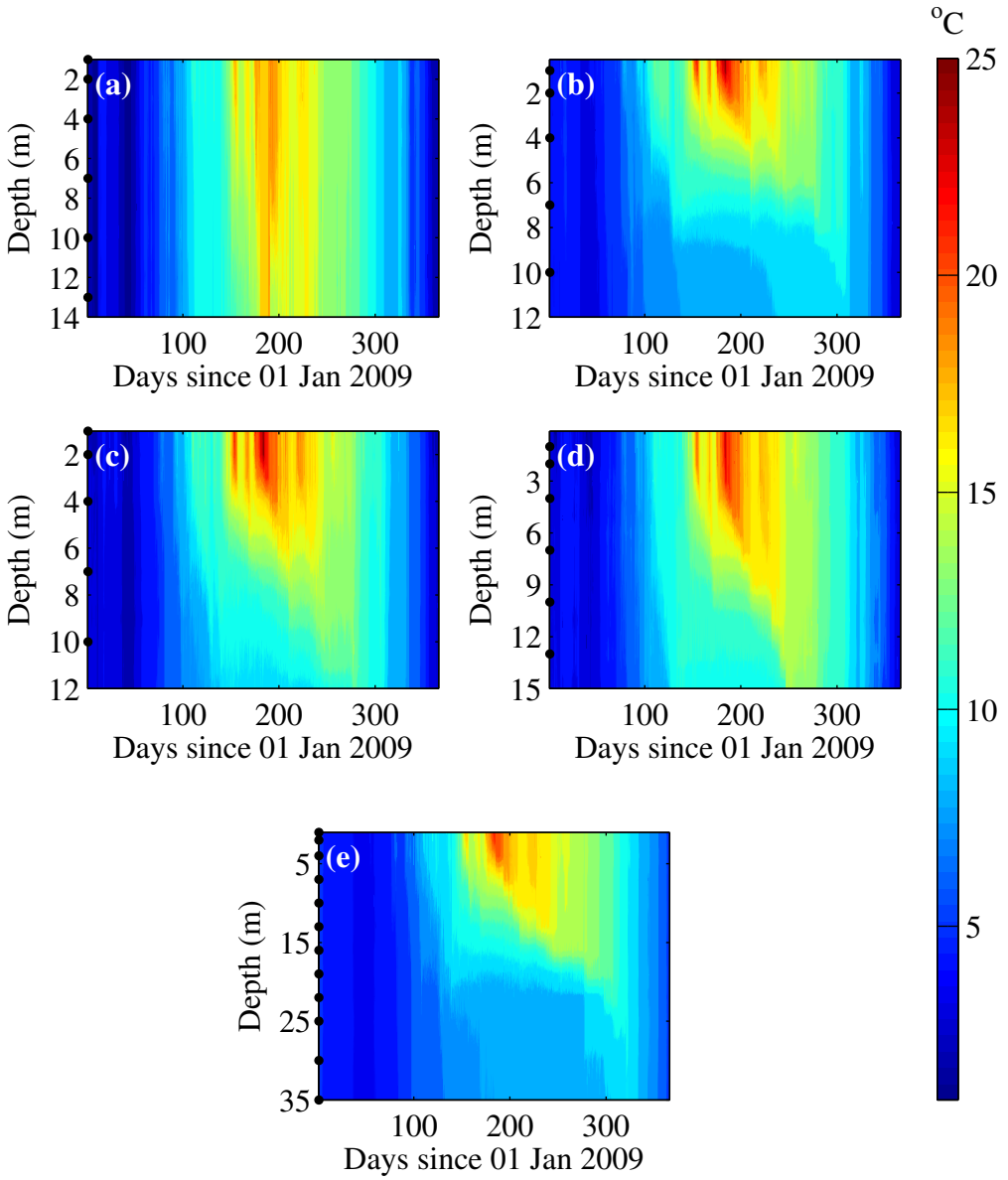

Figure 5.1: High-resolution (hourly) water column temperature profiles for (a) Bassenthwaite Lake; (b) Blelham Tarn; (c) Esthwaite Water; (d) Loweswater; and (e) Windermere South Basin. Buoy thermistor depths are shown on the left edge (black circles). Note the different depth scales for each of the lakes.

5.3 Meteorological data and calculated energy fluxes

In 2009, using Loweswater as an example, air temperature had a clear and expected seasonal cycle (Fig. 5.2a), varying from, on average, less than 5 °C in winter to more than 15 °C in summer. Surface water temperature, similar to air temperature, followed a typical annual pattern, being high in summer and low in winter (Fig. 5.2a). Unlike air temperature, however, surface water temperatures varied much less at diel timescales, often fluctuating by less than 2 °C of the daily-averaged temperature. Relative humidity was continuously high, averaging 80 % with humidity in summer typically being lower than in winter (Fig. 5.2b). Incoming short-wave radiation was highly variable at the seasonal timescale (Fig. 5.2c) with an annual average of approximately 100 W m^{-2}. Maximum monthly-averaged incoming short-wave radiation, however, was much greater, reaching 220 W m^{-2} in mid-June, corresponding to the summer solstice. The annually-averaged wind speed was about 3 m s^{-1} with little systematic seasonal pattern (Fig. 5.2d), although average wind speeds were marginally lower in summer (June, July, August) than in winter (January, February). Similar seasonal patterns were evident among all of the study sites (data not shown).

There was a recognisable seasonal cycle among the majority of the heat flux components as well as the total surface heat flux in Loweswater (Fig. 5.3). The net incoming short-wave radiation was highly variable (Fig. 5.3a), differing most from the measured short-wave radiation during winter, due to the increase in short-wave albedo during these months. Incoming long-wave radiation (Fig. 5.3b) was often lower than the outgoing long-wave radiation throughout the year, being approximately 40 W m^{-2} lower on average (i.e. annual average for the

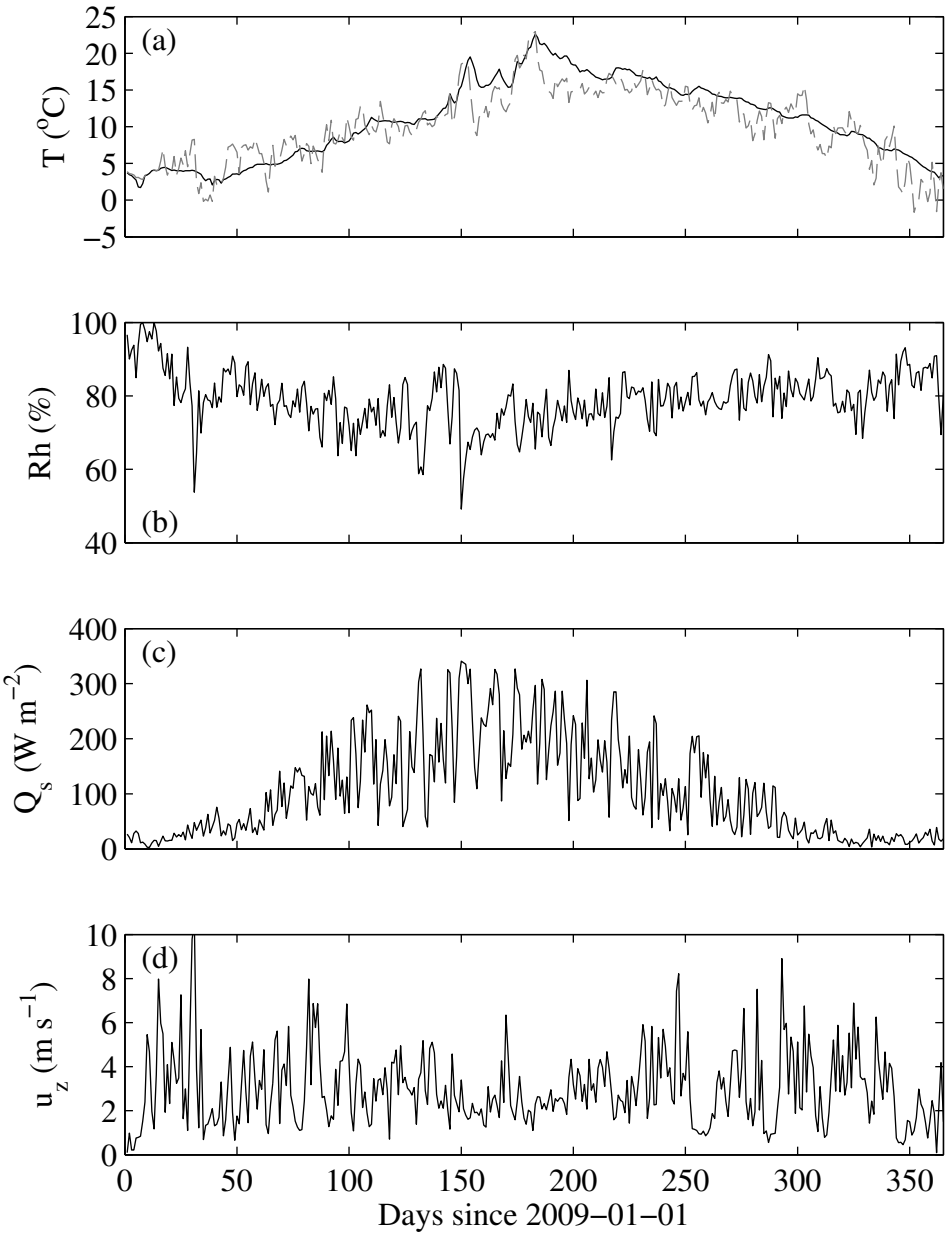

Figure 5.2: Daily-averaged meteorological measurements for Loweswater showing (a) air (dashed line) and surface water (black line) temperature; (b) relative humidity; (c) incoming short-wave radiation; and (d) wind speed at the measurement height.

hourly data). Both latent and sensible heat fluxes followed a seasonal cycle, being large in summer and low in winter (Fig. 5.3c). Of the two turbulent fluxes, the latent heat flux was the largest in Loweswater, being approximately 15 W m^{-2} larger as an annual average (i.e. annual average for the hourly data). There was a clear seasonal cycle in the total surface heat flux which was predominantly negative (i.e. cooling) in winter and positive (i.e. heating) in summer (Fig. 5.3d). Similarly, the individual heat flux terms calculated for the remaining four lakes included in this analysis were highly variable with large variations at the seasonal timescales (data not shown).

5.4 Drivers of mixing depth in the five lakes

The monthly-averaged heating within the upper mixed layer, Q_{zmix}, varied throughout the year, being positive (i.e. heating) in summer and negative (i.e. cooling) in winter (Fig. 5.4a). All of the lakes had a positive Q_{zmix} for seven months (Mar, Apr, May, Jun, Jul, Aug, Sep) and a negative Q_{zmix} for five months (Jan, Feb, Oct, Nov, Dec). The magnitude of heating, however, varied from month to month. The maximum positive monthly-averaged total surface heat flux was calculated for Windermere South Basin (95 W m^{-2}) in April and the maximum negative monthly-averaged total surface heat flux was calculated for Windermere South Basin (97 W m^{-2}) in December. The monthly-averaged heat flux within the upper mixed layer varied only marginally among the lakes. The largest difference between Q_{zmix}, for example, was calculated as 38 W m^{-2} in December and 36 W m^{-2} in April. By calculating the annual average, however, the total surface heat flux only differed by 5 W m^{-2}.

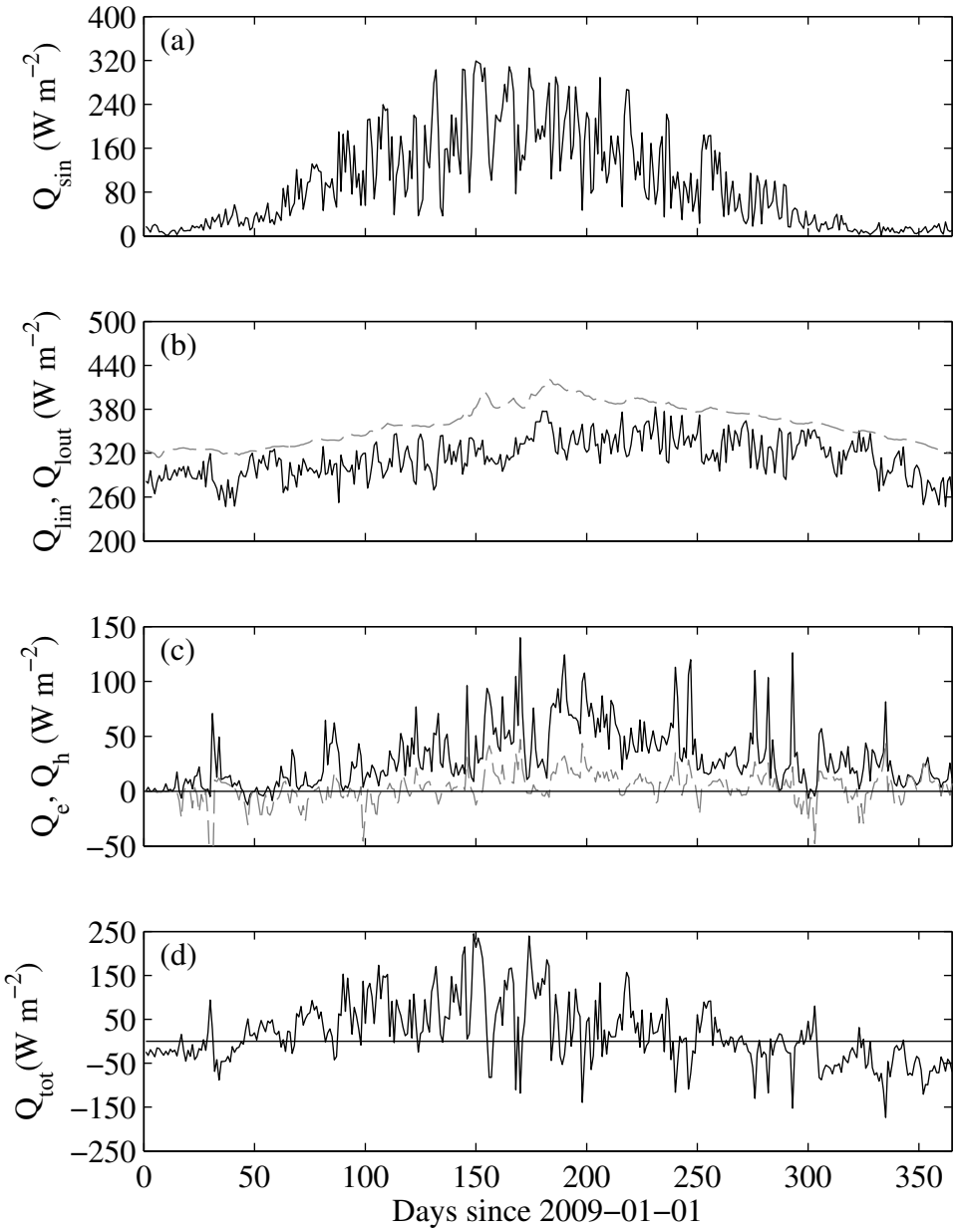

Figure 5.3: Daily-averaged heat fluxes for Loweswater showing (a) net incoming short-wave radiation; (b) outgoing (grey dashed line) and incoming (black line) long-wave radiation; (c) sensible (grey dashed line) and latent (black line) heat fluxes; and (d) total surface heat flux.

Monthly-averaged wind speed corrected to a height of 10 m above the lake surface, u_{10}, varied considerably among the lakes (Fig. 5.4b). The highest monthly-averaged wind speed was measured in two of the largest lakes by surface area, Bassenthwaite Lake and Windermere South Basin, and the lowest monthly-averaged wind speed was measured in the smallest lake by surface area, Blelham Tarn. The large difference in wind speed among the lakes is evident through most of the year, in particular during November where the monthly-averaged wind speed at Bassenthwaite Lake (5.5 m s^{-1}) was more than double the monthly-averaged wind speed at Blelham Tarn (2.2 m s^{-1}). For the lakes studied here, the relationship between wind speed and lake area is complicated by the surrounding topography. Higher than expected wind speeds, for example, were measured in Loweswater due to the lake being located at the end of a valley which ultimately leads to increasing wind speed. This increase in wind speed, however, matched the variation in mixing depth (Fig. 5.4c), that is those lakes with higher wind speeds also had deeper upper mixed layer depths.

The greatest difference in mixing depth among the five lakes was observed in winter when the lakes were vertically mixed, and thus, the mixing depth is equal to maximum lake depth (Fig. 5.4c). During the summer, however, the lakes are thermally stratified, and the mixing depth is influenced by u_{10}. The summer (June, July, and August) average mixing depth was greatest for Windermere South Basin (9.4 m) and smallest for Blelham Tarn (2.8 m) and Esthwaite Water (4.6 m), whereas Loweswater had an intermediate average mixing depth of 6.9 m.

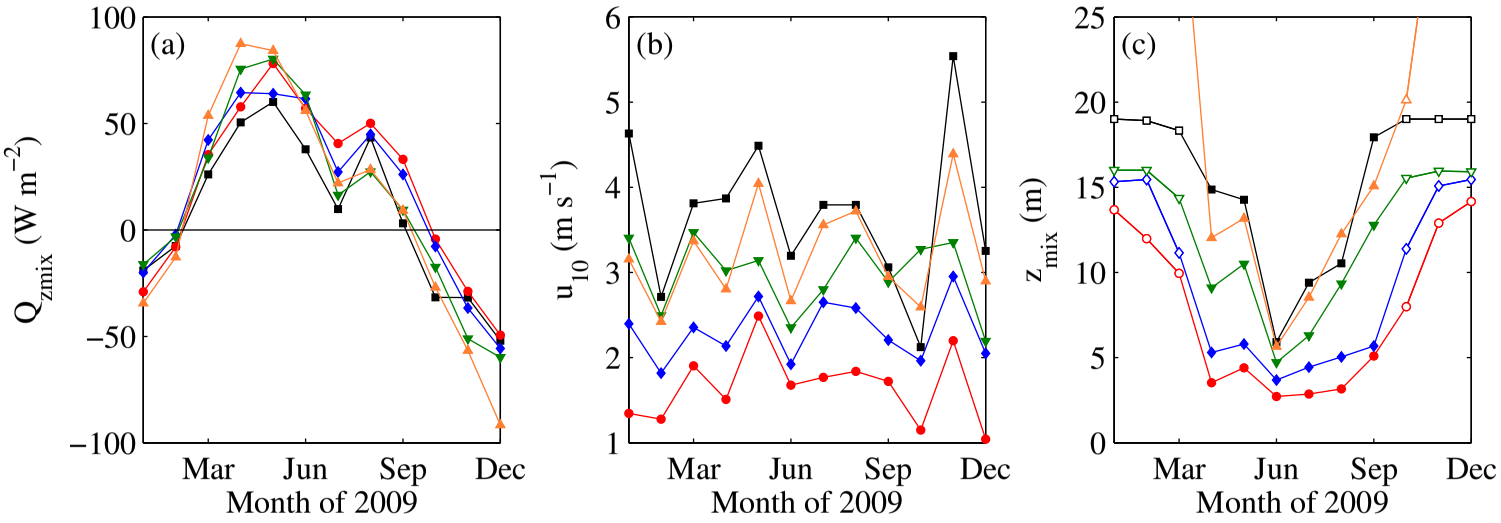

Figure 5.4: Monthly-averaged (a) heat flux influencing the upper mixed layer; (b) wind speed estimated at a height of 10 m above the lake surface; and (c) depth of the upper mixed layer for the stratified (filled circles) and non-stratified (unfilled circles) periods for Bassenthwaite Lake (black), Blelham Tarn (red), Esthwaite Water (blue), Loweswater (green), and Windermere South Basin (orange).

5.5 Monthly-averaged diel temperature cycle

The monthly-averaged diel temperature cycle varied among the lakes (Fig. 5.5a). A distinct seasonal variability in the magnitude of the diel cycle, however, was evident among all of the sites, with a minimum and maximum monthly-averaged diel range occurring in winter and summer, respectively. A maximum monthly-averaged diel surface temperature range of 1.6 °C was calculated for Blelham Tarn during June and a minimum monthly-averaged diel temperature range (= 0.1 °C) was observed for Windermere South Basin in January. In comparison to Blelham Tarn, the other lakes had reduced diel temperature cycles (Fig. 5.5b). The magnitude of the monthly-averaged diel temperature ranges in Windermere South Basin, for example, varied by just over half of that in Blelham Tarn. While the monthly-averaged diel cycle was always less than 2 °C, diel cycles on individual days could be substantially larger than this. The greatest observed diel temperature range was 5.1 °C for Blelham Tarn and 2.3 °C for Windermere South Basin with the maximum diel temperature range for the remaining lakes between these values (Fig. 5.5c).

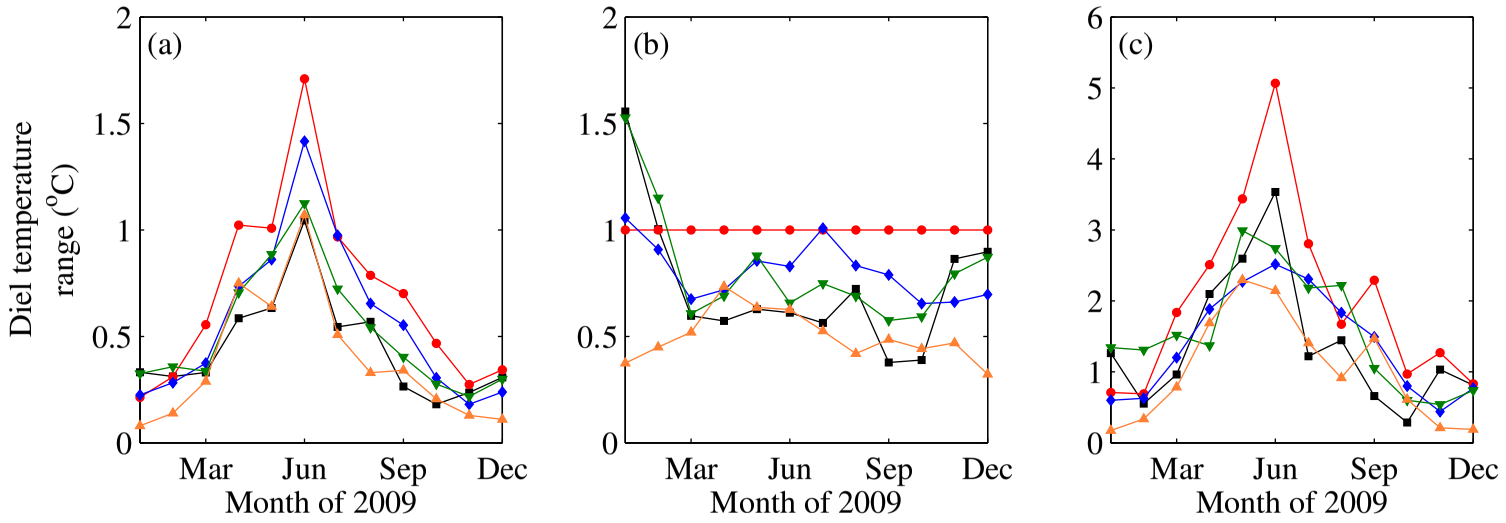

Figure 5.5: (a) Monthly-averaged diel temperature range for Bassenthwaite Lake (black), Blelham Tarn (red), Esthwaite Water (blue), Loweswater (green), and Windermere South Basin (orange); (b) ratio of the monthly-averaged diel temperature range of each lake to that of Blelham Tarn; and (c) maximum diel temperature range for each month. Note the change in the y-axis between the individual panels.

5.6 Monthly correlations between the diel temperature range, upper mixed layer depth, wind speed and lake surface area

For May through October, there was a significant correlation ($p < 0.05$) between the diel temperature range and z_{mix} among all of the lakes (Fig. 5.6). The monthly-averaged diel temperature range, for example, was largest for the lakes with the smallest monthly-averaged z_{mix}. The highest Pearson's correlation was calculated in June, which coincides with the period of maximum stratification strength and minimum z_{mix}. As previously stated, the mixing depth is equal to maximum lake depth during winter. The correlations and significance levels shown for the mixed periods (Jan, Feb, Mar, Nov, and Dec), therefore, have limited meaning in this context.

The correlation between the wind speed estimated at a height of 10 m, u_{10}, and the depth of the upper mixed layer, z_{mix}, varied through the year (Fig. 5.7). Pearson's correlation was significant ($p < 0.05$) from April through September, indicating that u_{10} significantly influenced z_{mix} during these months. This was not true in winter, however, when the lakes were fully mixed. The wind speed estimated at a height of 10 m was also significantly correlated with lake surface area through most of the year where the larger lakes experienced higher winds (Fig. 5.8). Similar to the relationship between u_{10} and z_{mix}, the relationship between u_{10} and lake area was most significant in July with a calculated Pearson's correlation of 0.97. The correlation and consequently the significance of the relationship then declined from July through October. The calculated Pear-

son's correlations, which illustrate the relationship between the diel temperature range, wind speed, the depth of the upper mixed layer, and lake surface area, are shown in Fig. 5.9. The connection between these factors can, therefore, be explained by the correlation between the diel temperature range and the depth of the upper mixed layer, which in these lakes is predominantly influenced by wind speed, and the correlation between wind speed and lake size.

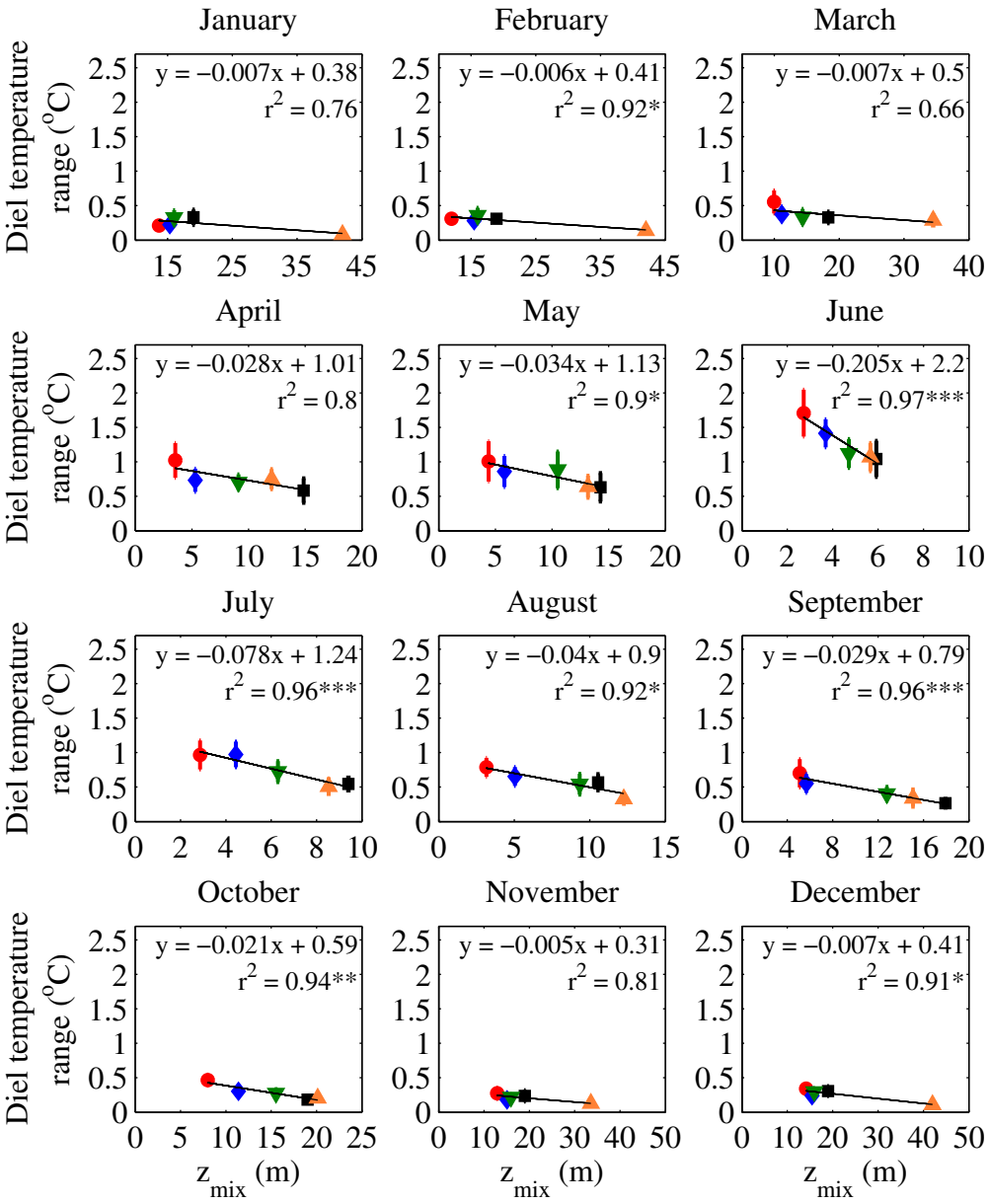

Figure 5.6: Scatter plots of the relationship between the monthly-averaged diel temperature range and the depth of the upper mixed layer, z_{mix}, for Bassenthwaite Lake (black), Blelham Tarn (red), Esthwaite Water (blue), Loweswater (green), and Windermere South Basin (orange). The statistical significance is shown as $***$ for $p < 0.001$, $**$ for $p < 0.01$, and $*$ for $p < 0.05$. The 95 % confidence intervals are shown for the temperature data. Note the change in the x-axis.

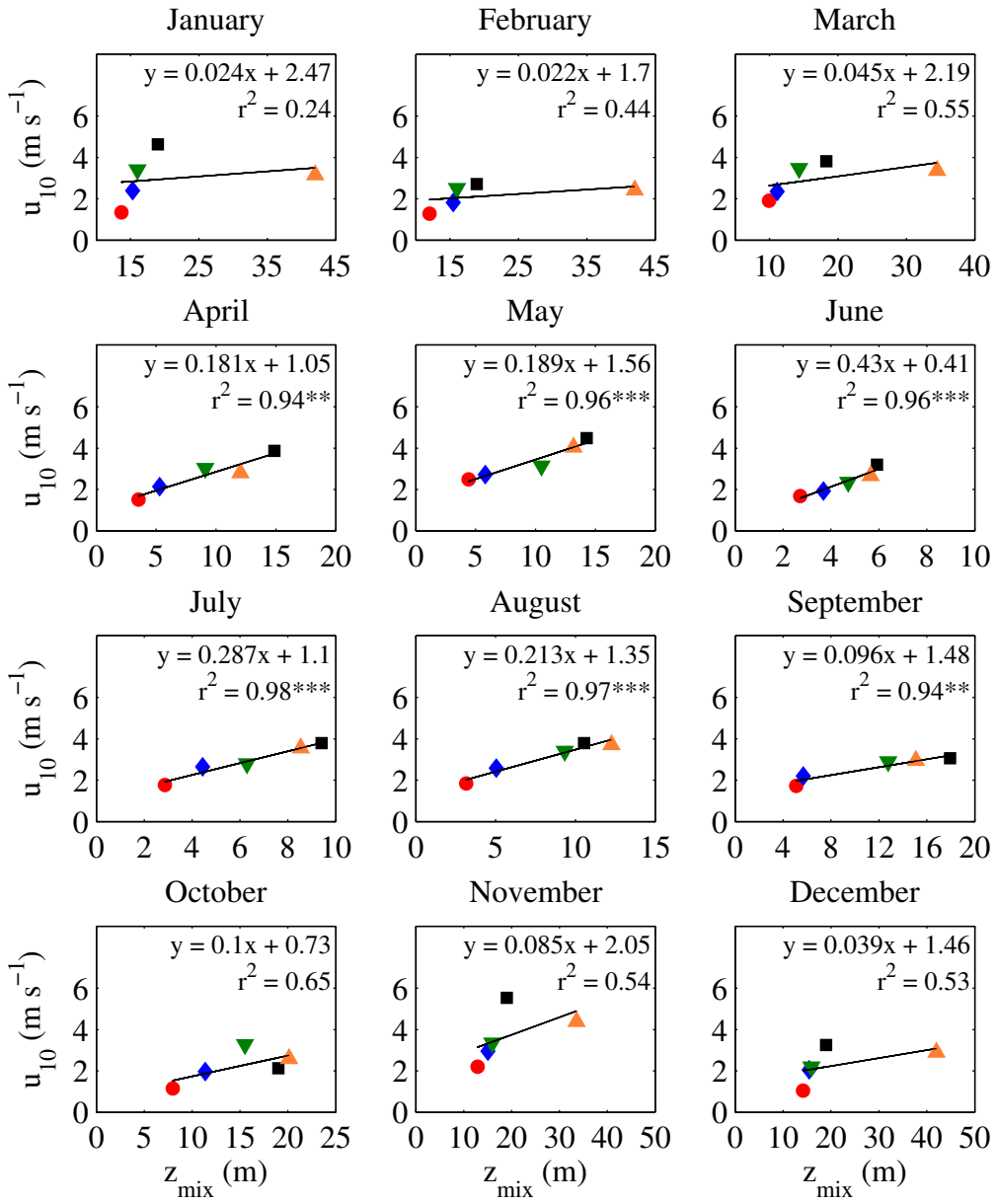

Figure 5.7: Scatter plots of the relationship between the monthly-averaged depth of the upper mixed layer, z_{mix}, and the wind speed estimated at a height of 10 m above the lake surface, u_{10}, for Bassenthwaite Lake (black), Blelham Tarn (red), Esthwaite Water (blue), Loweswater (green), and Windermere South Basin (orange). The statistical significance is shown as $***$ for $p < 0.001$, $**$ for $p < 0.01$, and $*$ for $p < 0.05$. Note the change in the x-axis.

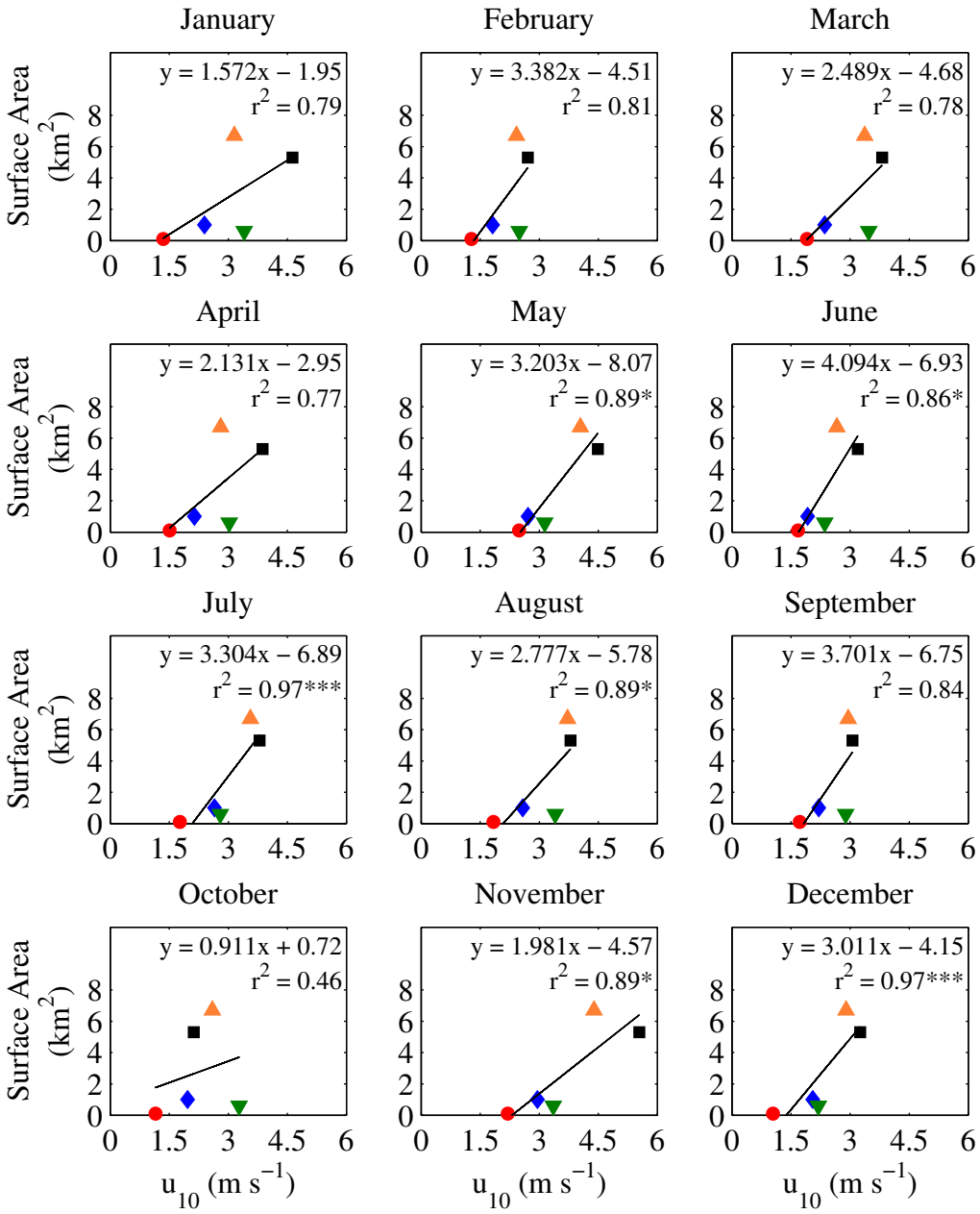

Figure 5.8: Same as Fig. 5.7 but for the relationship between the wind speed estimated at a height of 10 m above the lake surface, u_{10}, and lake surface area.

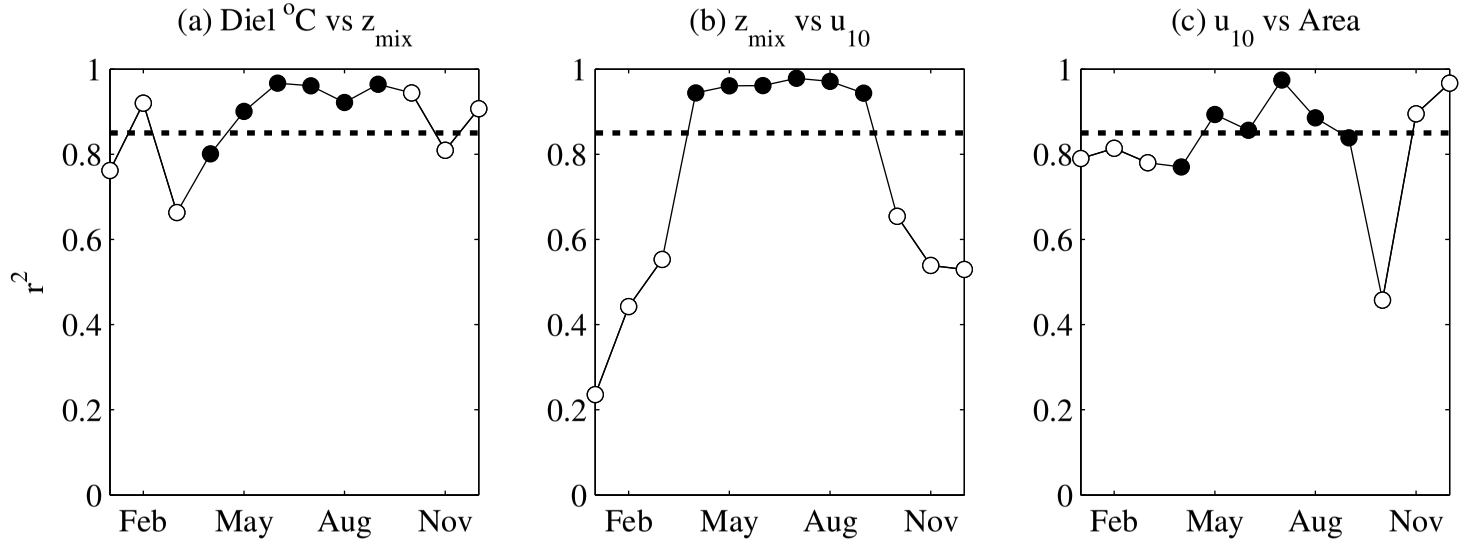

Figure 5.9: Monthly-averaged comparisons of Pearson's correlations for the stratified (filled circles) and non-stratified (unfilled circles) periods between (a) diel temperature range and the depth of the upper mixed layer; (b) depth of the upper mixed layer and the wind speed estimated at a height of 10 m above the lake surface; and (c) wind speed estimated at a height of 10 m above the lake surface and lake surface area. The dashed line illustrates the correlations that are statistically significant ($p < 0.05$), where points above this line are significant and those below the line are not.

Due to the significant relationship between the diel temperature range and z_{mix}, as well as the significant relationship between z_{mix} and u_{10}, there was also a significant relationship between the diel temperature range and u_{10} for some months (Fig. 5.10). There was a non-significant relationship between the diel temperature range and u_{10} during winter, for example, but a significant correlation was maintained for other months (April, May, June, July, September). Furthermore, the relationship between u_{10} and lake surface area, resulted in a significant ($p < 0.05$) relationship between the diel temperature range and lake surface area during some of the summer months (Fig. 5.11). In May, for example, Pearson's correlation between the diel temperature range and lake surface area was calculated as 0.98, being significant at the $p < 0.001$ level. The light attenuation coefficient, K_d, however, was only significantly correlated with the diel temperature range during August (Fig. 5.12). A correlation of 0.97, for example, was calculated in August, being the only statistically significant Pearson's correlation calculated between the diel temperature range and K_d for these lakes. The degree of coherence between the diel temperature range and Q_{zmix} was minimal through the majority of the year, illustrating that the magnitude of mixed layer heating did not significantly influence the diel temperature cycle (Fig. 5.13). The correlation between Q_{zmix} and the diel temperature range was statistically significant during September, however, where a Pearson's correlation of 0.98 was calculated. For the remainder of the stratified months Pearson's correlation was not statistically significant. The seasonal variability in the monthly-averaged Pearson's correlations are demonstrated in Fig. 5.14.

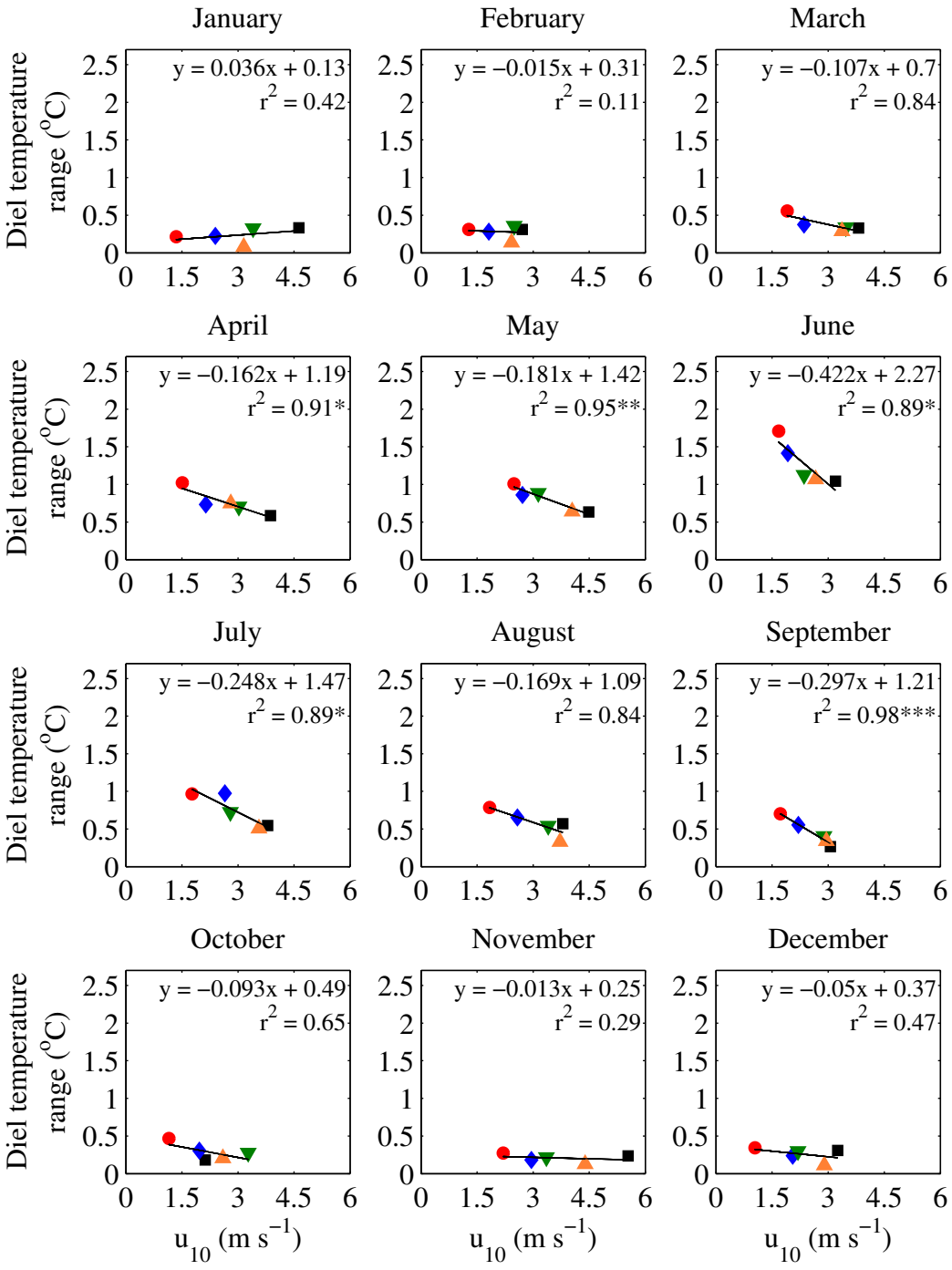

Figure 5.10: Same as Fig. 5.7 but for the relationship between the wind speed estimated at a height of 10 m above the lake surface, u_{10}, and the diel temperature range.

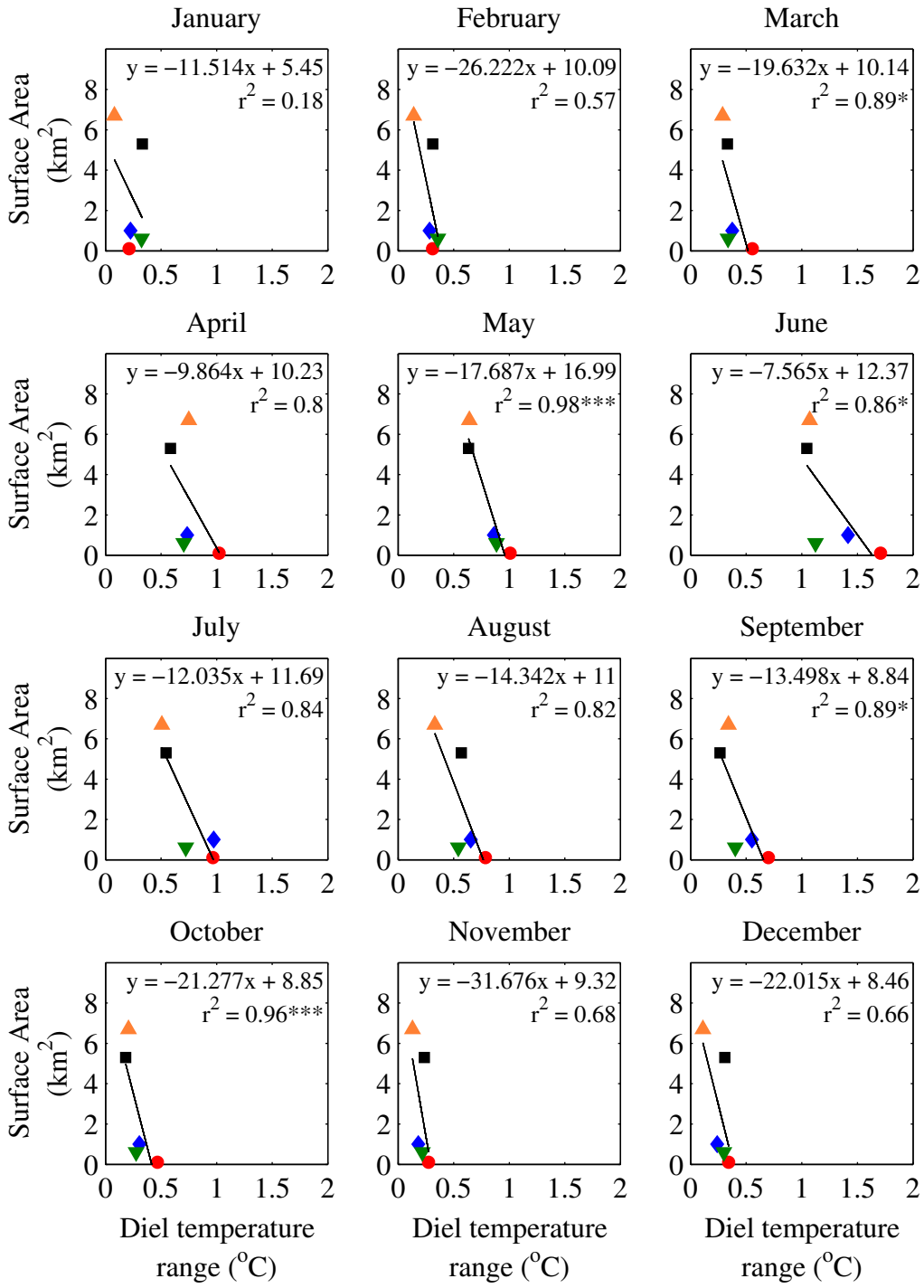

Figure 5.11: Same as Fig. 5.7 but for the relationship between the diel temperature range and lake surface area.

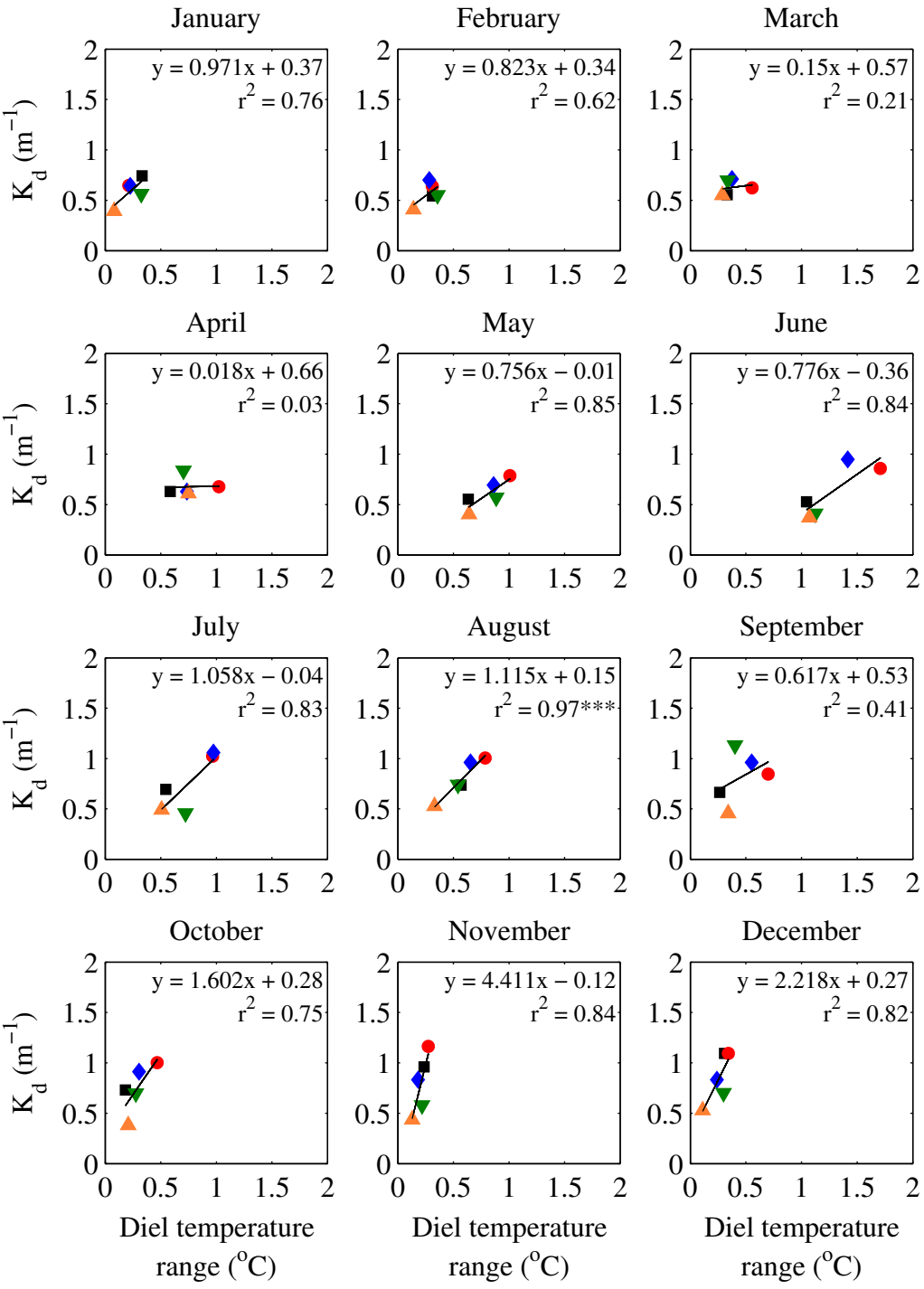

Figure 5.12: Same as Fig. 5.7 but for the relationship between the diel temperature range and the light attenuation coefficient, K_d.

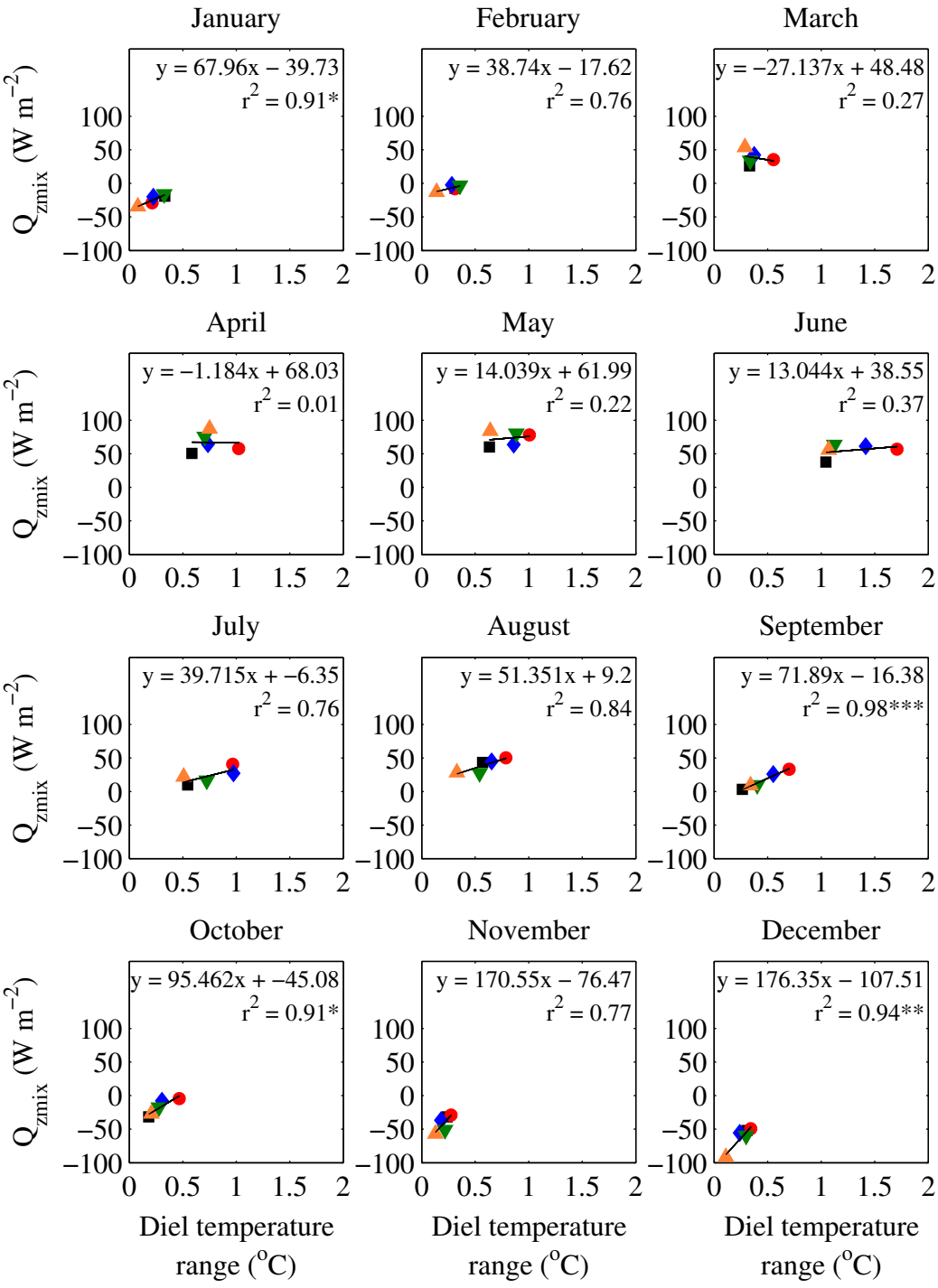

Figure 5.13: Same as Fig. 5.7 but for the relationship between the diel temperature range and upper mixed layer heating, Q_{zmix}.

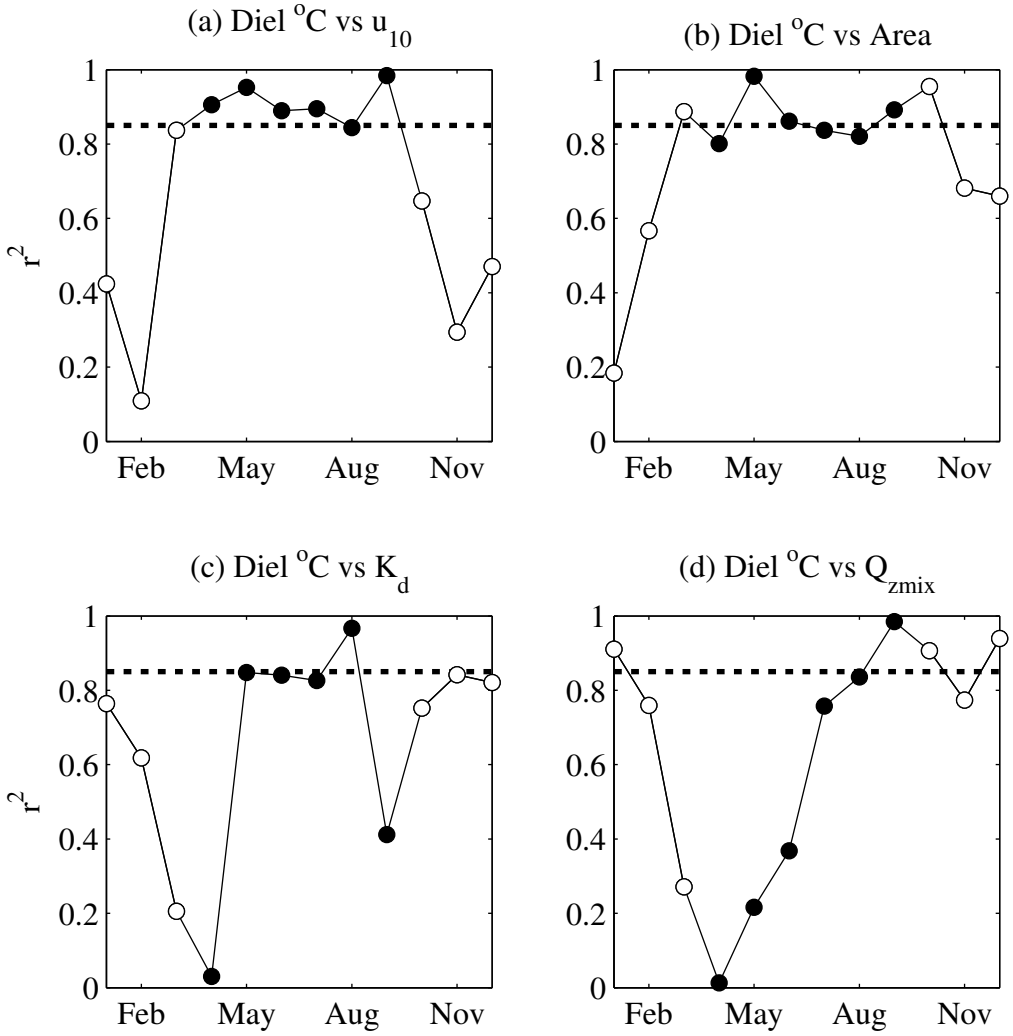

Figure 5.14: Monthly-averaged comparisons of Pearson's correlations for the stratified (filled circles) and non-stratified (unfilled circles) periods between (a) diel temperature range and the wind speed estimated at a height of 10 m above the lake surface; (b) diel temperature range and lake surface area; (c) diel temperature range and the light attenuation coefficient; and (d) diel temperature range and upper mixed layer heating. The dashed line illustrates the correlations that are statistically significant ($p < 0.05$).

5.7 Relationship between the diel temperature range and the depth of the upper mixed layer

The summer-averaged diel temperature range was statistically related to the summer-averaged z_{mix} with an r^2 of 0.91 (Fig. 5.15). Though there was a very high linear correlation for this small range of lakes, the relationship was better represented by a non-linear relationship of the form $y = ax^b$. By applying a power law relationship, the annual mean diel temperature cycle was related to the depth of z_{mix} by $y = 1.8858x^{-0.515}$ with an r^2 of 0.97. This means that the diel temperature range is expected to be even larger for lakes with mixed depths that are shallower than the ones investigated here.

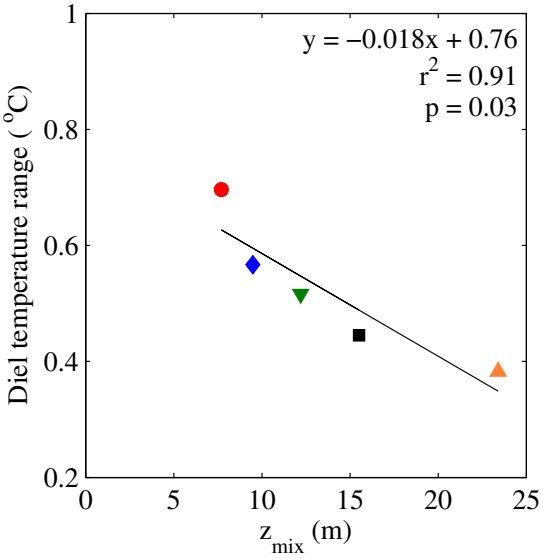

Figure 5.15: Relationship between the average diel temperature range and the average depth of the upper mixed layer during the stratified period. The different colours represent Bassenthwaite Lake (black), Blelham Tarn (red), Esthwaite Water (blue), Loweswater (green), and Windermere South Basin (orange).

Chapter 6

Diel variation in surface water temperature varies with lake size

6.1 Introduction

In Chapters 3, 4 and 5 of this dissertation the diel range in lake surface water temperature was shown to be predominantly influenced by the depth of the upper mixed layer. For lakes with shallower mixed layers, for example, atmospheric heating is concentrated over a smaller volume resulting in a larger diel temperature range than that experienced by lakes with deeper mixed layers. The depth of the upper mixed layer, however, is influenced by a number of lake specific characteristics such as lake size, water clarity, and the geographic location of the lake. Lake surface area, for example, can affect the wind speed at the lake surface, which in turn can alter the mixing depth. Water clarity can alter the absorption of solar radiation at the lake surface, and thus, influence water temperature. The geographic location of the lake can also influence lake temperature,

where latitude and altitude are known to control the local weather that directly influences the lake as well as the mixing processes within. These lake specific factors were discussed in detail in Chapter 1. In this chapter, the influence of lake area, water clarity, latitude and altitude on the diel range in surface water temperature is investigated for a large distribution of temperate lakes (Table 2.1).

6.2 Data transformation

To reduce the influence of a minority of extreme values in the raw data (Table 2.1), the explanatory variables (surface area, latitude, and K_d) were transformed. There is no need to transform latitude, the absolute value can be calculated and latitude can be used as a proxy for distance from the equator (irrespective of hemisphere). For lake surface area, a log transformation is applied. Similar to Fee et al. (1996), the light attenuation coefficient, K_d, is converted to percent transmission per metre as:

$$I_z = 100 \times \exp^{(K_d)}. \tag{6.1}$$

6.3 Which explanatory variable best describes the diel range in surface water temperature?

The objective of this part of the investigation is to determine the relationship between the diel temperature range and four explanatory variables (lake surface area, I_z, latitude, and altitude) for 74 of the 100 lakes (i.e. those that had data for

each of the explanatory variables). To begin, the data were assessed for collinearity between the explanatory variables, as well as the relationship between the explanatory variables and the response variable. The highest degree of collinearity was calculated between the diel surface water temperature range and lake surface area. There was also a high degree of collinearity between the percent transmission per metre, I_z, and the diel surface water temperature range. There does not seem to be any high correlation among the explanatory variables (i.e. for these lakes none of the explanatory variables correlate with one another).

A multiple linear regression model was first used in an attempt to explain the relationship between each of the explanatory variables and the diel temperature range. The multiple regression model was written as:

$$Diel_i = \beta_0 + \beta_1 \text{Area}_i + \beta_2 \text{Lat}_i + \beta_3 \text{Alt}_i + \beta_4 \text{Iz}_i + \varepsilon_i, \tag{6.2}$$

where β_0 is the intercept, β_1 to β_4 are the slope parameters of the fitted model, and ε_i is the residual error, where $i = 1 : n$ and n is the number of observations. The model validation graphs clearly illustrate that the model does not fit the data well (Fig. 6.1). Clear patterns are present, for example, between the residuals and the fitted values, and also the residuals are clearly not normally distributed. The model diagnostics also suggest that some observations may potentially have high influence, as shown by the relationship between the standardised residuals and the leverage. The model is also clearly violating the independence assumption where clear patterns are evident between the model residuals and the explanatory variables (Fig. 6.2). Specifically, there seems to be a strong dependence of the residual error and lake surface area where a substantial increase in the residuals

is evident at low lake surface area values. The remaining explanatory variables demonstrate a weaker relationship with the residuals.

To account for the observed increase in residual spread at low lake surface area values, a second-order polynomial function is included in the model. This may be expressed mathematically as:

$$Diel_i = \beta_0 + \beta_1 \text{Area}_i^2 + \beta_2 \text{Lat}_i + \beta_3 \text{Alt}_i + \beta_4 \text{Iz}_i + \varepsilon_i. \quad (6.3)$$

The model validation graphs, however, still demonstrate patterns in the residual error (Fig. 6.3). The relationship between the residuals and the fitted values, for example, are clearly not random. The Q-Q plot seems more promising than for the simple linear model (equation 6.2), although the model still seems to be violating the assumption of normality at some of the extreme values for the residuals. The standardised residuals also suggests that some observations will have high influence. A strong relationship is also observed between the model residuals and lake surface area (Fig. 6.4).

The relationship between the diel surface water temperature range and each of the explanatory variables was then examined by a generalised additive model (GAM) with a Gamma error distribution and a log-link function. A Gamma error distribution was appropriate since the observed diel surface water temperature range varied on a continuous scale and had a positive skew. The GAM may be written as:

$$\log(\text{Diel}_i) = \beta_0 + f_1 \text{Area}_i + \beta_2 \text{Lat}_i + \beta_3 \text{Alt}_i + \beta_4 \text{Iz}_i + \varepsilon_i, \quad (6.4)$$

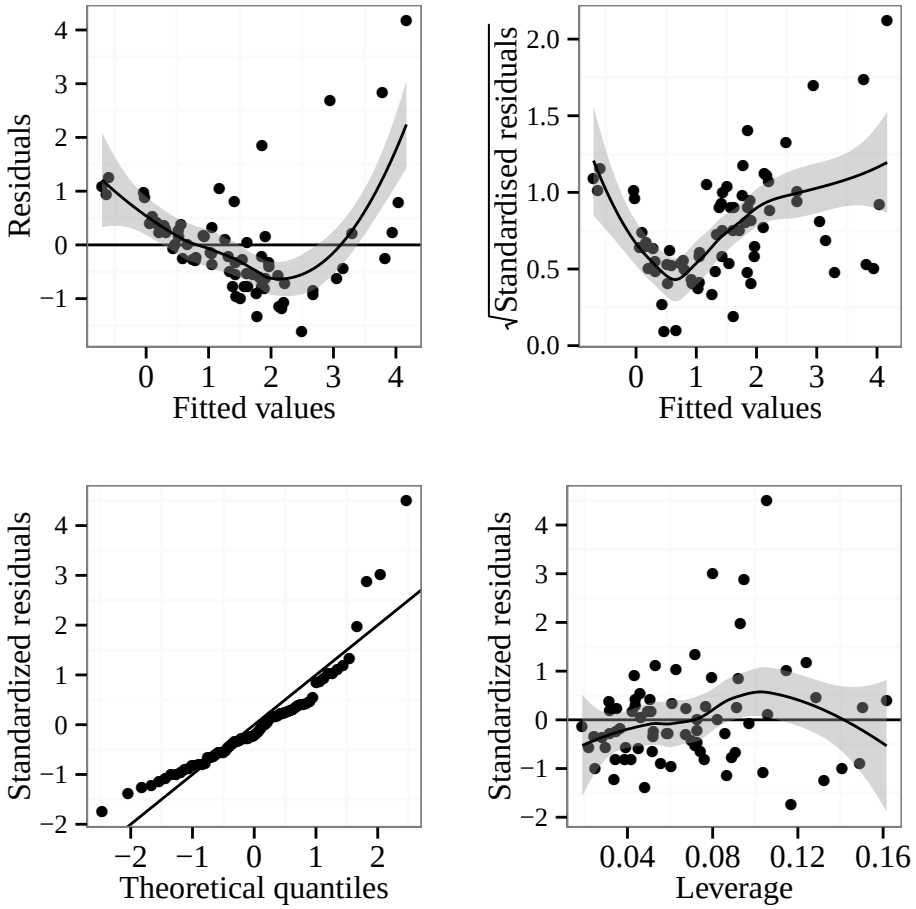

Figure 6.1: Model validation graphs obtained by applying a linear regression model to the diel surface water temperature range data. The upper left and upper right panels show the relationship between the residuals and the fitted values, a LOESS smoother is added to aid visual interpretation. The bottom left panel is a QQ-plot used to check for normality, and the lower right panel shows the standardised residuals versus leverage.

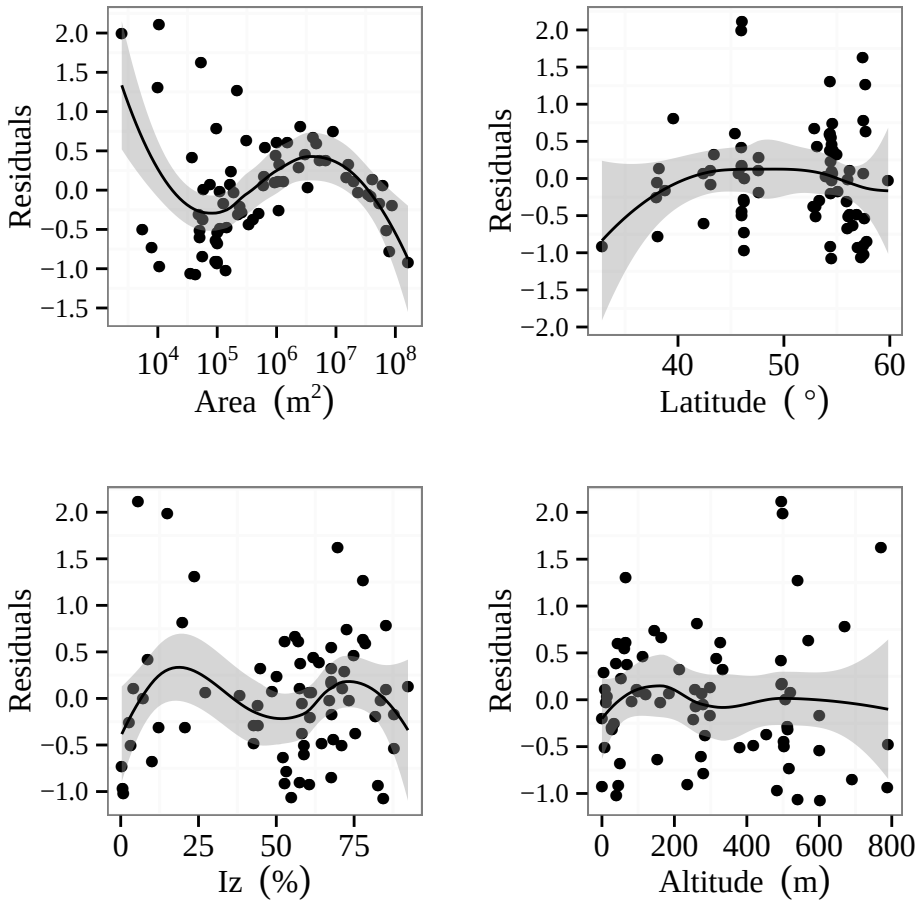

Figure 6.2: Relationship between model residuals for the linear regression model and each of the four explanatory variables. A LOESS smoother is added to aid visual interpretation.

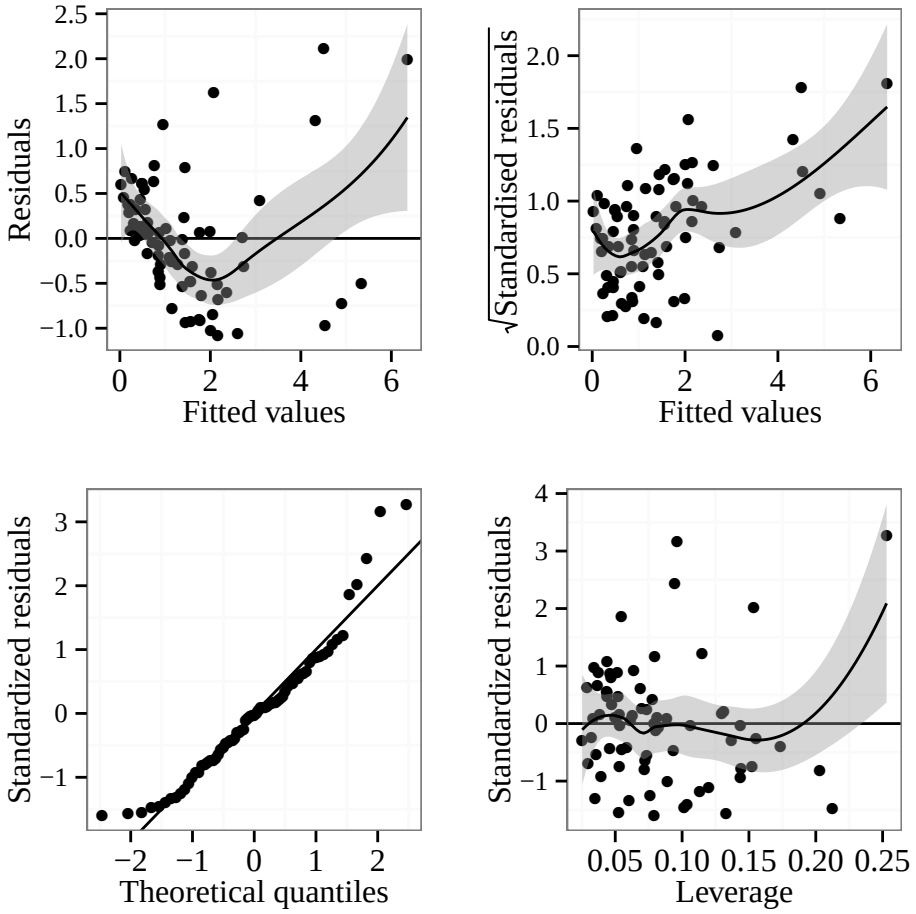

Figure 6.3: Same as Fig. 6.1 but for a linear regression model with a polynomial function applied to lake surface area.

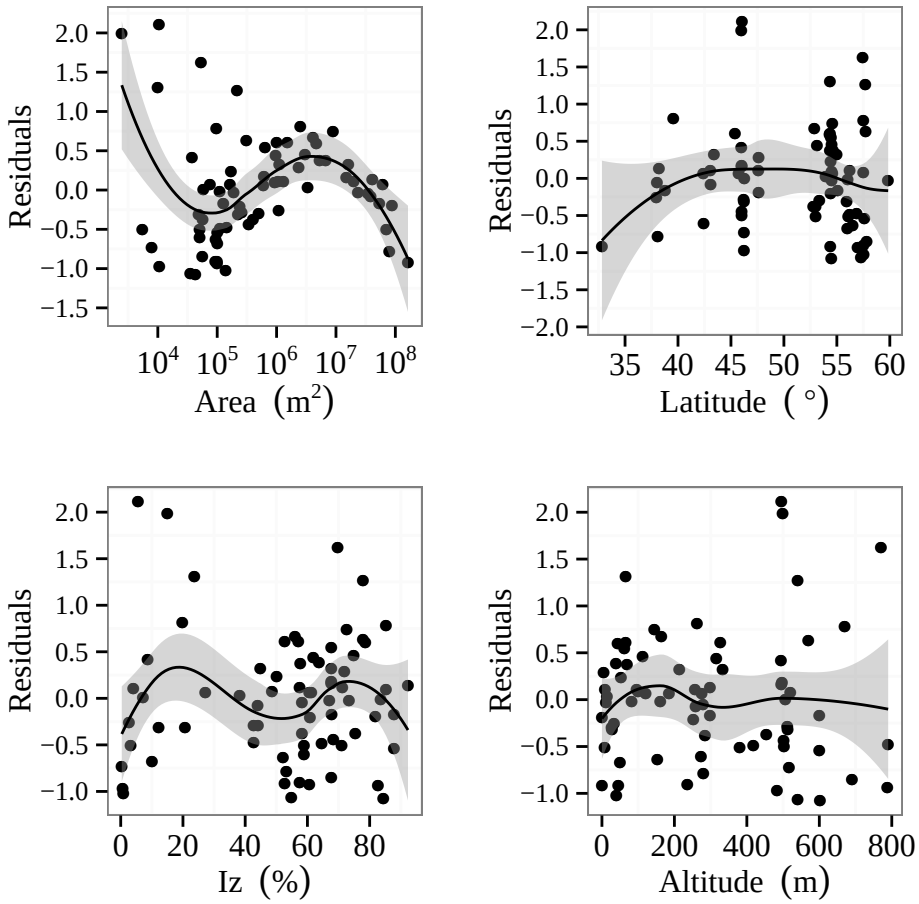

Figure 6.4: Same as Fig. 6.2 but for a linear regression model with a polynomial function applied to lake surface area.

where f_1 is a smoothing function (Hastie and Tibshirani, 1990). Initial inspection of the model residuals did not reveal any reasons for concern as the residuals did not demonstrate any clear patterns (Fig. 6.5). The numerical output of the model indicates that the smoother is significant ($p < 0.001$); hence, there is a significant non-linear relationship between the diel temperature range and lake surface area. The numerical output also indicates that the model explained 79.6 % of the variance.

The model expressed in equation 6.4 represents the global model (i.e. including all of the explanatory variables). In order to select the best possible combination of explanatory variables contained within the global model the dredge function from the R package MuMIn (Barton, 2014) was used. The dredge function is essentially a data mining method used to uncover relationships in the data. Models were compared using the adjusted Akaike Information Criterion (AICc) statistic, as recommended by Burnham and Anderson (1998) and discussed in Chapter 2 of this dissertation. Calculated AICc weights indicated that, for each of the parameters under consideration, no single statistical model received overwhelming support. Rather, a set of top-ranking models received similar levels of support (Table 6.1). The top models, however, consistently included a lake surface area effect.

The confidence set of models were used to derive relative importance values and model-averaged effect sizes for each of the explanatory variables. Relative importance represents the probability of a variable being present in the best-performing model and is calculated in MuMIn using the relative Akaike weights of models within the confidence set (Burnham and Anderson, 1998). For the candidate set of models, lake surface area was calculated as having the highest

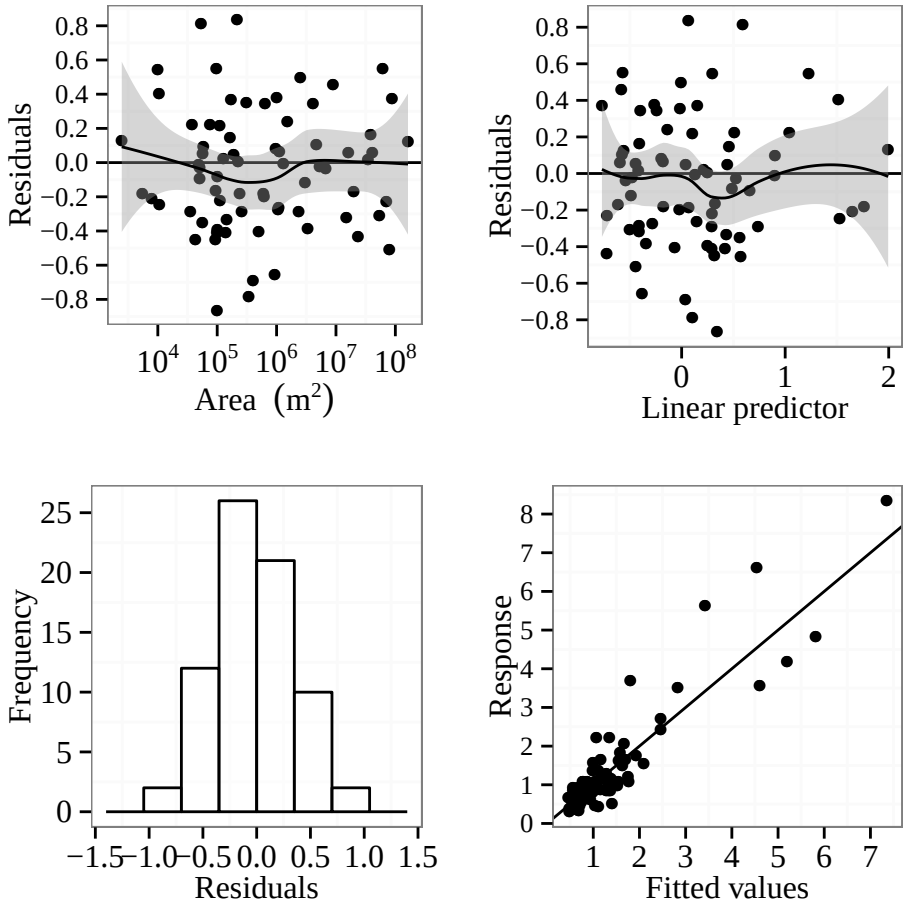

Figure 6.5: Model validation graphs for the generalised additive model. The upper left panel shows the relationship between the model residuals and lake surface area; the upper right panels show the relationship between the residuals and the linear predictor. A LOESS smoother is added to aid visual interpretation. The bottom left panel is a histogram to check for normality, and the lower right panel shows the residuals against the fitted values.

Table 6.1: The confidence set of models ranked according to their adjusted Akaike Information Criterion (AICc) statistic.

Model	AIC_c	ΔAIC_c	Akaike weight
$\log(\text{Diel}_i) = \beta_0 + f_1(\text{Area}_i) + \beta_3 \text{Alt}_i + \beta_4 \text{Iz}_i + \varepsilon_i$	82.5	0.00	0.274
$\log(\text{Diel}_i) = \beta_0 + f_1(\text{Area}_i) + \beta_4 \text{Iz}_i + \varepsilon_i$	82.6	0.09	0.262
$\log(\text{Diel}_i) = \beta_0 + f_1(\text{Area}_i) + \beta_2 \text{Lat}_i + \beta_4 \text{Iz}_i + \varepsilon_i$	83.6	1.05	0.162
$\log(\text{Diel}_i) = \beta_0 + f_1(\text{Area}_i) + \beta_2 \text{Lat}_i + \varepsilon_i$	84.3	1.74	0.115
$\log(\text{Diel}_i) = \beta_0 + f_1(\text{Area}_i) + \beta_2 \text{Lat}_i + \beta_3 \text{Alt}_i + \beta_4 \text{Iz}_i + \varepsilon_i$	84.4	1.84	0.109
$\log(\text{Diel}_i) = \beta_0 + f_1(\text{Area}_i) + \beta_2 \text{Lat}_i + \beta_3 \text{Alt}_i + \varepsilon_i$	86.4	3.83	0.040

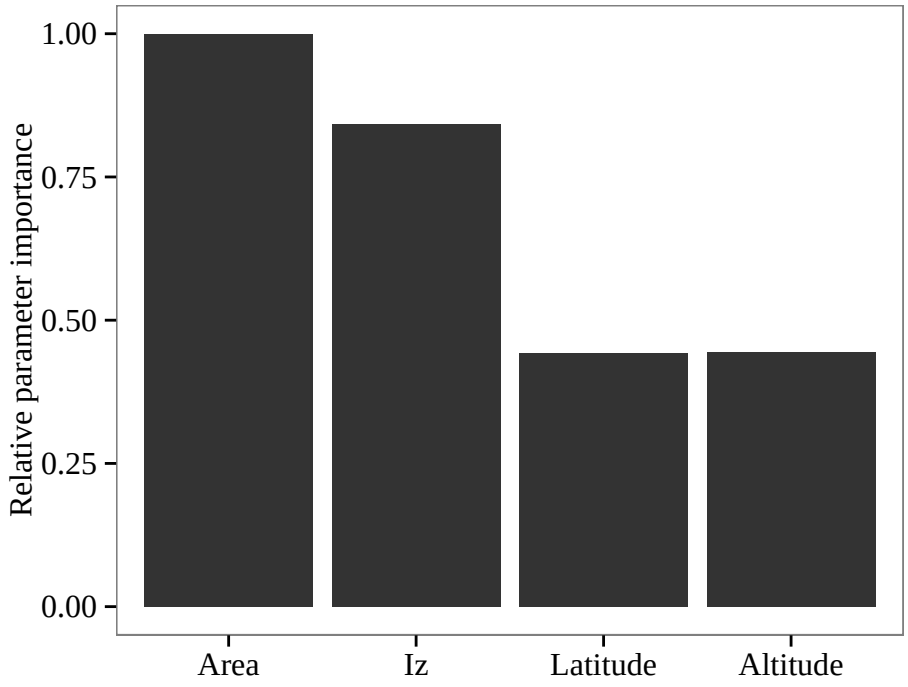

Figure 6.6: The relative importance of lake surface area, I_z, latitude, and altitude in the candidate set of models.

relative parameter importance, followed by I_z, which had a relative importance of 0.83 and latitude and altitude which have an importance of 0.44 (Fig. 6.6).

The model-averaged parameters (i.e. of the confidence set of models) were then used to predict the influence of lake surface area on the diel temperature range (Fig. 6.7), which was based on weighted means of the remaining coefficients from the confidence set of models. The model-averaged prediction demonstrated that the diel temperature range increases with decreasing lake surface area. For the other terms included in the global model, model-averaged effect sizes were calculated for each explanatory variable by averaging the parameter estimates across each model in which a given parameter occurred. A

significant effect of a parameter is indicated where the confidence interval does not overlap with zero (Grueber et al., 2011). These results demonstrated that the model-averaged effects sizes were only significant for I_z, although being relatively small. This confirmed that lake surface area was the most important explanatory variable for explaining the diel range in lake surface water temperature from the observed measurements. Furthermore, the global model identified that the relationship between the diel temperature range and lake surface area was highly significant ($p < 0.001$), while water clarity was only just significant ($p < 0.05$).

6.4 At what surface area is the diel temperature range significantly increasing?

Lake surface area had a strong influence on the diel temperature range. By simply plotting the observed diel temperature range against lake surface area, a clear pattern emerges (Fig. 6.8). The diel temperature range, for example, was much smaller for the larger lakes, and appears to considerably increase for the smaller lakes. To determine at what lake surface area was the diel temperature range significantly increasing (i.e. when surface area had a significant influence on the diel temperature range), a statistical model was used. As the global model (equation 6.4) demonstrated that I_z, latitude and altitude has a minimal influence on the diel temperature range, a similar model was used to express the relationship between the diel temperature range and lake surface area alone. Similar to equa-

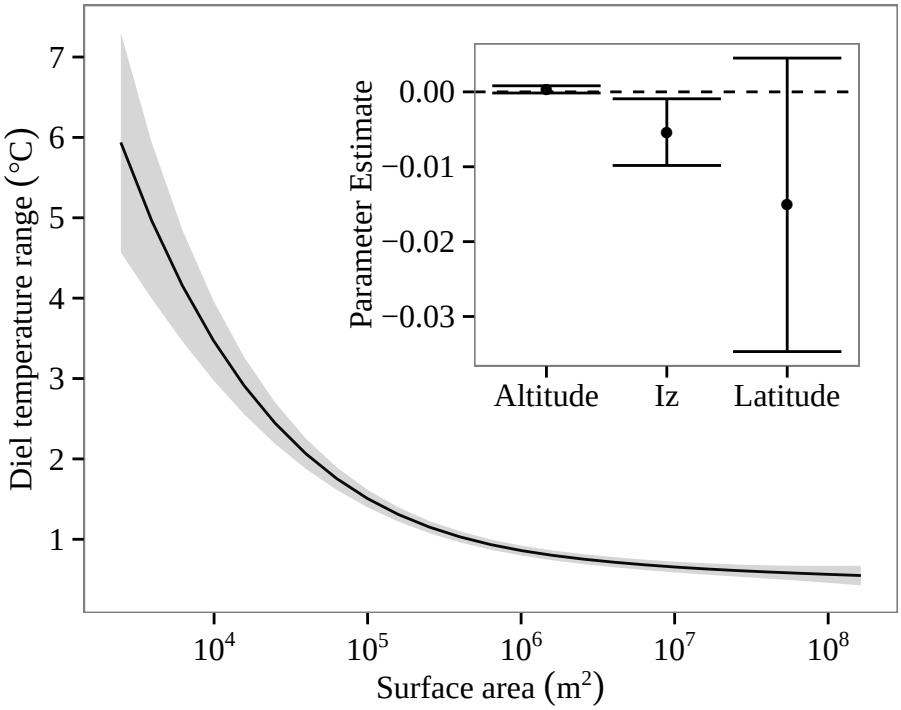

Figure 6.7: Predicted relationship between lake surface area and the diel surface water temperature range from the model averages of the candidate set of models and the model-averaged slope parameters for the relationship between the diel surface water temperature range and the remaining explanatory variables (inset). Filled circles indicate the model-averaged slope parameter estimate for each relationship, and whiskers indicate the 95 % confidence interval for the estimate. Dashed horizontal line indicates zero.

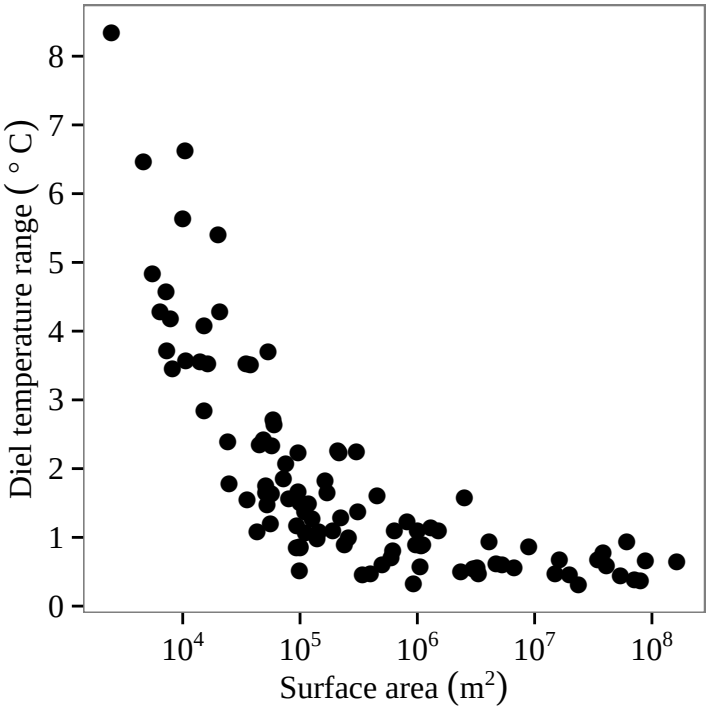

Figure 6.8: Relationship between the observed diel surface water temperature range and lake surface area.

tion 6.4, a GAM with a gamma error distribution was chosen to model the diel range as a function of lake surface area. This model can be written as:

$$\log(\text{Diel}_i) = \beta_0 + f_1\text{Area}_i + \varepsilon_i. \tag{6.5}$$

For this model, data from 100 lakes was used. Diagnostics checks did not reveal any problems associated with the residuals (Fig. 6.9). The numerical output identified that the model explained 78.1 % of the variance and had an r^2 of 0.82 ($p < 0.001$). The confidence intervals for the fitted GAM demonstrated that the

model was sufficiently capturing the variation in the diel temperature range (Fig. 6.10). The GAM was also re-computed using only 74 lakes (i.e. same as equation 6.4) to demonstrate the minimal influence that the number of observations has on the fitted model. This was confirmed as the GAM for the 74 lakes fits within the confidence intervals for the GAM computed with 100 lakes.

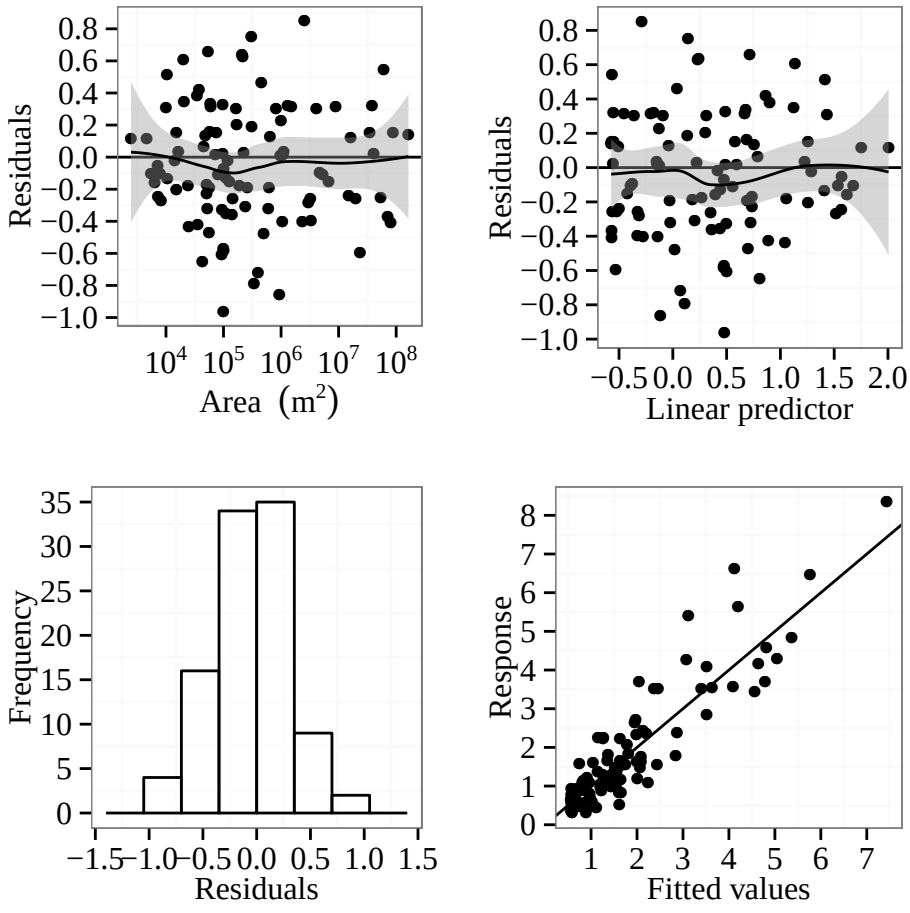

Figure 6.9: Same as Fig. 6.5 but for the generalised additive model with only lake surface area as an explanatory variable.

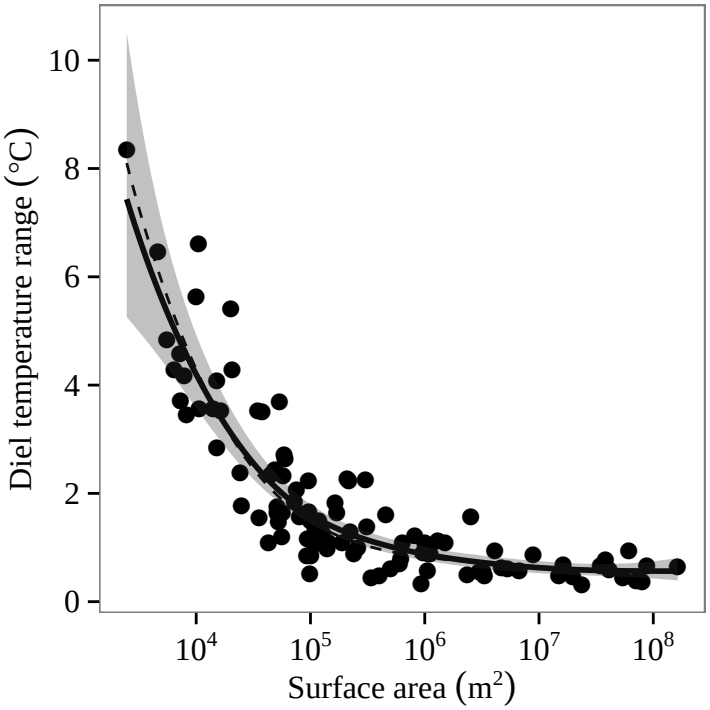

Figure 6.10: Same as Fig. 6.8 but with GAM fit for 100 (solid black line) and 74 (thin dashed line) lakes superimposed.

In order to estimate the lake surface area at which the diel temperature range starts to significantly increase, the rate of change of the fitted model needed to be calculated to see if rate of change is sufficient to reject the null hypothesis that the slope of the relationship is 0 at a given point. For a linear regression model the estimated rate of change would be $\bar{\beta}$, the slope of the regression line. It could then be determined if the non-zero estimate for the slope is distinguishable from 0 given the uncertainty in the estimate. The slope or the estimate $\bar{\beta}$ is the first derivative of the regression line. Technically, this is the instantaneous rate of change of the function that defines the line, an idea that can be extended to any

function, even one as potentially complex as a fitted spline function in the GAM. An issue with using a GAM, however, is that we do not have the full equation for the spline from which to extract the derivatives. As we have a fitted model, however, the finite difference method can be used to estimate the derivatives. Finite differences is a technique by which derivatives of functions are approximated between a given value and a small increment (Fig. 6.11).

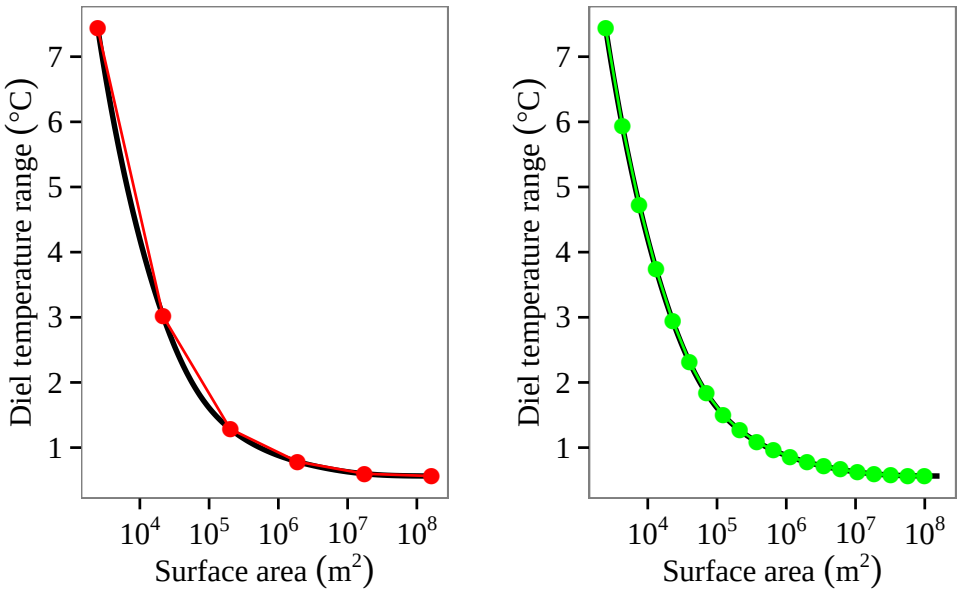

Figure 6.11: Illustration of the finite differences approach to estimating derivatives of a function.

Consider the situation in the left hand plot of Fig. 6.11. The black line is the fitted spline. Superimposed on the spline are six points, between pairs of which we can approximate the first derivative of the function. We know the distance along the x-axis (surface area) between each pair of points and we can evaluate the value of the function on the y-axis by predicting from the model for the

indicated points. The derivatives are reasonably well approximated using this method at some instances using just a selected number of points, but in other places this approach either under or over estimates the derivative of the function. The solution is to evaluate the slope at more points that are located closer together on the function. The right hand plot in Fig. 6.11 shows the finite difference method for increased number of points. The accuracy of this method will increase by using points that are closer together. Eventually, the points would be infinitely close so that the first derivative would be calculated exactly.

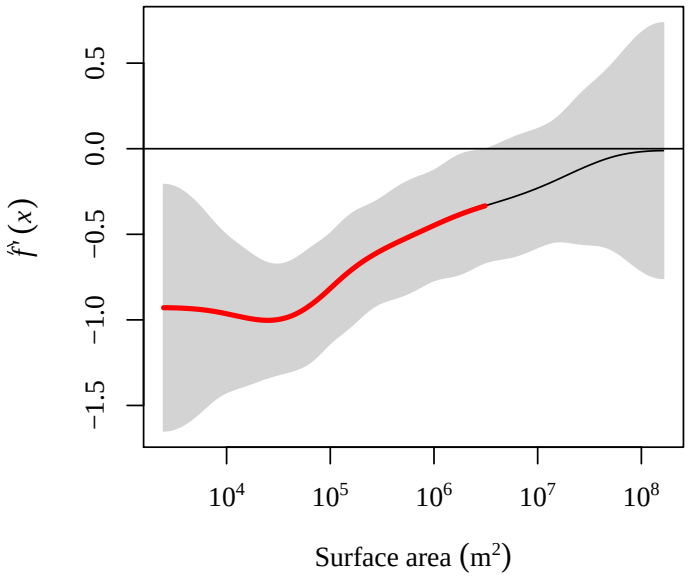

Figure 6.12: Time series of first derivatives of the fitted model. The red line indicates those parts of the model fit that are statistically significantly changing and the grey region show the confidence intervals for the first derivatives.

The first derivative of the model identifies one clear region of statistically significant change in diel surface water temperature range with respect to surface

area (Fig. 6.12). Periods of significant change in diel surface water temperature range are then superimposed on the observed data (Fig. 6.13). The derivatives suggest a significant increase in the diel temperature range for lakes smaller than 3.2 km^2 whereas those above this threshold are not significantly changing with respect to surface area.

The expected diel temperature range, which is calculated here from first principles, as shown in Chapter 2 of this dissertation, was in close agreement with the observed values, with a RMSE of 0.6 °C. The expected diel temperature range, for example, is low for the large lakes and high for the smaller lakes. Only 23 of the lakes had meteorological and depth-resolved temperature measurements, which are needed to estimate the diel range. The smallest lake that the expected range could be calculated for was Trout Bog (USA) which had an expected diel range of 3.88 °C. The lowest expected diel temperature range was calculated for one of the largest lakes, Waikaremoana (0.2 °C).

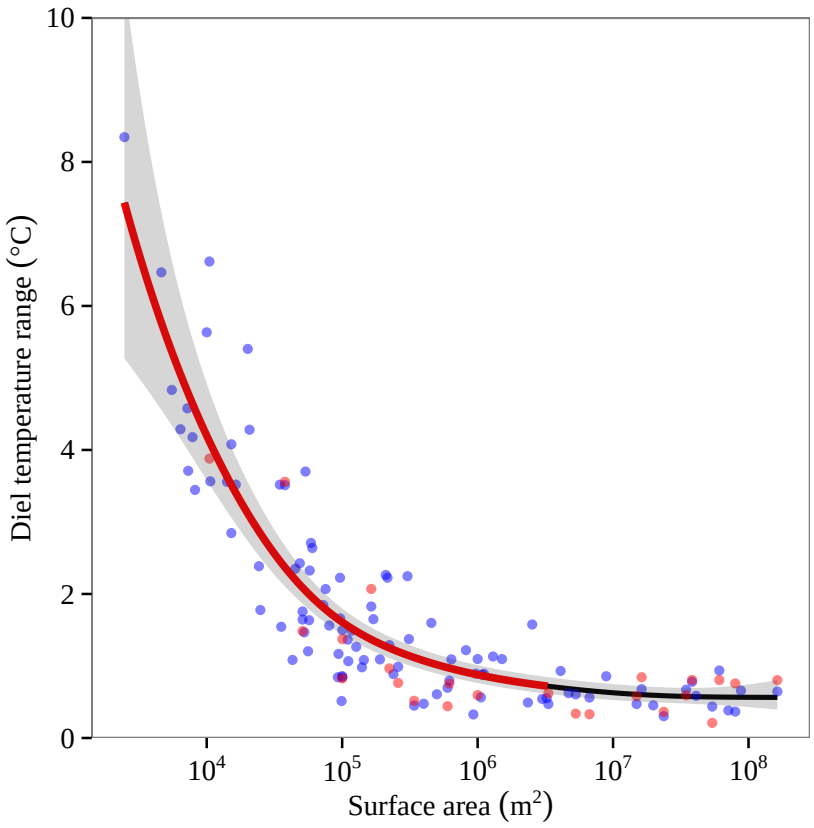

Figure 6.13: Relationship between the observed (blue circles) and expected (red circles) diel surface water temperature range and lake surface area with the GAM fit and 95 % confidence limits overlaid (grey). The red line indicates those parts that are statistically significantly increasing.

On individual days, temperature ranges could be much greater than the summer-averaged values. During a two-week period in mid-summer, for example, the diel temperature range in Jekl Bog (USA), the smallest lake in the data set, could be as high as 15 °C, which was an order of magnitude larger than some of the larger lakes, such as the nearby Sparkling Lake, which had a maximum diel tempera-

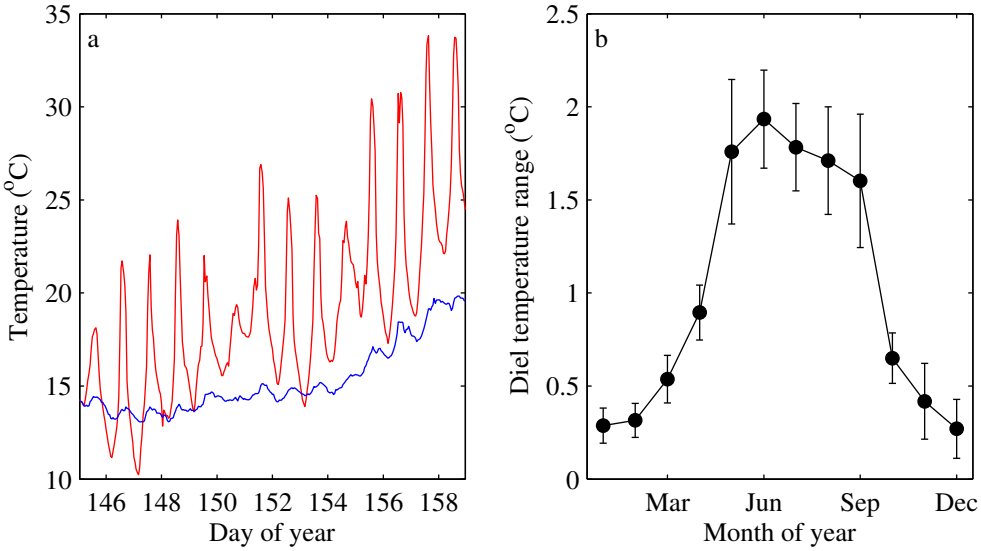

Figure 6.14: Example of hourly-resolution near-surface lake water temperature variation at Jekl Bog, Wisconsin, USA (red) and Sparkling Lake (blue), which are < 2 km apart. b, Seasonal change in near-surface diel temperature range for 96 Northern Hemisphere lakes with 95 % confidence intervals (note that not all lakes had data for the whole year).

ture range of only 1.1 °C in the same period (Fig . 6.14a). Similarly, the diel temperature range will vary seasonally, being greatest in summer when energy exchanges across the lake surface are greatest and least in winter when surface heating is minimal (Fig. 6.14b).

In order to understand the implications that the relationship between the diel temperature range and lake size may have on a global scale, the global abundance and size distribution of the worlds lakes was estimated. To estimate the global abundance and size distribution of lakes, the method presented by Downing et al. (2006) was followed. They describe that the size distribution of lakes has been

observed to follow a Pareto distribution, with the probability density function

$$pdf\left(A_0\right) = ck^c A_0^{-(c+1)}, \tag{6.6}$$

where $c = 1.06079$ is the shape parameter (Downing et al., 2006) and $k = 0.001$ is the smallest possible lake size (km^2). The number of lakes between a given size range, A_{min} and A_{max}, is estimated as:

$$N_{A_{max}-A_{min}} = -N_t k^c \left(A_{max}^{-c} - A_{min}^{-c}\right), \tag{6.7}$$

where $N_t = 3.04 \times 10^8$ is the total number of the worlds lakes and A_{min} and A_{max} are the minimum and maximum lake size for a given size range. The average size and total area covered by lakes in a given size range can then be calculated as:

$$\bar{A}_{A_{min}-A_{max}} = c \times \frac{-A_{max}A_{min}^c + A_{max}^c A_{min}}{(c-1)\left(A_{max}^c - A_{min}^c\right)}. \tag{6.8}$$

The total land area covered by lakes of any size can be calculated as the product of equation 6.7 and equation 6.8. The calculated numbers, average sizes, and areas of the world's lakes are shown in Table 6.2.

Table 6.2: The numbers, average sizes, and areas of world lakes calculated from equations 6.7 and 6.8 following Downing et al. (2006).

A_{min} (km^2)	A_{max} (km^2)	Number of lakes	Average lake area (km^2)
0.001	0.01	277,422,033	2.496×10^{-3}
0.01	0.1	24,118,536	2.495×10^{-2}
0.1	1	2,096,819	2.496×10^{-1}
1	10	182,293	2.496×10^{0}
10	100	15,905	2.470×10^{1}
100	1,000	1,330	2.480×10^{2}
1,000	10,000	105	2.456×10^{3}
10,000	100,000	16	3.198×10^{4}
$>$ 100,000		1	3.781×10^{5}

Using the method shown above, the global population of the world's lakes was estimated as approximately 304 million. Of the global population of lakes, the statistical method above suggests that 77 % of lakes are smaller than 0.004 $\times$ 10^6 m^2. Thus, from these estimates, over three quarters of the world's lakes will experience a summer-averaged diel temperature range in excess of 6 °C. Similarly an estimated 96 % of lakes are smaller than 0.02 $\times$ 10^6 m^2 and likely to experience a summer-averaged diel temperature range of greater than 3 °C. Although recent estimates from satellite imagery (Verpoorter et al., 2014) suggest that the statistical method described by Downing et al. (2006) overestimates the

number of small lakes in the world, it confirms that the majority of the lakes in the world are small (< 0.01 km^2). Therefore, on the basis of recent satellite imagery, it can be estimated that over 90 million of the world's lakes (with a surface area of between 0.002 to 0.01 km^2) will have a summer diel surface temperature range of up to 6 °C.

Chapter 7

Discussion

7.1 Introduction

A hierarchy of environmental conditions can influence the functioning of a lake. Climate is a first-order control that can affect the ecosystem through a complex series of direct and indirect mechanisms. Indirect mechanisms include the effect of climate on the catchment. Processes such as weathering, microbial activity, vegetation decomposition and productivity, for example, can influence the lake through the transfer of solutes and particulates from the catchment. Climate can also influence the lake directly by altering the lake's thermal and hydrological budgets. Improving our understanding of lake function, therefore, most logically begins at the lake surface by focusing on the direct effects of climate.

7.2 The transfer of energy at the air-water interface

The dynamic coupling between a lake and the atmosphere depends on the transfer of momentum, heat and material at the air-water interface. It is the quantities of these fluxes that influence physical processes within lakes, and in turn, have a major impact on lake ecology. In order to understand fully the workings of lakes it is therefore imperative to have a detailed understanding of the atmospheric forcing at the lake surface, and to understand how different atmospheric conditions can affect the system. This is particularly true in the context of climate change (e.g. De Stasio et al., 1996; Winder and Schindler, 2004) where it is necessary to be able to quantify these fluxes under present climate conditions, in order to be able to detect any future changes in them (Betts et al., 1996).

The exchange of energy at the air-water interface is driven by a number of meteorological parameters such as air temperature, cloud cover, relative humidity, and wind speed. The exchange of energy is often represented by bulk formulae, which allow the surface energy fluxes to be calculated according to frequently measured variables. However, these formulae also require the use of transfer coefficients. Various reviews on transfer coefficients (e.g. Blanc, 1985; Garratt, 1977, 1994) have suggested a number of factors on which they depend, in particular, wind speed and atmospheric stability (e.g. Verburg and Antenucci, 2010).

Wind speed is often considered as one of the most important parameters controlling the transfer of energy at the air-water interface. Higher wind speeds increase wave height and therefore roughness length, which in turn act to in-

crease the transfer coefficient (Brutsaert, 1982). At low wind speeds, however, gravity waves cease to be the most important interface between the water and the overlying atmosphere, and other mechanisms control the value of the transfer coefficients (Chang and Grossman, 1999). As seen in this dissertation, atmospheric stability can also cause large variations in the transfer coefficients as the more stable the atmosphere the more restricted is the mixing from higher levels towards the air-water interface (Deardorff, 1968). Therefore, the transfer coefficient is higher in an unstable atmosphere than a stable atmosphere.

Actual estimates of the transfer coefficient vary enormously in the literature (Garratt, 1994), where an order of magnitude increase between values in stable low wind speed conditions and those in unstable high wind conditions have been reported (Smith, 1988). Similarly, the drag coefficient, which is a dimensionless quantity, has been shown to vary from less than 1×10^{-3} to nearly 3×10^{-3} (Blanc, 1985) during different wind regimes, and some investigations have even shown that during similar wind conditions, the drag coefficient can vary by more than 50 % (Blanc, 1985; Hsu, 1986). As shown in this dissertation, estimates of transfer coefficient can also vary by over an order of magnitude within a 24 hour period.

Although the transfer coefficient can vary greatly at a range of temporal scales, owing to different atmospheric forcing, some researchers often parametrise it as a constant. The constant used, however, can vary greatly in the literature (Table 7.1) where some studies may even use a different constant for the same lake driven by the same meteorological forcing. This is common in modelling studies where the constant used for a given lake can vary by an order of magnitude (e.g. Stepanenko et al., 2014). As the transfer coefficient varies as a function of wind

speed, however, several researchers have used different constants depending on a pre-determined wind speed threshold (e.g. Read et al., 2011). Others estimate the transfer coefficient from a simple function of wind speed (e.g. Markfort et al., 2010). In order to obtain accurate estimates for the transfer coefficients, however, the influence of wind speed and atmospheric stability must be accounted for (e.g. Verburg and Antenucci, 2010).

Similar to the drag coefficient, the transfer coefficients for heat (C_h) and

Table 7.1: List of commonly used drag coefficient constants (dimensionless) including some example references.

Value	Description	Reference
0.001	Modelling study of Lake Valkea-Kotinen (Finland) using SimStrat (Goudsmit et al., 2002; Perroud et al., 2009)	Stepanenko et al. (2014)
0.001	Limnological tool for lake physics. C_d values valid for wind speed < 5 m s^{-1}	Read et al. (2011)
0.0011	Modelling study of Lake Valkea-Kotinen (Finland) using LAKEoneD (Jöhnk et al., 2008; Jöhnk and Umlauf, 2001)	Stepanenko et al. (2014)
0.0013	Gas transfer velocity estimates	Crusius and Wanninkhof (2003) Vachon et al. (2010)
0.0014	Used to estimate physical wind forcing following Wüest et al. (2000)	Mackay et al. (2014)
0.0015	Limnological tool for lake physics. C_d values valid for wind speed ≥ 5 m s^{-1}	Read et al. (2011)
0.0018	Modelling study of Lake Valkea-Kotinen (Finland) using FLake (Kirillin et al., 2011; Mironov, 2008; Mironov et al., 2010)	Stepanenko et al. (2014)
0.0045	Modelling study of Lake Valkea-Kotinen (Finland) using CLM4-LISSS (Hostetler and Bartlein, 1990; Subin et al., 2012)	Stepanenko et al. (2014)
0.012	Modelling study of Lake Valkea-Kotinen (Finland) using LAKE (Stepanenko et al., 2011)	Stepanenko et al. (2014)

humidity (C_e) can also vary in the literature. These transfer coefficients are im-

portant as they determine the rate of exchange of heat and humidity at the air-water interface. Unlike the drag coefficient, traditional estimates of C_h and C_e tend to support a fairly constant value over a range of wind speeds. Friehe and Schmitt (1976), for example, recommended a constant C_{e10} of $1.32 \times 10^{-3} \pm 0.007$ on the basis of several turbulence-based datasets where the highest wind speed was 4 m s^{-1}. Smith (1989) suggested a constant value of $1.2 \times 10^{-3} \pm 0.1$ for winds between 4 and 14 m s^{-1}. For higher wind speeds, DeCosmo et al. (1996) suggested a constant value of $1.12 \times 10^{-3} \pm 0.24$ for wind speeds up to 18 m s^{-1}. For C_{h10}, Friehe and Schmitt (1976) obtained slightly different values for unstable and stable atmospheric conditions (0.97×10^{-3} and 0.86×10^{-3}, respectively). Smith (1988) suggested a C_{h10} of 1.0×10^{-3} whereas DeCosmo et al. (1996) suggested that $C_{h10} = C_{e10}$. For low wind speed regimes, however, the transfer coefficients, C_{e10} and C_{h10}, have been shown to increase as the wind decreases below approximately 2 m s^{-1} (Bradley et al., 1991; Liu et al., 1979).

The transfer coefficients for heat and humidity have been examined extensively in the literature. Pond et al. (1974), for example, examined results for C_h and C_e determined from profile measurements while Friehe and Schmitt (1976) compiled data from nine experiments using covariance fluxes. It was the much quoted comparison of bulk transfer coefficients schemes by Blanc (1985), however, which drew attention to the substantial differences between the different schemes used in their calculation, and the consequent uncertainty in flux estimates. Blanc (1985) demonstrated that different bulk transfer coefficient schemes resulted in a typical maximum variation of 70 % for an average sensible heat flux determination of $\pm$ 25 W m^{-2}, and 45 % for an average latent heat flux determination of $\pm$ 40 W m^{-2}. This illustrates that uncertainties can arise by

using different transfer coefficient schemes.

In Table 7.2, the transfer coefficients for heat and humidity are shown from published studies for four freshwater lakes, including Lake Valkea-Kotinen (Nordbo et al., 2011), Lake Tämnaren (Heikinheimo et al., 1999), Ross Rarnett Reservoir (Liu et al., 2009) and Great Slave Lake (Blanken et al., 2003). Thus demonstrating the large variability in C_{e10} and C_{h10} values. For example, C_{e10} ranges from 1.0×10^{-3} to 2.0×10^{-3} and C_{h10} ranges from 0.4×10^{-3} to 1.5×10^{-3}. As mentioned for the transfer coefficient for momentum, the transfer coefficients for the scalar terms must be corrected for wind speed and atmospheric stability which is essential when comparing between lakes. In addition, it is also important to take atmospheric stability into account when applying literature values, which are conventionally based at a height of 10 m, to a different measurement height.

Table 7.2: Examples of transfer coefficients for heat and humidity (dimensionless) used in the literature.

Lake	C_{e10}	C_{e10}	Reference
Lake Taihu, China	$1.8 \times 10^{-3} \pm 0.02$	$1.5 \times 10^{-3} \pm 0.02$	Xiao et al. (2013)
Lake Valkea-Kotinen, Finland	$1.0 \times 10^{-3} \pm 0.04$	$1.0 \times 10^{-3} \pm 0.09$	Nordbo et al. (2011)
Lake Tämnaren, Sweden	$1.0 \times 10^{-3} \pm 0.4$	$1.3 \times 10^{-3} \pm 0.35$	Heikinheimo et al. (1999)
Ross Rarnett Reservoir, Mississippi, USA	$1.2 \times 10^{-3} \pm 0.06$	$1.1 \times 10^{-3} \pm 0.09$	Liu et al. (2009)
Great Slave Lake, Canada	$2.0 \times 10^{-3} \pm 0.19$	$0.4 \times 10^{-3} \pm 0.05$	Blanken et al. (2003)

Meteorological conditions above the lake, as well as influencing the turbulent surface fluxes, can also influence the surface energy budget by altering some of the radiative fluxes. Incoming long-wave radiation, for example, can be influenced by factors such as air temperature and cloud cover and can affect greatly the exchange of long-wave radiation at the air-water interface. As incoming long-wave radiation is not commonly measured, however, various techniques have been developed in recent years to estimate incoming long-wave radiation based on near-surface measurements (Table 7.3). These methods have had varying degrees of success, and new techniques continue to be developed. The main issue with the majority of these methods, however, is that they are often developed empirically at one location. In addition, these methods were originally developed for long-term averages and therefore are much less accurate at shorter timescales. Furthermore, many of these methods require cloud cover observations, which are not often recorded above the lake.

Table 7.3: List of commonly used bulk formulae for net long-wave radiation at the lake surface. Here D is the dew point depression calculated as the difference between the dew point temperature and the air temperature; ε_z is the emissivity of the air; and nc is cloud cover; all other terms are described in Chapter 2 of this dissertation. For information on how to calculate the net long-wave radiation following these methods please refer to the cited text.

Reference	Formula
Brutsaert (1982)	$\varepsilon_w \sigma T_0^4 - \varepsilon_z \sigma T_z^4 \left(1 + 0.17 nc^2\right)$
Gill (1982)	$0.985 \sigma T_0^4 \left[0.39 - \left(0.05 \times e_z^{0.5}\right)\right] \left[1 - \left(0.6 \times nc^2\right)\right]$
Bignami et al. (1995)	$\varepsilon_w \sigma T_0^4 - \sigma T_z^4 \left(0.653 + 0.00535 e_z\right) \left(1 + 0.1762 nc^2\right)$
Josey et al. (2003)	$\varepsilon_w \sigma T_0^4 - (1 - 0.045)\, \sigma [T_z + 10.77 nc^2 + 2.34 nc - 18.44 + 0.84 (D + 4.01)]^4$

The method used in this dissertation aimed to overcome the limitations imposed by other long-wave formulae. Most importantly, cloud cover was estimated based on the ratio of clear-sky to observed incoming short-wave radiation, and thus was not required as an input variable. This allowed the incoming long-wave radiation to be calculated accurately at high temporal resolution, as common cloud cover observations would be daily-averaged values at best (Crawford and Duchon, 1999). The method also incorporates an annual sinusoidal variation in effective clear-sky atmospheric emissivity, based on typical climatological variations in near-surface vapor pressure which results in an accurate seasonal variation in the incoming long-wave radiation.

Although incoming long-wave radiation can contribute substantially to the total surface energy fluxes, the most important component of this budget is arguably incoming short-wave radiation (e.g. Fink et al., 2014). This was shown, during this dissertation, to be true in Esthwaite Water where the exchange of radiant energy was dominated by short-wave radiation, being a larger contributor to the total surface heat flux than net long-wave radiation as well as the turbulent fluxes of latent and sensible heat. This was also shown by Fink et al. (2014) for Lake Constance (Germany, Switzerland, Austria) where it was shown that incoming short-wave radiation contributed most to lake warming during the past three decades.

As the surface energy budget is often dominated by incoming short-wave radiation, it stands to reason that the amount of reflected short-wave radiation at the lake surface will also have a considerable influence on the total surface fluxes. An increase in short-wave radiation, for example, will ultimately lead to an increase in the amount of short-wave radiation reflected back to the atmosphere.

As the reflected short-wave radiation is rarely measured on lakes it must be estimated from empirical relationships, the most common of which is in terms of α_{sw}, commonly known as the albedo, which is the proportion of short-wave radiation that is reflected back to space. As α_{sw} is not frequently measured, however, it is common to average the reflectance over time, and to set α_{sw} as a function of latitude in suitable tables (Table 7.4), from which data are drawn as needed. Various forms of these tables are found in the literature (e.g. Cogley, 1979) and many studies take values directly from these (e.g. Hummel and Reck, 1979). An issue with using monthly-averaged albedo values, however, is that they tend to over-predict by day and under-predict at dusk and dawn. Similarly, some studies often use a constant for α_{sw}, irrespective of time of year (Table 7.5). For water quality or thermal models which require mean daily parametrisations, for example, a mean annual value of $\alpha_{sw} = 0.06$, based on Lake Hefner studies (e.g. Parker and Krenkel, 1970), is often used. However, Cogley (1979) suggests that an annual global mean value of $\alpha_{sw} = 0.08$ is more appropriate. On short timescales (i.e. diel timescale) it is important to include the zenith angle effect. The method demonstrated in this dissertation was based on Fresnel's law which can be used to estimate the diel variation in short-wave reflectance.

7.3 Accurate calculation of surface energy fluxes

Accurate estimates of the surface energy fluxes are currently made with eddy covariance techniques (e.g. Liu et al., 2009; Nordbo et al., 2011; Vesala et al., 2006) where a number of long-term eddy covariance data on surface energy fluxes have

Table 7.4: Monthly-averaged albedo of open water. Taken from Cogley (1979).

	Month												
$\varphi(^\circ)$	Jan	Feb	Mar	Apr	May	Jun	Jul	Aug	Sep	Oct	Nov	Dec	Year
80-90	-	0.30	0.33	0.25	0.17	0.13	0.15	0.23	0.32	0.30	-	-	0.18
70-80	0.30	0.34	0.27	0.18	0.14	0.12	0.13	0.16	0.24	0.33	0.30	-	0.16
60-70	0.34	0.28	0.19	0.12	0.10	0.10	0.10	0.11	0.16	0.25	0.34	0.33	0.13
50-60	0.26	0.19	0.13	0.09	0.08	0.08	0.08	0.09	0.11	0.17	0.25	0.29	0.11
40-50	0.18	0.13	0.10	0.08	0.07	0.07	0.07	0.08	0.09	0.12	0.17	0.20	0.09
30-40	0.12	0.10	0.08	0.07	0.07	0.07	0.07	0.07	0.08	0.09	0.12	0.13	0.08
20-30	0.09	0.08	0.07	0.07	0.06	0.06	0.06	0.06	0.07	0.08	0.09	0.10	0.07
10-20	0.08	0.07	0.07	0.06	0.06	0.06	0.06	0.06	0.06	0.07	0.08	0.08	0.07
0-10	0.07	0.07	0.06	0.06	0.07	0.07	0.07	0.06	0.06	0.07	0.07	0.07	0.07

Table 7.5: List of commonly used short-wave albedo values and example references of where they have been used.

Value	Reference
0.03	Fink et al. (2014)
0.05	Sadro et al. (2011)
0.06	Parker and Krenkel (1970)
0.07	Mackay et al. (2011)
0.08	Cogley (1979b)

recently been reported (e.g. Rouse et al., 2008). Eddy covariance techniques are expensive, however, and have only been applied to a limited number of lakes. In this dissertation, the energy fluxes were calculated from more routinely measured variables using a bulk parametrisation method thus allowing the fluxes to be calculated with relative ease. By developing the Lake Heat Flux Analyzer program, the work presented in this dissertation will overcome the difficulty of comparing surface flux estimates from various sites by using a consistent calculation. The surface energy fluxes can be calculated rapidly by the Lake Heat Flux Analyzer program and provide a much needed tool for the expanding global network of instrumented lakes. The limnological community has already benefited from data analysis approaches such as wavelet analysis (Torrence and Compo, 1998) and Lake Analyzer (Read et al., 2011; Winslow et al., 2013) that have been used in global scale research (e.g. Read et al., 2012; Read and Rose, 2013; Winder and Cloern, 2010). Similarly, Lake Heat Flux Analyzer can be used for global scale research by calculating the surface fluxes using the same method, which is essential for cross-site collaboration.

Lake Heat Flux Analyzer was developed in this dissertation was created for the rapid calculation of the surface energy fluxes from instrumented lake buoy data. The accuracy of its results will obviously depend upon the quality of the input data. The program does not include quality control procedures and assumes that instrument calibration has been performed. The algorithms also assume that the input data are measured on the lake, particularly wind speed, which will vary from that measured on land (Markfort et al., 2010) and will have a substantial influence on the turbulent surface fluxes. A wind-sheltering coefficient is often applied to land-based wind measurements in numerical models to account for the

difference in roughness lengths between land and open water (Brutsaert, 1982). If a sheltering coefficient is used prior to running Lake Heat Flux Analyzer, the results should be interpreted with caution.

Future demands for more accurate modelling approaches will require a more detailed simulation of surface fluxes. The methods currently used to estimate transfer coefficients are derived from the ocean and therefore may not cover all of the difficulties associated with lakes of varying size. Small lakes, for example, are often characterised by low wind speeds, potentially extreme stabilities, and waves that have not attained equilibrium with forcing conditions and sufficiently shallow depths to compromise wave shape (Wüest and Lorke, 2003). The transfer coefficients have been described to be influenced by wave-age, where younger waves are considered more effective at transferring momentum at the air-water interface, with wave-age itself being implicitly related to wind speed and fetch (e.g. Donelan et al., 1993). Only when the wave-state reaches equilibrium with the atmosphere is the efficiency of transfer reduced to open ocean values. By using the transfer coefficients calculated from the open ocean, even when taking atmospheric stability and wind speed into account, limnologists are in danger of severely underestimating the turbulent fluxes across the air-water interface.

The main advantages and limitations of the Lake Heat Flux Analyzer program are shown in Table 7.6. One of its main advantages is that it uses data that are readily available on lake monitoring stations. The program also takes into account the most important processes known to affect heat fluxes, which are well established in the literature. The program can also calculate at a range of temporal scales, and thus allows the surface fluxes to be calculated at high tem-

Table 7.6: List of the advantages and limitations of the Lake Heat Flux Analyzer program.

Advantages	Limitations
- Allows quick and standardised calculations to be performed to enable comparative analysis	- Formulae are not necessarily as accurate in all parts of the world
- Calculate on hourly timescale	- Formulae may be more accurate under certain conditions
- All formulae used are well established in the literature	- Fluxes may be more accurately calculated by other methods during certain conditions or in certain parts of the world
- Uses readily available data	
- Takes into account the most important processes known to affect energy fluxes	

poral resolution, as well as allowing quick and standardised calculations to be performed to enable comparative studies. Lake Heat Flux Analyzer has a number of limitations. For example, there are many bulk transfer coefficient schemes that are described in the literature (e.g. Fairall et al., 1996; Friehe and Schmitt, 1976; Liu et al., 1979; Zeng et al., 1998). There is, therefore, no single, universally accepted bulk transfer coefficient scheme. Some schemes, for example, may have a higher degree of accuracy in some regions or under different atmospheric conditions but are not as accurate in other regions and under different atmospheric conditions. It is, therefore, difficult to select the most appropriate bulk transfer coefficient scheme.

7.4 The influence of atmospheric forcing on the thermal structure of lakes

Atmospheric fluxes of momentum, heat and freshwater at the lake surface drive vertical mixing and buoyancy forces that result in a subsequent change in the water temperature at all depths. The role of atmospheric forcing on the thermal structure of lakes has been extensively studied in recent years, where the role of wind speed and heat exchange processes at the lake surface has received much attention. An increase in surface heating during summer, for example, has been shown to result in a vertical layering of the water column where a warm surface layer is often separated from a cool bottom layer by a temperature driven density gradient known as the thermocline. The depth of the upper mixed layer plays an important role in several physical, chemical and biological processes in lakes. It has been shown, for example, to influence light availability per unit volume to phytoplankton (MacIntyre, 1993), the supply of oxygen to the hypolimnion and sediment (Foley et al., 2012) and also influence the vertical distribution of species (Clegg et al., 2007; Mellard et al., 2011).

The depth of the upper mixed layer varies with time owing to the variability in water clarity and atmospheric forcing. The thickness of the mixed layer indicates the amount of water and heat that directly interacts with the atmosphere. The concept of the upper mixed layer is arbitrary, and can be based on different parameters (e.g. temperature, density, oxygen). The most common definition of the upper mixed layer is in terms of the change in temperature with depth. The criteria used to determine the mixing depth, however, varies considerably in the literature (Table 7.7).

Table 7.7: List of commonly used criterion for defining the depth of the upper mixed layer.

Example	Criterion
Van de Bogert et al. (2012)	The first depth at which the temperature change
Staehr and Sand-Jensen (2007)	is > 1 °C m^{-1}
Coloso et al. (2011)	The shallowest depth at which the rate of density
Solomon et al. (2013)	change exceeds 0.075 kg m^{-3} m^{-1}
Coloso et al. (2008)	The depth where the temperature changes more
	than 1 °C per half metre
Fee et al. (1996)	The region where the temperature gradient
	is less than 1 °C m^{-1}
Read et al. (2011)	The region above the thermocline where the
	density gradient was less than 0.5 kg m^{-3}
Kara et al. (2000)	The depth where the temperature differs by
Thomson and Fine (2003)	0.2 °C relative to that measured at the surface
Kelly and Qiu (1995)	The depth where the difference between
	the lake surface and that at depth = 0.5 °C

Most definitions for the depth of the upper mixed layer can be classified into two groups: (i) gradient-based criteria, where z_{mix} is the depth where the vertical gradient of a given property reaches a threshold value, and (ii) difference-based criteria, where z_{mix} is the depth where a property has changed by a certain amount from a near-surface reference value. Previous studies have shown that well-resolved vertical profiles are necessary to use successfully gradient-based criteria (Brainerd and Gregg, 1995). In the oceans, for example, Dong et al. (2008) demonstrated that the presence of anomalous spikes and perturbations in vertical profiles could lead to erroneously low z_{mix}, where it was found that the gradient-based z_{mix} deviates from the difference-based z_{mix} by as much as 100 m. Each of the definitions, therefore, have different implications for mixing and consequences for different elements within the lake. During this dissertation, a difference-based criteria was used in order to account for the different vertical resolution of temperature measurements included in the 100 lakes.

7.5 Onset of thermal stratification from surface measurements

The onset of thermal stratification in lakes can be estimated by using any of the definitions described in Table 7.7, where stratification onset is considered as when the criterion is met for the first time. As such, any two different definitions of stratification onset will not produce the same answer in all situations. In lakes, one of the most commonly used criterion for defining the onset of ther-

mal stratification is when the temperature difference between the epilimnion and the hypolimnion first exceeds 1 °C (e.g. Stefan et al., 1996). A common issue with determining if a lake is thermally stratified, however, is that depth-resolved temperature measurements are required. During this dissertation, an alternative method for estimating the onset of thermal stratification was provided. The method involved analysing the temporal variability in the diel surface water temperature range and relating the diel cycle to the onset of thermal stratification. This method is therefore the first to estimate the onset of thermal stratification from surface temperature measurements alone.

There are sound theoretical reasons why the diel cycle in lake surface water temperature can be influenced by thermal stratification to the extent that important information about the vertical thermal structure of the lake may be gleaned from surface water temperature measurements alone. By calculating accurately the surface energy fluxes with the Lake Heat Flux Analyzer program, the expected diel temperature range identified that a considerable increase in the diel cycle is expected when the depth of the upper mixed layer is shallow, as is the case during the onset of thermal stratification. Furthermore, as the onset of thermal stratification is typified by a change from an isothermal lake to a lake with a relatively shallow mixed depth (e.g. Körtzinger et al., 2008), the timing of this onset can be estimated by measuring changing surface water temperature over time. There are a number of assumptions with this method, however, which include (i) the depth of the upper mixed layer does not change much during the day, (ii) a minimal amount of heat is lost beneath the base of the upper mixed layer, and (iii) heat is distributed evenly throughout the upper mixed layer. The results shown in this dissertation suggest that these approximations are sufficiently rea-

sonable to allow the onset of thermal stratification to be estimated accurately.

The applicability of any definition of stratification onset is compromised by periods of transient stratification. Such periods are common throughout the year in polymictic lakes, such as Bassenthwaite Lake or Rotorua, where stratification is weak and readily broken down by wind and convective mixing. However, transient periods of thermal stratification also exist in other lakes, particularly prior to the onset of continuous thermal stratification, where periods of high net incoming radiation and low wind forcing may cause the lake to become temporarily stratified. The stratification criterion used in this dissertation only considered a lake to be thermally stratified when the criterion was maintained for a period of at least 48 hours. This ensures that the method can be used to estimate the onset of extended thermal stratification and not identify transient stratification events.

An alternative method to estimate thermal stratification without knowing water temperature at depth is to use a numerical lake physics model (e.g. Peeters et al., 2002). Such numerical process-based models, however, require detailed and local time series of meteorological measurements. Traditionally, relatively few lakes have sufficient data, and lake modellers often use meteorological measurements from local weather stations, introducing inaccuracies in the driving variables for the model and consequently reducing the accuracy in determining stratification timing. Other sources of uncertainty include observational uncertainty such as the accuracy of the sensors, parameter uncertainty and model uncertainty, all of which will influence the accuracy of the model.

The approach presented in this dissertation has the potential to be applied to other high-frequency data sets that are restricted to surface temperature measurements alone (e.g. Livingstone and Kernan, 2009). This method was developed,

however, using a limited number of lakes, none of which had a maximum depth of less than 15 m. It is expected that the method would also work in shallower lakes that stratify, but possibly with some loss of accuracy. By using the wavelet method for lakes that stratify, however, this work has shown that low cost sensors measuring surface water temperatures at 30-minute intervals can provide an improvement in the accuracy of estimating stratification when compared to traditional monitoring of depth-resolved temperatures at fortnightly intervals or more.

In the future, this approach may also be applicable to surface temperature measurements obtained from satellites. Remote sensing has the potential to retrieve such measurements, but is currently limited by the sampling frequency of sensors. Two measurements per day is the minimum required for wavelet analysis to capture a diel signal, as the sampling frequency necessary to capture any signal must exceed twice the frequency of that signal, and even at a low-frequency, the diel cycle would still be resolved to a reasonably high accuracy. The timing of these observations is also important; the method is most effective if the observations are equally spaced and are made at the times of maximum and minimum temperature.

New techniques applied to the Along Track Scanning Radiometer (ATSR) series of sensors have recently generated accurate and consistent lake surface temperature time series for greater than 250 large lakes globally (MacCallum and Merchant, 2012) from 1991 to 2009. In addition, the MODIS (Moderate Resolution Imaging Spectroradiometer) instruments on the Terra and Aqua polar-orbiting satellites provide information on sea surface temperature and land surface temperature measurements (Oesch et al., 2008; Reinart and Reinhold,

2008). MODIS can produce sea surface temperature over certain regions approximately 3 times per day. Lake surface water temperature retrieval, however, is currently limited to 1 km^2, and therefore, not possible for small lakes (MacCallum and Merchant, 2012).

One potential issue with satellite measurements, however, is that they record the skin temperature rather than the temperature at 1 m. This represents a temperature within a millimetre of the air-water interface and can differ from the bulk temperature by as much as a few degrees (Minnett, 2003). Although several techniques are currently used to infer bulk temperatures from skin temperature (Wilson et al., 2013), further analysis would be required to establish whether the methods described in this dissertation can be successfully used with satellite measurements of temperature. Nevertheless, this method can be used on the increasing number of high-frequency surface temperature measurements on lakes to provide an improved understanding on the recent trends in the onset of thermal stratification for lakes from around the world.

7.6 Variability in the thermal responses of lakes to atmospheric forcing

The thermal responses of a lake to atmospheric forcing will vary depending on a number of lake specific features such as lake size and water clarity (e.g. Fee et al., 1996; Mazumder and Taylor, 1994). Thus, the thermal characteristics of lakes situated within the same geographic region behave differently even though

they are exposed to the same climate. This was demonstrated during this dissertation where the monthly-averaged depth of the upper mixed layer for five lakes in the English Lake District were different throughout the year. The depth of the upper mixed layer for these lakes was primarily influenced by wind speed. In turn, wind speed was influenced by lake size. This relationship was complicated in these lakes, however, as Loweswater had higher than expected wind speed due to the lake being located at the end of a valley, with the fetch therefore being greater than just the length of the lake. The variation in wind speed, however, matched the variation in mixing depth where z_{mix} was highly related to u_{10} for each of the lakes during summer.

The variability in the thermal responses of lakes to atmospheric forcing has also been shown in other studies. Frempong (1983), for example, demonstrated that wind-induced mixing and vertical circulation induced by nocturnal cooling of surface water through evaporative and conductive processes modified the thermal structure of Esthwaite Water. The majority of studies, however, have used lower resolution measurements. Gorham and Boyce (1989), for example, investigated the thermal response of 54 lakes in Minnesota (USA) during summer in relation to lake size. It was shown that the depth of the thermocline, the region of maximum temperature difference within a water column, was significantly related to lake surface area. Similar results were reported by Fee et al. (1996), who demonstrated that the depth of the upper mixed layer in 21 Canadian Shield lakes in northwestern Ontario was related to lake surface area for periods ranging from 2 to 23 years. They also demonstrated that water clarity had a statistically significant influence on the vertical thermal structure.

7.7 The diel range in lake surface water temperature

The depth of the upper mixed layer has a strong influence on the diel range in lake surface water temperature. For lakes with shallower mixed layers, for example, atmospheric heating is concentrated over a smaller volume resulting in a larger temperature range than that experienced by lakes with deeper mixed layers. As the depth of the upper mixed layer is influenced by lake size and water clarity, however, it was expected that the diel temperature range would also be influenced by these factors. Water clarity, for example, can influence the amount of radiation that penetrates to a given depth of the water column. This exponential decay can be expressed mathematically as:

$$I_z = I_0 \exp\left(-K_d \times z_{mix}\right). \tag{7.1}$$

According to this relationship, large values of K_d, therefore, result in a large proportion of light being absorbed at the lake surface, while small values of K_d results in a large amount of light penetrating deep into the water.

For five lakes situated in the English Lake District, the diel temperature range was significantly influenced by the depth of the upper mixed layer. For these lakes, lake surface area was also significantly related to the diel temperature range during some of the summer months. Water clarity, however, was not significantly correlated with the diel temperature range for the majority of the year, most likely because there was little difference in water clarity among the lakes. However, due to the exponential nature of the light penetration curve (equation

7.1), changes to small values of K_d would be expected to have a greater impact on the thermal structure of lakes than changes to large values of K_d. Therefore, even though K_d values for the lakes in the English Lake District are small and relatively similar, one would still expect there to be a considerable influence on the mixing depth. For these lakes, however, water clarity was not significantly influencing the diel temperature range.

The advantage of using five lakes in the English Lake District for assessing the variability in the diel temperature range is that the influence of water clarity and lake size on the diel range can be investigated without having to consider differences in the local climate. The disadvantage of using these lakes, however, is that the investigation did not include all of the drivers that influence lake temperature e.g. latitude and altitude, which can influence the amount of heating and cooling acting on a given lake.

Solar radiation varies substantially with latitude. Latitude, for example, can influence day length, and thus alter the heating period for a given day. In winter, the higher the latitude, the shorter the day length, and consequently the shorter the heating period. Between winter and the summer solstice, however, the day length increases, and the rate of increase is larger for higher latitudes. Therefore, during summer, the day length increases with increasing latitude. This means that during summer, the heating period for lakes at higher latitudes will be longer than those closer to the equator. The magnitude of heating, however, will be much less at higher latitudes due to the decrease in the solar elevation angle at noon. High solar elevation angles, for example, result in higher solar radiation. For example, if the sun is positioned directly overhead i.e. 90 °, incoming solar radiation strikes the Earth's surface at a right angle and is most intense. As the

solar elevation angle decreases, however, solar radiation is spread out over larger surfaces, thus reducing the intensity of the radiation. Furthermore, as the solar elevation angle decreases, a larger proportion of radiation is scattered and/or absorbed by air and dust in the overlying atmosphere, again altering the intensity of radiation reaching the surface.

The absorption and scattering of solar radiation is influenced by the distance in which solar radiation travels through the overlying atmosphere. As well as being influenced by latitude, the distance in which solar radiation travels prior to reaching a lake surface, may also be influenced by altitude. Furthermore, the amount of scattering molecules is lower at high altitude, due to lower air pressure, and thus scattering is less significant. Altitude has been shown in recent studies to influence lake surface water temperature, where increasing altitude, thus decreasing air temperature, tends to result in a decrease in surface water temperature (e.g. Livingstone et al., 2005, 1999). In this dissertation, latitude and altitude were, therefore, used as convenient proxies for local weather, representing lake location at single parameters.

In this study, neither lake size nor water clarity varied much among the lakes. Water clarity, however, can vary substantially among lakes, much more than the range of K_d values seen in the lakes in the English Lake District. Paavel et al. (2008), for example, found that the light attenuation coefficient in Estonian lakes can vary from 0.9 to 6.5 m^{-1}. Similarly, Read and Rose (2013) demonstrated that K_d varied between 0.93 and 3.51 m^{-1} in eight small lakes in Wisconsin and Michigan (USA). Over a greater spatial scale Rose et al. (2014) investigated 15 lakes from different countries which varied from 0.3 to 4.1 m^{-1}, and the investigation by Read et al. (2012) included K_d values from 0.4 to 6.1 m^{-1}. Within a

given lake K_d can also vary substantially. Clearwater Lake (Ontario, Canada), for example, experienced a doubling in K_d values from 0.15 to 0.31 m^{-1} (Tanentzap et al., 2008), which was explained to have been caused by an increase in dissolved organic carbon concentrations in the lake which were associated with deacidification (Dixit et al., 2001). Similarly, in Lake Annie (Florida, USA), the light attenuation coefficient has been shown to increase from 0.3 to 1.9 m^{-1} since 1993 (Gaiser et al., 2009), being driven by an accelerated transport of coloured dissolved organic matter from the catchment into the lake.

While the variability in water clarity among lakes does not often exceed an order of magnitude, the variability in lake size is often much greater. The investigation by Read et al. (2012), for example, consisted of 40 temperate lakes that ranged in over five orders of magnitude. Similarly, Mazumder and Taylor (1994) investigated the influence of water clarity on the thermal structure among lakes that varied by seven orders of magnitude and Fee et al. (1996) investigated the effect of lake size and water clarity on mixing depths in Canadian Shield lakes. Their analysis included lakes that ranged in size from 0.04 to 4900 km^2 and varied in K_d from 0.2 to 2.5 m^{-1}. To understand better the drivers of diel temperature ranges in lakes, a dataset that include a large range of K_d and surface area values is required.

As part of this project a dataset of 100 lakes ranging from 2468 m^2 to 1.63 $\times$ 10^8 m^2 in surface area and between 0.08 m^{-1} and 5.7 m^{-1} in water clarity was assembled. Diel temperature range was shown to be primarily influenced by lake size where the causal connection between lake size and the diel range was due to the association between lake size and the depth of the upper mixed layer. The diel temperature range was also shown to be significantly correlated ($p < 0.05$)

with water clarity but in comparison to lake area, it had a relatively small effect. It might be expected that other factors, such as lake location, would have a noticeable effect on the diel temperature range. In this dissertation, though, latitude spanned over 20° and altitude varied by over 2000 m, but still had a minimal effect on the diel temperature range. Though local conditions are likely to have some role to play, they are much less important than lake size. To a first approximation, area alone can be used to predict average summertime diel temperature ranges for lakes across the globe. For small lakes of similar size, however, it is expected that water clarity would be the dominant factor influencing the diel temperature range for the majority of the year. This was demonstrated by Houser (2006), who reported that the diel temperature cycle was more pronounced in coloured lakes in a study that involved lakes ranging from 0.008 km^2 to 0.03 km^2 in surface area.

7.8 Consequences of the diel range in lake surface water temperature

Temperature has a pervasive effect on lakes as it affects many within-lake processes. It is critical in determining the duration of ice cover (Magnuson et al., 2000), the timing and intensity of stratification and seasonal deep mixing (Livingstone, 2003) and the subsequent extent of anoxia (Foley et al., 2012). Biological growth rates (Butterwick et al., 2005), organism size (Atkinson, 1994), the timing of phenological events (Thackeray et al., 2008), the likelihood of toxic cyanobacterial blooms (Pearl and Huisman, 2008) and the available habitat for

fish species (Christie and Regier, 1988) are all controlled by water temperature. Similarly, the rates and equilibrium positions of chemical reactions (Stumm and Morgan, 2013), rates of metabolic processes (Yvon-Durocher et al., 2012), lake metabolism (Staehr and Sand-Jensen, 2006) and greenhouse gas emissions from lakes (Cole et al., 2007; Raymond et al., 2013) are all dependent on the water temperature in surface layers.

Diel temperature variation has the potential to affect many aspects of lake ecology as most physico-chemical and biological processes have a non-linear temperature dependence, including oxygen solubility and consequent effects on ecology (e.g. Verberk et al., 2011), rates of metabolic processes (e.g. Brown et al., 2004), organism size (Atkinson, 1994) and temperature tolerances of individual species (e.g. Huertas et al., 2011). Furthermore, the global role of inland waters in biogeochemical processes, such as the carbon cycle, for example, has become increasingly recognised in recent years (Cole et al., 2007; Raymond et al., 2013; Tranvik et al., 2009) and small lakes, because of their abundance, are an important component of this process (Downing, 2010). Estimates of global CO_2 losses from lakes are often calculated as the product of average CO_2 oversaturation and total lake area, but gas solubility is dependent on temperature. Thus, not taking into account the temperature variation means that actual CO_2 fluxes from lakes could be much different than expected.

Due to the observed relationship between the diel temperature range and water clarity, as well as the relationship between water clarity and dissolved organic carbon (DOC) concentrations, it is proposed here that, for a given lake, the diel temperature range has risen substantially in the past and will continue to increase in the future. For example, recent evidence has shown that surface waters have

been browning over the last few decades (Roulet and Moore, 2006), primarily ascribed to changes in DOC concentrations (Monteith et al., 2007; Vuorenmaa et al., 2006), with an expectation that this trend may continue (Larsen et al., 2011). There are multiple reasons for an increase in the transport of DOC to lake surface waters, including a drier climate (Freeman et al., 2001), wetter climate (Tranvik and Jansson, 2002), warmer temperatures (Lepistö et al., 2008), or declines in acid deposition (Monteith et al., 2007). It is therefore expected that this increase will have a substantial influence on the diel temperature range, as supported by the results presented in this dissertation.

7.9 Traditional limnological monitoring

Historically, physical limnologists have tended to study large lakes that are important for regional water supply (Fischer, 1979; Imberger, 1985), represent a large share of biodiversity (Verburg et al., 2003), and have a large influence on local climate (Austin and Colman, 2007; Desai et al., 2009). Similarly, most long-term monitoring programmes are undertaken on the larger lakes in a region (e.g. O'Reilly et al., 2003). Recent work, however, has refined the global estimate of the number of lakes as well as the areal contribution of these lakes (Downing et al., 2006). While areal estimates of small lakes likely require refinement (McDonald et al., 2012; Seekell and Pace, 2011; Verpoorter et al., 2014), small lakes undoubtedly dominate the global distribution of lake abundance (Downing et al., 2006; Verpoorter et al., 2014).

There has been a tendency to assume that small and large lakes operate in

similar ways. Much of our knowledge of physical limnology, for example, has been derived from physical oceanography (Csanady, 2001; McGillis et al., 2004; Wanninkhof, 1992), and while applicable to large lakes, likely fails to describe adequately the physical processes in small lakes. It has been shown, for example, that the relative importance of wind-driven and convective mixing varies with lake area (Read et al., 2012), that the transfer of energy at the lake surface, which is related to wave-age, is implicitly related to area (Donelan et al., 1993; Geernaert et al., 1986; Hsu, 1986) and here that diel temperature variation increases dramatically with decreasing lake area. Lake size also has a marked influence on ecology: many aquatic rates, processes, and quantities are more intense, complex, or abundant in small lakes than in larger lakes (Downing, 2010), which may, in fact, be driven, at least to some extent, by the diel range in lake surface water temperature. Macrophyte coverage is also proportionately greater in smaller lakes (Duarte et al., 1986) leading to enhanced production and habitat composition. Furthermore, in the pelagic zone, small lakes have more complex thermal structure than large lakes (Xenopoulos and Schindler, 2001). Small lakes are also important to the maintenance of regional biodiversity (e.g. Dodson et al., 2000; Elmber et al., 1994; Matuszek et al., 1990).

Traditional limnological monitoring, of at best weekly or two-weekly intervals, usually involves a temperature measurement at one time during the day. For large lakes, where the bulk of this historic monitoring effort has been focussed (Table 7.8), this measurement will be fairly representative of the surface temperature throughout the day. For small lakes, however, this measurement will only be representative of a small part of the large diel variation. Thus, our historic bias to the large rather than the small could be jeopardising our understanding

of lake ecosystems. The importance of surface temperature to lake ecology suggests that, for small lakes, resolving the diel cycle is therefore a necessity.

Table 7.8: List of long-term monitoring sites (Fink et al., 2014), shown in descending order according to their surface area.

Lake	Size (km^2)	Since	Source
Lake Superior	82,103	1979	Austin and Colman (2007)
Lake Huron	59,600	1979	Austin and Colman (2007)
Lake Michigan	58,000	1979	Austin and Colman (2007)
Lake Baikal	31,722	1945	Hampton et al. (2008)
Lake Mälaren	1,140	1965	Arvola et al. (2010)
Lake Constance	536	1962	Straile et al. (2003)
167 remotely sensed lakes	> 500 km^2	1985	Schneider and Hook (2010)
Lake Tahoe	496	1970	Coats et al. (2006)
Lake Zurich	89	1955	Livingstone (2003)
Lake Washington	88	1964	Arhonditsis et al. (2004)
Lake Geneva	21	1983	Gillet and Quentin (2006)
Windermere North Basin	8.2	1945	George (2010)
Windermere South Basin	6.7	1945	George (2010)
Esthwaite Water	1.0	1945	George (2010)
Blelham Tarn	0.1	1945	Foley et al. (2012)

7.10 Advantages of high temporal resolution data

The advantage of using high temporal resolution measurements to monitor lakes has been demonstrated in this dissertation. This is also shown in other studies which have focussed, for example, on lake metabolism (e.g. Staehr et al., 2010) and gas exchange between the lake and the atmosphere (e.g. MacIntyre et al.,

2010). The high temporal resolution information collected provides a more detailed picture of what happens within lakes in response to changing environmental conditions, and thus, are needed to understand how the different environmental pressures affect lakes and to forecast future responses. This is because lake condition can change rapidly and since the generation time of the largely microbial populations that control ecological structure and function is very short, of the order of days or less (Kent et al., 2007). Equally importantly, lakes are strongly influenced by short-term physical processes, such as strong wind events (e.g. MacIntyre et al., 2009), storm events (e.g. Klug et al., 2012), or even periods of hot weather (e.g. Jöhnk et al., 2008) which can influence lake temperature and mixing patterns and thus directly alter the environment in which the biology and chemistry within a lake operate.

Thermal stratification in lakes and reservoirs is a rather rapid process, where the lake can change from being fully mixed to a thermally stratified water column within a few days or even hours. In addition, thermal stratification can breakdown within a 24 hour period (e.g. Rueda-Valdivia and Schladow, 2009), due to high winds or convective cooling. High temporal resolution measurements can be used to monitor these sudden changes in the vertical thermal structure of lakes and with data processing tools such as Lake Analyzer (Read et al., 2011), can be used to effectively parse out the contributions of drivers such as wind, convective cooling, and de-stratifying forces that weaken vertical density gradients on measured biological signals (e.g. Robertson and Imberger, 1994). The development of the Lake Heat Flux Analyzer program in this dissertation will aid in developing an in-depth understanding of the causes and drivers of physical processes occurring within lakes. By calculating the exchange of energy at the lake surface

with Lake Heat Flux Analyzer and calculating the resulting physical processes with Lake Analyzer, researchers will be able to develop a detailed understanding of the physical processes in lakes at a range of temporal scales.

In this dissertation, the use of continuous high temporal resolution data was essential to improve our understanding of diel temperature fluctuations, a process which had not previously been investigated in great detail. Traditionally, measurements of diel temperature fluctuations would require manual temperature measurements to be made at selected times of the day or from automatic measurements for selected periods. Frempong (1983), for example, investigated the diel thermal structure of Esthwaite Water (UK) on seven selected days during different stages of thermal stratification. His study demonstrated that the vertical thermal structure of the water column and the energy budget varied throughout the day at different times of the year for this relatively small English Lake. Due to the need of high temporal resolution measurements, however, Frempong's study could not resolve the continual change in the surface fluxes nor the diel temperature range, and thus could not demonstrate how the diel cycles varied with a range of meteorological conditions. Frempong's study, however, identified a clear diel range in meteorological conditions and the resulting energy fluxes during selected periods of the year. Similar to Frempong's study, the work presented in this dissertation, with the use of high temporal resolution measurements, demonstrated that the surface energy fluxes varied at diel timescales, which ultimately influenced the diel temperature cycle. The exchange of latent and sensible heat, for example, was shown to vary substantially throughout the day. The magnitude of the total surface heat flux was also shown to greatly vary over a diel cycle, owing to the large diel range in wind speed, relative humidity,

incoming short-wave radiation, air temperature, and surface water temperature.

Being able to calculate surface fluxes at different timescales is of great importance for understanding the different drivers of atmospheric forcing on the lake. Lenters et al. (2005), for example, investigated the seasonal, intraseasonal, and interannual variation in lake evaporation in Sparkling Lake (Wisconsin). Variations in evaporation rates were found on a wide range of timescales. Due to the large diel range in the main driving parameters of lake evaporation, however, a substantial diel variation in evaporation rates would also be expected. For example, Frempong (1983) identified that the evaporative heat flux for Esthwaite Water varied considerably throughout the day, being largest at midday. This was also confirmed for Esthwaite Water during this dissertation.

7.11 Advantages of a global network of limnological monitoring stations

A network of monitoring stations makes high temporal resolution datasets even more powerful, since different lakes can be compared at a range of temporal scales. The insights gained by the United Kingdom Upland Waters Monitoring Network (UKUWMN), previously known as the United Kingdom Acid Waters Monitoring Network (UKAWMN), is a prime example of the benefits that can arise from networking monitoring stations. The data collected in the UKUWMN has, for example, been used to address many key issues in science, such as the long-term chemical recovery of lakes from acidification (Battarbee et al., 2014; Evans and Monteith, 2001, 2002) and the impacts of climate change on upland

waters (e.g. Evans, 2005; Futter et al., 2009; Thompson, 2012). Other monitoring networks, such as the United Kingdom Lake Ecological Observatory Network (UKLEON), which is more focussed on high temporal resolution measurements, can be used to compare short-term processes such as mixing events, among a gradient of lake types, and thus be used to demonstrate how different lakes will respond to similar conditions.

Monitoring networks are even more useful when they include lakes that are distributed from around the world. A global network of monitoring stations, such as GLEON, for example, allow comparison studies for different systems from around the world, which can therefore be used to answer research questions on a much larger scale. The diel range in lake surface water temperature, for example, could only be shown in this dissertation to vary substantially as a function of lake size, by comparing data from a large number of lake types from around the world. A smaller dataset, such as that shown in this dissertation for the English Lake District, could provide similar results but the full scale of any relationship will become clearer, and more significant, by including a greater range of lakes. This was illustrated in this dissertation, where the relationship between lake size and the diel temperature cycle was not realised until a larger dataset was used.

A global dataset is essential for testing new hypotheses and methods. Pierson et al. (2011), for example, used GLEON data to test a new method for estimating the timing of ice-on, ice-off, and thus, the duration of ice cover for lakes from around the world. Similarly, in this dissertation, the method presented for estimating the onset of thermal stratification, was applied to seven lakes from three countries (United Kingdom, United States of America, and New Zealand) to test

whether it could be used successfully across a geographical and morphological range of lakes. Without testing these new methods in various lakes, there is no way of knowing if the accuracy of the method will be the same across different lake types.

As a global network of monitoring stations results in a large volume of data to accumulate from around the world, they can be used to answer key science questions that span broad geographic regions and ecosystem gradients. In order to compare among lakes, however, the process in question needs to be calculated following the same method. This was initially demonstrated for the limnological community by the development of the Lake Analyzer software (Read et al., 2011). Following from the relative success of Lake Analyzer, the Lake Heat Flux Analyzer software developed in this dissertation to calculate accurately the energy fluxes at the air-water interface, thus enabling comparative studies, which with sensor networks, can span gradients of climate, land-use, hydro-physiography, and time.

Chapter 8

Conclusions and future work

8.1 Introduction

This dissertation has sought to explore the drivers, consequences, and associations of the diel range in lake surface water temperature. The original contributions of this work include the development of an open source numerical program called Lake Heat Flux Analyzer, designed to calculate accurately the surface energy fluxes in lakes and reservoirs, which can then be used to estimate the diel range in lake surface water temperature; and the development of a method for estimating the onset of thermal stratification from the diel range in surface water temperature. The results presented in this dissertation also demonstrated that the diel range in surface temperature differs among five lakes in the English Lake District, driven by essentially the same climate, but characterised by different morphometric features; and that the diel range in surface water temperature for a large distribution of lakes is primarily influenced by lake size. Furthermore, this dissertation has demonstrated that the relationship between the diel temperature range and lake size is non-linear with lakes smaller than 3.2 km^2 having a higher diel temperature range than larger lakes. The main conclusions and implications

of the work are detailed below.

8.2 Conclusions

While accounting for only 3 % of the Earth's surface (Downing et al., 2006), lakes are vital habitats that provide essential resources for a wide range of species. Lakes, however, are regarded as one of the most imperilled ecosystems in the world (Dudgeon et al., 2006; Sala et al., 2000), and are increasingly threatened by a wide range of stressors (e.g. Ormerod et al., 2010). In order to understand how lakes respond to these different stressors, a detailed understanding of lake function is required. Climate is a first-order control on lake function which affects the lake through a number of different mechanisms. Of the various ways in which the climate can affect a lake, the most direct is through its affect on the lake surface and the transfer of energy at the air-water interface.

Direct measurements of surface energy fluxes in lakes are expensive. A large amount of research has therefore focussed on the derivation of appropriate methods to estimate these fluxes from relatively well known and frequently measured variables such as air temperature, wind speed, short-wave radiation, relative humidity, and surface water temperature. Recent developments in aquatic sensor technology have made it possible to measure these parameters in lakes automatically from *in situ* platforms. These monitoring stations show promise for addressing science questions that span broad geographic regions and ecosystem gradients, but adequate tools are required to process this information.

An open source numerical program called 'Lake Heat Flux Analyzer' was

developed during this PhD to calculate accurately the surface energy fluxes in lakes and reservoirs. Available outputs from Lake Heat Flux Analyzer include the surface fluxes of momentum, sensible and latent heat and their corresponding transfer coefficients, incoming and outgoing long-wave radiation, evaporation rates and wind speed, temperature and humidity corrected to a height of 10 m above the lake surface. Lake Heat Flux Analyzer can be used to process data from multiple lakes rapidly. It provides a means of calculating the surface fluxes using the same method, thereby facilitating global comparisons of high-frequency data from lake buoys. In addition, the program allows the surface energy fluxes to be calculated at a range of temporal scales (e.g. Lenters et al., 2005), which is of great importance for understanding the different drivers of atmospheric forcing on the lake. Quantifying these physical processes is also central to understanding lake dynamics and their contribution to global biogeochemical cycles, as gas exchange at the air-water interface is influenced greatly by the surface energy fluxes. The methods followed for estimating the surface energy fluxes were presented in Chapter 2.

The surface energy fluxes were calculated for Esthwaite Water in the English Lake District and were used to estimate the expected diel range in lake surface water temperature following a predictive method. A theoretical analysis showed that the diel temperature range for Esthwaite Water was primarily influenced by the depth of the upper mixed layer. As the diel temperature range is highest when the upper mixed layer is shallow, as is the case during the onset of thermal stratification i.e. when the lake changes from being isothermal to being stratified, it was hypothesised that the onset of thermal stratification could be estimated by measuring the change in the diel temperature range over time.

During this dissertation, it was demonstrated that the magnitude of the diel range in surface water temperature could be used to estimate accurately the onset of thermal stratification. The accuracy of using the diel range as an estimate of the onset of thermal stratification was assessed by applying two methods based on the calculation of (1) the absolute difference in the observed diel surface temperature range, and (2) the magnitude of the diel cycle from wavelet analysis. The study demonstrated that the onset of thermal stratification can be detected accurately by wavelet analysis with a root mean square error of 2.1 days and by the observed diel temperature method with a root mean square error of 11.8 days. This approach enables existing, and future, high-resolution surface water datasets to be used to detect the onset of lake stratification. Furthermore, the continuously increasing observational powers of satellites may eventually result in surface water temperature being measured at a sufficiently high temporal resolution at the spatial scales of small lakes to allow the onset of thermal stratification to be detected remotely. Thus, expanding the number of lakes for which we can estimate stratification onset, which is useful for determining the climate's effect on lakes. In addition, this method allows for stratification onset to be estimated relatively cheaply where instead of having to buy numerous water temperature sensors, one temperature sensor at the lake surface can provide a relatively accurate estimate of stratification onset.

For a given lake, the diel range in lake surface water temperature can vary throughout the year, owing to the difference in the depth of the upper mixed layer. The depth of the upper mixed layer, however, is influenced by a number of lake specific factors such as surface area and water clarity. It was, therefore, expected that the diel temperature range was also influenced by these primary

factors. For five lakes in the English Lake District, driven by essentially the same climate, the diel temperature range was found to be lowest for the largest lake, Windermere, which varied by approximately half that of the smallest lake, Blelham Tarn. A significant correlation between the diel temperature range and lake area was observed in summer due to the larger lakes being exposed to higher wind speeds, in turn leading to larger shear and ultimately wind mixing, and consequently leading to large mixing depths and thus low diel temperature range. As only five lakes were included in the investigation, however, the statistical significance of this relationship was not very high.

For a large data-set, comprised of 100 lakes, the relationship between the diel temperature range and lake surface area was shown to be highly significant during the summer months. The diel temperature range was also shown to be significantly correlated with water clarity but in comparison to lake area, it had a relatively small effect. Thus, area alone was shown to predict accurately the summer-averaged diel temperature ranges. Furthermore, by using a generalised additive model, this study highlighted that lakes smaller than 3.2 km^2 are likely to have a diel temperature range of over 6 $^{\circ}$C. In contrast, for lakes with larger surface areas, the diel surface temperature range in summer was < 2 $^{\circ}$C but did not vary with lake area.

The present study is the first to demonstrate that the diel temperature range varies as a function of lake surface area. This finding is of great scientific interest as it allows the diel temperature range to be estimated by knowing only the lake's surface area. Furthermore, due to the relationship between lake surface area and the diel temperature range, as well as the relationship between lake area and the number of lakes in the world, the relationship between the diel tem-

perature range and the number of lakes in the world has been identified. Thus, the results demonstrated in this dissertation has improved our understanding of a large proportion of the world's lakes, thus allowing the diel temperature range to be estimated accurately for unmeasured lakes. In addition, this dissertation has also highlighted the importance of acknowledging the diel temperature cycle when upscaling processes to global cycles.

Temperature has a pervasive effect on lakes and the significant variability in diel range noted here has implications for many processes that affect biogeochemical cycling in lakes. These include the solubility of gases and the rates and equilibrium positions of chemical reactions (Stumm and Morgan, 2013), rates of metabolic processes (Brown et al., 2004; Yvon-Durocher et al., 2012) and growth (Butterwick et al., 2005). Perhaps the most critical aspect involves global biogeochemical cycles, particularly of carbon. Lakes are important sources of CO_2 to the atmosphere (Cole et al., 2007; Raymond et al., 2013) and small lakes, because of their abundance, are important contributors to this process (Downing, 2010). For example, water temperature influences CO_2 solubility. A temperature difference of 6 °C, as demonstrated in this dissertation, would equate to approximately a 20 % variation in CO_2 solubility. Therefore, when estimating total CO_2 losses from lakes, which is driven by the difference in CO_2 concentration between the lake and the atmosphere, failing to include the diel variability in water temperature could introduce an additional error into global estimates of CO_2 losses from lakes.

8.3 Prospects for future work

This dissertation research has produced a number of helpful and innovative products, including shared methods, publications, and seeds for future collaboration. Many of these elements can be improved by future research campaigns, and there are a number of targeted objectives that would represent legitimate contributions to the field of limnology in the future. In addition, a number of suggestions for possible future research have developed from the insights gained in this dissertation.

This dissertation resulted in the development of an open source numerical program called 'Lake Heat Flux Analyzer'. Given the rapid processing of lake buoy data, and calculation of surface energy fluxes, that takes place with the Lake Heat Flux Analyzer program, it would be beneficial to conduct a global comparison study of the surface energy terms. Specifically, developing an understanding of how the individual terms of the surface energy budget varies across a diverse range of lakes, and how the processes occurring at the air-water interface vary as a function of lake size, would be of great interest. One of the main driving forces of the turbulent fluxes in lakes is wind speed; it would therefore be of great scientific interest to compare wind speed measurements among sites of varying sizes. Currently, many lake stations from around the world measure wind speed, but the measurements are often made at different measurement heights, thus limiting the usefulness of a comparison study. By using the Lake Heat Flux Analyzer program, however, users are able to standardise wind speed measurements to a height of 10 m according to the appropriate scaling laws, and thus, conduct a meaningful comparative study.

An extensive data set of high temporal resolution measurements has been analysed. With this data set it would be possible to investigate the diel ranges in wind speed, atmospheric stability, transfer coefficients for momentum, heat and humidity, evaporation rates, convective mixing for lakes from around the world. That is, investigate how these terms differ during the day and night and investigate if they vary as a function of lake morphometry.

Future improvements to the Lake Heat Flux Analyzer program include the possible inclusion of gas exchange equations to estimate the atmospheric exchange of oxygen, carbon dioxide and other material at the air-water interface. Additional variables needed to calculate these exchanges include the light attenuation coefficient, K_d, depth-resolved water temperature measurements to calculate the depth of the upper mixed layer, and the gas concentration in question (e.g. oxygen) at the lake surface and the atmosphere. An additional use for the Lake Heat Flux Analyzer program may be in its inclusion into the 1-D hydrodynamic model, General Lake Model (GLM), which at present uses a constant of 1.3×10^{-3} for the transfer coefficients, although having all of the input variables required to calculate the transfer coefficients as described by the Lake Heat Flux analyzer program. It has been shown in this thesis that the transfer coefficient can vary drastically from this constant value, and thus by ignoring the variability in the transfer coefficients at these scales would lead to erroneous estimates in the GLM. It would, therefore, be a substantial improvement to the GLM if the algorithm for calculating the transfer coefficients were incorporated into the GLM framework. It is also suggested that new transfer coefficients should be derived for lakes which may account for variation caused by, for example, sheltering and fetch-limitation of wind. With this in mind, the numerical code has been written

in an easily accessible manner, so that when new approaches are developed, they can be easily incorporated into the program

References

Abell, J. M., Özkundakci, D., Hamilton, D. P. and Miller, S. D., 2011, Relationship between land use and nitrogen and phosphorus in New Zealand lakes, *Marine and Freshwater Research* **62**(2), 162–175.

Adams, W. and Lasenby, D., 1978, The role of ice and snow in lake heat budgets, *Limnology and Oceanography* **23**(5), 1025–1028.

Adrian, R., Deneke, R., Mischke, U., Stellmacher, R. and Lederer, P., 1995, A Long-term study of the Heiligensee (1975-1992) - Evidence for effects of climatic change on the dynamics of eutrophied lake ecosystems, *Archiv Fur Hydrobiologie* **133**(3), 315–337.

Antenucci, J. P., Imberger, J. and Saggio, A., 2000, Seasonal evolution of the basin-scale internal wave field in a large stratified lake, *Limnology and Oceanography* **45**(7), 1621–1638.

Arhonditsis, G. B. and Brett, M. T., 2005*a*, Eutrophication model for Lake Washington (USA): Part I. Model description and sensitivity analysis, *Ecological Modelling* **187**(2-3), 140–178.

Arhonditsis, G. B. and Brett, M. T., 2005*b*, Eutrophication model for Lake Wash-

ington (USA): Part II. Model calibration and system dynamics analysis, *Ecological Modelling* **187**(2-3), 179–200.

Arhonditsis, G. B., Brett, M. T., DeGasperi, C. L. and Schindler, D. E., 2004, Effects of climatic variability on the thermal properties of Lake Washington, *Limnology and Oceanography* **49**(1), 256–270.

Arvola, L., George, G. D., Livingstone, D. M., Jarvinen, M., Blenckner, T., Dokulil, M. T., Jennings, E., Aonghusa, C. N., Noges, P., Noges, T. and Weyhenmeyer, G. A., 2010, The Impact of the Changing Climate on the Thermal Characteristics of Lakes, *in* George, G, ed., 'Impact of climate change on European lakes', Aquatic Ecology Series, pp. 85–101. doi: 10.1007/978-90-481-2945-4_6.

Atkinson, D., 1994, Temperature and organism size - A biological law for ectotherms?, *Advances in Ecological Research* **25**, 1–58.

Atwater, M. A. and Brown, P. S., 1974, Numerical computations of the latitudinal variation of solar radiation for an atmosphere of varying opacity, *Journal of Applied Meteorology* **13**, 289–297.

Austin, J. A. and Colman, S. M., 2008, A century of temperature variability in Lake Superior, *Limnology and Oceanography* **53**(6), 2724–2730.

Austin, J. M. and Colman, S. M., 2007, Lake Superior summer water temperatures are increasing more rapidly than regional air temperatures: A positive ice-albedo feedback, *Geophysical Research Letters* **34**(6). doi: 10.1029/2006GL029021.

Baines, S., Webster, K., Kratz, T., Carpenter, S. and Magnuson, J., 2000, Synchronous behavior of temperature, calcium, and chlorophyll in lakes of northern Wisconsin, *Ecology* **81**(3), 815–825. doi: 10.1890/0012-9658(2000)081[0815:SBOTCA]2.0.CO;2.

Barton, K., 2014, *MuMIn: Multi-model inference*. R package version 1.10.0. **URL:** *http://CRAN.R-project.org/package=MuMIn*

Bastviken, D., Cole, J. J., Pace, M. L. and Tranvik, L. J., 2004, Methane emissions from lakes: Dependence of lake characteristics, two regional assessments, and a global estimate, *Global Biogeochemical Cycles* **18**(4). doi: 10.1029/2004GB002238.

Bastviken, D., Tranvik, L. J., Downing, J. A., Crill, P. M. and Enrich-Prast, A., 2011, Freshwater methane emissions offset the continental carbon sink, *Science* **331**(6013), 50.

Battarbee, R. W., Shilland, E. M., Kernan, M., Monteith, D. T. and Curtis, C. J., 2014, Recovery of acidified surface waters from acidification in the United Kingdom after twenty years of chemical and biological monitoring (1988-2008), *Ecological Indicators* **37**(B), 267–273. doi: 10.1016/j.ecolind.2013.10.011.

Benson, B. J., Lenters, J. D., Magnuson, J. J., Stubbs, M., Kratz, T. K., Dillon, P. J., Hecky, R. E. and Lathrop, R. C., 2000, Regional coherence of climatic and lake thermal variables of four lake districts in the Upper Great Lakes Region of North America, *Freshwater Biology* **43**, 517–527.

Betts, A. K., Ball, J. H., Beljaars, A. C. M., Miller, M. J. and Viterbo, P. A., 1996, The land surface-atmosphere interaction: A review based on observational and global modeling perspectives, *Journal of Geophysical Research: Atmospheres* **101**(D3), 7209–7225. doi: 10.1029/95JD02135.

Bignami, F., Marullo, S., Santoleri, R. and Schiano, M. E., 1995, Longwave radiation budget in the Mediterranean Sea, *Journal of Geophysical Research: Oceans* **100**(C2), 2501–2514. doi: 10.1029/94JC02496.

Blanc, T. V., 1985, Variation of bulk-derived surface flux, stability, and roughness results due to the use of different transfer coefficient schemes, *Journal of Physical Oceanography* **15**, 650–669.

Blanken, P. D., Rouse, W. R. and Schertzer, W. M., 2003, Enhancement of evaporation from a large northern lake by the entrainment of warm, dry air, *Journal of Hyrdometeorology* **4**(4), 680–693. doi: 10.1175/1525-7541(2003)004¡0680:EOEFAL¿2.0.CO;2.

Bleiker, W. and Schanz, F., 1997, Light climate as the key factor controlling the spring dynamics of phytoplankton in Lake Zürich, *Aquatic Sciences* **59**(2), 135–157.

Bloch, I. and Weyhenmeyer, G. A., 2012, Long-term changes in physical and chemical conditions of nutrient-poor lakes along a latitudinal gradient: is there a coherent phytoplankton community response?, *Aquatic Sciences* **74**(1), 77–85.

Boehrer, B. and Schultze, M., 2008, Stratification of lakes, *Reviews of Geophysics* **46**(2). doi: 10.1029/206RG000210.

Bolton, D., 1980, The computation of equivalent potential temperature, *Monthly Weather Review* **108**, 1046–1053.

Bradley, E. F., Coppin, P. A. and Godfrey, J. S., 1991, Measurements of sensible and latent heat flux in the western equatorial pacific ocean, *Journal of Geophysical Research: Oceans (1978–2012)* **96**(S01), 3375–3389.

Brainerd, K. E. and Gregg, M. C., 1995, Surface mixed and mixing layer depths, *Deep Sea Research Part I: Oceanographic Research Papers* **42**(9), 1521 – 1543. doi: http://dx.doi.org/10.1016/0967-0637(95)00068-H.
URL: *http://www.sciencedirect.com/science/article/pii/096706379500068H*

Breau, C., Cunjak, R. A. and Peake, S. J., 2011, Behaviour during elevated water temperatures: can physiology explain movement of juvenille Atlantic salmon to cool water?, *Journal of Animal Ecology* **80**(4), 844–853.

Brooks, A. and Zastrow, J., 2002, The potential influence of climate change on offshore primary production in Lake Michigan, *Journal of Great Lakes Research* **28**(4), 597–607.

Brown, J. H., Gillooly, J. F., Allen, A. P., Savage, V. M. and West, G. B., 2004, Toward a metabolic theory of ecology, *Ecology* **85**(7), 1771–1789.

Brutsaert, W., 1982, *Evaporation into the atmosphere: Theory, history and applications*, Environmental Fluid Mechanics, Springer.

Burger, D. F., Hamilton, D. P. and Pilditch, C. A., 2008, Modelling the relative importance of internal and external nutrient loads on water column nutrient

concentrations and phytoplankton biomass in a shallow polymictic lake, *Ecological Modelling* **211**(3-4), 411–423.

Burnham, K. P. and Anderson, D. R., 1998, *Model Selection and Inference: A Practical Information-theoretic Approach: with 21 Illustrations*, Springer-Verlag.

Butterwick, C., Heaney, S. I. and Talling, J. F., 2005, Diversity in the influence of temperature on the growth rates of freshwater algae, and its ecological relevance, *Freshwater Biology* **50**(2), 291–300.

Carpenter, S. R. and Brock, W. A., 2006, Rising variance: a leading indicator of ecological transition, *Ecology Letters* **9**(3), 311–318. doi: 10.1111/j.1461-0248.2005.00877.x.

Carpenter, S. R., Cole, J. J., Pace, M. L., Batt, R., Brock, W. A., Cline, T., Coloso, J., Hodgson, J. R., Kitchell, J. F., Seekell, D. A., Smith, L. and Weidel, B., 2011, Early warnings of regime shifts: A whole-ecosystem experiment, *Science* **332**(6033), 1079–1082. doi: 10.1126/science.1203672.

Chang, H. R. and Grossman, R. L., 1999, Evaluation of bulk surface flux algorithms for light wind conditions using data from the coupled ocean-atmosphere response experiment (COARE), *Quarterly Journal of the Royal Meteorological Society* **125**(557), 1551–1588.

Christie, G. and Regier, H., 1988, Measures of optimal thermal habitat and their relationship to yields for 4 commercial fish species, *Canadian Journal of Fisheries and Aquatic Sciences* **45**, 301–314.

Churchill, J. H. and Kerfoot, W. C., 2007, The impact of surface heat flux and wind on thermal stratification in Portage Lake, Michigan, *Journal of Great Lakes Research* **33**(1), 143–155. doi: 10.3394/0380-1330(2007)33[143:TIOSHF]2.0.CO;2.

Clegg, M. R., Maberly, S. C. and Jones, R. I., 2007, Behavioral response as a predictor of seasonal depth distribution and vertical niche separation in freshwater phytoplanktonic flagellates, *Limnology and Oceanography* **52**(1), 441–455.

Coats, R., Perez-Losada, J., Schladow, G., Richards, R. and Goldman, C., 2006, The warming of Lake Tahoe, *Climatic Change* **76**(1-2), 121–148.

Cogley, J. G., 1979, Albedo of water as a function of latitude, *Monthly Weather Review* **107**(6), 775–781.

Cogley, J. G., 1979b, *The Albedo of Water at Different Seasons and Latitudes*, Occasional paper, Department of Geography, Trent University.

Cole, J. J., Prairie, Y. T., Caraco, N. F., McDowell, W. H., Tranvik, L. J., Striegl, R. G., Duarte, C. M., Kortelainen, P., Downing, J. A., Middelburg, J. J. and Melack, J. M., 2007, Plumbing the global carbon cycle: Integrating inland waters into the terrestrial carbon budget, *Ecosystems* **10**(1), 172–185.

Coloso, J. J., Cole, J. J., Hanson, P. C. and Pace, M. L., 2008, Depth-integrated, continuous estimates of metabolism in a clear-water lake, *Canadian Journal of Fisheries and Aquatic Sciences* **65**(4), 712–722. doi: 10.1139/F08-006.

Coloso, J. J., Cole, J. J. and Pace, M. L., 2011, Short-term variation in ther-

mal stratification complicates estimation of lake metabolism, *Aquatic Sciences* **73**(2), 305–315.

Crawford, T. M. and Duchon, C. E., 1999, An improved parameterization for estimating effective atmospheric emissivity for use in calculating daytime downwelling longwave radiation, *Journal of Applied Meteorology* **38**, 474–480.

Crusius, J. and Wanninkhof, R., 2003, Gas transfer velocities measured at low wind speed over a lake, *Limnology and Oceanography* **48**(3), 1010–1017.

Csanady, G. T., 2001, *Air-Sea Interaction: Laws and Mechanisms*, Cambridge University Press.

Daly, K. L., Byrne, R. H., Dickson, A. G., Gallager, S. M., Perry, M. J. and Tivet, T. K., 2011, Chemical and biological sensors for time-series research: Current status and new directions, *Marine Technology Society Journal* **38**(2), 121–143.

Davies-Colley, R. J., 1988, Mixing depths in New Zealand lakes, *New Zealand Journal of Marine and Freshwater Research* **22**(4), 517–528.

Davies, J. A., Robinson, P. J. and Nunez, M., 1971, Field determinations of surface emissivity and temperature for Lake Ontario, *Journal of Applied Meteorology* **10**(4), 811–819.

De Cesare, G., Boillat, J. L. and Schleiss, A. J., 2006, Circulation in stratified lakes due to flood-induced turbidity currents, *ASCE Journal of Environmental Engineering* **132**(11), 1508–1517. doi: 10.1061/(ASCE)0733-9372(2006)132:11(1508).

De Stasio, B. T., Hill, D. K., Kleinhans, J. M., Nibbelink, N. P. and Magnuson, J. J., 1996, Potential effects of global climate change on small north-temperate lakes: physics, fish and plankton, *Limnology and Oceanography* **41**(5), 1136–1149.

Deardorff, J. W., 1968, Dependence of air-sea transfer coefficients on bulk stability, *Journal of Geophysical Research* **73**(8), 2549–2557.

Deardorff, J. W., Willis, G. E. and Lilly, D. K., 1969, Laboratory investigation of non-steady penetrative convection, *Journal of Fluid Mechanics* **35**, 7–31.

DeCosmo, J., Katsaros, K. B., Smith, S. D., Anderson, R. J., Oost, W. A., Bumke, K. and Chadwick, H., 1996, Air-sea exchange of water vapor and sensible heat: The humidity exchange over the sea (hexos) results, *Journal of Geophysical Research: Oceans (1978–2012)* **101**(C5), 12001–12016.

Desai, A. R., Austin, J. A., Bennington, V. and McKinley, G. A., 2009, Stronger winds over a large lake in response to weakening air-to-lake temperature gradient, *Nature Geoscience* **2**, 855–858.

Dixit, S. S., Keller, W., Dixit, A. S. and Smol, J. P., 2001, Diatom-inferred dissolved organic carbon reconstructions provide assessments of past uv-b penetration in canadian shield lakes, *Canadian Journal of Fisheries and Aquatic Sciences* **58**, 543–550.

Dodson, S. I., Arnott, S. E. and Cottingham, K. L., 2000, The relationship in lake communities between primary productivity and species richness, *Ecology* **81**(10), 2662–2679.

Dokulil, M. T., Jagsch, A., George, G. D., Anneville, O., Jankowski, T., Wahl, B., Lenhart, B., Blenckner, T. and Teubner, K., 2006, Twenty years of spatially coherent deepwater warming in lakes across europe related to the North Atlantic Oscillation, *Limnology and Oceanography* **51**(6), 2787–2793.

Donelan, M. A., Dobson, F. W., Smith, S. D. and Anderson, R. J., 1993, On the dependence of sea-surface roughness on wave development, *Journal of Physical Oceanography* **23**(9), 2143–2149. doi: 10.1175/1520-0485(1993)023¡2143:OTDOSS¿2.0.CO;2.

Dong, S., Sprintall, J., Gille, S. T. and Talley, L., 2008, Southern ocean mixed-layer depth from Argo float profiles, *Journal of Geophysical Research: Oceans* **113**(C6). doi: 10.1029/2006JC004051.

Downing, J. A., 2010, Emerging global role of small lakes and ponds: little things mean a lot, *Limnetica* **29**(1), 9–24.

Downing, J. A., Prairie, Y. T., Cole, J. J., Duarte, C. M., Tranvik, L. J., Striegl, R. G., McDowell, W. H., Kortelainen, P., Caraco, N. F., Melack, J. M. and Middelburg, J. J., 2006, The global abundance and size distribution of lakes, ponds, and impoundments, *Limnology and Oceanography* **51**(5), 2388–2397.

Duarte, C. M., Kalff, J. and Peters, R. H., 1986, Patterns in biomass and cover of aquatic macrophytes in lakes, *Canadian Journal of Fisheries and Aquatic Sciences* **43**, 1900–1908.

Dudgeon, D., Arthington, A. H., Gessner, M. O., Kawabata, Z., Knowler, D. J., Leveque, C., Naiman, R. J., Prieur-Richard, A., Soto, D., Stiassny, M. L. J.

and Sullivan, C. A., 2006, Freshwater biodiversity: importance, threats, status and conservation challenges, *Biological Reviews* **81**(2), 163–182.

Edinger, J. E., Duttweiler, D. W. and Geyer, J. C., 1968, The response of water temperature to meteorological conditions, *Water Resources Research* **4**(5), 1137–1143.

Elliott, J. A. and Bell, V. A., 2011, Predicting the potential long-term influence of climate change on vendace (*Coregonus albula*) habitat in Bassenthwaite Lake, UK, *Freshwater Biology* **56**(2), 395–405.

Elmber, J. Nummi, P., Pöysä, H. and Sjöberg, K., 1994, Relationships between species number, lake size and resource diversity in assemblages of breeding waterfowl, *Journal of Biogeography* **21**(1), 75–84.

Eugster, W., Kling, G., Jonas, T., McFadden, J. P., Wüest, A., MacIntyre, S. and Chapin, F. S., 2003, CO_2 exchange between air and water in an arctic alaskan and midlatitude Swiss lake: Importance of convective mixing, *Journal of Geophysical Research: Atmospheres* **108**(D12). doi: 10.1029/2002JD002653.

Evans, C. D., 2005, Modelling the effects of climate change on an acidic upland stream, *Biogeochemistry* **74**(1), 21–46.

Evans, C. D. and Monteith, D. T., 2001, Chemical trends at lakes and streams in the uk acid waters monitoring network, 1988-2000, *Hydrology and Earth System Sciences* **5**, 351–366.

Evans, C. D. and Monteith, D. T., 2002, Natural and anthropogenic changes in the chemistry of six uk mountain lakes, *Water, Air and Soil Pollution* **2**, 33–46.

Fairall, C. W., Bradley, E. F., Hare, J. E., Grachev, A. A. and Edson, J. B., 2003, Bulk parameterization of air-sea fluxes: Updates and verification for the COARE algorithm, *Journal of Climate* **16**, 571–591.

Fairall, C. W., Bradley, E. F., Rogers, D. P., Edson, J. B. and Young, G. S., 1996, Bulk parameterization of air-sea fluxes for Tropical Ocean-Global Atmosphere Coupled-Ocean Atmosphere Response Experiment, *Journal of Geophysical Research Oceans* **101**, 3747–3764. doi: 10.1029/95JCO3205.

Fee, E. J., Hecky, R. E., Kasian, S. E. M. and Cruikshank, D. R., 1996, Effects of lake size, water clarity, and climatic variability on mixing depths in Canadian Shield lakes, *Limnology and Oceanography* **41**(5), 912–920.

Fink, G., Schmid, M., Wahl, B., Wolf, T. and Wüest, A., 2014, Heat flux modifications related to climate-induced warming of large European lakes, *Water Resources Research* **50**(3), 2072–2085. doi: 10.1002/2013WR014448.

Fischer, H. B., 1979, *Mixing in Inland and Coastal Waters*, Academic Press.

Flower, R. J. and Battarbee, R. W., 1983, Diatom evidence for recent acidification of two scottish lochs, *Nature* **305**, 130–133.

Foley, B., Jones, I. D., Maberly, S. C. and Rippey, B., 2012, Long-term changes in oxygen depletion in a small temperate lake: effect of climate change and eutrophication, *Freshwater Biology* **57**(2), 278–289.

France, R., 1997, Land-water linkages: Influences of riparian deforestation on lake thermocline depth and possible consequences for cold stenotherms, *Canadian Journal of Fisheries and Aquatic Sciences* **54**(6), 1299–1305.

Freeman, C., Evans, C. D., Monteith, D., Reynolds, B. and Fenner, N., 2001, Export of organic carbon from peat soils, *Nature* **412**(6849), 785–785.

Frempong, E., 1983, Diel aspects of the thermal structure and energy budget of a small English lake, *Freshwater Biology* **13**(1), 89–102. doi: DOI: 10.1111/j.1365-2427.1983.tb00660.x.

Friehe, C. A. and Schmitt, K. F., 1976, Parameterization of air-sea interface fluxes of sensible heat and moisture by the bulk aerodynamic formulas, *Journal of Physical Oceanography* **6**(6), 801–809.

Futter, M., Helliwell, R., Hutchins, M. and Aherne, J., 2009, Modelling the effects of changing climate and nitrogen deposition on nitrate dynamics in a scottish mountain catchment.

Gabor, D., 1946, Theory of communication. Part 1: The analysis of information, *Electrical Engineers - Part III: Radio and Communication Engineering, Journal of the Institution of* **93**(26), 429–441. doi: 10.1049/ji-3-2.1946.0074.

Gaiser, E., Deyrup, N., Bachmann, R., Battoe, L. and Swain, H., 2009, Effects of climate variability on transparency and thermal structure in subtropical, monomictic Lake Annie, Florida, *Fundamental and Applied Limnology / Archiv fr Hydrobiologie* **175**(3), 217–230. doi: doi:10.1127/1863-9135/2009/0175-0217.

Gal, G., Hipsey, M. R., Parparov, A., Wagner, U., Makler, V. and Zohary, T., 2009, Implementation of ecological modeling as en effective management and investigation tool: Lake Kinneret as a case study, *Ecological Modelling* **220**(13-14), 1697–1718.

Garneau, M., Posch, T., Hitz, G., Pomerleau, F., Pradalier, C., Siegwart, R. and Pernthaler, J., 2013, Short-term displacement of *Planktothrix rubescens* (cyanobacteria) in a pre-alpine lake observed using an autonomous sampling platform, *Limnology and Oceanography* **58**(5), 1892–1906.

Garratt, J. R., 1977, Review of drag coefficients over oceans and continents, *Monthly Weather Review* **105**, 915–929.

Garratt, J. R., 1994, *The atmospheric boundary layer*, Cambridge University Press.

Geernaert, G. L., Katsaros, K. B. and Richter, K., 1986, Variation of the drag coefficient and its dependence on sea state, *Journal of Geophysical Research: Oceans* **91**(C6), 7667–7679. doi: 10.1029/JC091iC06p07667.

George, D. G., 2007, The impact of the North Atlantic Oscillation on the development of ice on Lake Windermere, *Climatic Change* **81**(3-4), 455–468. doi: 10.1007/s10584-006-9115-5.

George, D. G., Maberly, S. C. and Hewitt, D. P., 2004, The influence of the North Atlantic Oscillation on the physical, chemical and biological characteristics of four lakes in the English Lake District, *Freshwater Biology* **49**(6), 760–774.

George, D. G. and Taylor, A. H., 1995, UK lake plankton and the Gulf Stream, *Nature* **378**(6553), 139.

George, G. D., 2010, The impact of year-to-year changes in the weather on the seasonal dynamics of lakes, *in* 'Freshwater Forum', Vol. 23.

George, G. D., Hurley, M. and Hewitt, D., 2007, The impact of climate change on the physical characteristics of the larger lakes in the English Lake District, *Freshwater Biology* **52**(9), 1647–1666.

Gerten, D. and Adrian, R., 2000, Climate-driven changes in spring plankton dynamics and the sensitivity of shallow polymictic lakes to the North Atlantic Oscillation, *Limnology and Oceanography* **45**(5), 1058–1066.

Gill, A. E., 1982, *Atmosphere-Ocean dynamics*, International Geophysics, Elsevier Science.

Gillet, C. and Quentin, P., 2006, Effects of temperature changes on the reproductive cycle of reach in Lake Geneva from 1983 to 2001, *Journal of Fish Biology* **69**, 518–535. doi: 10.1111/j/1095-8649.2006.01123.x.

Gleick, P. H., 1993, *Water in crisis: A guide to the world's fresh water resources.*, Oxford University Press, Inc.

Goldman, C. R., Mason, D. T. and Hobbie, J. E., 1967, Two Antarctic desert lakes, *Limnology and Oceanography* **12**(2), 295–310.

Gorham, E. and Boyce, F. M., 1989, Influence of lake surface area and depth upon thermal stratification and the depth of the summer thermocline, *Journal of Great Lakes Research* **15**(2), 233 – 245.

Goudsmit, G. H., Burchard, H., Peeters, F. and Wüest, A., 2002, Application of k-ε turbulence models to enclosed basins: The role of internal seiches, *Journal of Geophysical Research: Oceans* **107**(C12), 23–1–23–13. doi: 10.1029/2001JC000954.

Goudsmit, G. H., Lemcke, G., Livingstone, D. M., Lotter, A. F., Müller, B. and Sturm, M., 2000, Hagelseewli: a fascinating high mountain lake - suitable for palaeoclimate studies?, *Verhandlungen des Internationalen Verein Limnologie* **27**, 1013–1022.

Graf, W. H. and Mortimer, C. H., 1979, *Hydrodynamics of Lakes*, Developments in Water Science, Elsevier Science.

Grinsted, A., Moore, J. C. and Jevrejeva, S., 2004, Application of the cross wavelet transform and wavelet coherence to geophysical time series, *Nonlinear Processes in Geophysics* **11**, 561–566.

Grueber, C. E., Nakagawa, S., Laws, R. J. and Jamieson, I. G., 2011, Multimodel inference in ecology and evolution: challenges and solutions, *Journal of Evolutionary Biology* **24**(4), 699–711.

Gueymard, C. A., Myers, D. and Emery, K., 2002, Proposed reference irradiance spectra for solar energy systems testing, *Solar Energy* **73**(6), 443 – 467.

Håkanson, L., Parparov, A. and Hambright, K. D., 2000, Modelling the impact of water level fluctuations on water quality (suspended particulate matter) in Lake Kinneret, Israel, *Ecological Modelling* **128**(2-3), 101 – 125.

Hambright, K. D., Gophen, M. and Serruya, S., 1994, Influence of long-term climatic hanges on the stratification of a subtropical, warm monomictic lake, *Limnology and Oceanography* **39**(5), 1233–1242.

Hampton, S. E., Izmest'Eva, L. R., Moore, M. V., Katz, S. L., Dennis, B. and Silow, E. A., 2008, Sixty years of environmental change in the world's largest

freshwater lake - Lake Baikal, Siberia, *Global Change Biology* **14**(8), 1947–1958. doi: 10.1111/j.1365-2486.2008.01616.x.

Hanson, P. C., Carpenter, S. R., Armstrong, D. E., Stanley, E. H. and Kratz, T. K., 2006, Lake dissolved inorganic carbon and dissolved oxygen: Changing drivers from days to decades, *Ecological Monographs* **76**, 343–363.

Hardewig, I., Pörtner, H. O. and van Dijk, P., 2004, Hows does the cold stenothermal gadoid *Lota lota* survive high water temperatures during summer?, *Journal of Comparative Physiology B* **174**, 149–156.

Hari, R. E., Livingstone, D. M., Siber, R., Burkhardt-Holm, P. and Güttinger, H., 2006, Consequences of climatic change for water temperature and brown trout populations in alpine rivers and streams, *Global Change Biology* **12**(1), 10–26. doi: 10.1111/j.1365-2486.2005.001051.x.

Harris, G. P. and Griffiths, F. B., 1987, On means and variances in aquatic food chains and recruitment to the fisheries, *Freshwater Biology* **17**(2), 381–386.

Hart, J. K. and Martinez, K., 2006, Environmental sensor networks: A revolution in the earth system science?, *Earth-Science Reviews* **78**(3-4), 177–191.

Harvey, H. H. and Coombs, J. F., 1971, Physical and chemical limnology of the lakes of Manitoulin Island, *Journal of the Fisheries Research Board of Canada* **28**(12), 1883–1897.

Hastie, T. and Tibshirani, R., 1990, *Generalized Additive Models*, Taylor & Francis.

Heikinheimo, M., Kangas, M., Tourula, T., Venalainen, A. and Tattari, S., 1999, Momentum and heat fluxes over lakes Tamnaren and Raksjo determined by the bulk-aerodynamic and eddy-correlation methods, *Agricultural and Forest Meteorology* **98-9**, 521–534. doi: 10.1016/S0168-1923(99)00121-5.

Heiskanen, J. J., Mammarella, I., Haapanala, S., Pumpanen, J., Vesala, T., MacIntyre, S. and Ojala, A., 2014, Effects of cooling and internal wave motions on gas transfer coefficients in a boreal lake, *Tellus Series B-Chemical and Physical Meteorology* **66**(22827). doi: 10.3402/tellusb.v66.22827.

Henderson-Sellers, B., 1986, Calculating the surface energy balance for lake and reservoir modelling: A review, *Reviews of Geophysics* **24**(3), 625–649.

Hickman, M., 1979, Phytoplankton of shallow lakes: seasonal succession, standing crop and the chief determinants of primary productivity, 1 Cooking Lake, Alberta, Canada, *Holarctic Ecology* **1**(4), 337–350.

Hicks, B. B., 1972, Some evaluations of drag and bulk transfer coefficients over water bodies of different sizes, *Boundary Layer Meteorology* **3**(2), 201–213.

Hill, D. K. and Magnuson, J. J., 1990, Potential effects of global climate warming on the growth and prey consumption of Great-Lakes fish, *Transactions of the American Fisheries Society* **119**(2), 265–275. doi: 10.1577/1548-8659(1990)119¡0265:PEOGCW¿2.3.CO;2.

Hipsey, M. R., Bruce, L. C., Boon, C., Bruggeman, J., Bolding, K. and Hamilton, D. P., 2012, *GLM-FABM model overview and user documentation. The University of Western Australia technical manual, Perth, Australia*.

Hocking, G. C. and Străskraba, M., 1999, The effect of light extinction on thermal stratification in reservoirs and lakes, *Internaltional Review of Hydrobiology* **84**(6), 535–556.

Hofman, A. R., Armstrong, D. E. and Lathrop, R. C., 2013, Influence of phosphorus scavenging by iron in contrasting dimictic lakes, *Canadian Journal of Fisheries and Aquatic Sciences* **70**(7), 941–952.

Hostetler, S. W. and Bartlein, P. J., 1990, Simulation of lake evaporation with application to modeling lake level variations of Harney-Malheur Lake, Oregon, *Water Resources Research* **26**(10), 2603–2612. doi: 10.1029/90WR01240.

Houghton, H. G., 1954, On the annual heat balance of the northern hemisphere, *Journal of Meteorology* **11**(1), 1–9.

Houser, J. N., 2006, Water color affects the stratification, surface temperature, heat content, and mean epilimnetic irradiance of small lakes, *Canadian Journal of Fisheries and Aquatic Sciences* **63**(11), 2447–2455.

Hsu, S. A., 1986, A mechanism for the increase of wind stress (drag) coefficient with wind speed over water surfaces: A parametric model, *Journal of Physical Oceanography* **16**, 144–150.

Huertas, I. E., Rouco, M., López-Rodas, V. and Costas, E., 2011, Warming will affect phytoplankton differently: evidence through a mechanistic approach, *Proceedings of the Royal Society B: Biological Sciences* . doi: 10.1098/rspb.2011.0160.

Huisman, J., Sharples, J., Stroom, J. M., Visser, P. M., Kardinaal, W. E. A.,

Verspagen, J. M. H. and Sommeijer, B., 2004, Changes in turbulent mixing shift competition for light between phytoplankton species, *Ecology* **85**(11), 2960–2970.

Hummel, J. R. and Reck, R. A., 1979, A global surface albedo model, *Journal of Applied Meteorology* **18**(3), 239–253.

Hurrell, J., 1995, Decadal trends in the North Atlantic Oscillation - Regional temperatures and precipitation, *Science* **269**(5224), 676–679. doi: 10.1126/science.269.5224.676.

Hutchinson, G. E. and Edmondson, Y. H., 1957, *A treatise on limnology*, number 1, Wiley.

Hutter, K., Wang, Y. and Chubarenko, I. P., 2010, *Physics of Lakes: Volume 1: Foundation of the Mathematical and Physical Background*, Advances in Geophysical and Environmental Mechanics and Mathematics, Springer.

Idso, S. B., 1973, On the concept of lake stability, *Limnology and Oceanography* **18**(4), 681–683.

Imberger, J., 1985, The diurnal mixed layer, *Limnology and Oceanography* **30**(4), 737–770.

Imberger, J., 1998, *Physical Processes in Lakes and Oceans*, Coastal and estuarine studies, American Geophysical Union.

Imberger, J. and Hamblin, P., 1982, Dynamics of lakes, reservoirs, and cooling ponds, *Annual Reviews of Fluid Mechanics* **14**, 153–187.

Imberger, J. and Patterson, J., 1989, *Physical limnology*, Environmental Dynamics Reference ED-284-JI.

Imboden, D. and Wüest, A., 1995, Mixing Mechanisms in Lakes, *in* A. Lerman, D. Imboden and J. Gat, eds, 'Physics and Chemistry of Lakes', Springer Berlin Heidelberg, pp. 83–138.

Jakkila, J., Lepparanta, M., Kawamura, T., Shirasawa, K. and Salonen, K., 2009, Radiation transfer and heat budget during the ice season in Lake Pääjärvi, Finland, *Aquatic Ecology* **43**(3), 681–692.

Jellison, R. and Melack, J. M., 1993, Meromixis in hypersaline Mono Lake, California. 1. Stratification and vertical mixing during the onset, persistence, and breakdown of meromixis., *Limnology and Oceanography* **38**(5), 1008–1019.

Jennings, E. and Allott, N., 2006, Position of the Gulf Stream influences lake nitrate concentrations in SW Ireland, *Aquatic Sciences* **68**(4), 482–489. doi: 10.1007/s00027-006-0847-0.

Jennings, E., Jones, S., Arvola, L., Staehr, P. A., Gaiser, E., Jones, I. D., Weathers, K. C., Weyhenmeyer, G. A., Chiu, C. and de Eyto, E., 2010, Episodic events in lakes: an analysis of drivers, effects, and responses using high-frequency data, *Freshwater Biology* **57**(3), 589–601.

Jöhnk, K. D., Huisman, J., Sharples, J., Sommeijer, B., Visser, P. M. and Stroom, J. M., 2008, Summer heatwaves promote blooms of harmful cyanobacteria, *Global Change Biology* **14**(3), 495–512. doi: 10.1111/j.1365-2486.2007.01510.x.

Jöhnk, K. D. and Umlauf, L., 2001, Modelling the metalimnetic oxygen minimum in a medium sized alpine lake, *Ecological Modelling* **136**(1), 67–80. doi: 10.1016/S0304-3800(00)00381-1.

Jones, I. D., George, G. D. and Reynolds, C. S., 2005, Quantifying effects of phytoplankton on the heat budgets of two large limnetic enclosures, *Freshwater Biology* **50**(7), 1239–1247.

Jones, I. D., Winfield, I. J. and Carse, F., 2008, Assessment of long-term changes in habitat availability for arctic charr (*Salvelinus alpines*) in a temperate lake using oxygen profiles and hydroacoustic surveys, *Freshwater Biology* **53**(2), 393–402.

Jones, P. D., New, M., Parker, D. E., Martin, S. and Rigor, I. G., 1999, Surface air temperature and its changes over the past 150 years, *Reviews of Geophysics* **37**(2), 173–199. doi: 10.1029/1999RG900002.

Jones, P. D., Osborn, T. J. and Briffa, K. R., 1997, Estimating sampling errors in large-scale temperature averages, *Journal of Climate* **10**, 2548–2568.

Jones, R. I. and Arvola, L., 1984, Light penetration ands some related characteristics in small forest lakes in southern finland, *Verhandlungen Internationale Vereinigung für Theoretische und Angewante Limnologie* **22**, 811–816.

Josey, S. A., Pascal, R. W., Taylor, P. K. and Yelland, M. J., 2003, A new formula for determining the atmospheric longwave flux at the ocean surface at midhigh latitudes, *Journal of Geophysical Research: Oceans* **108**(4). doi: 10.1029/2002JC001418.

Kaiser, G., 2011, *A Friendly Guide to Wavelets*, Modern Birkhauser Classics, Birkhäuser Boston.

Kara, A. B., Rochford, P. A. and Hurlburt, H. E., 2000, An optimal definition for ocean mixed layer depth, *Journal of Geophysical Research: Oceans* **105**(C7), 16803–16821. doi: 10.1029/2000JC900072.

Kara, E. L., Hanson, P. C., Hamilton, D. P., Hipsey, M. R., McMahon, K. D., Read, J. S., Winslow, L. A., Dedrick, J., Rose, K. C., Carey, C. C., Bertilsson, S., Marques, D., Beversdorf, L., Miller, T., Wu, C., Hsieh, Y., Gaiser, E. and Kratz, T. K., 2012, Time-scale dependence in numerical simulations: Assessment of physical, chemical, and biological predictions in a stratified lake at temporal scales of hours to months, *Environmental Modelling and Software* **35**, 104 – 121.

Keller, W. B., Heneberry, J., Leduc, J., Gunn, J. and Yan, N., 2006, Variations in epilimnion thickness in small boreal shield lakes: Relationships with transparency, weather and acidification, *Environmental Monitoring and Assessment* **115**(1-3), 419–431. doi: 10.1007/s10661-006-7237-x.

Keller, W. and Conlon, M., 1994, Crustacean zooplankton communities and lake morphometry in precambrian shield lakes, *Canadian Journal of Fisheries and Aquatic Sciences* **51**(11), 2424–2434.

Kelly, K. A. and Qiu, B., 1995, Heat flux estimates for the western North Atlantic. 1. Assimilation of satellite data into a mixed-layer model, *Journal of Physical Oceanography* **25**(10), 2344–2360. doi: 10.1175/1520-0485(1995)025¡2344:HFEFTW¿2.0.CO;2.

Kempe, S., 1984, Sinks of the anthropogenically enhanced carbon cycle in surface fresh waters, *Journal of Geophysical Research: Atmospheres* **89**(D3), 4657–4676.

Kent, A. D., Yannarell, A. C., Rusak, J. A., Triplett, E. W. and McMahon, K. D., 2007, Synchrony in aquatic microbial community dynamics, *Multidisciplinary Journal of Microbial Ecology* **1**, 38–47.

Kirillin, G., Hochschild, J., Mironov, D., Terzhevik, A., Golosov, S. and Nuetzmann, G., 2011, FLake-Global: Online lake model with worldwide coverage, *Environmental Modelling & Software* **26**(5), 683–684. doi: 10.1016/j.envsoft.2010.12.004.

Kirk, J., 1994, *Light and photosynthesis in aquatic ecosystems*, Cambridge University Press.

Klausmeier, C. A. and Litchman, E., 2001, Algal games: The vertical distribution of phytoplankton in poorly mixed water columns, *Limnology and Oceanography* **46**(8), 1998–2007.

Kling, G. W., 1988, Comparative transparency, depth of mixing, and stability of stratification in lakes of Cameroon, West Africa, *Limnology and Oceanography* **33**(1), 27–40.

Klug, J. L., Richardson, D. C., Ewing, H. A., Hargreaves, B. R., Samal, N. R., Vachon, D., Pierson, D. C., Lindsey, A. M., O'Donnel, D. M., Effler, S. W. and Weather, K. C., 2012, Ecosystem effects of a tropical cyclone on a network of lakes in northeastern North America, *Environmental Science and Technology* **46**(21), 11693–11701.

Kondratyev, K., 1969, *Radiation in the atmosphere*, International Geophysics, Elsevier Science.

Körtzinger, A., Send, U., Lampitt, R. S., Hartman, S., Wallace, D. W. R., Karstensen, J., Villagarcia, M. G., Llinás, O. and DeGrandpre, M. D., 2008, The seasonal pco_2 cycle at 49°N/16.5°W in the northeastern Atlantic Ocean and what it tells us about biological productivity, *Journal of Geophysical Research* **113**(C4).

Kratz, T. K., Deegan, L. A., Harmon, M. E. and Lauenroth, W. K., 2003, Ecological variability in space and time: Insights gained from the US LTER program, *BioScience* **53**(1), 57–67.

Kratz, T. K., Soranno, P. A., Baines, S. B., Benson, B. J., Magnuson, J. J., Frost, T. M. and Lathrop, R. C., 1998, Interannual synchronous dynamics in north temperate lakes in Wisconsin, USA, *in* D. G. George, J. G. Jones, P. Puncochar, C. S. Reynolds and D. W. Sutcliffe, eds, 'Management of lakes and reservoirs during global climate change', Vol. 42 of *Nato Advanced Science Institutes Series, Sub-Ser 2, Environmental Security*, pp. 273–287.

Kristensen, P., Søndergaard, M. and Jeppesen, E., 1992, Resuspension in a shallow eutrophic lake, *Hydrobiologia* **228**(1), 101–109.

Kumar, A., 2003, *Aquatic Ecosystems*, A.P.H. Publishing Corporation.

Lafrenière, M. and Sharp, M., 2003, Wavelet analysis of inter-annual variability in the runoff regimes of glacial and nival stream catchments, Bow Lake, Alberta, *Hydrological Processes* **17**(6), 1093–1118.

Larsen, S., Andersen, T. and Hessen, D. O., 2011, Climate change predicted to cause severe increase of organic carbon in lakes, *Global Change Biology* **17**(2), 1186–1192.

Le Quéré, C., Raupach, M. R., Canadell, J. G., Marland, G., Bopp, L., Ciais, P., Conway, T. J., Doney, S. C., Feely, R. A., Foster, P., Friedlingstein, P., Gurney, K., Houghton, R. A., House, J. I., Huntingford, C., Levy, P. E., Lomas, M. R., Majkut, J., Metzl, N., Ometto, J. P., Peters, G. P., Prentice, I. C., Randerson, J. T., Running, S. W., Sarmiento, J. L., Schuster, U., Sitch, S., Takahashi, T., Viovy, N., van der Werf, G. R. and Woodward, F. I., 2009, Trends in the sources and sinks of carbon dioxide, *Nature Geoscience* **2**(12), 831–836. doi: 10.1038/ngeo689.

Lehman, J. T., 2002, Mixing patterns and plankton biomass of the St. Lawrence Great Lakes under climate change scenarios, *Journal of Great Lakes Research* **28**(4), 583–596.

Leibold, M. A., 1990, Resources and predators can affect the vertical distribution of zooplankton, *Limnology and Oceanography* **35**(4), 938–944.

Lemckert, C. J., Antenucci, J. P. and Saggio, A .and Imberger, J., 2004, Physical properties of turbulent benthic boundary layers generated by internal waves, *Journal of Hydraulic Engineering-ASCE* **130**(1), 58–69. doi: 10.1061/(ASCE)0733-9429(2004)130:1(58).

Lemmin, U. and Amouroux, A., 2012, *The Influence of Climate Change on Lake Geneva*, John Wiley & Sons, Ltd, pp. 201–217. doi: 10.1002/9781118470596.ch12.

Lenters, J. D., Kratz, T. K. and Bowser, C. J., 2005, Effects of climate variability on lake evaporation: Results from a long-term energy budget study of Sparkling Lake, northern Wisconsin (USA), *Journal of Hydrology* **308**(1-4), 168–195.

Lepistö, A., Kortelainen, P. and Mattsson, T., 2008, Increased organic c and n leaching in a northern boreal river basin in finland, *Global Biogeochemical Cycles* **22**(3).

Lewis, W., 1973, Thermal regime of Lake Lanao (Philippines) and its theoretical implications for tropical lakes, *Limnology and Oceanography* **18**(2), 200–217.

Lewis, W. M., 1983, A revised classification of lakes based on mixing, *Canadian Journal of Fisheries and Aquatic Sciences* **40**(10), 1779–1787.

Likens, G., ed., 1985, *An Ecosystem Approach to Aquatic Ecology: Mirror Lake and Its Environment*, Springer-Verlag New York, Inc.

Litchman, E., 2000, Growth rates of phytoplankton under fluctuating light, *Freshwater Biology* **44**(2), 223–235.

Liu, H., Zhang, Y., Liu, S., Jiang, H., Sheng, L. and Williams, Q. L., 2009, Eddy covariance measurements of surface energy budget and evaporation in a cool season over southern open water in Mississippi, *Journal of Geophysical Research-Atmospheres* **114**. doi: 10.1029/2008JD010891.

Liu, W. T., Katsaros, K. B. and Businger, J. A., 1979, Bulk parameterization of air-sea exchanges of heat and water vapor including the molecular constraints at the interface, *Journal of the Atmospheric Sciences* **36**(9), 1722–1735.

Livingstone, D. M., 2001, Large-scale climatic forcing detected in historical observations of lake ice break-up, *in* Williams, W. D., ed., 'International Association of Theoretical and Applied Limnology, vol 27, pt 5, Proceedings', Vol. 27 of *International Association of Theoretical and Applied Limnology - Proceedings*, pp. 2775–2783.

Livingstone, D. M., 2003, Impact of secular climate change on the thermal structure of a large temperate central European lake, *Climatic Change* **57**(1-2), 205–225.

Livingstone, D. M., Adrian, R., Arvola, L., Blenckner, T., Dokulil, M. T., Hari, R. E., George, G., Jankowski, T., Järvinen, M., Jennings, E., Nõges, P., Nõges, T., Straile, D. and Weyhenmeyer, G. A., 2010, Regional and supra-regional coherence in limnological variables, *in* G. D. George, ed., 'The impact of climate change on european lakes', Vol. 4 of *Aquatic Ecology Series*, Springer Netherlands, pp. 311–337.

Livingstone, D. M. and Dokulil, M. T., 2001, Eighty years of spatially coherent Austrian lake surface temperatures and their relationship to regional air temperature and the North Atlantic Oscillation, *Limnology and Oceanography* **46**(5), 1220–1227.

Livingstone, D. M. and Imboden, D. M., 1989, Annual heat balance and equilibrium temperature of Lake Aegeri, Switzerland, *Aquatic Sciences* **51**(4), 351–369.

Livingstone, D. M. and Kernan, M., 2009, Regional coherence and geographi-

cal variability in the surface water temperatures of Scottish Highland lochs, *Advances in Limnology* **62**, 367–378.

Livingstone, D. M. and Lotter, A. F., 1998, The relationship between air and water temperatures in lakes of the Swiss Plateau: a case study with palaeolimnological implications, *Journal of Paleolimnology* **19**(2), 181–198. doi: 10.1023/A:1007904817619.

Livingstone, D. M., Lotter, A. F. and Kettle, H., 2005, Altitude-dependent differences in the primary physical response of mountain lakes to climatic forcing, *Limnology and Oceanography* **50**(4), 1313–1325. doi: DOI: 10.4319/lo.2005.50.4.1313.

Livingstone, D. M., Lotter, A. F. and Walker, I. R., 1999, The decrease in summer surface water temperature with altitude in Swiss Alpine Lakes: A comparison with air temperature lapse rates, *Arctic, Antarctic, and Alpine Research* **31**(4), 341–352.

Lorke, A. and Wüest, A., 2005, Application of coherent ADCP for turbulence measurements in the bottom boundary layer, *Journal of Atmospheric and Oceanic technology* **22**, 1821–1828.

Lowe, P. R., 1977, An approximating polynomial for the computation of saturation vapor pressure, *Journal of Applied Meteorology* **16**, 100–103.

Maberly, S. C., 1996, Diel, episodic and seasonal changes in pH and concentrations of inorganic carbon in a productive lake, *Freshwater Biology* **35**(3), 579–598.

Maberly, S. C. and Elliott, J. A., 2012, Insights from long-term studies in the Windermere catchment: external stressors, internal interactions and the structure and function of lake ecosystems, *Freshwater Biology* **57**, 233–243.

MacCallum, S. N. and Merchant, C. J., 2012, Surface water temperature observations of large lakes by optimal estimation, *Canadian Journal of Remote Sensing* **38**(1), 25–45.

MacIntyre, S., 1993, Vertical mixing in a shallow, eutrophic lake: Possible consequences for the light climate of phytoplankton, *Limnology and Oceanography* **38**(4), 798–817.

MacIntyre, S., Eugster, W. and Kling, G. W., 2001, *The Critical Importance of Buoyancy Flux for Gas Flux Across the Air-Water Interface*, American Geophysical Union, pp. 135–139. doi: 10.1029/GM127p0135.

MacIntyre, S., Flynn, K. M., Jellison, R. and Romero, J. R., 1999, Boundary mixing and nutrient fluxes in Mono Lake, California, *Limnology and Oceanography* **44**(3), 512–529.

MacIntyre, S., Fram, J. P., Kushner, P. J., Bettez, N. D., O'Brien, W. J., Hobbie, J. E. and Kling, G. W., 2009, Climate-related variations in mixing dynamics in an Alaskan arctic lake, *Limnology and Oceanography* **54**(6, part 2), 2401–2417.

MacIntyre, S., Jonsson, A., Jansson, M., Âberg, J., Turney, D. E. and Miller, S. D., 2010, Buoyancy flux, turbulence, and the gas transfer coefficient in a stratified lake, *Geophysical Research Letters* **37**. doi: 10.1029/2010GL044164.

MacIntyre, S. and Melack, J. M., 1982, Meromixis in an equatorial African soda lake, *Limnology and Oceanography* **27**(4), 595–609.

MacIntyre, S. and Melack, J. M., 2009, Mixing dynamics in lakes across climatic zones, *in* G. E. Likens, ed., 'Encyclopedia of Inland Waters', Academic Press, pp. 603 – 612.

MacIntyre, S., Romero, J. R. and Kling, G. W., 2002, Spatial-temporal variability in mixed layer deepening and lateral advection in an embayment of Lake Victoria, East Africa, *Limnology and Oceanography* **47**(3), 656–671.

Mackay, E. B., Folkard, A. M. and Jones, I. D., 2014, Interannual variations in atmospheric forcing determine trajectories of hypolimnetic soluble reactive phosphorus supply in a eutrophic lake, *Freshwater Biology* **59**(8), 1646–1658. doi: 10.1111/fwb.12371.

Mackay, E. B., Jones, I. D., Folkard, A. M. and Barker, P. A., 2012, Contribution of sediment focussing to heterogeneity of organic carbon and phosphorus burial in small lakes, *Freshwater Biology* **57**(2), 290–304.

Mackay, E. B., Jones, I. D., Thackeray, S. J. and Folkard, A. M., 2011, Spatial heterogeneity in a small, temperate lake during archetypal weak forcing conditions, *Fundamental and Applied Limnology* **179**(1), 27–40.

Magnuson, J. J., Benson, B. J. and Kratz, T. K., 1990, Temporal coherence in the limnology of a suite of lakes in Wisconsin, U.S.A., *Freshwater Biology* **23**(1), 145–159.

Magnuson, J. J., Crowder, L. B. and Medvick, P. A., 1979, Temperature as an ecological resource, *American Zoologist* **19**(1), 331–343.

Magnuson, J. J., Robertson, D. M., Benson, B. J., Wynne, R. H., Livingstone, D. M., Arai, T., Assel, R. A., Barry, R. G., Card, V., Kuusisto, E., Granin, N. G., Prowse, T. D., Stewart, K. M. and Vuglinski, V. S., 2000, Historical trends in lake and river ice cover in the Northern Hemisphere, *Science* **289**(5485), 1743–1746. doi: 10.1126/science.289.5485.1743.

Magnuson, J. J., Webster, K. E., Assel, R. A., Bowser, C. J., Dillon, P. J., Eaton, J. G., Evans, H. E., Fee, E. J., Hall, R. I., Mortsch, L. R., Schindler, D. W. and Quinn, F. H., 1997, Potential effects of climate changes on aquatic systems: Laurentian Great Lakes and Precambrian Shield Region, *Hydrological Processes* **11**(8), 825–871.

Manly, B. F. ., 2008, *Statistics for Environmental Science and Management, Second Edition*, Chapman & Hall/CRC Applied Environmental Statistics, Taylor & Francis.

Markensten, H., Moore, K. and Persson, I., 2010, Simulated lake phytoplankton composition shifts toward cyanobacteria dominance in a future warmer climate, *Ecological Applications* **20**(3), 752–767.

Markfort, C. D., Perez, A. L. S., Thill, J. W., Jaster, D. A., Porté-Agel, F. and Stefan, H. G., 2010, Wind sheltering of a lake by a tree canopy or bluff topography, *Water Resources Research* **46**. doi: 10.1029/2009WR007759.

Markfort, C. D., Porté-Agel, F. and Stefan, H. G., 2012, Canopy-wake dynam-

ics and wind sheltering effects on earth surface fluxes, *Environmental Fluid Mechanics* **14**(3), 663–697. doi: 10.1007/s10652-013-9313-4.

Masson, S., Pinel-Alloul, B. and Dutilleul, P., 2004, Spatial heterogeneity of zooplankton biomass and size structure in southern Quebec lakes: variation among lakes and within lake among epi-, meta- and hypolimnion strata, *Journal of Plankton Research* **26**(12), 1441–1458.

Matuszek, J. E., Goodier, J. and Wales, D. L., 1990, The occurence of cyprinidae and other small fish species in relation to pH in Ontario Lakes., *Transactions of the American Fisheries Society* **119**(5), 850–861.

Mazumder, A. and Taylor, W. D., 1994, Thermal structure of lakes varying in size and water clarity, *Limnology and Oceanography* **39**(4), 968–976.

Mazumder, A., Taylor, W. D., Mcqueen, D. J., and Lean, D. R. S., 1990, Effects of fish and plankton on lake temperature and mixing depth, *Science* **247**(4940), 312–315.

Millennium Ecosystem Assessment, 2005, *Ecosystems and human well-being: Synthesis*, Island Press, Washington, DC.

McCombie, A., 1959, Some relations between air temperatures and the surface water temperatures of lakes, *Limnology and Oceanography* **4**(3), 252–258.

McDonald, C. P., Rover, J. A., Stets, E. G. and Striegl, R. G., 2012, The regional abundance and size distribution of lakes and reservoirs in the United States and implications for estimates of global lake extent, *Limnology and Oceanography* **57**(2), 597–606.

McDonald, J. E., 1960, Direct absorption of solar radiation by atmospheric water vapor, *Journal of Meteorology* **17**(3), 319–328.

McDowell, R. W. and Hamilton, D. P., 2013, Nutrients and eutrophication: introduction, *Marine and Freshwater Research* **64**(3), 3–6.

McGillis, W. R., Edson, J. B., Zappa, C. J., Ware, J. D., McKenna, S. P., Terray, E. A., Hare, J. E., Fairall, C. W., Drennan, W., Donelan, M., DeGrandpre, M. D., Wanninkhof, R. and Feely, R. A., 2004, Air-sea co_2 exchange in the equatorial pacific, *Journal of Geophysical Research: Oceans* **109**(C8). doi: 10.1029/2003JC002256.

Mellard, J. P., Yoshiyama, E. L., Litchman, E. and Klausmeier, C. A., 2011, The vertical distribution of phytoplankton in stratified water columns, *Journal of Theoretical Biology* **269**(1), 16–30.

Meyers, T. P. and Dale, R. F., 1983, Predicting daily insolation with hourly cloud height and coverage, *Journal of Climate and Applied Meteorology* **22**(4), 537–545.

Minnett, P. J., 2003, Radiometric measurements of the sea-surface skin temperature: The competing roles of the diurnal thermocline and the cool skin, *International Journal of Remote Sensing* **24**, 5033–5047.

Mironov, D., 2008, Parameterization of lakes in numerical weather prediction. description of a lake model. cosmo technical report, no. 11., Technical report, Deutscher Wetterdienst, Germany: Offenbach am Main, 41 pp.

Mironov, D., Heise, E., Kourzeneva, E., Ritter, B., Schneider, N. and Terzhevik,

A., 2010, Implementation of the lake parameterisation scheme FLake into the numerical weather prediction model COSMO, *Boreal Environment Research* **15**(2), 218–230.

Monin, A. S. and Obukhov, A. M., 1954, Basic laws of turbulent mixing in the atmosphere near the ground, *J. Akad. Nauk. SSR Geofiz. Inst* **24**, 163–187.

Monismith, S. G., 1985, Wind-forced motions in stratified lakes and their effect on mixed-layer shear, *Limnology and Oceanography* **30**(4), 771–783.

Monismith, S. G. and MacIntyre, S., 2009, The surface mixed layer in lakes and reservoirs, *in* G. E. Likens, ed., 'Encyclopedia of Inland Waters', Academic Press, pp. 636 – 650.

Monteith, D. T., Stoddard, J. L., Evans, C. D., de Wit, H. A., Forsius, M., Hogasen, T., Wilander, A., Skjelkvale, B. L., Jeffries, D. S., Vuorenmaa, J., Keller, B., Kopácek, J. and Vesely, J., 2007, Dissolved organic carbon trends resulting from changes in atmospheric deposition chemistry, *Nature* **450**, 537–540.

Moore, M. V., Folt, C. L. and Stemberger, R. S., 1996, Consequences of elevated temperatures for zooplankton assemblages in temperate lakes., *Fundamental and Applied Limnology* **135**, 289–319.

Morimer, C. H., 1941, The exchange of dissolved substances between mud and water in lakes, *Journal of Ecology* **29**(2), 280–329.

Morris, D. P., Zagarese, H., Williamson, C. E., Balseiro, E. G., Hargreaves, B. R., Modenutti, B., Moeller, R. and Queimalinos, C., 1995, The attenuation of so-

lar UV radiation in lakes and the role of dissolved organic carbon, *Limnology and Oceanography* **40**(8), 1381–1391.

Moss, B., 2007, Shallow lakes, the water framework directive and life. what should it all be about?, *in* R. Gulati, E. Lammens, N. Pauw and E. Donk, eds, 'Shallow Lakes in a Changing World', Vol. 196 of *Developments in Hydrobiology*, Springer Netherlands, pp. 381–394.

Myrup, L. O., Powell, T. M., Godden, D. A. and Goldman, C. R., 1979, Climatological estimate of the average monthly energy and water budgets of Lake Tahoe, California-Nevada, *Water Resources Research* **15**(6), 1499–1508.

Nõges, T., 2004, Reflection of the changes of the North Atlantic Oscillation index and the Gulf Stream Position Index in the hydrology and phytoplankton of Võrtsjärv, a large, shallow lake in Estonia, *Boreal Environment Research* **9**(5), 401–407.

Nordbo, A., Launiainen, S., Mammarella, I., Lepparanta, M., Huotari, J., Ojala, A. and Vesala, T., 2011, Long-term energy flux measurements and energy balance over a small boreal lake using eddy covariance technique, *Journal of Geophysical Research-Atmospheres* **116**. doi: 10.1029/2010JD014542.

Oesch, D., Jaquest, J. M., Klaus, R. and Schenker, P., 2008, Multi-scale thermal pattern monitoring of a large lake (Lake Geneva) using a multi-sensor approach, *International Journal of Remote Sensing* **29**(20), 5785–5808.

Olesen, B. and Maberly, S. C., 2001, The effect of high levels of visible levels and ultra-violet radiation on the photosynthesis of photoplankton from a freshwater lake, *Archuv für Hydrobiologie* **151**, 301–315.

O'Reilly, C. M., Alin, S. R., Plisnier, P., Cohen, A. S. and McKee, A., 2003, Climate change decreases aquatic ecosystem productivity of Lake Tanganyika, Africa, *Nature* **424**, 766–768.

Ormerod, S. J., Dobson, M., Hildrew, A. G. and Townsend, C. R., 2010, Multiple stressors in freshwater ecosystems, *Freshwater Biology* **55**, 1–4.

Ostrovsky, I., Yacobi, Y. Z., Walline, P. and Kalikhman, Y., 1996, Seiche-induced water mixing: Its impact on lake productivity, *Limnology and Oceanography* **41**(2), 323–332.

Paavel, B., Arst, H. and Reinart, A., 2008, Variability of bio-optical parameters in two North-European large lakes, *Hydrobiologia* **599**, 201–211. doi: 10.1007/s10750-007-9200-4.

Parker, F. L. and Krenkel, P. A., 1970, *CRC Physical and Engineering Aspects of Thermal Pollution*, CRC Press.

Pearl, H. W. and Huisman, J., 2008, Blooms like it hot, *Science* **320**(5872), 57–58.

Peeters, F., Livingstone, D. M., Goudsmit, G., Kipfer, R. and Forster, R., 2002, Modeling 50 years of historical temperature profiles in a large central European lake, *Limnology and Oceanography* **47**(1), 186–197.

Percival, D. B. and Walden, A., 2006, *Wavelet Methods for Time Series Analysis*, Cambridge Series in Statistics and Probabilistic Mathematics, Cambridge University Press.

Pérez-Fuentetaja, A., Dillon, P. J., Yan, N. D. and McQueen, D. J., 1999, Significance of dissolved organic carbon in the prediction of thermocline depth in small Canadian shield lakes, *Aquatic Ecology* **33**, 127–133.

Pernica, P., Wells, M. G. and MacIntyre, S., 2014, Persistent weak thermal stratification inhibits mixing in the epilimnion of north-temperate Lake Opeongo, Canada, *Aquatic Sciences* **76**(2), 187–201. doi: 10.1007/s00027-013-0328-1.

Perroud, M., Goyette, S., Martynov, A., Beniston, M. and Anneville, O., 2009, Simulation of multiannual thermal profiles in deep Lake Geneva: A comparison of one-dimensional lake models, *Limnology and Oceanography* **54**(5), 1574–1594. doi: 10.4319/lo.2009.54.5.1574.

Peters, R. H. and Downing, J. A., 1984, Empirical analysis of zooplankton filtering and feeding rates, *Limnology and Oceanography* **29**(4), 763–784.

Pierson, D. C., Weyhenmeyer, G. A., Arvola, L., Benson, B., Blenckner, T., Kratz, T., Livingstone, D. M., Merkensten, H., Pettersson, K. and Weathers, K. C., 2011, An automated method to monitor lake ice phenology, *Limnology and Oceanography: Methods* **9**, 74–83.

Pilotti, M., G., V. and Leoni, B., 2013, Data set for hydrodynamic lake model calibration: A deep prealpine case, *Water Resources Research* **49**(10), 7159–7163.

Pond, S., Fissel, D. B. and Paulson, C. A., 1974, A note on bulk aerodynamic coefficients for sensible heat and moisture fluxes, *Boundary Layer Meteorology* **6**(1-2), 333–339.

Porter, J., Arzberger, P., Braun, H., Bryant, P., Gage, S., Hansen, T., Hanson, P., Lin, C., Lin, F., Kratz, T. K., Michener, W., Shapiro, S. and Williams, T., 2005, Wireless sensor networks for ecology, *BioScience* **55**(7), 561–572.

Porter, J. H., Nagy, E., Kratz, T. K., Hanson, P. C., Collins, S. L. and Arzberger, P., 2009, New eyes on the world: Advanced sensors for ecology, *BioScience* **59**(5), 385–397.

Post, D. M., Pace, M. L. and Hairston, N. G., 2000, Ecosystem size determines food-chain length in lakes, *Nature* **405**, 1047–1049.

Quayle, W. C., Peck, L. S., Peat, H., Ellis-Evans, J. C. and Harrigan, P. R., 2002, Extreme responses to climate change in Antarctic lakes, *Science* **295**(5555), 645. doi: 10.1126/science.1064074.

Ramsbottom, A., 1976, *Depth charts of the Cumbrian Lakes*, Freshwater Biological Association.

Rask, M., Arvola, L. and Salonen, K., 1993, Effects of catchment deforestation and burning on the limnology of a small forest lake in southern Finland, *in* Sladeckova, A, ed., 'International Association of Theoretical and Applied Limnology - Proceedings, vol 25, pt 1', Vol. 25 of *International Association of Theoretical and Applied Limnology - Proceedings*, pp. 525–528.

Raymond, P. A., Hartmann, J., Lauerwald, R., Sobek, S., McDonald, C., Hoover, M., Butman, D., Striegl, R., Mayorga, E., Humborg, C., Kortelainen, P., Dürr, H., Meybeck, M., Ciais, P. and Guth, P., 2013, Global carbon dioxide emissions from inland waters, *Nature* **503**, 355–359.

Read, J. S., Hamilton, D. P., Desai, A. R., Rose, K. C., MacIntyre, S., Lenters, J. D., Smyth, R. L., Hanson, P. C., Cole, J. J., Staehr, P. A., Rusak, J. A., Pierson, D. C., Brookes, J. D., Laas, A. and Wu, C. H., 2012, Lake-size dependency of wind shear and convection as controls on gas exchange, *Geophysical Research Letters* **39**(9). doi: 10.1029/2012GL051886.

Read, J. S., Hamilton, D. P., Jones, I. D., Muraoka, K., Winslow, L. A., Kroiss, R., Wu, C. H. and Gaiser, E., 2011, Derivation of lake mixing and stratification indices from high-resolution lake buoy data, *Environmental Modelling and Software* **26**(11), 1325 – 1336.

Read, J. S. and Rose, K. C., 2013, Physical responses of small temperate lakes to variation in dissolved organic carbon concentrations, *Limnology and Oceanography* **58**(3), 921–931.

Reinart, A. and Reinhold, M., 2008, Mapping surface temperature in large lakes with MODIS data, *Remote Sensing of Environments* **112**(2), 603–611.

Reynolds, C. S., 1984, *The Ecology of Freshwater Phytoplankton*, Cambridge Studies in Ecology, Cambridge University Press.

Rhodes, G., Porter, J. and Pickup, R. W., 2012, The bacteriology of windermere and its catchment: insights from 70 years of study, *Freshwater Biology* **57**(2), 305–320. doi: 10.1111/j.1365-2427.2011.02700.x.

Robertson, D. M. and Imberger, J., 1994, Lake Number, a quantitative indicator of mixing used to estimate changes in dissolved oxygen, *Internationale Revue Der Gesamten Hydrobiologie* **79**(2), 159–176.

Robertson, D. M. and Ragotzkie, R. A., 1990, Changes in the thermal structure of moderate to large sized lakes in response to changes in air temperature, *Aquatic Sciences* **52**(4), 360–380. doi: 10.1007/BF00879763.

Robertson, E. and Barry, P. J., 1985, The water and energy balances of Perch Lake (1969 to 1980), *Atmosphere-Ocean* **23**(3), 238–253.

Romero, J. R., Jellison, R. and Melack, J. M., 1998, Stratification, vertical mixing, and upward ammonium flux in hypersaline Mono Lake, California, *Archiv Fur Hydrobiologie* **142**(3), 283–315.

Rose, K. C., Winslow, L. A., Read, J. S., Read, E. K., Solomon, C. T., Adrian, R. and Hanson, P. C., 2014, Improving the precision of lake ecosystem metabolism estimates by identifying predictors of model uncertainty, *Limnology and Oceanography: Methods* **12**, 303–312. doi: 10.4319/lom.2014.12.303.

Rouen, M., George, G. D., Kelly, J., Lee, M. and Moreno-Ostos, E., 2005, High-resolution automatic water quality monitoring systems applied to catchment and reservoir monitoring, *Freshwater Forum* **23**, 20–37.

Roulet, N. and Moore, T. R., 2006, Environmental chemistry: Browning the waters, *Nature* **444**, 283–284.

Rouse, W., Oswald, C., Binyamin, J., Blanken, P., Schertzer, W. and Spence, C., 2003, Interannual and seasonal variability of the surface energy balance and temperature of central Great Slave Lake, *Journal of Hydrometeorology* **4**, 720–730.

Rouse, W. R., Blanken, P. D., Bussieres, N., Walker, A. E., Oswald, C. J., Schertzer, W. M. and Spence, C., 2008, An investigation of the Thermal and Energy Balance Regimes of Great Slave and Great Bear Lakes, *Journal of Hydrometeorology* **9**(6), 1318–1333. doi: 10.1175/2008JHM977.1.

Rueda-Valdivia, F. J. and Schladow, G., 2009, Mixing and stratification in lakes of varying horizontal length scales: Scaling arguments and energy partitioning, *Limnology and Oceanography* **54**(6), 2003–2017.

Sadro, S., Melack, J. M. and MacIntyre, S., 2011, Depth-integrated estimates of ecosystem metabolism in a high-elevation lake (Emerald Lake, Sierra Nevada, California), *Limnology and Oceanography* **56**(5), 1764–1780. doi: 10.4319/lo.2011.56.5.1764.

Saggio, A. and Imberger, J., 1998, Internal wave weather in a stratified lake, *Limnology and Oceanography* **43**(8), 1780–1795.

Sahlberg, J., 2003, Physical modelling of the Akkajaure reservoir, *Hydrology and Earth system Sciences* **7**(3), 268–282.

Sala, O. E., Chapin, F. S., Armesto, J. J., Berlow, E., Bloomfield, J., Dirzo, R., Huber-Sanwald, E., Huenneke, L. F., Jackson, R. B., Kinzig, A., Leemans, R., Lodge, D. M., Mooney, H. A., Oesterheld, M., Poff, N. L., Sykes, M. T., Walker, B. H., Walker, M. and Wall, D. H., 2000, Biodiversity - global biodiversity scenarios for the year 2100, *Science* **287**(5459), 1770–1774.

Scheffer, M., Carpenter, S. R., Foley, J. A., Folke, C. and Walker, B., 2001, Catastrophic shifts in ecosystems, *Nature* **413**, 591–596.

Schertzer, W. M., Saylor, J. H., Boyce, F. M., Robertson, D. G. and Rosa, F., 1987, Seasonal thermal cycle of Lake Erie, *Journal of Great Lakes Research* **13**, 468–486.

Schindler, D. W., 1974a, Eutrophication and recovery in experimental lakes: Implications for lake management, *Science* **184**(4139), 897–899. doi: 10.1126/science.184.4139.897.

Schindler, D. W., 2009, Lakes as sentinels and integrators for the effects of climate change on watersheds, airsheds, and landscapes, *Limnology and Oceanography* **54**(6, 2), 2349–2358. doi: 10.4319/lo.2009.54.6_part_2.2349.

Schindler, D. W., Beauty, K. G., Fee, E. J., Cruikshank, D. R., DeBruyn, E. R., Findlay, D. L., Linsey, G. A., Shearer, J. A., Stainton, M. P. and Turner, M. A., 1990, Effects of climatic warming on lakes of the central boreal forest, *Science* **250**(4983), 967–970.

Schindler, D. W. Kalff, J., Welch, H. E., Brunskill, G. J., Kling, H. and Kritsch, N., 1974c, Eutrophication in the high arctic - Meretta Lake, Cornwallis Island (75°N Lat.), *Journal of the Fisheries Research Board of Canada* **31**, 647–662.

Schindler, D. W., Welch, H. E., Kalff, J., Brunskill, G. J. and Kritsch, N., 1974b, Physical and chemical limnology of Char Lake, Cornwallis Island (75°N Lat.), *Journal of the Fisheries Research Board of Canada* **31**, 585–607.

Schneider, P. and Hook, S. J., 2010, Space observations of inland water bodies show rapid surface warming since 1985, *Geophysical Research Letters* **37**(22). doi: 10.1029/2010GL045059.

Scully, N. M., Leavitt, P. R. and Carpenter, S. R., 2000, Century-long effects of forest harvest on the physical structure and autotrophic community of a small temperate lake, *Canadian Journal of Fisheries and Aquatic Sciences* **57**(S2), 50–59.

Seekell, D. A. and Pace, M. L., 2011, Does the Pareto distribution adequately describe the size-distribution of lakes?, *Limnology and Oceanography* **56**(1), 350–356.

Shade, A., Carey, C. C., Kara, E. L., Bertilsson, S., McMahon, D. and Smith, M. C., 2009, Can the black box be cracked? The augmentation of microbial ecology by high-resolution, automated sensing technologies, *The IMSE Journal* **3**(8), 881–888.

Shintani, T., de la Fuente, A., Nino, Y. and Imberger, J., 2010, Generalizations of the Wedderburn number: Parameterizing upwelling in stratified lakes, *Limnology and Oceanography* **55**(3), 1377–1389.

Shuter, B. J., Schlesinger, D. A. and Zimmerman, A. P., 1983, Empirical predictions of annual surface water temperature cycle in North American lakes, *Canadian Journal of Fisheries and Aquatic Sciences* **40**(10), 1838–1845.

Simpson, J. H., Wiles, P. J. and Lincoln, B. J., 2011, Internal seiche modes and bottom boundary-layer dissipation in a temperate lake from acoustic measurements, *Limnology and Oceanography* **56**, 1893–1906.

Smith, S. D., 1988, Coefficients for sea surface wind stress, heat flux, and wind profiles as a function of wind speed and temperature, *Journal of Geophysical Research: Oceans* **93**, 15467–15472. doi: 10.1029/JC093iC12p15467.

Smith, S. D., 1989, Water vapor flux at the sea surface, *Boundary-Layer Meteorology* **47**(1-4), 277–293.

Smith, S. D., 1998, Coefficients for sea surface wind stress, heat flux, and wind profiles as a function of wind speed and temperature, *Journal of Geophysical Research* **93**, 15467–15472.

Smith, W. L., 1966, Note on the relationship between total precipitable water and surface dewpoint, *Journal of Applied Meteorology* **5**, 726–727.

Snucins, E. and Gunn, J., 2000, Interannual variation in the thermal structure of clear and colored lakes, *Limnology and Oceanography* **45**(7), 1639–1646.

Solomon, C. T., Bruesewitz, D. A., Richardson, D. C., Rose, K. C., Van de Bogert, M. C., Hanson, P. C., Kratz, T. K., Larget, B., Adrian, R., Babin, B. L., Chih-Yu, C., Hamilton, D. P., Gaiser, E., Hendricks, S., Istvánovics, V., Laas, A., O'Donnell, D. M., Pace, M. L., Ryder, E., Staehr, P. A., Torgersen, T. S., Vanni, M., Weathers, K. C. and Zhu, G., 2013, Ecosystem respiration: Drivers of daily variability and background respiration in lakes around the globe, *Limnology and Oceanography* **58**, 849–866.

Spigel, R. H. and Imberger, J., 1980, The classification of mixed-layer dynamics of lakes of small to medium size, *Journal of physical oceanography* **10**(7), 1104–1121.

Staehr, P. A., Bade, D., Van De Bogert, M. C., Koch, G. R., Williamson, C. L., Hanson, P. C., Cole, J. J. and Kratz, T. K., 2010, Lake metabolism and the diel oxygen technique: State of the science, *Limnology and Oceanography: Methods* **8**, 628–644.

Staehr, P. A. and Sand-Jensen, K., 2007, Temporal dynamics and regulation of lake metabolism, *Limnology and Oceanography* **52**(1), 108–120.

Staehr, P. and Sand-Jensen, K., 2006, Seasonal changes in temperature and nutrient control of photosynthesis, respiration and growth of natural phytoplankton communities, *Freshwater Biology* **51**, 249–262.

Steedman, R. J. and Kushneriuk, R. S., 2000, Effects of experimental clearcut logging on thermal stratification, dissolved oxygen, and lake trout (Salvelinus namaycush) habitat volume in three small boreal forest lakes, *Canadian Journal of Fisheries and Aquatic Sciences* **57**(2), 82–91. doi: 10.1139/cjfas-57-S2-82.

Stefan, H. G., Hondzo, M., Fang, X., Eaton, J. G. and McCormick, J. H., 1996, Simulated long-term temperature and dissolved oxygen characteristics of lakes in the north-central United States and associated fish habitat limit, *Limnology and Oceanography* **41**(5), 1124–1135.

Stepanenko, V. M., Joehnk, K. D., Machulskaya, E., Perroud, M., Subin, Z., Nordbo, A., Mammarella, I. and Mironov, D., 2014, Simulation of surface energy fluxes and stratification of a small boreal lake by a set of one-dimensional models, *Tellus Series A-Dynamic Meteorology and Oceanography* **66**. doi: 10.3402/tellusa.v66.21389.

Stepanenko, V. M., Machul'skaya, E. E., Glagolev, M. V. and Lykossov, V. N., 2011, Numerical Modeling of Methane Emissions from Lakes in the Permafrost Zone, *Izvestiya Atmospheric and Oceanic Physics* **47**(2), 252–264. doi: 10.1134/S0001433811020113.

Stevens, C. L. and Lawrence, G. A., 1997, Estimation of wind-forced internal seiche amplitudes in lakes and reservoirs, with data from British Columbia, Canada, *Aquatic Sciences* **59**(2), 115–134.

Straile, D., 2002, North Atlantic Oscillation synchronizes food-web interactions in central European lakes, *Proceedings of the Royal Society of London. Series B: Biological Sciences* **269**(1489), 391–395.

Straile, D. and Adrian, R., 2000, The North Atlantic Oscillation and plankton dynamics in two European lakes-two variations on a general theme, *Global Change Biology* **6**(6), 663–670.

Straile, D., Johnk, K. and Rossknecht, H., 2003, Complex effects of winter warming on the physicochemical characteristics of a deep lake, *Limnology and Oceanography* **48**(4), 1432–1438.

Straile, D. and Stenseth, N., 2007, The North Atlantic Oscillation and ecology: links between historical time-series, and lessons regarding future climate warming, *Climate Research* **34**(3), 259.

Strong, C. and Maberly, S. C., 2011, The influence of atmospheric wave dynamics on interannual variation in the surface temperature of lakes in the English Lake District, *Global Change Biology* **17**(6), 2013–2022.

Stumm, W. and Morgan, J., 2013, *Aquatic Chemistry: Chemical Equilibria and Rates in Natural Waters*, Environmental Science and Technology: A Wiley-Interscience Series of Texts and Monographs, Wiley.

Sturrock, A., Winter, T. and Rosenberry, D., 1992, Energy budget evaporation

from Williams Lake: A closed lake in north central Minnesota, *Water Resources Research* **28**(6), 1605–1617. doi: DOI: 10.1029/92WR00553.

Subin, Z. M., Riley, W. J. and Mironov, D., 2012, An improved lake model for climate simulations: Model structure, evaluation, and sensaitivity analyses in CESM1, *Journal of Advances in Modeling Earth Systems* **4**(1). doi: 10.1029/2011MS000072.

Sverdrup, H., 1953, On conditions for the vernal blooming of phytoplankton, *Journal of Marine Science* **18**(3), 287–295.

Sweers, H. E., 1976, A nomogram to estimate the heat-exchange coefficient at the air-water interface as a function of wind spees and temperature: A critical survey of some literature, *Journal of Hydrology* **30**(4), 375–401.

Tanentzap, A. J., Taylor, P. A., Yan, N. D. and Salmon, J. R., 2007, On sundbury-area wind speeds - a tale of forest regeneration, *Journal of Applied Meteorology and Climatology* pp. 1645–1654.

Tanentzap, A., Yan, N., Keller, B., Girard, R., Heneberry, J., Gunn, J., Hamilton, D. and Taylor, P., 2008, Cooling lakes while the world warms: Effects of forest regrowth and increased dissolved organic matter on the thermal regime of a temperate, urban lake, *Limnology and Oceanography* **53**(1), 404–410.

Thackeray, S. J., George, D. G., Jones, R. I. and Winfield, I. J., 2006b, Statistical quantification of the effect of thermal stratification on patterns of dispersion in a freshwater zooplankton community, *Aquatic Ecology* **40**, 23–32.

Thackeray, S. J., Henrys, P. A., Jones, I. D. and Feutchmayr, H., 2012,

Eight decades of phenological change for a freshwater cladoceran: what are the consequences of our definition of seasonal timing?, *Freshwater Biology* **57**(2), 345–359. doi: 10.1111/j.1365-2427.2011.02614.x.

Thackeray, S. J., Jones, I. D. and Maberly, S. C., 2008, Long-term change in the phenology of spring phytoplankton: Species-specific responses to nutrient enrichment and climatic change, *Journal of Ecology* **96**(3), 523–535.

Thackeray, S. J., Maberly, S. C. and Winfield, I. J., 2006a, The ecology of Bassenthwaite Lake (English Lake District), *Freshwater Forumn* **25**, 1–80.

Thiebaut, S. and Vennel, R., 2010, Observation of a fast continental shelf wave generated by a storm impacting Newfoundland using wavelet and cross-wavelet analyses, *Journal of Physical Oceanography* **40**(2), 417–428.

Thompson, J. R., 2012, Modelling the impacts of climate change on upland catchments in southwest scotland using mike she and the ukcp09 probabilistic projections, *Hydrology Research* **43**(4), 507–530.

Thompson, R. O. R. Y., 1976, Climatological models of the surface mixed layer in the ocean, *Journal of Physical Oceanography* **6**, 496–503.

Thomson, R. E. and Fine, I. V., 2003, Estimating mixed layer depth from oceanic profile data, *Journal of Atmospheric and Oceanic Technology* **20**(2), 319–329. doi: 10.1175/1520-0426(2003)020¡0319:EMLDFO¿2.0.CO;2.

Torrence, C. and Compo, G. P., 1998, A practical guide to wavelet analysis, *Bulletin of the American Meteorological Society* **79**(1), 61–78.

Tranvik, L. J., Downing, J. A., Cotner, J. B., Loiselle, S. A., Striegl, R. G., Ballatore, T. J., Dillon, P., Finlay, K., Fortino, K., Knoll, L. B., Kortelainen, P. L., Kutser, T., Larsen, S., Laurion, I., Leech, D. M., McCallister, S. L., McKnight, D. M., Melack, J. M., Overholt, E., Porter, J. A., Prairie, Y., Renwick, W. H., Roland, F., Sherman, B. S., Schindler, D. W., Sobek, S., Tremblay, A., Vanni, M. J., Verschoor, A. M., von Wachenfeldt, E. and Weyhenmeyer, G. A., 2009, Lakes and reservoirs as regulators of carbon cycling and climate, *Limnology and Oceanography* **54**(6, Part 2), 2298–2314.

Tranvik, L. J. and Jansson, M., 2002, Climate change (communication arising): terrestrial export of organic carbon, *Nature* **415**(6874), 861–862.

Trolle, D., Hamilton, D. P., Pilditch, C. A., Duggan, I. C. and Jeppesen, E., 2011, Predicting the effects of climate change on trophic status of three morphologically varying lakes: implications for lake restoration and management, *Environmental Modelling and Software* **26**, 354–370.

Trolle, D., Skovgaard, H. and Jeppesen, E., 2008, The water framework directive: Setting the phosphorus loading target for a deep lake in Denmark using the 1d lake ecosystem model DYRESM-CAEDYM, *Ecological Modelling* **219**, 138–152.

Vachon, D. and Prairie, Y. T., 2013, The ecosystem size and shape dependence of gas transfer velocity versus wind speed relationship in lakes, *Canadian Journal of Fisheries and Aquatic Sciences* **70**, 1757–1764.

Vachon, D., Prairie, Y. T. and Cole, J. J., 2010, The relationship between near-surface turbulence and gas transfer velocity in freshwater systems and its im-

plications for floating chamber measurements of gas exchange, *Limnology and Oceanography* **55**(4), 1723–1732. doi: 10.4319/lo.2010.55.4.1723.

Van de Bogert, M. C., Bade, D. L., Carpenter, S. R., Cole, J. J., Pace, M. L., Hanson, P. C. and Langman, O. C., 2012, Spatial heterogeneity strongly affects estimates of ecosystem metabolism in two north temperate lakes, *Limnology and Oceanography* **57**(6), 1689–1700. doi: 10.4319/lo.2012.57.6.1689.

Verberk, W., Bilton, D., Calosi, P. and Spicer, J., 2011, Oxygen supply in aquatic ectotherms: Partial pressure and solubility together explain biodiversity and size patterns, *Ecology* **92**(8), 1565–1572.

Verburg, P. and Antenucci, J. P., 2010, Persistent unstable atmospheric boundary enhances sensible and latent heat loss in a tropical great lake: Lake Tanganyika, *Geophysical Research Letters* **115**. doi: 10.1029/2009JD012839.

Verburg, P., Hecky, R. and Kling, H., 2003, Ecological consequences of a century of warming in Lake Tanganuika, *Science* **301**, 505–507.

Verpoorter, C., Kutser, T., Seekell, D. A. and Tranvik, L. J., 2014, A global inventory of lakes based on high-resolution satellite imagery, *Geophysical Research Letters* . doi: 10.1002/2014GL060641.

Vesala, T., Huotari, J., Rannik, U., Suni, T., Smolander, S., Sogachev, A., Launiainen, S. and Ojala, A., 2006, Eddy covariance measurements of carbon exchange and latent and sensible heat fluxes over a boreal lake for a full open-water period, *Journal of Geophysical Research-Atmospheres* **111**(D11). doi: 10.1029/2005JD006365.

Vidal, J., MacIntyre, S., McPhee-Shaw, E. E., Shaw, W. J. and Monismith, S. G., 2013, Temporal and spatial variability of the internal wave field in a lake with complex morphometry, *Limnology and Oceanography* **58**(5), 1557–1580. doi: 10.4319/lo.2013.58.5.1557.

Vidal, J., Rueda, F. and Casamitjana, X., 2007, The seasonal evolution of high vertical-mode internal waves in a deep reservoir, *Limnology and Oceanography* **52**(6), 2656–2667.

Vincent, W., 1981, Production strategies in Antarctic inland waters: phytoplankton eco-physiology in a permanently ice-covered lake, *Ecology* **62**, 1215–1224.

Vincent, W. F., MacIntyre, S., Spigel, R. H. and Laurion, I., 2008, *The physical limnology of high latitude lakes*, Oxford University Press, Oxford, U. K.

Vollmer, M., Bootsma, H., Hecky, R., Patterson, G., Halfman, J., Edmond, J., Eccles, D. and Weiss, R., 2005, Deep-water warming trend in Lake Malawi, East Africa, *Limnology and Oceanography* **50**(2), 727–732.

von Einem, J. and Granéli, W., 2010, Effects of fetch and dissolved organic carbon on epilimnion depth and light climate in small forest lakes in southern Sweden, *Limnology and Oceanography* **55**, 920–930.

Vuorenmaa, J., Forsius, M. and Mannio, J., 2006, Increasing trends of total organic carbon concentrations in small forest lakes in finland from 1987 to 2003, *Science of the Total Environment* **365**, 47–65.

Wain, D. J. and Rehman, C. R., 2010, Transport by an intrusion generated by boundary mixing in a lake, *Water Resources Research* **46**. doi: 10.1029/2009WR008391.

Wanninkhof, R., 1992, Relationship between wind speed and gas exchange over the ocean, *Journal of Geophysical Research: Oceans* **97**(C5), 7373–7382. doi: DOI: 10.1029/92JC00188.

Watras, C., Read, J., Holman, K., Liu, Z., Song, Y., Watras, A., Morgan, S. and Stanley, E., 2014, Decadal oscillation of lakes and aquifers in the upper great lakes region of north america: Hydroclimatic implications, *Geophysical Research Letters* **41**(2), 456–462. doi: 10.1002/2013GL058679.

Watson, E. R., 1904, Movements of the waters of Loch Ness as indicated by temperature observations, *Geographical Journal* **24**, 430–437.

Wedderburn, E. M., 1907, The temperature of the freshwater lochs of Scotland with special reference to Loch Ness, *The Royal Society of Edinburgh* **45**, 407–489.

Wetzel, R., 1975, *Limnology*, W.B. Saunders, Philadelphia, London, and Toronto.

Weyhenmeyer, G. A., Livingstone, D. M., Meili, M., Jensen, O., Benson, B. and Magnuson, J. J., 2011, Large geographical differences in the sensitivity of ice-covered lakes and rivers in the Northern Hemisphere to temperature changes, *Global Change Biology* **17**(1), 268–275. doi: 10.1111/j.1365-2486.2010.02249.x.

Williamson, C. E., Saros, J. E. and Schindler, D. W., 2009, Sentinels of change, *Science* **323**(5916), 887–888. doi: 10.1126/science.1169443.

Wilson, R., Hook, S., Schneider, P. and Schladow, S., 2013, Skin and bulk temperature difference at Lake Tahoe: A case study on lake skin effect, *Journal of Geophysical Research Atmospheres* **118**, 332–346.

Winder, M. and Cloern, J., 2010, The annual cycles of phytoplankton biomass, *Philosophical Transactions of the Royal Society B: Biological Sciences* **365**(1555), 3215–3226.

Winder, M., Jassby, A. D. and Nally, R. M., 2011, Synergies between climate anomalies and hydrological modifications facilitate estuarine biotic invasions, *Ecology Letters* **14**, 749–757.

Winder, M., Reuter, J. and Schladow, S., 2009, Lake warming favours small-sized planktonic diatom species, *Proceedings of the Royal Society B-Biological Sciences* **276**(1656), 427–435.

Winder, M. and Schindler, D. E., 2004, Climate effects on the phenology of lake processes, *Global Change Biology* **10**, 1844–1956.

Winfield, I. J., Fletcher, J. M. and James, B. J., 2012, Long-term changes in the diet of pike (*Esox lucius*), the top aquatic predator in a changing windermere, *Freshwater Biology* **57**(2), 373–383. doi: 10.1111/j.1365-2427.2011.02607.x.

Winslow, L. A., Read, J. S., Woolway, R. I., Brentrup, J. and Zwart, J., 2013, *rLakeAnalyzer: Package for the analysis of lake physics*.
URL: *http://CRAN.R-project.org/package=rLakeAnalyzer*

Woolway, R. I., Maberly, S. C., Jones, I. D. and Feuchtmayr, H., 2014, A novel method for estimating the onset of thermal stratification in lakes from surface water measurements, *Water Resources Research* **50**(6), 5131–5140. doi: 10.1002/2013WR014975.

Wüest, A. and Lorke, A., 2003, Small-scale hydrodynamics in lakes, *Annual Review of Fluid Mechanics* **35**, 373–412. doi: 10.1146/annurev.fluid.35.101101.161220.

Wüest, A., Piepke, G. and Van Senden, D., 2000, Turbulent kinetic energy balance as a tool for estimating vertical diffusivity in wind-forced stratified waters, *Limnology and Oceanography* **45**(6), 1388–1400.

Xenopoulos, M. A. and Schindler, D. W., 2001, The environmental control of near surface thermoclines in boreal lakes, *Ecosystems* **4**, 699–707.

Xiao, W., Liu, S., Wang, W., Yang, D., Xu, J., Cao, C., Li, H. and Lee, X., 2013, Transfer Coefficients of Momentum, Heat and Water Vapour in the Atmospheric Surface Layer of a Large Freshwater Lake, *Boundary-layer Meteorology* **148**(3), 479–494. doi: 10.1007/s10546-013-9827-9.

Yeates, P. and Imberger, J. C., 2003, Pseudo two-dimensional simulations of internal and boundary fluxes in stratified lakes and reservoirs, *International Journal of River Basin Management* **1**(4), 297–319. doi: 10.1080/15715124.2003.9635214.

Yvon-Durocher, G., Caffrey, J. M., Cescatti, A., Dossena, M., del Giorgio, P., Gasol, J. M., Montoya, J. M., Pumpanen, J., Staehr, P. A., Trimmer, M., Woodward, G. and Allen, A. P., 2012, Reconciling the temperature dependence of

respiration across timescales and ecosystem types, *Nature* **487**(7408), 472–476. doi: 10.1038/nature11205.

Zeng, X., Zhao, M. and Dickinson, R., 1998, Intercomparison of bulk aerodynamic algorithms for the computation of sea surface fluxes using TOGA COARE and TAO data, *Journal of Climate* **11**, 2628–2644.

Zohary, T. and Ostrovsky, I., 2011, Ecological impacts of excessive water level fluctuations in stratified shallow lakes., *Inland Waters* **1**, 47–59.